
On the Elasticity of Stiff Polymer Networks

Claus Heußinger



München 2007

On the Elasticity of Stiff Polymer Networks

Claus Heußinger

Dissertation
an der Fakultät für Physik
der Ludwig–Maximilians–Universität
München

vorgelegt von
Claus Heußinger
aus Kulmbach

München, den 30.08.2007

Erstgutachter: Prof. Dr. Erwin Frey
Zweitgutachter: Prof. Dr. Klaus Kroy
Tag der mündlichen Prüfung: 15.10.2007

Contents

Zusammenfassung	ix
1 Introduction	1
1.1 Biology and technology	1
1.2 Single filaments	2
1.3 F-Actin rheology	4
2 Affine and non-affine deformations	7
2.1 Elasticity theory and affine deformations	7
2.2 The Cauchy-Born expansion and non-affine deformations	9
2.3 Stiff polymer networks	12
3 Modelling strategy	15
3.1 Entropic vs. energetic elasticity	15
3.2 Bundles	17
4 Athermal response: floppy modes	19
4.1 Results of simulations	19
4.2 Granular limit	20
5 Thermal response: non-affinity length-scale	25
6 Conclusion	27
6.1 Universal aspects	27
6.2 Outlook	28
7 Publications	29
7.1 Bundles	29
- Statistical Mechanics of Semiflexible Bundles of Wormlike Polymer Chains	31
- Cytoskeletal bundle mechanics	35
7.2 Athermal Response	68
- Floppy Modes and Nonaffine Deformations in Random Fiber Networks .	69
- Non-affine rubber elasticity for stiff polymer networks	73
- Mechanics of Bundled Semiflexible Polymer Networks	85

- Force distribution and force chains in random stiff fiber networks	89
7.3 Thermal Response	96
- Stiff Polymers, Foams, and Fiber Networks	97
- The Role of Architecture in the Elastic Response of Semiflexible Polymer and Fiber Networks	101
A Fascin Networks	117
Bibliography	119
Danksagung	127

List of Figures

1.1	Fluorescence image of actin cyotskeleton; electron micrograph of vimentin cytoskeleton	2
1.2	Confocal light micrograph of in vitro fibrin network	3
1.3	Illustration of the deformation modes of stiff polymers	4
1.4	Electron micrograph of F-actin solution; illustration of the tube concept . .	5
2.1	Illustration of affine deformations in homogeneous media	8
2.2	Illustration of the elasticity of a one-dimensional crystal	10
2.3	Illustration of the non-affine motion in granular assemblies	11
3.1	Computer generated cellular network and random fibrous network	16
3.2	Electron micrograph of F-actin bundle; computer generated bundle of cross-linked worm-like chains	17
4.1	Vibrational eigenmodes of model stiff polymer network	21

Zusammenfassung

Diese Arbeit beschäftigt sich mit der Bestimmung elastischer Konstanten in amorphen Materialien. Im Mittelpunkt steht die Elastizität heterogener Netzwerke aus steifen, stabartigen Polymeren. Diese Netzwerke spielen eine wichtige Rolle in der Zell-Biologie, z.B. in der Form des Zytoskeletts, welchem die Zelle einen Großteil ihrer mechanischen und dynamischen Eigenschaften verdankt. Außerhalb der Zelle werden vergleichbare Polymer-Netzwerke unter anderem in der Haut (Kollagen) oder bei der Wundheilung (Fibrin) gebildet. Eingang ins Alltagsleben haben solche Faser-Systeme schon seit mehreren Jahrhunderten gefunden – in Form von Papier, einem Netzwerk aus langen Zellulosefasern.

In den Kapiteln 1 bis 6 der vorliegenden Arbeit wird versucht, die wichtigsten Ergebnisse zusammenfassend darzustellen und in den Kontext der aktuellen Forschung einzuordnen. Die Details finden sich im Kapitel 7, in dem die zugehörigen wissenschaftlichen Artikel abgedruckt sind.

Bei der Bestimmung der elastischen Konstanten im Rahmen der Elastizitätstheorie erhält der Begriff der “Affinität” eine besondere Bedeutung, da er das Deformationsfeld *homogener* elastischer Systeme charakterisiert. Im Gegensatz dazu ist es in den hier interessierenden *heterogenen* Materialsystemen gerade die Abwesenheit dieser affinen Deformationen, die im Mittelpunkt des Interesses steht. Im Verlauf der Arbeit wird deutlich, wie Nichtaffinität aus einem Zusammenspiel geometrischer Eigenschaften der Mikrostruktur und mechanischer Eigenschaften der Einzelpolymere entstehen kann. Durch die Kombination von Computersimulation und analytischer Beschreibung werden wichtige Aspekte bezüglich der Rolle der heterogenen Mikrostruktur in der Ausbildung makroskopischer Elastizität geklärt. Der Berücksichtigung nicht-affiner Deformationen kommt dabei außerordentliche Bedeutung bei der präzisen Bestimmung makroskopischer elastischer Konstanten zu.

Die Modellierung setzt sich im Wesentlichen aus zwei Komponenten zusammen: der Definition der Netzwerkstruktur und der Spezifikation der elastischen Eigenschaften der Einzelpolymere.

Es zeigt sich, dass die Struktur der Polymer-Netzwerke im Allgemeinen durch zwei Längenskalen beschrieben werden muss. Neben der mittleren Maschenweite a tritt eine mesoskopische Längenskala $l_f \gg a$ auf, die aus der stabartigen Form der Polymere folgt. Es wird gezeigt, dass diese “Faserlänge” – und nicht die Maschenweite – die Rolle der Einheitszelle des Polymernetzwerkes spielt.

Neben dieser geometrischen Komponente spielen die elastischen Eigenschaften der Ein-

zelpolymere eine wesentliche Rolle für die makroskopische Elastizität. Diese orientieren sich zum Einen an den bekannten Kraft-Ausdehnungs-Relationen steifer Polymere und können mit Hilfe des “worm-like chain” Modells berechnet werden. Darüber hinaus wird ein neues “worm-like bundle” Modell entwickelt, das vergleichbare Aussagen zu statistischen und mechanischen Eigenschaften von Polymer-*Bündeln* erlaubt.

Der erste Teil der Arbeit beschäftigt sich mit der athermischen Elastizität der Netzwerke, d.h. der entropische Anteil der Kraft-Ausdehnungs-Relation wird vernachlässigt. Eine selbst-konsistente “effective-medium” Theorie wird entwickelt, die auf der Annahme beruht, dass die Filamente sich wie *inextensible*, biegesteife Stäbe verhalten. Die Annahme der Inextensibilität kann mit der anisotropen Elastizität steifer Polymere begründet werden, deren Biegesteifigkeit, k_{\perp} , im Allgemeinen sehr viel kleiner ist, als deren Strecksteifigkeit, $k_{\parallel} \gg k_{\perp}$. Das sich ergebende nicht-affine Deformationsfeld kann explizit konstruiert werden (“non-affine floppy modes”) und erlaubt eine Berechnung der elastischen Konstanten der Netzwerke, welche mit den Ergebnissen früherer Simulationen übereinstimmen. Desweiteren erlaubt die Theorie, in Verbindung mit dem “worm-like bundle” Modell, eine Erklärung der rheologischen Eigenschaften eines in-vitro Modellsystems aus verknüpften Polymerbündeln.

Der zweite Teil der Arbeit diskutiert thermische Effekte, indem die entropische Strecksteifigkeit der Polymere in der Modellierung berücksichtigt wird. Es besteht ein charakteristischer Unterschied zwischen diesem entropischen Beitrag zur Strecksteifigkeit, k_{\parallel} , und einem energetischen Beitrag, k_s , der sich z.B. aus der Streckung des Polymer-Rückgrats ergibt. Dieser Unterschied betrifft die Abhängigkeit von der Länge l des betrachteten Polymersegments. Die starke Abhängigkeit $k_{\parallel} \sim l^{-4}$ (im Vergleich zu $k_s \sim l^{-1}$) führt dazu, dass thermische Netzwerke steifer Polymere eine starke Sensitivität für strukturelle Unordnung aufweisen, die in athermischen Netzwerken nicht vorhanden ist. Im numerischen Modellsystem äußert sich dieser Effekt durch die Existenz einer Nichtaffinitäts-Länge und dazugehöriger anomaler Exponenten der elastischen Konstanten. Ein Skalenargument wird entwickelt, das den Zusammenhang aufzeigt zwischen Heterogenität des Netzwerks (hier charakterisiert durch die Verteilung $P(l)$) und elastischer Eigenschaften des Einzelpolymers ($k_{\parallel}(l)$).

Chapter 1

Introduction

1.1 Biology and technology

Textbook pictures of eukaryotic cells quite generally convey a very colorful impression of the crowded environment in which cellular processes have to take place. While Mitochondria, the Golgi complex, and other organelles are drawn in vivid colors and detailed morphologies, the cytoskeleton, one of the largest organelles of the cell, only occupies very little space and sometimes is not depicted at all ¹. While this is possibly due to the difficulty to graphically reproduce in a lucid way a structure as complex and heterogeneous as the cytoskeleton, it certainly does not do justice to the importance of this extraordinary organelle.

The cytoskeleton is a rigid yet flexible and dynamic network of protein filaments of varying length and stiffness [2]. The most important components are filamentous actin (F-actin), microtubules as well as intermediate filaments like keratin or vimentin (1.1). For each of the filaments there is a range of accessory proteins which mediate their interactions and control the properties of their assembly [84, 51]. Microtubules not only act as highways for the transport of cargo by motor proteins, but also form e.g. the mitotic spindle that during mitosis distributes the duplicated DNA on the daughter cells. In motile cells, actin filaments form the lamellipodium, a dynamical sheet-like structure at the leading edge that generates the forces necessary for moving the cell forward.

One of the principal tasks of the cytoskeleton is to impart (passive) mechanical stability to the cell. At the same time, however, it needs to be able to actively reorganize its structure to support as complicated tasks as cell migration or mitosis. All these processes rely on the interplay between regulatory mechanisms and the material properties of the cytoskeleton. Understanding the mechanical properties of the individual protein filament as well as its higher order assemblies is therefore a pre-requisite in understanding any such biological process.

Other examples for filamentous polymer networks may be found outside the cell, e.g. in the form of the collagen network in the skin, or the fibrin-based structures [80] that

¹See for example the search results produced by Google for the expression “eukaryotic cell”.

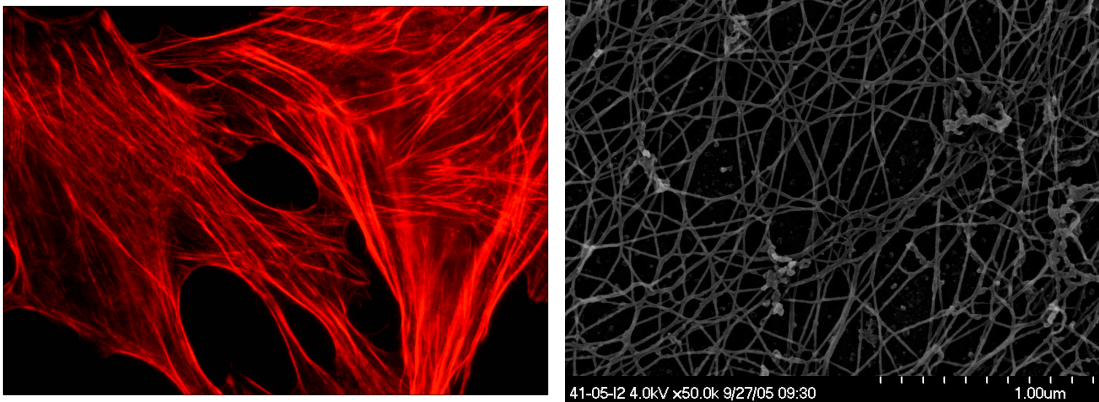


Figure 1.1: (Left) A light microscopy image of fluorescently labeled actin filaments (in mouse-embryonic osteoblasts; courtesy of Oliver Lieleg). (Right) By vapor-depositing a small layer of metal, intermediate filaments (here vimentin) and their cytoskeletal structures can be visualized under an electron microscope (courtesy of Michael Beil).

are generated during clotting of blood in the process of wound healing (Fig. 1.2). Similar networks made of cellulose fibers have found their ubiquitous application in modern day society in the form of paper sheets. Finally, carbon nanotubes and their assemblies are predicted to have important technological applications which are just beginning to be explored [35, 33, 34].

1.2 Single filaments

The filaments comprising the cytoskeleton strongly differ by the value of their persistence length, l_p , which is defined as the length-scale at which bending energy and thermal energy are comparable, $l_p = \kappa/k_B T$. Here, $k_B T \approx 4\text{pN} \cdot \text{nm}$ is the thermal energy at room temperature and κ is the bending stiffness of the filament (with units Energy \times Length). Microtubules are relatively stiff, with persistence lengths in the millimeter range [18, 58], which is much larger than the typical size of a cell. On the other hand, the persistence length of F-actin is $l_p \approx 17\mu\text{m}$ [39, 37, 24], which makes it “semiflexible” on the scale of the cell. Intermediate filaments are even more flexible with a persistence length below the micrometer scale [42].

The model usually adopted for a theoretical description of semiflexible polymers is the “wormlike chain” model [64]. Within this model the polymer is described as a smooth inextensible line $\mathbf{r}(s)$ of total length l parametrized in terms of the arc length s . The mechanical properties are determined by the Hamiltonian

$$H_{\text{WLC}} = \frac{\kappa}{2} \int_0^l ds \left(\frac{\partial \mathbf{t}}{\partial s} \right)^2, \quad (1.1)$$

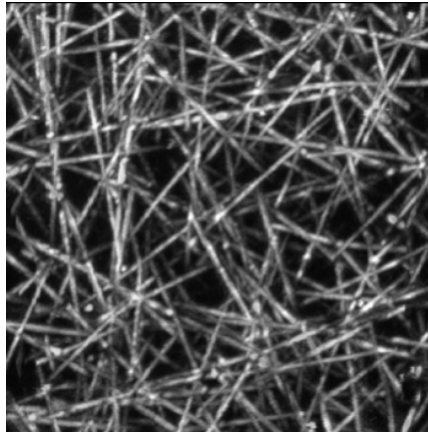


Figure 1.2: In vitro fibrin network (taken from Ref. [11] with permission). The establishment of a fibrin network is one of the first steps in the process of wound healing. The network traps proteins and prevents further blood loss. It also provides the main structural support until new collagen fibers are deposited.

which measures the bending energy of the particular conformation with tangent vectors $\mathbf{t} = \partial \mathbf{r} / \partial s$.

The ground-state or zero temperature properties of the WLC are well established for more than two centuries and can be found in any text-book on elasticity/beam theory ². In view of the thermal environment in the cell, however, the statistical properties of the WLC are of greater interest. One of the few exact results available is the exponential decay of the tangent-tangent correlation function $\langle \mathbf{t}(s)\mathbf{t}(s') \rangle = \exp(-|s - s'|/l_p)$, which is sometimes taken as the defining relation for the persistence length. Quite frequently, “weakly bending” approximations are adopted that allow further analytical results to be obtained, for example the probability distribution for end-to-end distances [81], or the linear response to forces [49, 43]. The latter is of particular interest when filaments are imbedded into networks as it demonstrates how forces can be transmitted from one filament to the next.

As one can infer from their extended, rodlike shape, stiff polymers are highly anisotropic elastic objects [43]. Their force response may be characterized in terms of two qualitatively different deformation modes (Fig. 1.3). The linear response to *longitudinal* forces (stretching) is primarily due to the presence of thermally excited undulations similar to the (isotropic) stiffness of flexible polymers. The resulting effective spring constant,

$$k_{\parallel} \sim \kappa l_p / l^4, \quad (1.2)$$

depends on the intrinsic bending stiffness of the polymer κ , as well as on the temperature-dependent persistence length $l_p \sim T^{-1}$ indicating the entropic origin of the stretching

²In fact, Leonard Euler, one of the founding fathers of beam theory was born in 1707, i.e. exactly 300 years ago.

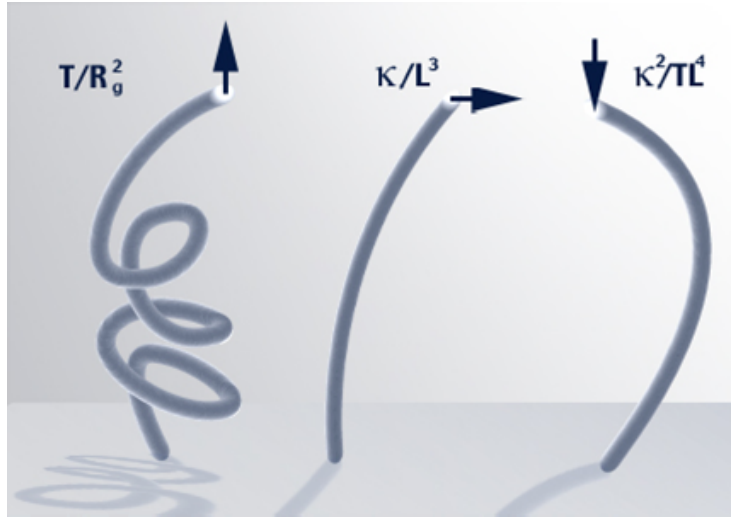


Figure 1.3: Illustration of the anisotropic response properties of stiff polymers as compared to the isotropic response of flexible chains (courtesy of Erwin Frey).

response. Note, that the temperature dependence, $k_{\parallel} \sim T^{-1}$, is quite different from that observed in flexible polymers ($k_{\text{flex}} \sim T$), and leads to a divergence at $T = 0$ that reflects the inextensibility of the polymer backbone. No such temperature dependence is present in the resistance of the polymer to *transverse* forces (bending). This is predominantly an energetic effect, leading to an increase in energy rather than to a decrease in entropy. The corresponding spring constant

$$k_{\perp} \sim \kappa/l^3, \quad (1.3)$$

is independent of the persistence length l_p .

1.3 F-Actin rheology

Having characterized the properties of single filaments, we proceed to discuss the properties of their assemblies. Out of the diverse toolbox of biological stiff polymers, F-actin has emerged as a model system, which allows precise and reproducible in vitro rheological measurements, for example in determining the frequency-dependent shear modulus $G(\omega)$. Already the simplest system, a one-component isotropic solution of actin filaments shows complex viscoelastic properties and represents an interesting model-system being studied for many years. One of the main quantities of interest is the plateau value of the shear modulus found at intermediate timescales where single polymer bending fluctuations are equilibrated, yet center of mass motion is negligible. The generally accepted theory [53, 31, 36, 68] for the concentration dependence of the plateau modulus is based on the free energy change ΔF of confining a single polymer of length l to a tube of diameter d . This is calculated as $\Delta F \sim k_B T l / l_e$ and defines the “deflection length” $l_d \propto l_p^{1/3} d^{2/3}$ that specifies

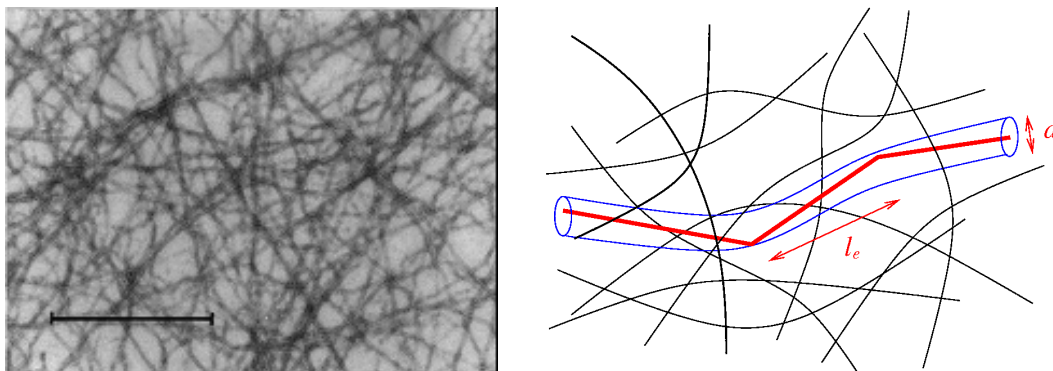


Figure 1.4: (Left) Electron micrograph of a reconstituted entangled F-Actin solution (taken from Ref. [26] with permission). (Right) Illustration of the concept of the tube. The deflection length l_d is the length-scale over which the confined polymer collides with the surrounding tube.

the length between two consecutive collisions of the polymer with its tube (Fig. 1.4). The diameter d itself is a consequence of the structural arrangement of the tubes in the solution, which is believed to be well represented by a random assembly of straight fibers (compare with the fibrin network structure, Fig. 1.2). Even though the resulting scaling of the modulus with concentration as $G \sim c^{7/5}$ is by now well established experimentally [32, 67, 89, 57], computer simulations to study the geometrical as well as elastic properties of this “fibrous” network structure have only recently been realized [62, 83, 61].

Upon the addition of cross-linking proteins or other regulating agents one can induce structural changes to modify the network architecture in many ways [46, 85, 76, 77, 75]. The detailed mechanisms that lead to a particular structure, however, are far from being understood. In general, there will be a complex interplay of polymer kinetics, thermal fluctuations and chemical as well as mechanical properties of the polymers and the cross-linking agents yielding a particular architecture relevant for a given physical situation.

A common feature frequently encountered, is the bundling transition [59, 69, 74, 21, 77], where bundles start to form above a critical linker concentration that depends on the polymer concentration as well as on the linker type. Attempts have been made to describe this transition with a virial expansion [7], with a Flory-Huggins theory [91] or with field theoretic methods [5], however, a detailed picture especially what regards the role of polymer bending undulations is still missing. In this respect, actin bundled and cross-linked with fascin may become a valuable model system. In recent experiments (see Chapter 7.2) an increasing fascin-to-actin ratio has been shown to lead to a direct transition between the two stable phases of an isotropic network of *filaments* and a network of *bundles*. While the origin of the transition itself remains unclear, a consistent interpretation of the observed rheological properties within the bundle regime is possible, as will be explained in more detail below.

Chapter 2

Affine and non-affine deformations

2.1 Elasticity theory and affine deformations

Classical elasticity is a continuum theory that deals with the large scale deformation properties of homogeneous solid systems. It relates stresses and strains by introducing a set of phenomenological parameters that characterizes the elastic properties on wave lengths large compared with any other structural length scale [45]. In linear elasticity these parameters are combined in a constant tensor \mathbf{C} which allows to write the elastic energy $E = \int d\mathbf{r} e(\mathbf{r})$ as the quadratic form

$$e(\mathbf{r}) = \frac{1}{2} \epsilon_{ij} C_{ijkl} \epsilon_{kl}, \quad (2.1)$$

where the strain tensor $\epsilon_{ij} = \frac{1}{2}(\partial_i u_j + \partial_j u_i)$ is defined as the symmetrized gradient of the displacement field $\mathbf{u}(\mathbf{r})$. While the 81 components of the tensor \mathbf{C} hint at the complex mathematical structure of the theory, it may be surprising that by symmetry arguments alone the number of independent components can be reduced to the minimum of two in the case of isotropic materials, for which the elastic energy can be written as

$$e(\mathbf{r}) = G \left(\epsilon_{ij} - \frac{1}{3} \delta_{ij} \epsilon_{ll} \right)^2 + \frac{K}{2} \epsilon_{ll}^2. \quad (2.2)$$

Here, the only remaining components of the tensor \mathbf{C} are the shear modulus G and the bulk modulus K .

A minimization of the elastic energy with respect to deformations $\mathbf{u}(\mathbf{x})$ yields the actual state of the system. The resulting equilibrium equation is most easily written in terms of the stress tensor $\sigma_{ij} = \partial e / \partial \epsilon_{ij}$, as

$$\frac{\partial \sigma_{ij}}{\partial x_j} = -f_i, \quad (2.3)$$

where an external force (density) \mathbf{f} is added to the right-hand side.

Eq. (2.3) has to be solved together with appropriate boundary conditions to obtain the displacement field. A particularly simple solution corresponds to the case of homogeneous

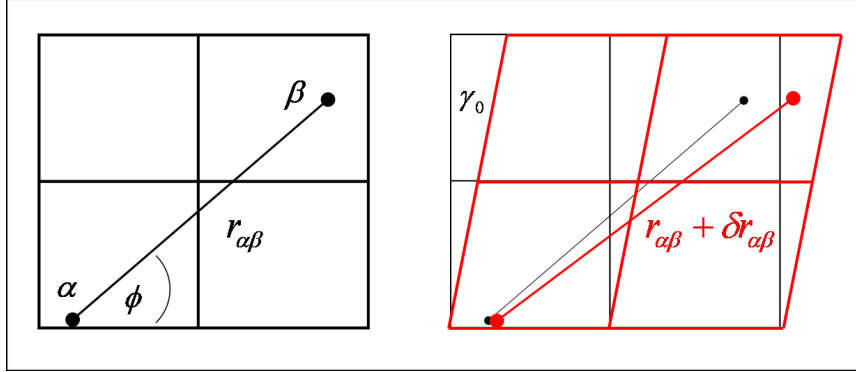


Figure 2.1: A grid drawn in the reference configuration is not distorted by an affine shear deformations γ_0 . The distance between the atoms α and β changes by the amount $\delta r_{\alpha\beta} = \gamma_0 \sin^2(\theta) r_{\alpha\beta}$.

or *affine deformations*, where the strain tensor is constant and independent of the spatial coordinates. In terms of the displacement field, $\mathbf{u}(\mathbf{x})$, this implies that a gradient expansion with respect to an arbitrary reference point \mathbf{R} ,

$$u_i(\mathbf{x}) = u_i(\mathbf{R}) + (\mathbf{x} - \mathbf{R}) \cdot \nabla u_i|_{\mathbf{R}}, \quad (2.4)$$

terminates after the leading order. In fact, mathematically an affine transformation is defined by the mapping $\mathbf{x} \mapsto \mathbf{u}(\mathbf{x}) = \mathbf{A}\mathbf{x} + \mathbf{b}$, where A and b are constants. As is visualized in Fig. 2.1 affine deformations do not lead to “distortions” of a grid that is defined in the undeformed configuration. A straight line in the reference state will still be straight after the deformation, while the distance $r_{\alpha\beta}$ between two points α, β changes in proportion to the distance itself, $\delta r_{\alpha\beta} \sim r_{\alpha\beta}$.

Two important cases of affine deformations have to be distinguished that allow the independent determination of the elastic moduli K and G .

An isotropic dilation is described by a diagonal strain tensor, $\epsilon_{ij} \sim \epsilon_0 \delta_{ij}$, where $\epsilon_0 = \Delta L/L$ corresponds to the relative change of the linear dimension L of the system. Under this deformation the elastic energy reduces to $E \sim L^d K \epsilon_0^2$. On the other hand, a pure shear results in a traceless strain tensor and $E \sim L^d G \gamma_0^2$ with the shear strain γ_0 . Thus, the moduli can be determined by the global energy change upon either dilating or shearing the system. While these relations are strictly valid only for the considered homogeneous systems, one may use them as operational definitions of effective “macroscopic” moduli also in the more general context of heterogeneous materials.

In fact it will be a central task of this thesis to associate macroscopic moduli to heterogeneous systems, where large scale inhomogeneities extend up to the scale of the system size. Concomitant with the existence of heterogeneities we expect, and indeed will find, that affine deformations only poorly represent the state of the system.

2.2 The Cauchy-Born expansion and non-affine deformations

While a description of heterogeneous materials may be based on a modified Eq. (2.2) with spatially varying functions $K(\mathbf{r})$ and $G(\mathbf{r})$, the presence of a discrete and random microstructure prohibits the smooth variation of the elastic moduli in the stiff polymer networks under consideration here. Rather a direct modeling of the individual “elastic building blocks” of the system is required.

In the context of crystal structures, where these building blocks are simply the atoms, this description is known as the Cauchy-Born expansion [6], and consists of specifying the potential energy of atom-atom interactions. The expansion proceeds by writing the energy up to second order in the deviation of the atomic positions from their reference state,

$$E(\{r_{\alpha\beta}\}) = E_0 + \sum \frac{\partial E}{\partial r_{\alpha\beta}} \Big|_0 \delta r_{\alpha\beta} + \frac{1}{2} \sum \frac{\partial^2 E}{\partial r_{\alpha\beta} \partial r_{\gamma\delta}} \Big|_0 \delta r_{\alpha\beta} \delta r_{\gamma\delta}. \quad (2.5)$$

Here, we follow Alexander [3] in using the distances $r_{\alpha\beta}$ between atoms α and β and their respective changes $\delta r_{\alpha\beta}$ as the primary variables. This has the advantage of guaranteeing rotational invariance to all orders in the expansion.

Eq. (2.5) is the microscopic counterpart to Eq. (2.1). The role of the strain tensor is taken by the variables $\delta r_{\alpha\beta}$, while the elastic constants are represented by the coefficients of the second order term, $\partial_{\alpha\beta} \partial_{\gamma\delta} E$. In the remainder of this thesis we will frequently call these coefficients “stiffnesses” or “spring constant” and relate to them by using the symbol k . By minimizing the energy for given boundary conditions, the atomic displacements and thus the macroscopic moduli are determined, quite analogously to solving Eq. (2.3).

One important distinction, however, relates to the presence of affine deformations. While affine deformations represent a solution to Eq. (2.3) for a special class of boundary conditions, there is no reason to expect this property in the case of the Cauchy-Born expansion. In fact, as soon as the unit cell consists of more than one atom, even crystalline materials, which are homogeneous on large scales, will display non-affine deformations on the scale of the unit cell. This interplay of affine and non-affine deformations can nicely be illustrated by the one-dimensional (1d) crystal, which admits a straightforward analytic solution (Fig. 2.2).

We denote the size of the unit cell by a . By connecting in series the stiffnesses $k_\mu \sim \partial_\mu^2 E$ of the interatomic potentials one can define an effective spring constant

$$\bar{k}^{-1} = \sum_{\text{unit cell}} k_\mu^{-1}, \quad (2.6)$$

that relates to the stiffness of the unit cell as a whole. The bulk modulus K can then be written as

$$K = a\bar{k}, \quad (2.7)$$

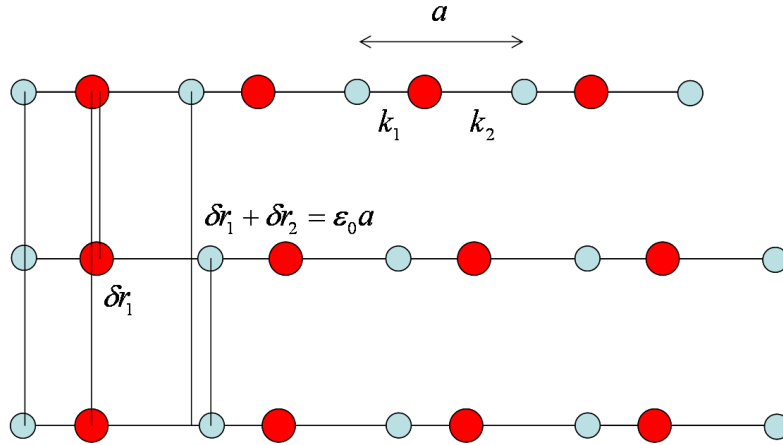


Figure 2.2: Illustration of the elasticity of a one-dimensional crystal with $M = 2$ atoms in the unit cell. The changes in interatomic distances, as compared to the initial configuration (top) are given by δr_1 and δr_2 . (middle) If the spring constants are equal, $k_1 = k_2 = k$, all deformations are affine and $\delta r_1 = \delta r_2 = a/2$. (bottom) In the extreme case that $k_1 = \infty$, the distance r_1 does not change and $\delta r_1 = 0$. The system can nevertheless have the same modulus as before by taking $k_2 = k/2$.

and thus depends on the k_μ only through the combination \bar{k} . In crystals with M atoms in the unit cell, the “internal” stiffnesses k_μ may therefore be varied, while keeping \bar{k} and thus the macroscopic modulus K constant. The associated changes in interatomic distances, which are given by $\delta r_\mu = \epsilon_0 a \bar{k} / k_\mu$, may therefore vary from affine to non-affine behaviour depending on the distribution of the bond stiffnesses k_μ . If all stiffnesses are roughly equal, $k_\mu \approx k$, the unit cell is effectively composed of only one atom and deformations are affine, $\delta r \approx \epsilon_0 a / M$. In this case, the displacement of the individual atom \mathbf{u}_α at R_α can be identified with the continuous displacement field $\mathbf{u}(\mathbf{R}_\alpha)$ defined in Eq. (2.4). If, on the other hand, the individual k_μ strongly differ in magnitude, the resulting deformations will be non-affine and Eq. (2.4) may not be related to the exact atomic displacements, but only to their coarse-grained version [25]. As a crystal is periodic, the scale of the non-affine deformations and thus the scale of the coarse-graining is naturally given by the size of the unit cell, a , which is the only length-scale of the system (besides the system-size L). In contrast, in random or amorphous systems unit cell and system size are formally equivalent, $a \equiv L$, and determining the “non-affinity scale” is a non-trivial task. For example, it has been noted that drawing the spring constants from a distribution $P(k)$ will result in non-affine deformations that (in 1d) grow with the size of the system as $\langle u_{na}^2 \rangle \sim L$ [13].

In this example the non-affinity results from polydispersity in the stiffnesses k_μ of the building blocks. A different type of non-affinity quite frequently occurs in the context of granular media [73, 50]. Recall that affine deformations are intimately connected to a

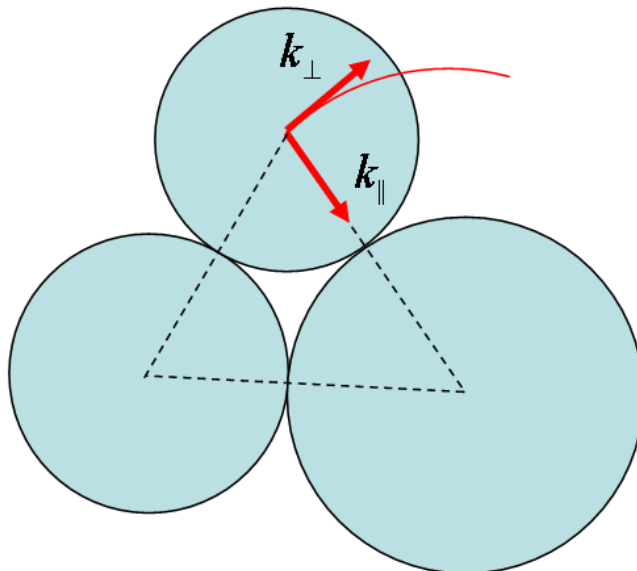


Figure 2.3: Non-affine motion resulting from the incompressibility of grains. An affine deformation would change the distance between the grains (k_{\parallel}), and is energetically much more expensive than the rolling motion perpendicular to the line of contact (k_{\perp}).

change in the distance between two points. In tightly packed systems of rigid grains, on the other hand, the distance between two elements in contact can not change (Fig. 2.3). The only motion possible is perpendicular to the line connecting the particle centers [15]. While the activation of these non-affine modes in granular systems in general results in the yielding of the system, one can also imagine a soft restoring force to inhibit this instability. The system will then be dominated by the transverse non-affine deformations, as long as there is a scale separation $k_{\perp}/k_{\parallel} \ll 1$, between the stiffness k_{\perp} of the non-affine transverse mode and the stiffness k_{\parallel} of the affine compressive mode.

As we will see below both types of non-affinities will be relevant for the accurate characterization of the deformation field in stiff polymer networks. The polydispersity in the spring constants k will be encountered as consequence of the ubiquitous structural randomness in connection with the strong length-dependence of the entropic stretching stiffness $k_{\parallel} \sim l^{-4}$, Eq. (1.2). The second type of non-affinity naturally occurs, as the scale separation between transverse (bending) and longitudinal (stretching) mode in stiff polymers is already implied by their fibrous appearance.

2.3 Stiff polymer networks

Current models [49, 43, 65] for the elasticity of stiff polymer networks (“affine models”) are based on the assumption that the non-affinity scale is on the order of the mesh-size, a . The modulus in this picture is simply given by the energy of the unit cell, $\bar{k}(\gamma a)^2$, times the number of cells per volume, $\nu \sim a^{-d}$ (in d dimensions). Similar to Eq. (2.6), the overbar denotes that the stiffnesses have to be taken on the scale of the average mesh-size. Because of the assumption of affine displacements no cooperativity between the elastic responses of individual elements can be possible. The effect of the assembled structure can simply be predicted by counting the number ν of building blocks, which are the individual meshes of size a . Accounting for the presence of the two deformation modes one can show [41] that the modulus is given by

$$G_{\text{aff}}^{-1} = a^{d-2} \left(A\bar{k}_{\perp}^{-1} + B\bar{k}_{\parallel}^{-1} \right), \quad (2.8)$$

where the two modes act as if they were springs connected in series. This equation represents the d -dimensional equivalent of Eq. (2.7).

It appears that this model can successfully be used to rationalize data of various cross-linked actin networks [21, 22]. Recently, extensions to the theory have been formulated to include nonlinear elasticity [72] as well as bundle formation [21], however, still on the mean-field level of affine segment deformations. While the details of the particular structure may enter the prefactors A and B in an involved way, this complication is usually eliminated by *choosing* the values appropriately (e.g. $A = 0$ in [49]). With this choice the affine theory is essentially equivalent to the classical theory of rubber elasticity in being based solely on the affine change of polymer end-to-end distances.

In the following we will show that these models are insufficient for several reasons.

1. As can be inferred from Figs. 1.2 and 1.4, stiff polymer networks are usually characterized by the presence of a mesoscopic length l_f that corresponds to the scale over which the polymers can be assumed to be straight. For isolated filaments this length-scale may be identified with the persistence length l_p . In networks the origin may be different and for example a consequence of the network generating processes itself. We will see that the presence of this length-scale drastically alters the elastic response as compared to systems where this scale is missing. In particular, it is shown that one has to view the entire polymer fiber as a “nonlocal” equivalent of the local unit cell of crystal structures. Thus, the entire fiber – and not just the individual mesh – forms the elementary building block of the network.
2. Bending and stretching stiffnesses in stiff polymer networks show the scale separation, $k_{\perp}/k_{\parallel} \ll 1$, characteristic for granular media. We will demonstrate how this “granular limit” leads to an elastic regime where, in striking contrast to the affine model (with $A = 0$), the stretching mode is fully frozen out and the elastic energy is completely dominated by highly non-affine bending deformations. We develop a theory that fully explains the anomalous elasticity found in this regime.

3. The presence of structural randomness induces a broad distribution of bond stiffnesses k , which may actually acquire polynomial tails. It will turn out that, similar to the 1d example given above, this results in deviations from affine behaviour on scales much larger than the mesh-size, a . We identify the microscopic mechanism that generates this non-affinity and clarify its consequences for the macroscopic moduli.

Chapter 3

Modelling strategy

The approach that we will adopt to model cross-linked stiff polymer networks is to neglect the intricate phase behaviour of the network, and to concentrate on given network structures and their specific influence in mediating the elastic or rheological properties. In this respect, we have found that *fibrous* and *cellular* networks (see Fig. 3.1) can provide two antipodal reference systems that may be used for the classification of real polymer networks. In fibrous networks the mesoscopic scale l_f is concomitant with a hierarchical architecture where small cells are generated within larger cells within even larger cells. In contrast, in cellular systems this length is absent. There, the structure is usually characterized quite well by only one hierarchy – that of the average unit cell. By studying both types of systems one can therefore assess the importance of the scale l_f on the macroscopic elastic properties.

3.1 Entropic vs. energetic elasticity

An important quantity to characterize the rheological properties is the low frequency shear modulus $G_0 = G(\omega \rightarrow 0)$, which takes a similar role as the plateau modulus in entangled solutions, and which can be calculated from the elastic energy stored in the strained network. In the spirit of the Cauchy-Born expansion, Eq. (2.5), the role of the atoms is now taken by the cross-links, which are moving in a potential energy landscape provided by the connecting polymers. While the applied macroscopic shear strain γ constrains the cross-links on the boundary ¹, those in the bulk are unconstrained to find the minimum energy configuration. In the harmonic approximation of Eq. (2.5) the potential energy is fully defined by “spring constants” k that characterize the linear response properties of polymer segments to forces applied at its ends.

As biological networks of stiff polymers are immersed in a thermal environment, in addition to the standard energetic elasticity, induced by an increase in energy, also entropic effects have to be accounted for. There are two main effects. In a thermal environment cross-links fluctuate and thus sample the full potential energy landscape with the appro-

¹In general, we employ periodic boundary conditions on all sides of the simulation volume.

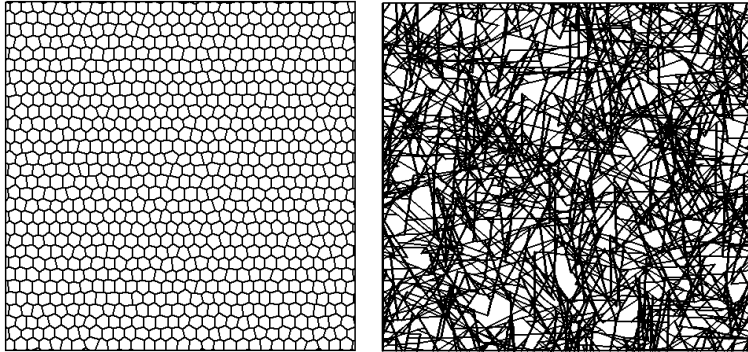


Figure 3.1: Illustration of the two different classes of network structures (2d) studied in this thesis. (Left) A cellular, foam-like structure with only small amounts of randomness. (Right) The random fibrous structure generated by randomly depositing fibers on a plane.

appropriate Boltzmann factor. Secondly, also the polymers are fluctuating and therefore the potential energy itself.

Both effects can in principle be accounted for by using proper Monte-Carlo techniques, which, however, goes beyond the scope of this thesis. In a first step, therefore, only the fluctuations of the polymers are accounted for. These can easily be incorporated into the above framework by including the conformational entropy of the polymers as an additional contribution to the potential energy landscape, which thus becomes a free energy landscape or a “potential of mean force”. The strategy is thereby similar to a Born-Oppenheimer approximation. Entropic contributions from the “slow variables”, the cross-link positions, are neglected, while the “fast” polymer degrees of freedom are assumed to be equilibrated at all times. Formally, this corresponds to integrating the partition function Z over the variables $\{r_\alpha\}$ pertaining to the polymers, while treating the remaining cross-link degrees of freedom $\{R_\alpha\}$ in saddle-point approximation,

$$\begin{aligned} Z &= \int_{R,r} \exp(-\beta H(r, R)) = \int_R \exp(-\beta F(R)) \\ &\rightarrow \exp(-\beta F(\bar{R})), \end{aligned} \quad (3.1)$$

where \bar{R} is obtained as solution to the saddle-point equation $\partial F/\partial R|_{\bar{R}} = 0$.

In fact, this approach is a standard manipulation in many condensed-matter problems. In particular it is used in the classical theory of rubber elasticity where only entropic contributions to the free energy landscape are present [63]. In the so-called fixed junction model, developed by Kuhn and others [44, 78, 19], one disregards the fluctuations of the cross-links and assumes them to deterministically follow the macroscopic strain in an affine way. The induced reduction of polymer conformational entropy is then captured by the definition of a purely entropic spring constant, $k_{\text{flex}} \sim T$, proportional to temperature T .

In contrast, the spring constants $k_\perp \sim \kappa/l^3$ and $k_\parallel \sim \kappa l_p/l^4$ relevant for stiff polymers resemble the mixed energetic/entropic nature of their elastic response. While the response

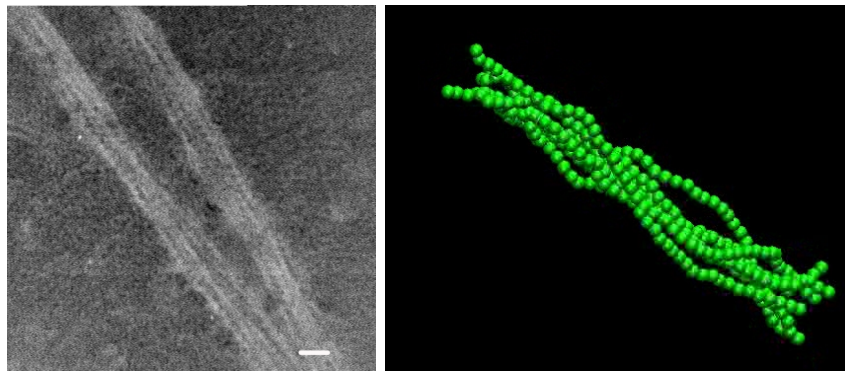


Figure 3.2: (Left) Electron micrograph of an F-actin bundle cross-linked by fascin (courtesy of Mireille Claessens). (Right) Snapshot from a Monte-Carlo simulation of a cross-linked bundle of worm-like chains (courtesy of Mark Bathe).

to forces transverse to the polymer axis is of energetic origin, the stretching response is due to the presence of thermally excited undulations and thus an entropic effect. In addition to these two main deformation modes, one can also include an energetic stretching stiffness by allowing for a finite extensibility of the polymer backbone [40]. This gives rise to a third spring constant

$$k_s \sim \kappa/lr^2, \quad (3.2)$$

which depends on the polymer cross-section radius r instead of on the persistence length l_p .

Note the distinct dependence of the enthalpic stretching stiffness, $k_s \sim l^{-1}$, on polymer length l as compared to the entropic stiffness, $k_{\parallel} \sim l^{-4}$. In networks with a distribution $P(l)$ of lengths, the two stretching modes will thus lead to fundamentally different elastic response properties. As indicated above, by accounting for the entropic origin, k_{\parallel} , of the single-polymer stretching elasticity, the networks acquire a strong susceptibility to polydispersity and structural randomness that is completely absent in athermal models.

3.2 Bundles

In view of the experiments on the actin/fascin system we also study the elastic properties of cross-linked semiflexible polymer *bundles* (see Fig. 3.2). A generalization of the wormlike chain model to bundles (“wormlike bundles”, WLB) allows the discussion of the statistical mechanics of filament bundles in much the same way as the WLC does for single filaments. It turns out that the response of a single bundle cannot be described on the basis of the constant bending stiffness κ introduced above. In contrast, a mode-number dependent bending stiffness $\kappa_B(q)$ has to be introduced that leads to a wealth of interesting and unexpected effects already on the level of the single bundle. Within the WLB model one

finds for a bundle of N filaments,

$$\kappa_B(q) = N\kappa \left[1 + \left(\frac{1}{N-1} + (q\lambda)^2 \right)^{-1} \right], \quad (3.3)$$

where the length-scale λ depends on the filament bending stiffness κ as well as on the mechanical properties of the cross-linking proteins. As a result of the analysis the tangent-tangent correlation function does not decay exponentially, but rather exhibits a complex structure at intermediate distances [16]. One also finds that the effective spring constants for stretching and bending, Eqs. (1.2) and (1.3), have to be modified as compared to the single filament case,

$$k_{\parallel}^B \sim \frac{N\kappa l_p}{l\lambda^3}, \quad k_{\perp}^B \sim \frac{N\kappa}{l\lambda^2}. \quad (3.4)$$

These expressions are valid as long as the third term in Eq. (3.3) dominates. Upon comparison with Eqs. (1.2) and (1.3) one finds that the dependence on polymer length l is altered. Both spring constants depend on polymer length as $k \sim l^{-1}$ similar to k_s .

An interesting consequence of Eq. (3.3) is furthermore that the Euler buckling load, $F_c \sim \kappa_B/l^2$, can become independent of the length of the bundle. This unique property may well be exploited in polymerizing biological bundles such as filopodia, which may increase their contour length against compressive loads without loss of mechanical stability.

Chapter 4

Athermal response: floppy modes

4.1 Results of simulations

In this section results are reported from the study of athermal filamentous networks (no bundles) in which the persistence length is assumed large enough for any thermal undulations to be frozen out completely. The polymer response is then characterized by the two spring constants k_{\perp} and k_s only. In fact, the resulting elastic element is identical to an Euler-Bernoulli beam.

Cellular structures with this type of material properties are well known as (open cell) foams. These materials and their closed cell analogs are ubiquitous in nature and many areas of technology. Examples range from liquid foams and froths as part of drinks or household detergents, to plastic and metallic foams used for insulation or shock absorption [79, 23]. The linear and nonlinear elastic as well as plastic properties of foams have been studied for many years. Particular interesting from the point of view of this thesis are numerical studies to assess the influence of randomness in size and type of the unit cell on the (magnitude of the) elastic moduli [71, 17, 90].

Quite generally, open-cell foams are characterized by rather slender beams $r \ll a$. One thus finds that the typical bending mode is softer than the stretching mode, $\bar{k}_s/\bar{k}_{\perp} \sim (a/r)^2 \gg 1$, and therefore dominates the modulus – mechanical foams are *bending dominated*. From Eq. (2.8) one thus finds (for $d = 2$)

$$G_{\text{foam}} \sim \bar{k}_{\perp}. \quad (4.1)$$

The fibrous architecture, on the other hand, is a well studied model system for the elastic properties of paper sheets, which are usually made of cellulose fibers. Quite contrary to the thin elastic elements making a foam, the cross-section of a cellulose fiber is large enough to make paper sheets dominated by the stretching mode [1]. Early theoretical approaches therefore neglect the bending stiffness of the fibers [12, 4], effectively replacing them by simple central force springs, which would lead to a modulus, $G \sim \bar{k}_s$ (this limit formally corresponds to $r \gg a$).

Recent studies on the random fibrous network structure (depicted in Fig. 3.1) are more tailored towards biological applications, however, without actually including the thermal

fluctuations ever present in soft matter systems [20, 82, 27, 28, 29, 30, 55]. These studies, focusing on the smaller aspect ratios appropriate for most important biological stiff polymers, identified a new elastic regime, where, similar to cellular foams, the bending mode predominates. In this regime the shear modulus was found to scale as

$$G_{\text{fiber}} \sim \bar{k}_{\perp} (l_f/a)^{\mu-3}, \quad (4.2)$$

which differs from Eq. (4.1) through the presence of the fiber length l_f . Quite surprisingly, the exponent μ , which specifies the susceptibility of the modulus to density changes, $G \sim \rho^{\mu}$, has a value as large as $\mu \approx 6.7$. What is more, deformations are found to be highly non-affine, again different from the affine deformations present in regular foams. A scaling ansatz for the shear modulus identified a length-scale ξ that takes the role of the average cell size a in governing the cross-over from the affine stretching regime ($r \gg \xi$) to the non-affine bending regime ($r \ll \xi$). While heuristic non-affinity measures have been devised to quantify the absence of affine deformations [27, 55], so far little was known about the actual nature of the deformations present in this regime.

In a first theoretical approach [4] the bending response was incorporated without accounting for the fiber length-scale l_f . The resulting affine theory directly leads to a modulus given by Eq. (4.1), i.e. to an exponent $\mu = 3$. Later Head *et al.* have proposed [28] to rationalize the emergent non-affinity by considering deviations from an affine reference state. A scaling argument is developed that considers perturbations to a perfectly affine deformation field brought about by lowering the radius from $r \gg \xi$, where the affine assumption holds, down to $r = \xi$. However, comparing with their simulation data the authors could not confirm the scaling picture unambiguously and acknowledged the need for further numerical as well as improved theoretical work [28]. Thus, non-affine elasticity in fibrous networks appears to be intrinsically a non-perturbative strong-coupling phenomenon.

4.2 Granular limit

The alternative approach pursued in this thesis utilizes an analogy to granular media, which is based on the recognition that a small value of $r \ll \xi$ at the same time corresponds to a large stretching stiffness, $k_s/k_{\perp} \gg 1$, indicating the fact that the polymers are nearly inextensible. The limit $r \rightarrow 0$ may thus be viewed analogously to the limit of incompressible grains characterized by a diverging Young's modulus. It is reasonable to assume that the deformation field in the non-affine regime ($0 < r \ll \xi$) reflects the inextensibility of the segments which is strictly present only at vanishing cross-section radius $r = 0$. Further indications of the relevance of this ‘‘granular limit’’ to the mechanics in the non-affine regime is provided by observing the spatial distribution of fiber axial forces. Similar to the force-chains of granular systems [38, 56] the highest axial forces are heterogeneously distributed and localized to well defined paths. Interestingly, the probability distribution of forces shows a universal scaling form with an intermediate power-law regime. As compared to the already unusual exponential tail found in granular systems [47, 14] this implies the build-up of even higher forces.

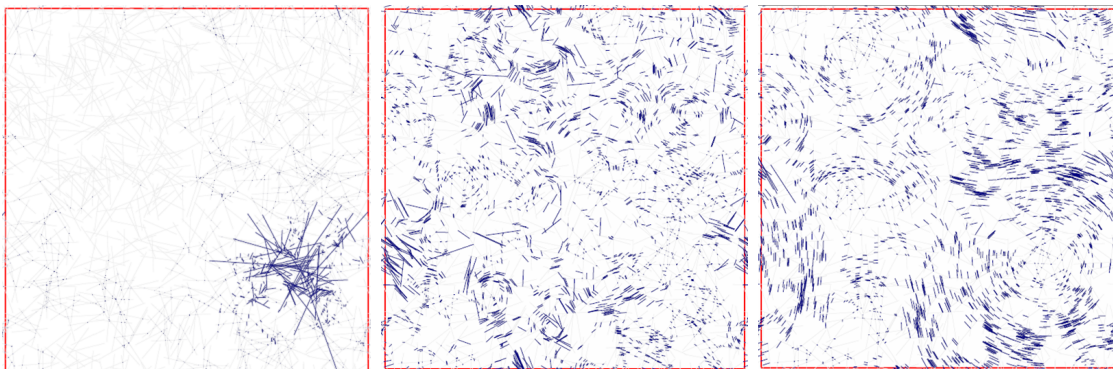


Figure 4.1: Three examples of vibrational eigenmodes constructed by a diagonalization of the set of local floppy modes (taken from [66], with permission). At high energies the modes retain a local character (left). At lower energies the modes start to delocalize, albeit in a random fashion (middle). At even lower energies spatial structures emerge in the form of characteristic vortices (right).

To determine the displacement field in the granular limit, one has to solve the purely geometric problem of finding those cross-link displacements that do not violate the imposed condition of segment inextensibility. This is a central problem of rigidity theory which goes back to the work of Maxwell [52, 8]. He argued that by increasing the number of connected neighbors z , a network of rigid, inextensible bars undergoes a transition from a floppy to a rigid state. For $z > z_c = 2d$ no cross-link displacements can be found without stretching the bars. Important examples of rigid networks are triangulated structures, which are routinely exploited in modern day steel construction, for example in building huge cantilever bridges like that over the Firth of Forth in Scotland or towers like Eiffel’s tower in Paris.

As cross-linking proteins can only link two filaments the coordination number relevant for biological stiff polymer networks is $z < 4$ and therefore below the rigidity transition both in two and in three dimensions. The geometric network is therefore floppy and it is possible to identify sets of cross-link displacements that keep the bars at constant length. These modes are called the “mechanisms” or the “floppy modes” of the structure. Their associated cross-link displacements $\{\bar{y}_i\}_{i=1..N_{xl}}$ provide a direct characterization of the deformation field in the non-affine bending dominated regime.

This concept of the rigidity transition and the associated floppy modes is of general applicability and has, for example, been utilized to study the unfolding of proteins [60], the glass transition in network glasses [10], as well as the jamming of soft repulsive spheres at zero temperature [54]. This latter system is characterized by an excess density of low frequency vibrational states (“boson peak”) [70], which is explained by spatially extended floppy modes present just below the jamming threshold [87, 88, 86]. By increasing the density across the transition additional contacts are generated. This stabilises the floppy modes, albeit at low frequencies, where they contribute to the boson peak. Quite analogously, the floppy modes of the polymer network are stabilized by the presence of the soft

bending mode, and thus contribute to the macroscopic elasticity in the bending dominated regime.

Unlike in the above mentioned systems, it is possible to explicitly construct the floppy modes in the model fiber network. It turns out, however, that this is only possible to linear order in the applied deformation¹. For finite deformations no floppy mode can be found and any internal rearrangement of the cross-links necessarily leads to stretching of fibers. In the linearized theory the floppy modes take the form of highly localized excitations which affect only single filaments and their immediate surroundings. They may be viewed as exotic examples of the well known elementary excitations in condensed matter systems (“floppions”) as it is not possible to break these excitations into smaller parts. This suggests to view the entire filament as the elementary building block (the unit cell) of the network, and not, as is frequently done in affine theories, the much smaller segments, spanning only the distance between two neighbouring cross-links along a filament. By orthonormalizing the set of floppy modes one obtains the vibrational normal modes of the network (Fig. 4.1), which can either be localized (at high energies) or delocalized (at lower energies) [66].

Having characterized the deformation field the next step is to calculate the elastic modulus. This is achieved by associating, on the level of a self-consistent effective medium theory, a bending energy to the floppy modes. In this approach one calculates the energy stored in the network upon imposing a floppy mode to a single fiber. The average elastic energy W is then given as self-consistent solution to the equation

$$W(k) = \left\langle \min_{y(s)} \left(W_b[y(s)] + \frac{1}{2} \sum_{i=1}^{N_{cl}} k (y(s_i) - \bar{y}_i)^2 \right) \right\rangle, \quad (4.3)$$

where the angular bracket relates to the ensemble average over the quenched random network structure. The first contribution on the right hand side relates to the bending energy in the fiber itself, given in terms of its transverse deflection $y(s)$. The second term arises from the interaction with the surrounding fibers at the locations s_i of the cross-links and acts like an elastic matrix of stiffness k . For large matrix stiffness the fiber is forced to closely follow the floppy-mode \bar{y}_i , such that its deflections $y(s_i) \approx \bar{y}_i$. If on the other hand the stiffness k is small, the fiber may freely deviate from the imposed floppy mode, and minimize its own bending energy. This, in turn, must lead to deformations in the surrounding matrix, which can only occur in the form of additional floppy modes. The energy scales of the floppy mode, W , and the stiffness of the medium, k , must therefore be identical and $W(k) \sim k$.

In contrast to the “bare floppion” defined on the geometric network, the excitation defined by Eq. (4.3) is “dressed” and incorporates fiber-matrix interactions on a Cayley-tree level. In this terminology, the branches of the tree are represented by the subsequent generations of neighbouring fibers. Since the details of the network structure only enter via the ensemble average (angular brackets), Eq. (4.3) is sufficiently general to be applicable to a variety of network architectures. For the specific model system studied here, it resulted in

¹In the language of structural engineering, these modes are “first order infinitesimal” mechanisms [9].

excellent confirmation of the scaling properties of the linear elastic modulus, by predicting $\mu \approx 6.75$.

The competition between the two energy contributions in connection with the random architecture of the network leads to the establishment of a length-scale l_{\min} that on a microscopic scale mediates the coupling of the fiber to the surrounding matrix. Since the stiffness $k_{\perp} \sim l^{-3}$ of the individual segment is strongly increasing with decreasing its length l , we found that segments with $l < l_{\min}$ rather deform the surrounding medium than being deformed itself, while longer segments $l > l_{\min}$ are not stiff enough to deform the medium. The scale l_{\min} therefore plays the role of a minimal length below which segments are stiff enough to remain undeformed. In terms of the deflections $y(s_i)$ of the fiber at the cross-links, this implies that long (and soft) segments are characterized by $y(s_i) \approx \bar{y}_i$, a situation where only small amounts of energy are stored in the surrounding medium. In contrast, short (and stiff) segments have crosslinks with vanishing transverse deflection $y(s_i) \approx 0$ and therefore only small amounts of bending energy. Equating the energy gain from reducing the bending energy in the short segments, with the energy loss from deforming the neighboring fibers, the length-scale l_{\min} can be determined as $l_{\min} \simeq 1/\rho^2 l_f$. The modulus in this scaling analysis is calculated as $G \sim \rho l_f \kappa / l_{\min}^3$ which leads to the exponent $\mu = 7$, consistent both with the network simulations and the solution to Eq. (4.3).

It has been mentioned above that the floppy modes can only be constructed for the linear elastic problem, while large deformations necessarily lead to stretching deformations that are much more expensive in energy. This is consistent with recent non-linear simulations [55], where an increasing modulus is explained on the basis of a cross-over to a stretching dominated regime. The floppy mode picture supports this view and provides it with a microscopic foundation.

Combining the calculation of the linear modulus with the onset of the non-linearity, as determined from a breakdown of the floppy-mode picture, it was possible to rationalize the rheological data obtained for a network of actin bundles cross-linked with fascin. By including the effects of the mode-dependent bending stiffness of Eq. (3.3), appropriate for filament bundles, the scaling properties of the modulus with actin and fascin concentration could be explained, as well as the critical strain, where nonlinear effects first start in (details of the scaling relations and their derivation can be found in Appendix A).

It is widely believed that bending can not provide a mechanism for strain-stiffening. Accordingly, experimental results both for the linear as well as the non-linear rheology are usually attributed to stretching deformations and the non-linear force-extension relation of a single polymer segment [21, 69]. In contrast, the picture we want to convey is that of a linear regime which is described by non-affine bending as given by the floppy modes of the network. The onset of strain stiffening is given by the limit of applicability of this concept, mediated by the presence of the fiber length l_f . The nonlinear elasticity is therefore due to geometric properties of the network rather than mechanical properties of the individual polymers. This suggests that the nonlinear rheology of stiff polymer networks reflects the subtle interplay of mechanical as well as geometrical effects and may not be as universal as commonly thought.

Chapter 5

Thermal response: non-affinity length-scale

While the previous section was dedicated to the athermal elasticity characterized by the spring constants k_{\perp} and k_s , here we want to incorporate thermal effects by considering in addition the entropic spring constant k_{\parallel} . As indicated above, the strong dependence of $k_{\parallel} \sim l^{-4}$ on the length l of the element, is expected to lead to qualitatively new elasticity in polydisperse networks.

We have quantified these effects by systematically studying cellular structures with varying degree of randomness as well as different types of unit cells. As a result we find that the affine prediction of Eq. (2.8) may safely be used only for highly ordered structures. Depending on the type of the unit cell, already small amounts of randomness strongly influence the order of magnitude of the modulus or its scaling properties. On the other hand, the elastic regime dominated by $k_s \sim l^{-1}$ only shows marginal susceptibility to randomness, as expected from its weak length-dependence. For the interpretation of experimental data based on the measurement of the shear modulus in thermally fluctuating polymer networks a precise knowledge of the network architecture therefore seems to be indispensable. For this it will be most important to develop new techniques that allow the characterization of the microstructure and monitor its changes upon deformation [48].

Further simulations in the random fibrous system allow to characterize in detail the interplay between network architecture and elastic properties of its constituents. In particular, we use the fiber length l_f to drive the system from the simple cellular structure with filaments as short as the mesh-size $l_f \approx a$, to a fully scale-invariant fibrous structure characterized by infinitely long filaments $l_f \rightarrow \infty$. Especially the latter limit allows for intricate scaling behavior that impressively demonstrates the qualitative difference between thermally fluctuating and purely mechanical, athermal elastic networks. While in principle the non-affine bending regime discussed in the preceding section can occur here as well, its strong dependence on fiber length leads to its suppression in the limit of infinitely long filaments. The remaining elastic regimes are then independent of l_f .

We have defined several types of networks that differ in the properties of the cross-links. In networks, where the angles at the cross-links are not allowed to change during

deformation, we found that the two deformation modes, (entropic) stretching and bending, act as if they were springs connected in parallel. The modulus is approximated by

$$G = a\bar{k}_\perp + b\bar{k}_\parallel, \quad (5.1)$$

where the prefactors a, b weakly depend on the scaling variable $y \sim \bar{k}_\parallel/\bar{k}_\perp \sim l_p/a$. Unlike in the “serial connection” described by Eq. (2.8), the network elasticity in the “parallel connection” found here is always dominated by the stiffer mode. This is qualitatively similar to a triangulated network, where the specific geometry of the unit cell always imposes stretching deformations on the system, no matter how soft the bending mode actually is. The fibrous architecture with increasingly long filaments apparently also suppresses the transition into a regime where the softer mode is dominant. By controlling the architecture of the network, the scale of the polymer length l_f therefore seems to implicitly influence the elastic properties of the system even in parameter regions where it does not enter the macroscopic elastic moduli explicitly.

Allowing the filaments to freely rotate at the cross-links, we also find an asymptotic scaling regime where stretching and bending modes contribute equally to the elastic energy. The modulus takes the form of a generalized geometric average

$$G \propto \bar{k}_\perp^{1-z} \bar{k}_\parallel^z, \quad (5.2)$$

with fractional exponent $z = 0.46$.

To explain this highly unusual finding it is crucial to consider the full distribution of spring constants $P(k_\parallel)$ instead of just the pre-averaged \bar{k}_\parallel^{-1} . Interestingly, due to the presence in the model network of arbitrarily short polymer segments, the distribution shows polynomial tails, $P(k_\parallel) \sim k_\parallel^{-5/4}$, characterized by a diverging mean value. Due to their exceedingly large stretching stiffness the small segments in the tails will resist deformation and thus stay in their unstrained configuration. This is analogous to the athermal case, where segments shorter than the threshold length l_{\min} remain undeformed, when imbedding the fiber in an elastic medium that imposes non-affine floppy mode deformations. A similar length-scale, l_c , is found here, when the polymer is imbedded in a medium that tries to enforce an affine deformation field. While segments longer than l_c follow the affine deformations, segments shorter than l_c stay relaxed and rather deform the surrounding medium. Equating the energy gain from reducing the stretching in the short segments, with the energy loss from deforming the neighboring polymers, results in the expression $l_c \sim \bar{l}(l_p/\bar{l})^{1/2}$ and for the modulus $G \sim \bar{k}_\parallel^{-1/2} \bar{k}_\perp^{1/2}$, which corresponds to a value of $z = 1/2$ in good agreement with the result of the simulations.

¹Recall, that the overbar encodes an averaging on the scale of the mesh-size.

Chapter 6

Conclusion

6.1 Universal aspects

In the course of this study two length-scales, l_{\min} and l_c , have been identified that, in their respective parameter regimes, govern the macroscopic elasticity in the random fibrous network structure. Their physical significance is to provide lower limits on the lengths of those segments that contribute to the elastic energy. The quite unusual scaling properties of the elastic moduli could be explained entirely in terms of these length-scales. One must be cautious, however, in using these scales and the associated exponents in other systems, as they are tightly connected to the Poissonian nature of the random fibrous architecture. The distribution of segment lengths is exponential and has a finite weight on zero length, which is quite unrealistic for in-vitro stiff polymer networks. While these networks are known to have a broad distribution of mesh-sizes one would nevertheless expect this distribution to be peaked at (or near) its average value.

So what has been learned if the testable predictions (the scaling properties of the moduli) are specific to a quite unrealistic, two-dimensional model system?

In fact, the analysis presented in this thesis goes way beyond reproducing the exponents obtained in the simulations. It does so by identifying the general physical principles that underlie the possible microscopic response of any stiff polymer network, be it completely random as the model system or highly regular, in two- or in three dimensions.

These principles are:

1. fiber length: The presence of a mesoscopic length-scale is probably the most important characteristic that distinguishes the morphology of networks formed with stiff polymers from networks with flexible polymers. As we have seen this length-scale contributes in an essential way to the establishment of the macroscopic elasticity. The unit cell of stiff polymer networks is not given by the scale of the mesh-size but by the scale of the entire polymer fiber.
2. inextensibility: In cases, where there is a scale separation between bending and stretching mode, a description in terms of the “granular limit” is possible. The

deformation field is non-affine on the scale of the fiber-length and can be characterized by localized elastic excitations (“floppions”). With this concept at hand the scaling properties of the elastic moduli can be calculated for any fibrous network architecture. In fact, we have shown that the theory can provide an explanation for experimentally observed rheological properties of an actin/fascin system.

3. polydispersity: In cases where the entropic stretching stiffness contributes to the elastic response, a consideration of the structural randomness is quite essential. This derives from the strong length-dependence of the entropic stiffness k_{\parallel} as compared to that of the backbone stretching stiffness k_s .

6.2 Outlook

While the experiments on the actin/fascin system have demonstrated the relevance of the ideas developed in this thesis, further validation is necessary. From the theoretical side, it would be interesting to clarify whether the floppy-mode concept, Eq. (4.3) can describe network elasticity in a *quantitative* fashion. One may also hope that the theory can be extended to finite frequencies to describe the full *visco-elastic* response of the network. A limitation of the theory originates in the neglect of cross-link *fluctuations*. This approximation has to be critically tested, for example with the help of Monte-Carlo simulations.

Even though the inextensibility of the individual polymers lies at the heart of the floppy-mode concept, one may think of extending the theory to include the finite but small entropic extensibility of the polymers. This may proceed in analogy to the weakly bending approximations, which make use of the small parameter $\epsilon = l/l_p \sim k_{\perp}/k_{\parallel}$.

Parallel to the development of the theory the finite-element simulations should be extended to include three-dimensional network structures. Realistic computer generated structures may, for example, become available as results of network polymerization schemes. Experimental structures could be obtained from suitable imaging techniques like confocal or electron microscopy. This could open the way to a combined theoretical, numerical, and experimental approach to the elasticity of stiff polymer networks. The results of rheological experiments could be compared with those of the computer simulations on the same network structure as well as the theoretical description developed in this thesis. For these studies it might become necessary to include nonlinearities in the constitutive response of the polymers. The highly non-linear stretching response of stiff polymers is expected to compete with the geometrical non-linearities that are a consequence of the fibrous network structure.

Chapter 7

Publications

7.1 Bundles

The two publications “Statistical Mechanics of Semiflexible Bundles of Wormlike Polymer Chains” and “Mechanics of cytoskeletal bundles” are concerned with mechanical and statistical properties of bundles of semiflexible polymers.

The “wormlike bundle” (WLB) model is developed that generalizes the well-known wormlike chain (WLC) model, which is applicable to single filaments. In this description the internal degrees of freedom of the bundle, in particular the relative sliding motion of neighboring filament pairs, give rise to a wavenumber dependent bending stiffness $\kappa_B(q)$. This leads to fundamentally new scaling properties of WLBs as compared to conventional WLCs, which are characterized by a constant bending stiffness κ_f .

Statistical Mechanics of Semiflexible Bundles of Wormlike Polymer Chains

Claus Heussinger, Mark Bathe, and Erwin Frey

Arnold Sommerfeld Center for Theoretical Physics and CeNS, Department of Physics, Ludwig-Maximilians-Universität München, Theresienstrasse 37, D-80333 München, Germany

(Received 13 February 2007; published 25 July 2007)

We demonstrate that a semiflexible bundle of wormlike chains exhibits a state-dependent bending stiffness that alters fundamentally its scaling behavior with respect to the standard wormlike chain. We explore the equilibrium conformational and mechanical behavior of wormlike bundles in isolation, in cross-linked networks, and in solution.

DOI: [10.1103/PhysRevLett.99.048101](https://doi.org/10.1103/PhysRevLett.99.048101)

PACS numbers: 87.16.Ka, 82.35.Lr, 83.10.-y, 87.15.La

In recent decades, the wormlike chain (WLC) has emerged as the standard model for the description of semiflexible polymers [1]. The defining property of a WLC is a mechanical bending stiffness κ_f that is an intrinsic material constant of the polymer. Within this framework, numerous correlation and response functions have been calculated, providing a comprehensive picture of the equilibrium and dynamical properties of WLCs [2–4]. A number of experimental studies have demonstrated the applicability of the WLC model to DNA [5] and *F*-actin [6], among other biological and synthetic polymers. Significant progress has also been made towards the description of the collective properties of WLCs, for example, in the form of entangled solutions. One of the hallmarks of this development is the scaling of the plateau shear modulus with concentration $G \sim c^{7/5}$ [7–9], which is well established experimentally [10,11].

Another important emerging class of semiflexible polymers consists of *bundles* of WLCs [12,13]. Semiflexible polymer bundles consisting of *F*-actin or microtubules are ubiquitous in biology [14] and have unique mechanical properties that may well be exploited in the design of nanomaterials [13]. As shown by Bathe *et al.* [15,16], wormlike bundles (WLBs) have a state-dependent bending stiffness κ_B that derives from a generic interplay between the high stiffness of individual filaments and their rather soft relative sliding motion. In this Letter, we demonstrate that this state dependence gives rise to fundamentally new behavior that cannot be reproduced trivially using existing relations for WLCs. We explore the consequences of a state-dependent bending stiffness on the statistical mechanics of isolated WLBs, as well as on the scaling behavior of their entangled solutions and cross-linked networks.

We consider the bending of ordered bundles with an isotropic cross section. A bundle consists of N filaments of length L and bending stiffness κ_f . Filaments are irreversibly cross-linked to their nearest neighbors by discrete cross-links with mean axial spacing δ . Cross-links are modeled to be compliant in shear along the bundle axis with finite shear stiffness k_\times and to be inextensible transverse to the bundle axis, thus fixing the interfilament distance b [17]. Bundle deformations are characterized

by the transverse deflection $\mathbf{r}_\perp(s)$ of the bundle neutral surface at axial position s along the backbone and by the stretching deformation $u_i(s)$ of filament i . The torsional stiffness of the bundle is assumed to be of the same order as the bending stiffness. Thus, as long as transverse deflections remain small (“weakly bending”), the two components of \mathbf{r}_\perp are decoupled, and the effects of twist are of higher order [18]. The bundle response may then be analyzed in planar deformation, where the bending stiffness results from the superposition of $2M = \sqrt{N}$ bundle layers.

The WLB Hamiltonian consists of three contributions $H_{\text{WLB}} = H_{\text{bend}} + H_{\text{stretch}} + H_{\text{shear}}$. The first term corresponds to the standard WLC Hamiltonian

$$H_{\text{bend}} = \frac{N\kappa_f}{2} \int_0^L ds \left(\frac{\partial^2 \mathbf{r}_\perp}{\partial s^2} \right)^2, \quad (1)$$

which is the same for each of the N filaments. The second term accounts for filament stretching

$$H_{\text{stretch}} = Mk_s \delta \int_0^L ds \sum_{i=-M}^{M-1} \left(\frac{\partial u_i}{\partial s} \right)^2, \quad (2)$$

where k_s is the single filament stretching stiffness on the scale of the cross-link spacing δ . No particular form for bending and stretching stiffnesses is assumed, but one may think of the filaments as homogeneous elastic beams with Young’s modulus E , for which $\kappa_f \sim Eb^4$ and $k_s \sim Eb^2/\delta$. Alternatively, k_s may represent the entropic elasticity of a WLC, for which $k_s \sim \kappa_f^2/T\delta^4$.

The third energy contribution H_{shear} results from the cross-link-induced coupling of neighboring filaments. To minimize the cross-link energy, any relative filament slip induced by cross-sectional rotations $\theta = \partial_s \mathbf{r}_\perp \equiv r'_\perp$ must be compensated by filament stretching (Fig. 1). This cross-link shear energy, which simply suppresses relative sliding motion of neighboring filaments, is given by

$$H_{\text{shear}} = \frac{Mk_\times}{\delta} \int_0^L ds \sum_{i=-M+1}^{M-1} \left(\Delta u_i + b \frac{\partial r_\perp}{\partial s} \right)^2, \quad (3)$$

where $\Delta u_i = u_i - u_{i-1}$. A related model for two filaments was introduced by Everaers, Bundschuh, and Kremer in

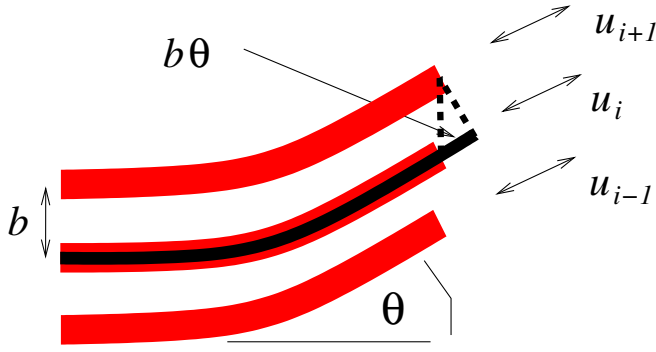


FIG. 1 (color online). Illustration of the geometry of a single bundle layer (the full bundle consists of $2M$ layers that are stacked in parallel). The bundle is deflected through the angle $\theta = r'_{\perp}$. If filament i stretches the amount $u_i = u_{i+1} + b\theta$, the cross-link (dashed line) remains undeformed with zero shear energy.

Ref. [19], where special emphasis was placed on the limit of inextensible filaments $k_s \rightarrow \infty$. In that model, the anisotropic bundle cross section leads to a coupling of in-plane and out-of-plane bending modes [20] that is absent in the present model because it has a symmetric cross section.

Functional differentiation of the Hamiltonian results in the (overdamped) equations of motion

$$N\kappa_f r_{\perp}'''' - \frac{2Mk_{\times}b}{\delta} \sum_i (\Delta u_i + br'_{\perp}) = F(r_{\perp}, s), \quad (4)$$

$$k_s \delta u_i'' + \frac{k_{\times}}{\delta} (\Delta u_{i+1} - \Delta u_i) = 0, \quad (5)$$

where F is a transverse force that may represent fluid drag, random thermal noise, or other external loading. To proceed, Eq. (5) is solved together with appropriate boundary conditions, so as to eliminate the u_i in Eq. (4). The calculations are most easily performed in Fourier space, where we write for the expansions $r_{\perp}(s) = \sum_n r_n \sin(n\pi s/L)$ and $u_i(s) = \sum_n u_{in} \cos(n\pi s/L)$, applicable to pinned boundary conditions. The resulting equation of motion for r_n then takes the simple form $\kappa_n q_n^4 r_n = F_n$, with a mode-number-dependent effective bending stiffness κ_n . The general result for κ_n is obtained using the standard ansatz $u_i \sim w^i$, which reduces Eq. (5) to an equation that is quadratic in w .

In the following, we present an approximate solution to Eqs. (4) and (5) that is based on the assumption that filament stretching increases *linearly* through the bundle cross section $u_i = \Delta u(i + 1/2)$ [21]. Although comparison with the exact solution demonstrates that u_i , in general, varies nonlinearly with i [22], it turns out that the effective bending stiffness κ_n is insensitive to this nonlinearity. At the same time, the linearization simplifies the formulas substantially, so that the effective bending stiffness is given in closed form by

$$\kappa_n = N\kappa_f \left[1 + \left(\frac{12\hat{\kappa}_f}{N-1} + (q_n\lambda)^2 \right)^{-1} \right], \quad (6)$$

with a dimensionless bending stiffness $\hat{\kappa}_f = \kappa_f/k_s \delta b^2$ and a length scale $\lambda = (L/\sqrt{\alpha}) \sqrt{M\hat{\kappa}_f/(M-1/2)}$ that depends on the shear stiffness k_{\times} via the dimensionless coupling parameter $\alpha = k_{\times}L^2/k_s\delta^2$.

For any given mode number $q_n \sim n/L$, three different elastic regimes emerge as asymptotic solutions for $N \gg 1$ and respective values of α [15,16]. For large shear stiffness ($\alpha \gg N$), the *fully coupled* bending scenario is obtained, where the bundle behaves like a homogeneous beam with $\kappa_n \sim N^2k_s$. For intermediate values of the shear stiffness ($1 \ll \alpha \ll N$), the bending stiffness in the *shear-dominated* regime is $\kappa_n \sim Nk_{\times}q_n^{-2}$ and the full mode-number dependence of Eq. (6) has to be accounted for. Finally, *decoupled bending* of N laterally independent, but transversely constrained, filaments is found in the limit of small cross-link shear stiffness ($\alpha \ll 1$), where the bending stiffness is simply $\kappa_n = N\kappa_f$.

In the particular limit of $N \rightarrow \infty$ and fixed bundle diameter $D = b\sqrt{N} \ll L$, Eq. (6) reduces to the Timoshenko model for beam bending [23], which was recently used to interpret bending stiffness measurements on microtubules [24,25] and carbon nanotube bundles [13]. In this limit,

$$\kappa_n = \frac{N^2\kappa_f}{1 + (q_n D)^2 E/12G}, \quad (7)$$

where we have used the expressions of k_s and κ_f for homogeneous beams and defined $G = k_{\times}/\delta$. While this limit serves as a consistency check for our mathematical analysis, real bundles consist of a finite, and often small, number of constituent filaments, for which Eq. (7) cannot be applied to describe the full range of bending behavior captured by Eq. (6). Indeed, in Eq. (7), no decoupled bending regime exists, and the bending stiffness vanishes as the cross-link shear stiffness approaches zero [26]. The condition $\alpha \sim N$ delineating the remaining two regimes can be rewritten as $E/G \sim (L/D)^2 \gg 1$, which reemphasizes the small value of cross-link shear stiffness in the intermediate regime.

For fixed values of (N, α) , the bundle bending stiffness Eq. (6) crosses over from fully coupled to decoupled bending via the intermediate regime as the mode number q_n is increased. Thus, different modes may belong to different elastic regimes, rendering the fluctuation properties of the bundle nontrivial and qualitatively different from single semiflexible polymers. This crossover is mediated by the length scale λ , which acts as a cutoff on the fluctuation spectrum: Whereas wavelengths $q_n^{-1} \ll \lambda$ belonging to the decoupled regime are characterized by a constant bending stiffness, modes with $q_n^{-1} \gg \lambda$ acquire a higher stiffness $\kappa_n \sim q_n^{-2}$ and are thereby suppressed. Finally, for even longer wavelengths $q_n^{-1} \gg \lambda\sqrt{N}$, the bending stiffness reattains a constant, limiting value. As an example (taken from Ref. [12]), we found $\lambda \approx 7 \mu\text{m}$ for actin/fascin bundles with $N \approx 30$, $L \approx 50 \mu\text{m}$.

In situations where modes pertaining to the intermediate regime are irrelevant, the q dependence of κ_n drops out, and one recovers the single WLC result, albeit with a renormalized persistence length $l_p \rightarrow Nl_p$ in the decoupled and $l_p \rightarrow N^2l_p$ in the fully coupled regimes, respectively. In other cases, calculation of the tangent-tangent correlation function demonstrates that the persistence length cannot be defined unambiguously. As indicated in Ref. [19], the correlation function does not decay exponentially but rather exhibits a complex structure at intermediate distances [22]. In the following, we will therefore explore the consequences on the statistical mechanics of the WLB, in particular, as regards the intermediate regime.

First, consider the force-extension relation as calculated from the end-to-end distance $R(F) = L - \sum_n k_B T / (\kappa_n q_n^2 + F)$, where F is the force applied to the bundle ends [27]. For small stretching forces, one may readily calculate the linear response coefficient $k_{\text{entr}} = F/[R(F) - R(0)]$ using a Taylor series expansion. The result in the intermediate regime is

$$k_{\text{entr}} \propto \frac{(N\kappa_f)^2}{L\lambda^3 k_B T} \quad (\lambda\sqrt{N} \gg L \gg \lambda), \quad (8)$$

which is inversely proportional to bundle length, like a mechanical beam. Importantly, the strong dependence of $k_{\text{entr}}(L) \sim L^{-4}$ applicable to single filaments (and the other two regimes) is lost. This has dramatic consequences on the plateau value of the shear modulus G in cross-linked bundle networks, which in affine theories [28] is assumed to be given in terms of k_{entr} by $G \sim k_{\text{entr}}(\xi)/\xi$, where the mesh size ξ depends on concentration c as $\xi \sim c^{-1/2}$. Accordingly, in the intermediate regime one finds $G \sim c$, which is a much weaker concentration dependence than $G \sim c^{5/2}$ [29] applicable to single filaments. It is worthwhile noting that the force-extension relation is strongly nonlinear (see Fig. 2), rendering the linear response valid only for very small relative extensions. In this particular example, the linear response formula deviates from the exact solution by 50% at only $\approx 3\%$ and $\approx 0.7\%$ strain in the decoupled and the fully coupled limits, respectively.

Bundle behavior under compressive forces further highlights the unusual properties of WLBs. Because the bending stiffness in the intermediate regime scales with the length of the bundle as $\kappa_B \sim L^2$, the Euler buckling force $F_c \sim \kappa_B/L^2 \sim N\kappa_f/\lambda^2$ is independent of bundle length. This unique property may well be exploited in polymerizing biological bundles such as filopodia, which may increase their contour length against compressive loads without loss of mechanical stability.

Complementary to the elasticity of cross-linked networks of WLBs, we turn next to the elasticity of their entangled solutions. The generally accepted theory for the concentration dependence of the plateau modulus of entangled WLCs is based on the free energy change ΔF of confining a polymer to a tube of diameter d [7,8]. The

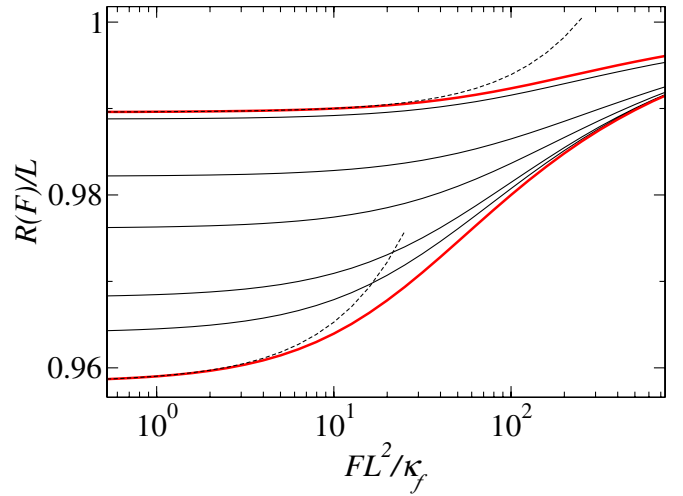


FIG. 2 (color online). End-to-end distance $R(F)/L$ as a function of stretching force FL^2/κ_f for a bundle of $N = 4$ filaments and $L = l_p$. The black curves correspond to $\lambda/L = 0.01, 0.1, \dots, 0.7$. The thick (red) curves relate to (bottom) decoupled and (top) fully coupled bending, respectively. The dashed lines correspond to the respective linear response regimes.

associated change in free energy is written as $\Delta F \sim k_B T L / l_d$, which defines the deflection length l_d to be the scale at which the polymer starts to interact with its enclosing tube. The deflection length itself is connected to the tube diameter d and the filament concentration c via the standard excluded volume argument [9] $l_d^2 d = l_d / c L$, which balances the excluded volume of the tube with the available volume per filament. All that remains is the calculation of the tube diameter d of a single polymer confined by the potential

$$V = \frac{N\kappa_f}{2l_c^4} \int_0^L ds r_{\perp}^2(s), \quad (9)$$

where the confinement length l_c is defined as a measure of the strength of the potential. While $l_c \equiv l_d$ in the standard WLC, we will see shortly that this does not hold for WLBs in the intermediate regime. First, consider the transverse fluctuations of an unconfined bundle, in particular, the average value $d_0^2 \equiv \frac{1}{L} \int_s \langle r_{\perp}^2(s) \rangle$. This is most easily calculated as

$$d_0^2 \sim L\lambda^2 / Nl_p \quad (\lambda\sqrt{N} \gg L \gg \lambda), \quad (10)$$

which has to be compared to the WLC result for which $d_0^2 \sim L^3 / l_p$. In the presence of the confining potential, the same calculation yields

$$d^2 \sim l_c^2 \lambda / Nl_p \quad (\lambda\sqrt{N} \gg l_c \gg \lambda). \quad (11)$$

For strong confinement $l_c \ll \lambda$, the potential suppresses all modes of the intermediate regime, and one recovers the expression valid for single filaments: $d^2 \sim l_c^3 / l_p$. The general result for the tube diameter is depicted in Fig. 3. As the

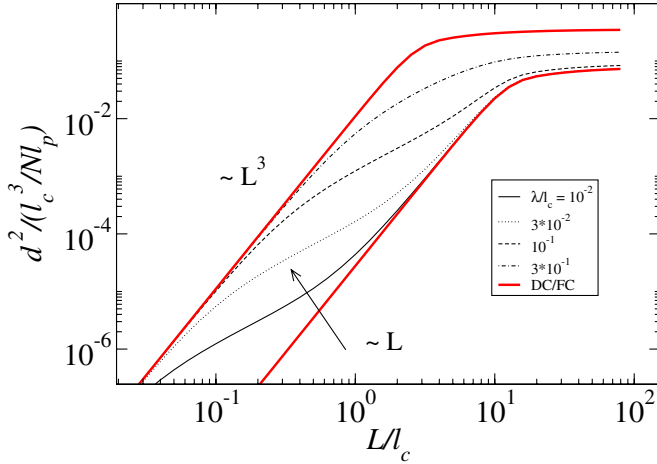


FIG. 3 (color online). Tube diameter $d^2/(l_c^3/Nl_p)$ as a function of contour length L/l_c for various λ/l_c and $M = 20$. Thick (red) curves correspond to (top) decoupled and (bottom) fully coupled bending, respectively. For short filaments, the intermediate regime is visible through the linear slope $d^2 \sim L$ [see Eq. (10)]. For long filaments, the fluctuations saturate. By increasing λ , the tube is becoming wider [Eq. (11)].

contour length L of the bundle is increased, it begins to “feel” the presence of its enclosing tube at the deflection length $L = l_d$. By comparing Eq. (10) with Eq. (11), one finds $l_d \sim l_c^2/\lambda$, which is valid in the intermediate regime. At the same time, $l_d \equiv l_c$ in the decoupled and fully coupled regimes, where the deflection and confinement lengths are identical.

One may use these results to rewrite the deflection length as a function of concentration c . In the intermediate regime, the result is $l_d^3 \sim Nl_p/(\lambda cL)^2$, which replaces the usual result $l_d^5 \sim Nl_p/(cL)^2$ valid in the decoupled regime (strong confinement). The free energy of confinement and the elastic plateau modulus $G \sim (cL)\Delta F/L$ now depend on λ and thus on the properties and density of the cross-links. The modulus displays a crossover that is *mediated by concentration*:

$$G \sim k_B T \begin{cases} (cL)^{5/3}(Nl_p)^{-1/3}\lambda^{2/3}, & c \ll c^*, \\ (cL)^{7/5}(Nl_p)^{-1/5}, & c \gg c^*, \end{cases} \quad (12)$$

where we defined the crossover concentration as $(cL)^* \sim \sqrt{Nl_p}\lambda^{-5/2}$. Below the even smaller concentration $c^{**} \sim c^*N^{-3/4}$, the fully coupled regime is entered, and the modulus again scales as $G \sim c^{7/5}$.

Having addressed equilibrium properties of WLBs, further consequences of the state-dependent bending stiffness on dynamic response functions remain to be explored, along with the effects of nonpermanent cross-links. Additional experiments [12,13,21,30] are required to test the applicability of the derived results to biological and synthetic bundles.

Funding from the Alexander von Humboldt Foundation (to M.B.), from the German Science Foundation (SFB

486), and from the German Excellence Initiative via the program “Nanosystems Initiative Munich (NIM)” is gratefully acknowledged.

- [1] N. Saitô, K. Takahashi, and Y. Yunoki, J. Phys. Soc. Jpn. **22**, 219 (1967).
- [2] R. Granek, J. Phys. II **7**, 1761 (1997).
- [3] J.F. Marko and E.D. Siggia, Macromolecules **28**, 8759 (1995).
- [4] J. Wilhelm and E. Frey, Phys. Rev. Lett. **77**, 2581 (1996).
- [5] C. Bustamante, J.F. Marko, E.D. Siggia, and S. Smith, Science **265**, 1599 (1994).
- [6] L. Le Goff, O. Hallatschek, E. Frey, and F. Amblard, Phys. Rev. Lett. **89**, 258101 (2002).
- [7] H. Isambert and A.C. Maggs, Macromolecules **29**, 1036 (1996).
- [8] T. Odjik, Macromolecules **16**, 1340 (1983).
- [9] A.N. Semenov, J. Chem. Soc., Faraday Trans. 2 **82**, 317 (1986).
- [10] B. Hinner *et al.*, Phys. Rev. Lett. **81**, 2614 (1998).
- [11] J. Xu, A. Palmer, and D. Wirtz, Macromolecules **31**, 6486 (1998).
- [12] M.M.A.E. Claessens, M. Bathe, E. Frey, and A.R. Bausch, Nat. Mater. **5**, 748 (2006).
- [13] A. Kis *et al.*, Nat. Mater. **3**, 153 (2004).
- [14] H. Lodish *et al.*, *Molecular Cell Biology* (Palgrave Macmillan, London, 2003), 5th ed.
- [15] M. Bathe, C. Heussinger, M. Claessens, A. Bausch, and E. Frey, arXiv:q-bio.BM/0607040.
- [16] M. Bathe, C. Heussinger, M. Claessens, A. Bausch, and E. Frey (to be published).
- [17] Typical protein elongational stiffnesses are of the order 1 N/m, while they are much softer in shear [12].
- [18] L.D. Landau and E.M. Lifshitz, *Theory of Elasticity* (Butterworth-Heinemann, Oxford, 1995), Vol. 7, 3rd ed.
- [19] R. Everaers, R. Bundschuh, and K. Kremer, Europhys. Lett. **29**, 263 (1995).
- [20] B. Mergell, M.R. Ejtehadi, and R. Everaers, Phys. Rev. E **66**, 011903 (2002).
- [21] J.A. Tolomeo and M.C. Holley, Biophys. J. **73**, 2241 (1997).
- [22] C. Heussinger *et al.* (to be published).
- [23] J.M. Gere and S.P. Timoshenko, *Mechanics of Materials* (Nelson Thornes Ltd., Cheltenham, 2002), 5th ed.
- [24] F. Pampaloni *et al.*, Proc. Natl. Acad. Sci. U.S.A. **103**, 10 248 (2006).
- [25] A. Kis *et al.*, Phys. Rev. Lett. **89**, 248101 (2002).
- [26] Reanalyzing the data of [24], we expect microtubules shorter than $L \approx 3.5 \mu\text{m}$ to be in the decoupled regime with a constant persistence length $l_p \approx 0.18 \text{ mm}$.
- [27] Note that a second contribution from the extensibility of the bundle backbone is neglected here for simplicity.
- [28] M. Rubinstein and R.H. Colby, *Polymer Physics* (Oxford University Press, New York, 2003).
- [29] F.C. MacKintosh, J. Käs, and P.A. Janmey, Phys. Rev. Lett. **75**, 4425 (1995).
- [30] O. Lieleg *et al.*, arXiv:cond-mat/0611752.

"This un-edited manuscript has been accepted for publication in Biophysical Journal and is freely available on BioFast at <http://www.biophysj.org>. The final copyedited version of the paper may be found at <http://www.biophysj.org>."

Cytoskeletal bundle mechanics

Mark Bathe[†], Claus Heussinger[†], Mireille M.A.E. Claessens[‡],
Andreas R. Bausch[‡], and Erwin Frey[†]

[†]Arnold Sommerfeld Zentrum für Theoretische Physik and Center for NanoScience
Ludwig–Maximilians–Universität München, Theresienstr. 37, 80333 Munich, Germany
and

[‡]Department of Biophysics E22
Technische Universität München, James Franck Str. 1, 85747 Garching, Germany

Abstract

The mechanical properties of cytoskeletal actin bundles play an essential role in numerous physiological processes including hearing, fertilization, cell migration and growth. Cells employ a multitude of actin-binding proteins to regulate actively bundle dimensions and crosslinking properties to suit biological function. The mechanical properties of actin bundles vary by orders of magnitude depending on diameter and length, crosslinking protein type and concentration, and constituent filament properties. Despite their importance to cell function, the molecular design principles responsible for this mechanical behavior remain unknown. Here, we examine the mechanics of cytoskeletal bundles using a molecular-based model that accounts for the discrete nature of constituent actin filaments and their distinct crosslinking proteins. A generic competition between filament stretching and crosslink shearing determines three markedly different regimes of mechanical response that are delineated by the relative values of two simple design parameters, revealing the universal nature of bundle bending mechanics. In each regime, bundle bending stiffness displays distinct scaling behavior with respect to bundle dimensions and molecular composition, as observed in reconstituted actin bundles *in vitro*. This mechanical behavior has direct implications on the physiological bending, buckling, and entropic stretching behavior of cytoskeletal processes, as well as reconstituted actin systems. Results are used to predict the bending regime of various *in vivo* cytoskeletal bundles that are not easily accessible to experiment and to generate hypotheses regarding implications of the isolated behavior on *in vivo* bundle function.

Introduction

Cytoskeletal actin bundles comprise numerous vital cellular processes including stereocilia, cytoskeletal stress fibers, the sperm acrosome, microvilli, and filopodia (Fig. 1) (1-3). The mechanical properties of these processes play essential roles in cell function—the bending stiffness of stereocilia mediates the senses of hearing and equilibrium (4, 5), the elasticity of cytoskeletal stress fibers enhance cellular resistance to mechanical deformation (6-13), the buckling resistance of the sperm acrosome facilitates egg cell penetration during fertilization (14, 15) and filopodial buckling resistance facilitates filopodial protrusion (16-20) and mediates actin turnover during neuronal growth and wound healing (21, 22). In addition to the preceding actin-based cytoskeletal bundles, cells also align microtubules to actively regulate nuclear positioning during mitosis (23, 24) and stabilize cell shape in the neuronal axon process (21) and outer pillar cells in the mammalian ear (25). Thus, a quantitative understanding of the molecular design principles responsible for the mechanical behavior of these ubiquitous cytoskeletal modules is important to gaining a mechanistic understanding of cell function (21, 26).

Bundle dimensions and internal constitution vary considerably depending on physiological function. Bundle length varies from several microns in microvilli and stress fibers to tens of microns in the sperm acrosome and hundreds of microns in neurosensory bristles (2, 3). Similarly, bundle diameters range from tens of filaments in filopodia to hundreds of filaments in stereocilia. Interestingly, actin bundle dimensions and the predominant crosslinking protein associated with various cytoskeletal processes are highly conserved across otherwise widely divergent species (27), suggesting specific and possibly mechanically-related functional constraints imposed during evolution (26, 28). Fascin is the predominant actin-binding protein (ABP) in filopodia and neurosensory bristles, fimbrin is prevalent in microvilli and stereocilia, scruin is present exclusively in the limulus sperm acrosome, and α -actinin predominates in cytoskeletal stress fibers. Despite the fundamental importance of actin bundle mechanical properties to cell function, the effects of bundle dimensions and crosslink composition on bundle mechanics remain poorly understood. Direct measurement of *in vivo* bundle mechanical response is limited by a number of complicating factors, rendering a systematic investigation of the effects of bundle dimensions and crosslinking protein composition on bundle mechanics impracticable.

As an alternative, the bending stiffness of reconstituted actin bundles was recently measured in a controlled *in vitro* assay (29). This enabled the systematic and broad exploration of the effects of bundle dimensions and actin-binding protein type and concentration on the bending stiffness of actin bundles. Bundle bending stiffness is the fundamental mechanical property of interest for inextensible bundles because once it is known, other physiologically relevant mechanical properties such as the critical buckling load or entropic stretching stiffness may be derived. In Ref. (29), the bending stiffness was found to depend in a complex manner on bundle composition, varying by orders of magnitude depending on crosslinking protein type and concentration, and bundle dimensions.

In this article, we employ a molecular-based model of crosslinked fiber bundles to explore the range of mechanical behavior of cytoskeletal actin bundles. The bending stiffness, κ_B , is found to depend on only two simple design parameters, the number of constituent filaments in the bundle, N , and a measure of the effectiveness of crosslinks in

mechanically coupling neighboring filaments, denoted α . The relative ratio of N to α is shown to delineate one of three distinct mechanical regimes that differ markedly in their dependence on bundle dimensions and internal constitution, highlighting the importance of the former on cytoskeletal bundle mechanics. The isolated mechanical behavior has direct implications on a number of disparate fields of biophysical research involving the physiological bending, buckling, and entropic stretching response of cytoskeletal processes involved in mechanosensation, fertilization, cell motility and neuronal growth, and may be used to predict the bending regime of *in vivo* cytoskeletal bundles that are not easily amenable to experimental measurement.

Model

We consider the linear bending response of fiber bundles of length L that consist of N cubically- or hexagonally-packed fibers, as is typical of highly crosslinked F-actin (15, 30, 31) (Fig. 2A). Each fiber is characterized geometrically at a coarse-grained molecular-scale by its cross-sectional dimension, d_f [m²], and contour length, L_f [m]. Fibers run the full length of the bundle ($L_f = L$) and are modeled mechanically as extensible Euler–Bernoulli beams (or extensible wormlike polymers) with stretching stiffness, $k_f := E_f A_f / \delta$ [N/m], and isotropic transverse bending stiffness, $\kappa_f := E_f I_f$ [Nm²]. E_f [N/m²] is the effective Young’s modulus of the fiber, A_f is its cross-sectional area, I_f [m⁴] is the moment of inertia of its cross-sectional area with respect to its neutral axis,^{§**} and δ [m] is the mean spacing between discrete crosslinks with effective shear stiffness k_x [N/m], and length, t [m]. Crosslinks are assumed to be irreversibly bound and inextensible, thereby constraining transverse fiber deflections to be equal but allowing interfiber relative slip. Bundle torsional stiffness is assumed to be of the same order as the bundle bending stiffness so that the effects of twist are of higher order and may safely be ignored in analyzing the linear bending response of stiff bundles for which the apparent bundle persistence length $l_p := \kappa_B / k_B T \gg L$ (32-35). In-plane bending of $2M := \sqrt{N}$ fiber layers crosslinked to their nearest neighbors in- and out-of-plane may then be considered, where the corresponding 3D bundle bending stiffness is related to its 2D counterpart by, $\kappa_B := 2M \kappa_{B(2D)}$ (Fig. 2A).^{††} Various types of biological fiber bundles have been modeled previously along similar lines (25, 31, 36, 37).

Bundle deformations are characterized by $r_\perp(x)$, the transverse deflection of the bundle neutral surface at axial position x along its backbone, and internal axial extensions of the constituent fibers. Let $u^{(k)}(x, \tilde{y})$ be the axial displacement field in the k^{th} fiber

[§] For molecular-scale objects, k_f and κ_f are fundamental independent observables that may be measured experimentally, whereas, E_f , A_f , and I_f are continuum mechanics equivalents that are ill-defined at the molecular-scale and thus only *effective* in their nature.

^{**} The neutral *surface* of a beam is the surface on which the bending-induced axial strain is zero. The intersection of that surface with any beam cross-section defines the neutral *axis* of the beam.

^{††} Effects of out-of-plane shear deformations present in hexagonally-packed bundles during planar bending, as well as finite-size geometric boundary effects, are ignored to leading order.

($k = -M, \dots, M - 1$) at a distance \tilde{y} from the *fiber* neutral axis. The associated local strain field $\varepsilon^{(k)} := u_{,x}^{(k)}$ then consists of a linear superposition of fiber bending and stretching contributions, $\varepsilon^{(k)} = -r_{\perp,xx} \tilde{y} + \bar{u}_{,x}^{(k)}$, where, $\bar{u}^{(k)}(x) = \frac{1}{A_f} \int_{A_f} u^{(k)}(x, \tilde{y}) dA_f$, a subscript comma is used to denote differentiation, and the standard small-displacement approximation $\rho \approx (r_{\perp,xx})^{-1}$ has been used for the neutral surface radius of curvature, ρ (Fig. 2B).

Crosslink shear displacements, ν , result from stretching and plane-cross-section-rotations of neighboring fibers, $\nu_j^{(k)} = \bar{u}^{(k)}(x_j) - \bar{u}^{(k-1)}(x_j) + (d_f + t)r_{\perp,x}(x_j)$, where j labels the crosslink at axial position $x_j = j\delta$ ($j = 1, 2, \dots, L/\delta$) and ($k = -M + 1, \dots, M - 1$). The shear displacement may be written equivalently in terms of the local fiber mean axial strain and inverse radius of curvature, $\nu_j^{(k)} = \int_0^{x_j} [\bar{\varepsilon}^{(k)} - \bar{\varepsilon}^{(k-1)} + (d_f + t)r_{\perp,xx}] dx$.

While the enthalpic stretching and bending stiffnesses of F-actin (38-40) and MTs (39, 41) are experimentally known, the shear stiffness of a given crosslink is often unknown. One exception is provided by the recent measurements of Claessens et al., (29), in which an *apparent* k_x was inferred for the ABPs fimbrin, fascin, and α -actinin in thermodynamic equilibrium. In other cases, k_x may in principle be calculated directly using atomistic-based simulation methods or measured using micromanipulation techniques. The effective length of the crosslinker, t , may be approximated using crystal structures (15, 42, 43) and δ estimated from chemical equilibrium and fiber packing considerations (30).

Biological crosslinks such as the ABPs fascin and fimbrin have finite off-rates, $k_{off} \sim 0.1 - 1 \text{ s}^{-1}$ (44, 45), and are therefore irreversibly-bound only on loading or deformation time scales that are shorter than k_{off}^{-1} . On longer time scales crosslinks may dissociate and rebind, thereby relaxing their shear deformation energy, such as in the coiled packing of the F-actin bundle of the sperm acrosome in which kinking via crosslink unbinding and subsequent inter-filament slip occurs (46). While the effects of crosslink unbinding/rebinding are of interest for understanding the viscoelastic response of cytoskeletal bundles, the present work is limited to conditions in which the loading time-scale is shorter than the crosslink off-rate, which may be mediated by force. The model may also be applied to conditions in which thermal fluctuations excite bundle bending modes provided that the relaxation time of the slowest (longest) wavelength mode is shorter than the crosslink off-rate and the appropriate mean number of bound crosslinks is employed (29). Extension of the present model to include dynamic crosslinks, molecular motors that mediate filament sliding, and filament (de)polymerization provide important model extensions that will be pursued as suitable experimental data become available to validate such developments (47-49).

In addition to their finite shear stiffness, crosslinks have a finite extensibility k_{\perp} [N/m] that could in principle allow for peristaltic (out-of-phase) fiber bending modes. Typical crosslinking proteins have an extensional stiffness, $k_{\perp} \sim 1 \text{ N/m}$ (50), however, that restricts the wavelength of these peristaltic modes to lengths at or below the typical

crosslink distance, δ , and ensuing transverse fluctuations are negligibly small.^{‡‡} Thus, actin bundles are tightly packed and ordered, as demonstrated by electron microscopy (30, 51), and the assumption of inextensible crosslinks is justified in analyzing their mechanical response.

The three-dimensional bundle bending stiffness can in general be expressed as a function of all the independent parameters of the model, $\kappa_B(N, L, k_f, \kappa_f, k_x, \delta, t)$, which in dimensionless form may be written, $\kappa_B^* = \kappa_B^*(N, k_x L^3 / \kappa_f, k_f L^3 / \kappa_f, L / \delta)$, in the limit of small crosslinks, where $\kappa_B^* := \kappa_B / \kappa_f$. We will demonstrate shortly, however, that κ_B^* depends only on the two independent dimensionless parameters, N , and the *fiber coupling parameter*,

$$\alpha := \frac{k_x L^2}{k_f \delta^2}, \quad (1)$$

which is evidently a measure of the competition between crosslink shearing and fiber stretching.

Numerical analysis

To elucidate the mechanics of bundle bending, we begin by examining the bending response of model fiber bundles subject to simple three-point bending computationally using the Finite Element (FE) method (Materials and Methods).^{§§} In analogy with experiment, κ_B is evaluated as a function of increasing fiber number N , for bundles of fixed α , which is akin to fixing the fiber and crosslink properties (Fig. 3A). *Decoupled bending* characterized by linear scaling is observed for small α and *fully coupled bending* for large α . Interestingly, between these two limits we also observe an *intermediate* range of α that displays a smooth crossover from quadratic- to linear-scaling in N . This is in contrast to a bending stiffness that is characterized simply by an α -dependent exponent a , $\kappa_B \sim N^a \kappa_f$ [$1 \leq a(\alpha) \leq 2$] (16, 36). Re-plotting κ_B^* as a function of α for a series of values for N indicates that this range is in fact part of a distinct intermediate regime where κ_B^* increases with increasing α (Fig. 3B). Moreover, any bundle that exhibits fully coupled bending behavior at any given α necessarily transitions into this regime with increasing bundle diameter. In what follows we perform a scaling analysis that considers the energetic competition between *fiber stretching* and *crosslink shearing* to elucidate the physical origin of the crossovers between each regime

^{‡‡} Crosslinks suppress fiber peristaltic modes to wavelengths, $\lambda \leq \lambda_{max} := (\kappa_f \delta / k_\perp)^{1/4}$, where $\lambda_{max} \approx 10$ nm for F-actin with $\kappa_f \approx 7 \times 10^{-26}$ Nm² (38, 39). The minimum axial distance between coplanar crosslinks in hexagonally-packed F-actin bundles is 37.5 nm (30). The associated transverse fluctuations are $r_\perp \sim 0.1 - 1$ nm, which is much less than the inter-axial spacing between fibers, $(d_f + t) \geq 10$ nm (30).

^{§§} Three-point beam bending refers to pinning or clamping a beam at its ends and applying a transverse point load at its center. The resultant load-deflection yields a measure of its apparent bending stiffness (Materials and Methods).

and to delineate their boundaries in (N, α) – space .

Scaling analysis

Consider a generic fiber bundle with a fixed characteristic radius of curvature, $\rho \approx (r_{\perp,xx})^{-1}$. In the decoupled limit individual fibers bend equally without stretching, whereas in the fully coupled limit crosslinks resist shear deformation so that fibers are forced to stretch and compress in addition to bend (Fig. 2B). Differences in fiber deformations in the decoupled, fully coupled, and intermediate regimes are thus manifest at fixed radius of curvature solely in differences in mean fiber stretching.

Accordingly, to isolate the crossover from the fully coupled to the intermediate regime we impose an infinitesimal stretching deformation, $\delta\bar{\varepsilon}^{(k)}$, that relaxes extensionally the fibers and thereby reduces the total fiber stretching energy, $W_{stretch}$, at the expense of an increase in crosslink shearing energy, W_{shear} . $\delta\bar{\varepsilon}^{(k)}$ is a characteristic deformation that is constant along the bundle axis but may differ between fiber layers, k . The crossover between the fully coupled and intermediate regimes is then determined by the point at which crosslink shearing becomes favorable to fiber stretching,

$\delta W_{stretch}[\delta\bar{\varepsilon}^{(k)}] = \delta W_{shear}[\delta\bar{\varepsilon}^{(k)}]$, where $\delta W_{stretch}[\delta\bar{\varepsilon}^{(k)}] = M \sum_{k=-M}^{M-1} \int_0^L dx \bar{F}^{(k)} \delta\bar{\varepsilon}^{(k)}$ is the variation in stretching energy and $\delta W_{shear}[\delta\bar{\varepsilon}^{(k)}] = M \sum_{k=-M+1}^{M-1} \sum_{j=1}^{L/\delta} F_{\times j}^{(k)} \delta v_j^{(k)}$ is the variation in crosslink shearing energy associated with the imposed relaxation $\delta\bar{\varepsilon}^{(k)}$ that results in the crosslink displacement, $\delta v_j^{(k)} = (\delta\bar{\varepsilon}^{(k)} - \delta\bar{\varepsilon}^{(k-1)})x_j$. The calculation of these energy variations requires that the mean-fiber-stretching-, $\bar{F}^{(k)}$, and crosslink-force, $F_{\times j}^{(k)}$, conjugate to the deformations $\delta\bar{\varepsilon}^{(k)}$ and $\delta v_j^{(k)}$ be evaluated, which we turn to next.

The mean axial force in the k^{th} fiber is related linearly to its mean axial strain by, $\bar{F}^{(k)} = E_f A_f \bar{\varepsilon}^{(k)}$, which in the fully coupled regime increases linearly with distance, y , from the *bundle* neutral axis, $\bar{\varepsilon}^{(k)} = -y(k)r_{\perp,xx} = -(k + \frac{1}{2})d_f r_{\perp,xx}$, so that,

$\bar{F}^{(k)} = -E_f A_f (k + \frac{1}{2})d_f r_{\perp,xx}$, like in a homogeneous Euler–Bernoulli beam (Fig. 2B). The limit of small crosslinks ($t \ll d_f$) has been assumed here for simplicity without loss of generality. It is precisely this fiber stretching force that gives rise to the additional bundle bending moment and higher associated bundle bending stiffness in the fully coupled regime. The crosslink force, $F_{\times j}^{(k)}$, is linearly related to its shear displacement via,

$F_{\times j}^{(k)} = k_{\times} v_j^{(k)}$, which is given by, $v_j^{(k)} \sim d_f r_{\perp,xx} x_j$, so that, $F_{\times j}^{(k)} \sim k_{\times} d_f r_{\perp,xx} x_j$, where a constant characteristic radius of curvature has been assumed in evaluating v , consistent with the present scaling picture. Note the differences between the expressions for the fiber axial force and the crosslink shear force: The former increases through the bundle *cross-section* whereas the latter increases along the bundle *axis*.

Variations in fiber stretching and crosslink shearing energy associated with the imposed relaxation $\delta\bar{\varepsilon}^{(k)}$ may now be calculated using the above results to yield,

$$\delta W_{stretch} \sim M E_f A_f d_f r_{\perp,xx} L \sum_{k=-M}^{M-1} k \delta\bar{\varepsilon}^{(k)} \quad \text{and}$$

$\delta W_{shear} \sim Mk_{\times} d_f r_{\perp,xx} \sum_{k=-M+1}^{M-1} (\delta \bar{\epsilon}^{(k)} - \delta \bar{\epsilon}^{(k-1)}) \sum_{j=1}^{L/\delta} x_j^2$, which may be re-written,

$$\delta W_{shear} \sim Mk_{\times} d_f r_{\perp,xx} (L^3 / \delta) \sum_{k=-M+1}^{M-1} (\delta \bar{\epsilon}^{(k)} - \delta \bar{\epsilon}^{(k-1)})$$
, after evaluation of the summation over crosslinks. Equating the resultant increase in crosslink shear energy with the decrease in fiber stretching energy and imposing arbitrary $\delta \bar{\epsilon}^{(k)}$ determines the location of the crossover, $NE_f A_f \sim k_{\times} L^2 / \delta$, which may be re-written, $\alpha \sim N$. Thus, the crossover from the fully coupled regime to the intermediate regime occurs at higher α for larger bundles, N . This result is due to the fact that in the fully coupled regime the fiber stretching energy scales with bundle *diameter* whereas the crosslink shearing energy scales with bundle *length*.

A similar analysis applies to the decoupled limit except that fibers are initially unstressed axially in the ground state. Finite Element results indicate that axial stretching is first induced in fibers at the outer boundary of the bundle in order to minimize the associated increase in $\delta W_{stretch}$, because inner fibers then remain in their relaxed state. This leads directly to a crossover that is bundle-diameter- and thus N -independent, which is given by the condition, $\alpha \sim 1$. Comparison of the crossovers between the decoupled–intermediate ($\alpha \sim 1$) and fully-coupled–intermediate ($\alpha \sim N$) regimes computed with the Finite Element model confirms the validity of the foregoing scaling arguments (Fig. 3B and Fig. 3B Inset), with some deviations for small N . Introduction of the finite-size, t , of the crosslinks increases the absolute value of the fully coupled bending stiffness, but it does not affect this scaling behavior.

Closed-form bundle bending stiffness expression

The fiber bundle model admits an analytical solution employing a continuum energetic approach (Appendix I). As in the Finite Element model, the total elastic energy of the bundle, $H[r_{\perp}(x), \bar{u}^{(k)}(x)]$, is given by fiber bending, H_{bend} , fiber stretching, $H_{stretch}$, and crosslink shearing, H_{shear} , contributions. The bending contribution is given by a linear superposition of the standard wormlike chain bending energy for each independent fiber, $H_{bend} = \frac{1}{2} N \kappa_f \int_0^L r_{\perp,xx}^2 dx$, because transverse fiber-displacements are equal. The fiber stretching energy is given by the axial strain energy,

$$H_{stretch} = ME_f A_f \sum_{k=-M}^{M-1} \int_0^L (\bar{u}_{,x}^{(k)})^2 dx$$
. Finally, crosslink shear energy is associated with crosslink deformation that results from neighboring fiber bending and stretching,

$$H_{shear} = \frac{Mk_{\times}}{\delta} \sum_{k=-M+1}^{M-1} \int_0^L [v^{(k)}(x)]^2 dx$$
.

The theoretical model contains $2M$ internal stretching degrees of freedom $\bar{u}^{(k)}$ in addition to the transverse bundle deflection, r_{\perp} , which is the principal observable of interest in measuring bundle response. Accordingly, the fiber stretching degrees of freedom are integrated over to obtain an *effective* bundle bending energy that depends solely on r_{\perp} , from which the *mode-number-dependent* effective bundle bending stiffness is (Appendix I),

$$\kappa_B(N, \alpha, q_j) = \kappa_f N \left(1 + \frac{\chi^2(N-1)}{1 + c(q_j) \frac{N + \sqrt{N}}{\alpha}} \right) \quad (2)$$

where $\chi := (d_f + t)/d_f$ accounts for the finite thickness of the crosslinks. The mode-number-dependent bending stiffness depends on the wave-numbers $q_j = j\pi/L$ through the non-dimensional factor $c(q_j) = (q_j L)^2/12$ and on the design parameters N and α isolated previously using scaling analysis. In three-point bending at zero temperature, the analytical solution for the bundle bending stiffness is well-approximated by Eq. (2) with a constant factor $c = 1$ for pinned ends and $c = 4$ for clamped ends, in quantitative agreement with the Finite Element results. In the limits of ($\alpha \ll 1$) and ($\alpha \gg N$), Eq. (2) reduces to the decoupled and fully coupled bending, respectively, and in the intermediate regime ($1 \ll \alpha \ll N$) exhibits the scaling, $\kappa_B \propto N k_x L^2$, which is independent of the mechanical properties of the underlying fibers. This demonstrates that the intermediate regime is dominated by shear-deformation of the crosslinks, so that intermediate and shear-dominated may be used interchangeably. This is in contrast to the decoupled and fully coupled regimes, in which the crosslink shear stiffness is effectively equal to zero and infinity, respectively.

The mode-number-dependence of κ_B demonstrates that in addition to being state-dependent (N, α), bundle bending stiffness is an *apparent* material property that depends on the nature in which the bundle is probed. This is in stark contrast to a standard wormlike polymer, which is defined as having an intrinsic bending stiffness that is state- and mode-number-independent (52, 53). Thus, inference of κ_B from “macroscopic” bundle observables such as the mean-square end-to-end distance, the zero-temperature force-deflection relation, or the fluctuation spectrum by associating the bundle with an equivalent wormlike polymer will yield different apparent values for κ_B . Of course, cytoskeletal bundles present in cellular processes are typically stiff ($l_p := \kappa_B / k_B T \gg L$) so that the lowest mode dominates their mechanical response. Accordingly, our primary interest is in the relative values of the isolated design parameters, N and α , which delineate the state-dependence of the bundle bending stiffness. The consequences of the mode-number dependence of κ_B on the statistical mechanical properties of bundles of wormlike chains is examined in separate work (54).

Connection to Timoshenko theory

Fiber bundles consisting of MT protofilaments (41, 55) and SWNTs (56, 57) have recently been analyzed using Timoshenko beam theory.^{***} In this approach, the heterogeneous microstructure of the bundle is ignored so that the bundle can instead be treated as a single homogeneous medium with effective macroscopic geometric and

^{***}Microtubules have been analogized to fiber bundles by treating protofilaments as individual fibers and inter-protofilament interactions as effective crosslinks.

mechanical properties. The bundle stiffness computed from Timoshenko theory for three-point bending with pinned boundary conditions may be written (58),

$\kappa_B = E_B I_B \left[1 + 12 E_B I_B / \beta G_B A_B L_B^2 \right]^{-1}$, where G_B is the effective bundle shear modulus and β is a cross-section-dependent shear-correction factor. To make a connection with the microscopic fiber-bundle theory employed in this work, interlayer shear displacements are assumed to be constant through the bundle cross-section and related to the macroscopic bundle shear strain by, $\gamma_B = v / d_f$, where the limit of small crosslinks is assumed ($t \ll d_f$). Setting the macroscopic bundle shear stress equal to the effective interlayer shear stress, $\tau^{macro} = G_B \gamma_B := \tau^{micro} = k_x v / d_f \delta$, then yields,

$\kappa_B = N^2 \kappa_f (1 + N / \alpha)^{-1}$, which is identical to the fiber-based model result when the limit ($N \gg 1$; $\alpha \gg 1$) is applied. Thus, Timoshenko theory converges to the same fully coupled bundle bending stiffness as the microscopic-based theory when, ($\alpha \gg N$), and crosses-over to the shear-dominated regime when, ($\alpha \sim N$) (Fig. 3B). Unlike the microscopic theory, however, Timoshenko theory is only asymptotically correct in the intermediate regime for large bundles ($N \gg 1$) and it fails drastically when ($\alpha \sim 1$) because it does not account explicitly for the heterogeneous underlying fiber structure of the bundle (Fig. 3B). Moreover, consideration of the underlying molecular structure of cytoskeletal bundles facilitates a connection to atomistic modeling to investigate the source of mesoscopically-observed parameters such as the crosslinker shear stiffness, as well as to examine the effects of underlying structural properties of the bundle such as fiber fracture, which we consider next.

Effect of fiber fracture

In certain cases, such as *Drosophila* bristles in their developmental phase and cytoskeletal stress fibers (10, 11), F-actin bundles are formed from short overlapping segments of fractured fibers that do not run the full length of the bundle (59). We tested the effect of fiber fracture on κ_B numerically by dividing each original mother-fiber in the Finite Element model into m daughter-fibers of equal length, $L_f < L$, where nearest-neighbor mother-fibers were randomly aligned with respect to one another (Supplementary Material). The primary mechanical consequence of fracture is that the fiber tension/compression propagation that is present in the fully coupled regime is eliminated. Instead, the pre-existing axial load carried by a fractured fiber is transferred to its nearest-neighbors via crosslink shear coupling. Intuitively, this transfer is most effective for high crosslink shear stiffnesses, low fracture densities, and large diameter bundles.

Quantitatively, for any bundle size (M, L) we find two distinct regimes delineated by the critical ratio, $\phi^* \approx M$, where $\phi := L / L_f$ is the fracture number density per fiber. As expected, for $\phi \ll \phi^*$ the bending response of the bundle is unaffected by fiber fracture. For $\phi \gg \phi^*$, however, the bundle response is strongly affected by fiber fracture and characterized by a renormalized coupling parameter $\alpha' := \alpha (\phi^* / \phi)^2$. In this

regime, the bundle behaves like m smaller sub-bundles of length L_f . While the critical density ϕ^* is derived from a planar 2D model, the fact that parallel planar fiber layers are assumed to bend independently implies that the same critical density applies to 3D bundles. This scaling behavior is also expected to apply to situations in which fractured segments are not monodisperse in length, as assumed here, as long as fractures are not aligned transversely but instead exhibit significant transverse disorder.

Application to in vitro F-actin bundles

The bending stiffness of F-actin bundles crosslinked by fascin, fimbrin, and non-specific PEG-induced depletion forces was recently measured experimentally using an *in vitro* droplet assay in which F-actin bundles form compact stable rings (29). In that work, bundle bending stiffness was analyzed using an existing analytical theory that depends in a complex manner on the numerous bundle parameters, $\kappa_B(N, L, k_f, \kappa_f, k_x, \delta, t)$ (25, 29). Using the present analytical bending stiffness [Eq. (2)] to fit each bending stiffness data point, (N_i, L_i, r) , at a given fascin:actin concentration ratio $r := c_{fascin} / c_{actin}$ yields a concentration-dependent effective interlayer shear modulus, $k_x / \delta = 1097 \pm 360, 352 \pm 49, 148 \pm 54, \text{ and } 27 \pm 7 \text{ Pa}$ for $r = 0.5, 0.2, 0.05, \text{ and } 0.02$, respectively, over the range of bundle diameters ($2 \leq N \leq 40$) and lengths ($14 \times 10^{-6} \text{ m} \leq L \leq 90 \times 10^{-6} \text{ m}$) examined. The dependence of k_x / δ on r is consistent with a standard Langmuir isotherm where the equilibrium mean spacing between crosslinks depends on crosslinker concentration as, $\delta \propto 1 / c_{fascin}$, with a constant apparent shear stiffness of, $k_x \approx 10^{-5} \text{ N/m}$, assuming a minimum in-plane axial crosslink spacing of 39 nm, $t = 0$, and $c = 5$ appropriate to the periodic boundary conditions used to model the ring-bundle examined experimentally (Appendix I). Employing a crosslinker dimension of $t = 10 \text{ nm}$ results in an apparent stiffness of $k_x \approx 10^{-6} \text{ N/m}$.^{†††} The uncertainty in model parameters including t and δ render the estimate of k_x only valid to within an order of magnitude. The dependence of bundle bending stiffness on bundle length, L , at fixed filament number, $N = 27 \pm 6$, provides additional evidence for the validity of the proposed mechanical model in which $\alpha := (k_x / E_f A_f)(L^2 / \delta)$ mediates the bending regime of crosslinked F-actin bundles, within the limited range of L capable of being probed experimentally at fixed N ($24 \times 10^{-6} \text{ m} \leq L \leq 55 \times 10^{-6} \text{ m}$) (Fig. 4).

In the absence of detailed information regarding the fine structure of the actin bundles examined, the preceding analysis assumes fiber fracture to be below the critical fracture density, $\phi \ll \phi^*$, and fibers to be ordered transversely. While the former assumption is consistent with the observation that phalloidin tends to anneal F-actin into stable, continuous filaments (61), and the latter is consistent with observations of the hexagonally ordered packing of fascin-actin bundles (3, 30, 62), direct examination of the fine structure of the *in vitro* ring bundles are needed to fully justify these assumptions.

^{†††} The present estimate for k_x differs somewhat from that published previously due to an erroneous bundle-length expression employed in that work (29, 60).

Unlike fascin-crosslinked bundles, bundles crosslinked by fimbrin and non-specific depletion forces exhibit a bending stiffness that is independent of the crosslinker concentration, where fimbrin-crosslinked bundles exhibit decoupled bending and depletion-force-induced bundles exhibit fully coupled over the range of bundle dimensions and crosslinker concentrations examined (29). While non-specific depletion-forces are likely to induce tight uni-polar packing between helical actin filaments (42) that would explain the fully coupled bending observed, the decoupled bending behavior observed for fimbrin may be hypothesized to be due either to an enhanced F-actin shear compliance associated with actin monomer tilting (63) mediated by fimbrin-binding, facile modes of shear deformation involving the actin-fimbrin binding interface (42), or fimbrin-actin dissociation/association kinetics. Indeed, the unusually low shear stiffness observed for fascin is also likely attributable to some combination of the aforementioned factors, which remain under active investigation. We believe that direct bundle stiffness measurements using optical tweezers or AFM to probe actively the nonlinear and nonequilibrium bending response of F-actin bundles are required together with molecular modeling of crosslinked actin bundles (64, 65) to understand the origin of the observed behavior, as well as to further validate the presently proposed interpretation of cytoskeletal bundle bending mechanics.

Bending stiffness state-diagram

The bending regime of *in vivo* cytoskeletal bundles may be predicted by evaluating the design parameters N and α using the apparent values of k_x determined experimentally (29) and known bundle dimensions (2, 3) (Fig. 5). Maximal bundle compliance is achieved by decoupled bending ($\alpha \ll 1$), whereas maximal bundle stiffness is achieved with fully coupled bending ($\alpha \gg N$). In the shear-dominated regime ($1 \ll \alpha \ll N$) bundle length or crosslink concentration may be varied to tune bundle bending stiffness by orders of magnitude.

The sperm acrosomal process is required to penetrate mechanically the outer jelly coat of the egg cell during fertilization (66, 67). The *limulus* (horseshoe crab) sperm acrosome consists of a tapered bundle of 15–80 hexagonally-packed F-actin fibers that are tightly crosslinked by scruin and run the full length ($L \approx 50 \mu\text{m}$) of the bundle. Macroscopic measurements of its bending stiffness have been made using hydrodynamic flow (66), where it was determined that the bundle exhibits fully coupled bending. This independent macroscopic observation is consistent with the *a priori* prediction of the fiber-based model, in which the ranges in N and α are determined from the parameters probed experimentally (Fig. 5). The shear stiffness of fascin is used as a lower-bound estimate for scruin because the molecular structure and interfilament packing of the latter suggest that it is considerably stiffer (15).

Vertebrate hair cell stereocilia are finger-like projections in the inner ear that serve as mechanochemical transducers for sound and motion (Fig. 1). Ranging from 1–10 μm in length, each stereocilium consists of up to 900 hexagonally-packed F-actin filaments crosslinked predominantly by fimbrin (2, 3, 68). Macroscopic measurements of the bending stiffness of hair cell stereocilia bundles and of the root of individual stereocilia made using microneedle manipulation (36) yielded decoupled bending behavior. Together with their short length, the very low effective stiffness of fimbrin

places their theoretical stiffness deep in the decoupled regime, consistent with these independent experimental observations (Fig. 5).

Brush-border microvilli ($N \approx 20 - 30$; $L \approx 1 - 5 \mu\text{m}$) are passive cellular processes that predominate in fimbrin and serve primarily to increase the apical surface area of intestinal epithelial cells (2, 3) (Fig. 1). Cytoskeletal stress fibers ($N \approx 10 - 40$; $L \approx 1 - 10 \mu\text{m}$) predominant in α -actinin (29) function mechanically to enhance the tensile stiffness of cells. Each of these processes is predicted to exhibit decoupled bending due to its relatively short length. Filopodia are active F-actin bundles present at the leading edge of motile cells and neuronal growth cones that increase in length during locomotion and growth (3) (Fig. 1). Consisting of 10–30 filaments, they are predominantly crosslinked by fascin and typically range from 1–10 μm , but may reach lengths of up to 30–40 μm in certain cases such as in the sea urchin embryo (16, 69). As a final actin-based example, we consider the 11 fascin-crosslinked bundles constituting the *Drosophila* neurosensory bristle. Each bundle is ≈ 400 microns long and contains 500–700 filaments in macrochaetes (59, 70) (Fig. 1). Using their full length, these bundles are predicted to lie at the interface of the fully coupled and intermediate regimes, despite their large diameter. Early in development, however, bristles consist of short overlapping bundle modules ($L_f \approx 3 \mu\text{m}$) (59). At this early stage the fiber fracture density,

$\phi := L / L_f \approx 100$, is less than the *critical fracture density*, $\phi^* \sim N \sim 10^2 - 10^3$, below which we find the fully-coupled–intermediate regime transition to be unaffected by fracture (Supplementary Material). Direct bending stiffness measurements would be of interest to verify this prediction.

Finally, noting that the bundle model employed in this work is generic to ordered fiber bundles, we also include in the state diagram MT bundles from outer pillar hair cells for which the interlayer shear modulus has been measured using micromanipulation and a fiber-based model ($N \approx 1000 - 3000$; $L \approx 70 - 120 \mu\text{m}$; $k_x / \delta \approx 1 \text{ kPa}$) (25).

The bending stiffness state diagram in Figure 5 provides preliminary, *ab initio* estimates for the bending regime of *in vivo* cytoskeletal actin bundles based on apparent values for k_x that have been inferred from a single type of *in vitro* experimental assay that probes the linear, equilibrium mechanical response of F-actin bundles. As noted earlier, significant further experimentation on *in vitro* and *in vivo* bundles using active measurement probes such as optical tweezers or AFM are needed to further validate these predictions, as well as to explore the nonlinear and nonequilibrium mechanical response of F-actin bundles. For example, an F-actin bundle that exhibits fully coupled or intermediate bending behavior on loading time-scales that are much shorter than the crosslink unbinding time-scale necessarily relaxes to the decoupled bending regime as crosslinks dissociate. Additionally, the rate of this relaxation will be accelerated in a manner that depends on the degree of bundle deformation. Notwithstanding, the importance of the present work is to isolate the generic design parameters N and α that reveal the universal nature of static cytoskeletal bundle mechanics, as well as their strong dependence on bundle geometry and crosslinker properties. While the quantitative values of N and α corresponding to specific cytoskeletal processes should be refined and further validated in the future, as well as modified to include effects of crosslink unbinding and nonlinear mechanical response present *in situ*, the importance of N and α in mediating

both the regime of cytoskeletal bundle bending, as well as crossovers between these regimes, is expected to apply.

Implications for *in situ* mechanical function

The isolated mechanical behavior of cytoskeletal bundles has direct implications on the *in situ* bending, buckling, and entropic stretching behavior of cytoskeletal bundles.

Decoupled bending exhibited by stereocilia not only maximizes the bending compliance of these cellular processes, but also relieves actin filament stretching/compression that grows linearly with distance from the bundle centerline in fully coupled bending, $F_k \propto k(d_f + t)E_f A_f / \rho$. Thus, fragility of actin filaments under axial strain that leads to filament fracture may provide an alternative criterion to design cytoskeletal bundles that exhibit decoupled bending in cellular processes such as stereocilia (71).

In contrast, fully coupled bending maximizes the mechanical resistance of the sperm acrosome to axial compressive forces that lead to structural failure at the critical buckling load, $F_{crit} \sim \kappa_B / L^2$. The isolated crossover from fully coupled to intermediate bending at the critical ratio $\alpha / N \sim 1$ provides a constraint on the design of cytoskeletal bundles for maximal mechanical stability under compressive loading. Also subject to compressive loading are invadopodia and filopodia, fascin-crosslinked actin bundles involved in tissue invasion, cell motility and axonal growth (16, 17). The results of this work suggest that as the length of these processes increases they transition from decoupled to intermediate regime bending, where F_{crit} becomes *independent* of length because $\kappa_B \propto L^2$ there. This is in stark contrast to a standard wormlike chain for which F_{crit} decreases strongly with increasing length. Thus, dynamic cytoskeletal processes such as filopodia may potentially increase their length without compromising their buckling stability in the intermediate regime, until they finally reach fully coupled bending, where F_{crit} becomes length-dependent again.

The entropic stretching response of F-actin bundles is suggested to play a role in the elasticity of reconstituted actin networks (45, 72, 73), biological tissues (74), and potentially cells (75, 76). Importantly, decoupled cytoskeletal actin bundles have an entropic stretching stiffness, $k_e \propto N^2 \kappa_f / L^4$, that is substantially lower than its fully coupled counterpart, $k_e \propto N^4 \kappa_f / L^4$, with a markedly different dependence on filament number, or bundle diameter. Additionally, the mode-number dependence of κ_B renders the dependence of k_e on bundle length relatively weak ($k_e \propto 1/L$) in this regime (8, 54, 73).

Taken together, these examples illustrate the direct implications that the state-dependent bending stiffness of cytoskeletal actin bundles isolated in the present work has on their *in situ* biomechanical behavior. Significant further experimentation is clearly warranted to better understand the complex nature of cytoskeletal bundle bending mechanics in cells and in reconstituted actin networks, in particular under physiological conditions of nonlinear and nonequilibrium loading present during cell migration (77). Additionally, extension of the present model to include the active, nonequilibrium stretching response of individual cytoskeletal stress fibers as mediated by myosin,

tropomyosin, and α -actinin provides an important avenue of development to facilitate the bottom-up prediction of cellular mechanics (8, 10, 11, 78).

Conclusions

Cytoskeletal bundles of crosslinked actin filaments form key structural components of a broad range of cellular processes. To date, a common conception has been that cytoskeletal bundles display two limiting bending behaviors, namely decoupled or fully coupled bending. Here, we demonstrate that their bending behavior is considerably more intricate, depending on global bundle dimensions, the shear stiffness of intervening crosslinks, and the stretching stiffness and fracture density of constituent fibers. We isolate two generic design parameters, N and α , that delineate the three distinct bending regimes of cytoskeletal bundles with markedly differing scaling properties. Experimental bending stiffness of *in vitro* fascin-crosslinked F-actin bundles, as well as existing *in vivo* measurements of the bending stiffness of the *limulus* sperm acrosome and of the stereocilium, validate our interpretation of F-actin bundle mechanics. The isolated state-dependence of fiber bundles has important implications for the physiological bending, buckling, and potential entropic stretching behavior of cytoskeletal processes, some of which are highlighted in this work. Finally, *ab initio* predictions for the bending regime of various cytoskeletal processes are presented in the form of a bending stiffness state diagram, which highlights the importance of bundle dimensions on bundle mechanical response.

Future experimentation using active mechanical probes will facilitate the extension of the present, static molecular-based model to include nonequilibrium effects of force-induced crosslink unbinding, filament dynamics including rupture and disassembly, and molecular motor mediated filament sliding and translocation as present in cytoskeletal stress fibers. While considerable additional experimentation in close collaboration with multi-scale modeling is needed to understand fully the intricate nature of cytoskeletal bundle mechanics, this challenging line of research should eventually facilitate a mechanistic, molecular-level understanding of the interplay between cellular mechanics and active cytoskeletal remodeling that has remained elusive to date.

Materials and Methods

Finite element modeling. Fibers are discretized identically in 2D using 2-node Hermitian beam elements with nodal degrees of freedom, $\{u_i, w_i, \theta_i\}$, where u_i is axial displacement, w_i is transverse deflection, and θ_i is in-plane rotation (79). Nodes on adjacent fibers are constrained to have equal transverse deflection. Crosslink shear stiffness is modeled using a general 2-node finite element that couples beam element nodes on nearest-neighbor fibers with stiffness matrix, $K_{ij} = \partial^2 E / \partial x_i \partial x_j$, where x_i denotes the nodal degree of freedom of the k^{th} fiber, $\{x_i : u^{(k)}, u^{(k-1)}, \theta^{(k)}, \theta^{(k-1)}\}$. The crosslink shear energy function is, $E = (k_x / 2) \left[(u^{(k)} - u^{(k-1)}) + (d_f / 2)(\theta^{(k)} + \theta^{(k-1)}) \right]^2$, where k_x is normalized properly to account for discretization. Three-point bending is simulated by applying pinned or clamped boundary conditions to the bundle ends and applying a transverse unit point load at the bundle mid-point, yielding the apparent wormlike chain bending stiffness, $\kappa_B := PL^3 / aw_{L/2}$, where $a = 48$ and $a = 192$ for pinned and clamped ends, respectively. Simulations are performed using the commercial Finite Element Software ADINA ver. 8.2.0 (Watertown, MA).

Experimental methods are as described in (29).

Appendix I Derivation of the mode-number-dependent bundle bending stiffness

The bundle Hamiltonian,

$$H[r_{\perp}(x), \bar{u}^{(k)}(x)] = \int_0^L dx \left\{ \frac{1}{2} N \kappa_f r_{\perp,xx}^2 + M E_f A_f \sum_{k=-M}^{M-1} (\bar{u}_{,x}^{(k)})^2 + \frac{M k_x}{\delta} \sum_{k=-M+1}^{M-1} [v^{(k)}(x)]^2 \right\} \quad (11)$$

may be simplified to depend only on r_{\perp} and the *relative* degree-of-stretching between fibers, $\Delta \bar{u}$, by employing the approximation that fiber-stretching varies linearly through the bundle cross-section (25), $\bar{u}^{(k)} = (k + \frac{1}{2}) \Delta \bar{u}$,

$$H[r_{\perp}(x), \Delta \bar{u}(x)] = \int_0^L dx \left\{ \frac{1}{2} N \kappa_f r_{\perp,xx}^2 + \frac{1}{6} M^2 (4M^2 - 1) E_f A_f \Delta \bar{u}_{,x}^2 + \dots \right. \\ \left. \dots + \frac{k_x}{\delta} M (2M - 1) [\Delta \bar{u} + (d_f + t) r_{\perp,x}]^2 \right\} \quad (12)$$

Fourier transformation of the Hamiltonian in Eq. (12) then results in the decomposition

$H = \sum_j H_j L / 2$, where the contribution of mode j to H is,

$$H_j = \frac{1}{2} N \kappa_f q_j^4 r_j^2 + \frac{1}{6} M^2 (4M^2 - 1) E_f A_f q_j^2 \Delta \bar{u}_j^2 + \frac{k_x}{\delta} M (2M - 1) [\Delta \bar{u}_j + (d_f + t) q_j r_j]^2 \quad (13)$$

and q_j denotes the wave-number associated with mode j . Minimization of Eq. (13) with respect to $\Delta \bar{u}_j$ yields the minimum value,

$$\Delta \bar{u}_j^* = \frac{-(d_f + t) q_j r_j}{1 + \frac{(q_j L)^2}{12} \frac{2M(2M+1)}{\alpha}} \quad (14)$$

and the corresponding reduced Hamiltonian,

$$H_j[r_j, \Delta \bar{u} = \Delta \bar{u}_j^*] = q_j^4 r_j^2 \left[\frac{1}{2} N \kappa_f + \frac{M^2 E_f A_f (d_f + t)^2 (4M^2 - 1)}{6 + \frac{(q_j L)^2 M (2M + 1)}{\alpha}} \right], \quad (15)$$

which yields the *mode-number-dependent effective bundle bending stiffness*,

$$\kappa_B(N, \alpha, q_j) = \kappa_f N \left[1 + \frac{\chi^2 (N - 1)}{1 + c(q_j) \frac{(N + \sqrt{N})}{\alpha}} \right] \quad (16)$$

where $\alpha = k_x L^2 / E_f A_f \delta$, $\kappa_f = E_f A_f d_f^2 / 12$, $N = (2M)^2$, $c(q_j) = (q_j L)^2 / 12$, and $\chi := (d_f + t) / d_f$ have been defined.

$\kappa_B(N, \alpha, q_j)$ may subsequently be employed to calculate the transverse deflection $r_\perp(x)$ corresponding to transverse loading $F(x)$ via back-transformation to real-space of,

$$\kappa_B(N, \alpha, q_j) q_j^4 r_j = -F_j \quad (17)$$

where F_j is the j^{th} Fourier component of the applied force. The transverse deflection is given by,

$$r_\perp(x) = R_0 - \sum_{j=1}^{\infty} \frac{F_j \phi(q_j x)}{q_j^4 \kappa_B(q_j, N, \alpha)} \quad (18)$$

where the eigenfunction $\phi(x)$ is given by sine and cosine for hinged and clamped boundary conditions, respectively, and R_0 is chosen such that the transverse deflection vanishes at the bundle ends.

While an exact evaluation of the sum in Eq. (18) in general yields a complex analytical expression, performing the sum without the “1” in the denominator of Eq. (16) and adding it back to the final result yields an approximate solution that is nearly identical to the exact result. The deflection of the bundle mid-point $r_\perp(x = L/2)$ may then be recast into the standard result from Euler–Bernouilli beam theory,

$$r_\perp(L/2) = -\frac{F_{L/2} L^3}{\beta \kappa_{B,eff}} \quad (19)$$

where $\beta = 48$ and 192 for pinned and clamped ends, respectively. The effective bending stiffness $\kappa_{B,eff}$ then has the same form as in Eq. (16) except with the (mode-number dependent) factor c substituted by the constant factors 1 and 4, as verified by comparison with the FE results.

Calculation of the equilibrium mean-square transverse displacement of the bundle backbone due to thermal fluctuations requires evaluation of,

$$r_\perp^2 := \frac{1}{L} \int_0^L \langle r_\perp^2(x) \rangle dx = 2 \sum_j \frac{k_B T / L}{q_j^4 \kappa_B(q_j, N, \alpha)} \quad (110)$$

where $q_j = j2\pi / L$ for periodic boundary conditions applicable to the ring-bundle system examined experimentally. This yields, $r_\perp^2 = k_B T L^3 / 720 \kappa_B$ (80), where the effective bundle bending stiffness is again given by Eq. (16) with $c = 5$.

Acknowledgements

We thank T. Svitkina for providing a high resolution version of the filopodium in Figure 1 and David P. Corey and John A. Assad for providing a high resolution version of the ciliary bundle in Figure 1. Funding from the German Science Foundation (SFB 413), the German Excellence Initiative via the NanoSystems Initiative Munich (NIM), and the Alexander von Humboldt Foundation in the form of a postgraduate research fellowship (to MB) is gratefully acknowledged.

References

1. Lodish, H., A. Berk, S. L. Zipursky, P. Matsudaira, D. Baltimore, and J. Darnell. 1999. *Molecular Cell Biology*. W.H. Freeman and Company, New York.
2. Bartles, J. R. 2000. Parallel actin bundles and their multiple actin-bundling proteins. *Current Opinion in Cell Biology* 12:72-78.
3. Revenu, C., R. Athman, S. Robine, and D. Louvard. 2004. The co-workers of actin filaments: From cell structures to signals. *Nature Reviews Molecular Cell Biology* 5:635-646.
4. Hudspeth, A. J., and D. P. Corey. 1977. Sensitivity, polarity, and conductance change in response of vertebrate hair cells to controlled mechanical stimuli. *Proceedings of the National Academy of Sciences of the United States of America* 74:2407-2411.
5. Kachar, B., W. E. Brownell, R. Altschuler, and J. Fex. 1986. Electrokinetic shape changes of cochlear outer hair cells. *Nature* 322:365-368.
6. Bursac, P., G. Lenormand, B. Fabry, M. Oliver, D. A. Weitz, V. Viasnoff, J. P. Butler, and J. J. Fredberg. 2005. Cytoskeletal remodelling and slow dynamics in the living cell. *Nature Materials* 4:557-561.
7. Huang, H. D., R. D. Kamm, and R. T. Lee. 2004. Cell mechanics and mechanotransduction: pathways, probes, and physiology. *American Journal of Physiology: Cell Physiology* 287:C1-C11.
8. Kumar, S., I. Z. Maxwell, A. Heisterkamp, T. R. Polte, T. P. Lele, M. Salanga, E. Mazur, and D. E. Ingber. 2006. Viscoelastic retraction of single living stress fibers and its impact on cell shape, cytoskeletal organization, and extracellular matrix mechanics. *Biophysical Journal* 90:3762-3773.
9. Ingber, D. E. 1993. Cellular Tensegrity - Defining New Rules of Biological Design that Govern the Cytoskeleton. *Journal of Cell Science* 104:613-627.
10. Hotulainen, P., and P. Lappalainen. 2006. Stress fibers are generated by two distinct actin assembly mechanisms in motile cells. *Journal of Cell Biology* 173:383-394.
11. Katoh, K., Y. Kano, M. Masuda, H. Onishi, and K. Fujiwara. 1998. Isolation and contraction of the stress fiber. *Molecular Biology of the Cell* 9:1919-1938.
12. Cramer, L. P., M. Siebert, and T. J. Mitchison. 1997. Identification of novel graded polarity actin filament bundles in locomoting heart fibroblasts: Implications for the generation of motile force. *Journal of Cell Biology* 136:1287-1305.
13. Costa, K. D., W. J. Hucker, and F. C. P. Yin. 2002. Buckling of actin stress fibers: A new wrinkle in the cytoskeletal tapestry. *Cell Motility And The Cytoskeleton* 52:266-274.
14. Miller, D. J., M. B. Macek, and B. D. Shur. 1992. Complementarity between sperm surface beta-1,4-galactosyl-transferase and egg-coat Zp3 mediates sperm egg binding. *Nature* 357:589-593.
15. Schmid, M. F., M. B. Sherman, P. Matsudaira, and W. Chiu. 2004. Structure of the acrosomal bundle. *Nature* 431:104-107.

16. Mogilner, A., and B. Rubinstein. 2005. The physics of filopodial protrusion. *Biophysical Journal* 89:782-795.
17. Atilgan, E., D. Wirtz, and S. X. Sun. 2006. Mechanics and dynamics of actin-driven thin membrane protrusions. *Biophysical Journal* 90:65-76.
18. Vignjevic, D., S. Kojima, Y. Aratyn, O. Danciu, T. Svitkina, and G. G. Borisy. 2006. Role of fascin in filopodial protrusion. *Journal of Cell Biology* 174:863-875.
19. Faix, J., and K. Rottner. 2005. The making of filopodia. *Current Opinion in Cell Biology* 18:18-25.
20. Aratyn, Y. S., T. E. Schaus, E. W. Taylor, and G. B. Borisy. 2007. Intrinsic Dynamic Behavior of Fascin in Filopodia. *Molecular Biology of the Cell* 18:3928-3940.
21. Rodriguez, O. C., A. W. Schaefer, C. A. Mandato, P. Forscher, W. M. Bement, and C. M. Waterman-Storer. 2003. Conserved microtubule-actin interactions in cell movement and morphogenesis. *Nature Cell Biology* 5:599-609.
22. Medeiros, N. A., D. T. Burnette, and P. Forscher. 2006. Myosin II functions in actin-bundle turnover in neuronal growth cones. *Nature Cell Biology* 8:215-226.
23. Karsenti, E., F. Nedelec, and T. Surrey. 2006. Modelling microtubule patterns. *Nature Cell Biology* 8:1204-1211.
24. Daga, R. R., K. G. Lee, S. Bratman, S. Salas-Pino, and F. Chang. 2006. Self-organization of microtubule bundles in anucleate fission yeast cells. *Nature Cell Biology* 8:1108-U1198.
25. Tolomeo, J. A., and M. C. Holley. 1997. Mechanics of microtubule bundles in pillar cells from the inner ear. *Biophysical Journal* 73:2241-2247.
26. Hartwell, L. H., J. J. Hopfield, S. Leibler, and A. W. Murray. 1999. From molecular to modular cell biology. *Nature* 402:C47-C52.
27. Kureishy, N., V. Sapountzi, S. Prag, N. Anilkumar, and J. C. Adams. 2002. Fascins, and their roles in cell structure and function. *Bioessays* 24:350-361.
28. Kirschner, M. W., and J. C. Gerhart. 2005. *The Plausibility of Life: Resolving Darwin's Dilemma*. Yale University Press, New Haven and London.
29. Claessens, M. M. A. E., M. Bathe, E. Frey, and A. R. Bausch. 2006. Actin-binding proteins sensitively mediate F-actin bundle stiffness. *Nature Materials* 5:748-753.
30. DeRosier, D. J., and L. G. Tilney. 1981. How actin filaments pack into bundles. *Cold Spring Harbor Symposia on Quantitative Biology* 46:525-540.
31. Tilney, L. G., E. H. Egelman, D. J. DeRosier, and J. C. Saunders. 1983. Actin filaments, stereocilia, and hair cells of the bird cochlea 2. Packing of actin filaments in the stereocilia and in the cuticular plate and what happens to the organization when the stereocilia are bent. *Journal of Cell Biology* 96:822-834.
32. Timoshenko, S. 1958. *Strength of Materials*. Van Nostrand Reinhold Company, New York.
33. Landau, L. D., and E. M. Lifshitz. 1995. *Theory of Elasticity*. Butterworth-Heinemann, Oxford.
34. Grason, G. M., and R. F. Bruinsma. 2007. Chirality and Equilibrium Biopolymer Bundles. *Physical Review Letters* 99:Art. No. 098101.

35. Wolgemuth, C. W., and S. X. Sun. 2006. Elasticity of alpha-Helical Coiled Coils. *Physical Review Letters* 97:Art. No. 248101.
36. Howard, J., and J. F. Ashmore. 1986. Stiffness of sensory hair bundles in the sacculus of the frog. *Hearing Research* 23:93-104.
37. Everaers, R., R. Bundschuh, and K. Kremer. 1995. Fluctuations and Stiffness of Double-Stranded Polymers: Railway-Track Model. *Europhysics Letters* 29:263-268.
38. LeGoff, L., O. Hallatschek, E. Frey, and F. Amblard. 2002. Tracer studies on F-actin fluctuations. *Physical Review Letters* 89:Art. No. 258101-258101.
39. Gittes, F., B. Mickey, J. Nettleton, and J. Howard. 1993. Flexural rigidity of microtubules and actin filaments measured from thermal fluctuations in shape. *Journal of Cell Biology* 120:923-934.
40. Kojima, H., A. Ishijima, and T. Yanagida. 1994. Direct measurement of stiffness of single actin-filaments with and without tropomyosin by in-vitro nanomanipulation. *Proceedings of the National Academy of Sciences of the United States of America* 91:12962-12966.
41. Pampaloni, F., G. Lattanzi, A. Jonas, T. Surrey, E. Frey, and E. L. Florin. 2006. Thermal fluctuations of grafted microtubules provide evidence of a length-dependent persistence length. *Proceedings of the National Academy of Sciences of the United States of America* 103:10248-10253.
42. Volkman, N., D. DeRosier, P. Matsudaira, and D. Hanein. 2001. An atomic model of actin filaments cross-linked by fimbrin and its implications for bundle assembly and function. *Journal of Cell Biology* 153:947-956.
43. Tang, J. H., D. W. Taylor, and K. A. Taylor. 2001. The three-dimensional structure of alpha-actinin obtained by cryoelectron microscopy suggests a model for Ca²⁺-dependent actin binding. *Journal of Molecular Biology* 310:845-858.
44. Goldmann, W. H., and G. Isenberg. 1993. Analysis of filamin and alpha-actinin binding to actin by the stopped-flow method. *FEBS Letters* 336:408-410.
45. Tseng, Y., E. Fedorov, J. M. McCaffery, S. C. Almo, and D. Wirtz. 2001. Micromechanics and ultrastructure of actin filament networks crosslinked by human fascin: A comparison with alpha-actinin. *Journal of Molecular Biology* 310:351-366.
46. Cohen, A. E., and L. Mahadevan. 2003. Kinks, rings, and rackets in filamentous structures. *Proceedings of the National Academy of Sciences of the United States of America* 100:12141-12146.
47. Kruse, K., S. Camalet, and F. Julicher. 2001. Self-propagating patterns in active filament bundles. *Physical Review Letters* 87:13.
48. Kruse, K., and F. Julicher. 2003. Self-organization and mechanical properties of active filament bundles. *Physical Review E* 67.
49. Bathe, M., and E. Frey. 2007. Work in progress.
50. Schwaiger, I., A. Kardinal, M. Schleicher, A. A. Noegel, and M. Rief. 2004. A mechanical unfolding intermediate in an actin-crosslinking protein. *Nature Structural & Molecular Biology* 11:81-85.
51. Small, J. V. 1981. Organization of Actin in the Leading Edge of Cultured Cells: Influence of Osmium Tetroxide and Dehydration on the Ultrastructure of Actin Meshworks. *The Journal of Cell Biology* 91:695-705.

52. Saito, N., K. Takahashi, and Y. Yunoki. 1967. Statistical Mechanical Theory of Stiff Chains. *Journal of the Physical Society of Japan* 22:219.
53. Yamakawa, H. 1973. Statistical mechanics of wormlike chains: Path integral and diagram methods. *Journal of Chemical Physics* 59:3811-3815.
54. Heussinger, C., M. Bathe, and E. Frey. 2007. Statistical Mechanics of Semiflexible Bundles of Wormlike Polymer Chains. *Physical Review Letters* 99:Art. No. 048101.
55. Kis, A., S. Kasas, B. Babic, A. J. Kulik, W. Benoit, G. A. D. Briggs, C. Schonenberger, S. Catsicas, and L. Forro. 2002. Nanomechanics of microtubules. *Physical Review Letters* 89.
56. Kis, A., G. Csanyi, J. P. Salvetat, T. N. Lee, E. Couteau, A. J. Kulik, W. Benoit, J. Brugger, and L. Forro. 2004. Reinforcement of single-walled carbon nanotube bundles by intertube bridging. *Nature Materials* 3:153-157.
57. Salvetat, J. P., G. A. D. Briggs, J. M. Bonard, R. R. Bacsa, A. J. Kulik, T. Stockli, N. A. Burnham, and L. Forro. 1999. Elastic and shear moduli of single-walled carbon nanotube ropes. *Physical Review Letters* 82:944-947.
58. Gere, J. M., and S. P. Timoshenko. 1997. *Mechanics of Materials*, 4th ed. Boston: PWS Publishing Co.
59. Guild, G. M., P. S. Connelly, L. Ruggiero, K. A. Vranich, and L. G. Tilney. 2003. Long continuous actin bundles in *Drosophila* bristles are constructed by overlapping short filaments. *Journal of Cell Biology* 162:1069-1077.
60. Claessens, M. M. A. E., M. Bathe, E. Frey, and A. R. Bausch. 2007. In preparation.
61. Isambert, H., P. Venier, A. C. Maggs, A. Fattoum, R. Kassab, D. Pantaloni, and M. F. Carlier. 1995. Flexibility of actin filaments derived from thermal fluctuations - Effect of bound nucleotide, phalloidin, and muscle regulatory proteins. *Journal of Biological Chemistry* 270:11437-11444.
62. Tilney, L. G., P. S. Connelly, K. A. Vranich, M. K. Shaw, and G. M. Guild. 2000. Regulation of actin filament cross-linking and bundle shape in *Drosophila* bristles. *Journal of Cell Biology* 148:87-99.
63. Orlova, A., A. Shvetsov, V. E. Galkin, D. S. Kudryashov, P. A. Rubenstein, E. H. Egelman, and E. Reisler. 2004. Actin-destabilizing factors disrupt filaments by means of a time reversal of polymerization. *Proceedings of the National Academy of Sciences of the United States of America* 101:17664-17668.
64. Bathe, M. 2007. A Finite Element framework for computation of protein normal modes and mechanical response. *Proteins: Structure, Function, and Bioinformatics* in press.
65. Bathe, M., and M. Karplus. 2007. Work in progress.
66. Shin, J. H., L. Mahadevan, P. T. So, and P. Matsudaira. 2004. Bending stiffness of a crystalline actin bundle. *Journal of Molecular Biology* 337:255-261.
67. Tilney, L. G. 1975. Actin Filaments in Acrosomal Reaction of *Limulus* Sperm - Motion Generated by Alterations in the Packing of the Filaments. *Journal of Cell Biology* 64:289-310.
68. Tilney, L. G., M. S. Tilney, and D. J. Derosier. 1992. Actin Filaments, Stereocilia, and Hair Cells: How Cells Count and Measure. *Annual Review of Cell Biology* 8:257-274.

69. Gustafson, T., and L. Wolpert. 1999. Studies on the cellular basis of morphogenesis in the sea urchin embryo - Directed movements of primary mesenchyme cells in normal and vegetalized larvae. *Experimental Cell Research* 253:288-295.
70. Tilney, L. G., P. Connelly, S. Smith, and G. M. Guild. 1996. F-actin bundles in *Drosophila* bristles are assembled from modules composed of short filaments. *Journal of Cell Biology* 135:1291-1308.
71. Tsuda, Y., H. Yasutake, A. Ishijima, and T. Yanagida. 1996. Torsional rigidity of single actin filaments and actin-actin bond breaking force under torsion measured directly by in vitro micromanipulation. *Proceedings of the National Academy of Sciences of the United States of America* 93:12937-12942.
72. Gardel, M. L., J. H. Shin, F. C. MacKintosh, L. Mahadevan, P. Matsudaira, and D. A. Weitz. 2004. Elastic behavior of cross-linked and bundled actin networks. *Science* 304:1301-1305.
73. Lielig, O., M. M. A. E. Claessens, C. Heussinger, E. Frey, and A. R. Bausch. 2007. Mechanics of bundled semiflexible polymer networks. *Physical Review Letters* 99:Art. No. 088102.
74. Storm, C., J. J. Pastore, F. C. MacKintosh, T. C. Lubensky, and P. A. Janmey. 2005. Nonlinear elasticity in biological gels. *Nature* 435:191-194.
75. Satcher, R. L., and C. F. Dewey. 1996. Theoretical estimates of mechanical properties of the endothelial cell cytoskeleton. *Biophysical Journal* 71:109-118.
76. Deng, L. H., X. Trepatt, J. P. Butler, E. Millet, K. G. Morgan, D. A. Weitz, and J. J. Fredberg. 2006. Fast and slow dynamics of the cytoskeleton. *Nature Materials* 5:636-640.
77. Abercrombie, M. 1980. Croonian Lecture, 1978 - Crawling Movement of Metazoan Cells. *Proceedings of the Royal Society of London Series B: Biological Sciences* 207:129-&.
78. Shemesh, T., B. Geiger, A. D. Bershadsky, and M. M. Kozlov. 2005. Focal adhesions as mechanosensors: A physical mechanism. *Proceedings of the National Academy of Sciences of the United States of America* 102:12383-12388.
79. Bathe, K. J. 1996. *Finite Element Procedures*. Prentice-Hall Inc., Upper Saddle River, New Jersey.
80. Camacho, C. J., M. E. Fisher, and R. R. P. Singh. 1991. Semiflexible Planar Polymeric Loops. *Journal of Chemical Physics*:5693-5700.
81. Svitkina, T. M., E. A. Bulanova, O. Y. Chaga, D. M. Vignjevic, S. Kojima, J. M. Vasiliev, and G. G. Borisy. 2003. Mechanism of filopodia initiation by reorganization of a dendritic network. *Journal of Cell Biology* 160:409-421.
82. Tilney, L. G., P. S. Connelly, L. Ruggiero, K. A. Vranich, G. M. Guild, and D. DeRosier. 2004. The role actin filaments play in providing the characteristic curved form of *Drosophila* bristles. *Molecular Biology of the Cell* 15:5481-5491.
83. Ono, S., Y. Yamakita, S. Yamashiro, P. T. Matsudaira, J. R. Gnarra, T. Obinata, and F. Matsumura. 1997. Identification of an actin binding region and a protein kinase C phosphorylation site on human fascin. *Journal of Biological Chemistry* 272:2527-2533.

84. Yamakita, Y., S. Ono, F. Matsumura, and S. Yamashiro. 1996. Phosphorylation of human fascin inhibits its actin binding and bundling activities. *Journal of Biological Chemistry* 271:12632-12638.
85. Heintzelman, M. B., and M. S. Mooseker. 1992. Assembly of the Intestinal Brush-Border Cytoskeleton. *Current Topics in Developmental Biology* 26:93-122.

Figure Legends

Figure 1 Fiber bundles consisting of F-actin. **(A)** Ciliary bundle from the sensory epithelium of a bullfrog saccule consisting of about 60 stereocilia. Courtesy David P. Corey and John A. Assad. **(B)** Filopodium protruding from the lamellipodium of a mouse melanoma cell. Reproduced from (81) by copyright permission of The Rockefeller University Press. **(C)** Epithelial microvilli. **(D)** *Drosophila* neurosensory micro- and macrochaete bristles. Reproduced from (82) with the permission of The American Society for Cell Biology.

Figure 2 Theoretical bundle model. **(A)** Crosslinked fiber bundle with $N = 16$ fibers. Discrete crosslinks (blue) couple nearest-neighbor fibers mechanically in stretching and bending. **(B)** (left) Deformed backbone of a fiber bundle subject to in-plane bending; (middle) close-up view of three typical fibers showing fiber and crosslink deformations in (faded gray lines) decoupled and (solid black lines) fully coupled bending; (right) transverse distributions of fiber axial displacement, $u^{(k)}(x, y)$, and strain, $\varepsilon^{(k)}(x, y)$, fields and (arrows) the mean axial displacement, $\bar{u}^{(k)}(x)$, in (faded gray lines) decoupled and (solid black lines) fully coupled bending.

Figure 3 Theoretical bundle bending stiffness. **(A)** Dependence of normalized bending stiffness, $\kappa_B^* := \kappa_B / \kappa_f$, on filament number, N , for various constant values of the fiber coupling parameter, $\alpha = \{10^{-1}, 10^0, 10^1, 10^2, 10^3, 10^4\}$ (bottom to top). Thick lines denote (bottom) decoupled and (top) fully coupled bending regimes. **(B)** Dependence of κ_B^* on α at constant $N = \{4, 9, 16, \dots, 100\}$ (bottom to top). Dotted lines correspond to Timoshenko theory predictions.

Inset to Figure 3B Dependence of the crossover values, α^{**} , of the fiber coupling parameter on bundle filament number, N , at the decoupled-to-intermediate (bottom curves) and fully-coupled-to-intermediate (top curves) regime crossovers for (squares) pinned and (circles) clamped boundary conditions. Solid lines indicate N -independent and linear-in- N scaling. Crossover values of α^{**} are defined by the value of α at which κ_B is within a factor of two of its limiting decoupled and fully coupled values.

Figure 4 Experimental and theoretical bending stiffness of fascin-crosslinked F-actin bundles for $N = 27 \pm 6$. Experimental bundle stiffness (symbols) is measured using a microemulsion droplet system for a range of fascin concentrations with corresponding mean spacings, δ : (black circles) 40 nm, (blue squares) 56 nm, (red diamonds) 68 nm, (green triangles) 225 nm, (pink crosses) 412 nm as described in (29). Bundle length is varied in an uncorrelated fashion by a factor of over two. Crosslinker axial spacing is calculated using a simple Langmuir isotherm approximation, $\delta = \delta_{min} (K_d + c_{fascin}) / c_{fascin}$ (83), where $\delta_{min} = 37.5$ nm is the minimum in-plane spacing between ABPs in hexagonally-ordered F-actin bundles (30) and $K_d = 0.5 \mu\text{M}$ is the fascin-actin

dissociation constant (84). Theoretical bundle stiffness (bold curve) is calculated using Eq. (2) with $c = 5$ (Appendix I) assuming $N = 27$ and bounding curves that account for experimental uncertainty are calculated using $N = 21$ and $N = 33$.

Figure 5 Bundle bending stiffness state-diagram for various cytoskeletal bundles. Dashed lines denote crossovers between (I) decoupled, (II) shear-dominated, and (III) fully coupled bending regimes. (a) Acrosomal process of the horseshoe crab sperm cell (66); (b) vertebrate hair cell stereocilia (2, 3, 68); (c) brush-border microvilli (2, 3, 85); (d) stress fibers; (e) filopodia (16); (f) *Drosophila* neurosensory bristles (59); (g) outer pillar hair cell MT bundles (25). Spacing between ABPs is taken to be the minimal in-plane value for hexagonally-packed bundles, $\delta = 37.5$ nm (30). Extensional stiffnesses are, $E_f A_f = 4.4 \times 10^{-8}$ N and 2.6×10^{-7} N, for F-actin (40) and MTs (39), respectively.

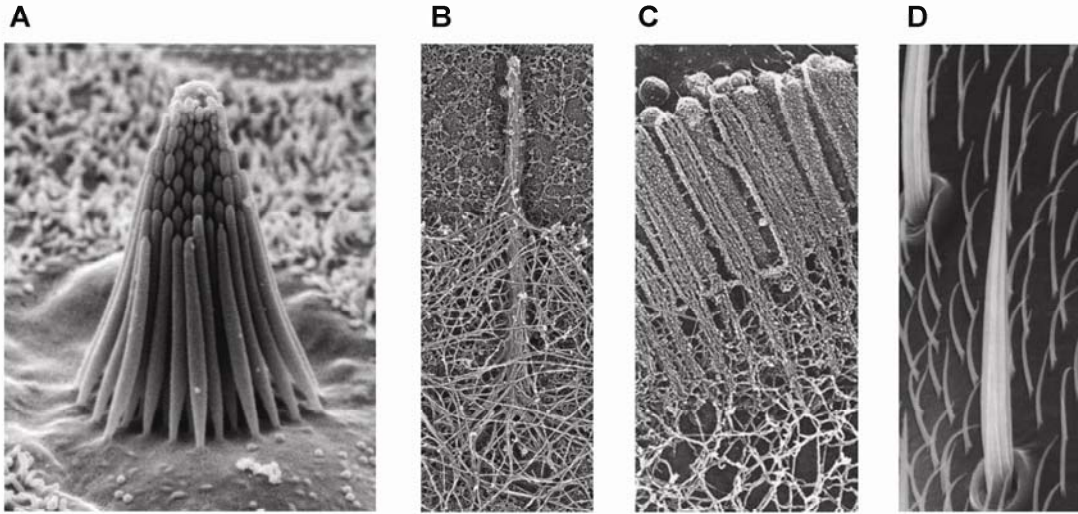


Figure 1

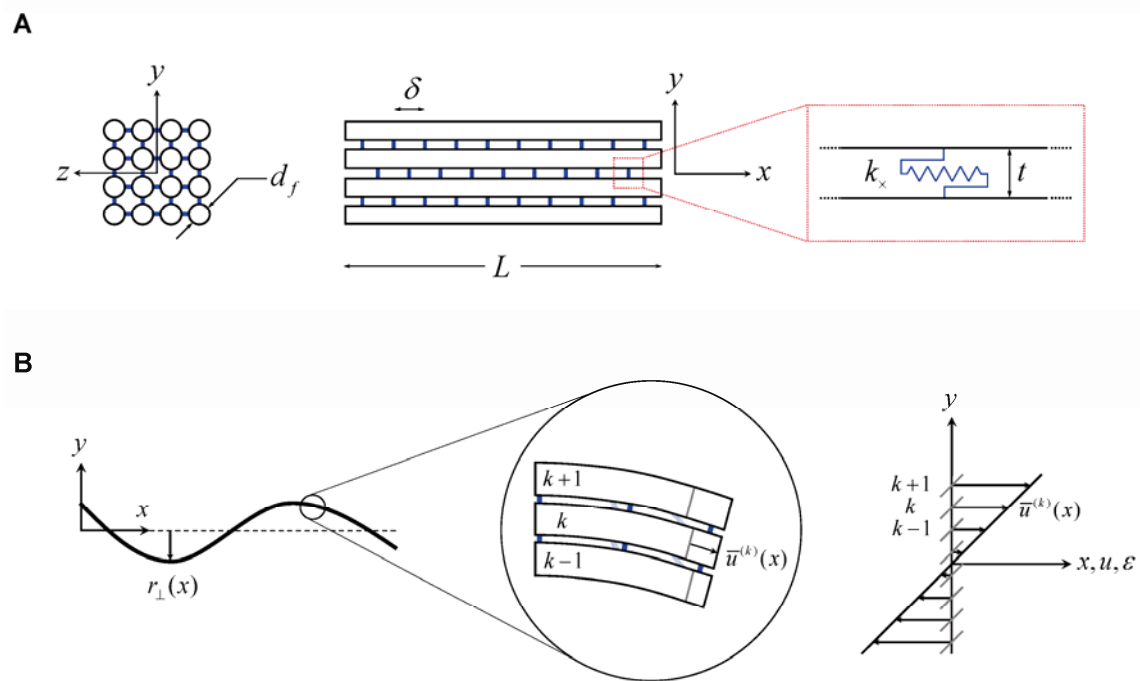
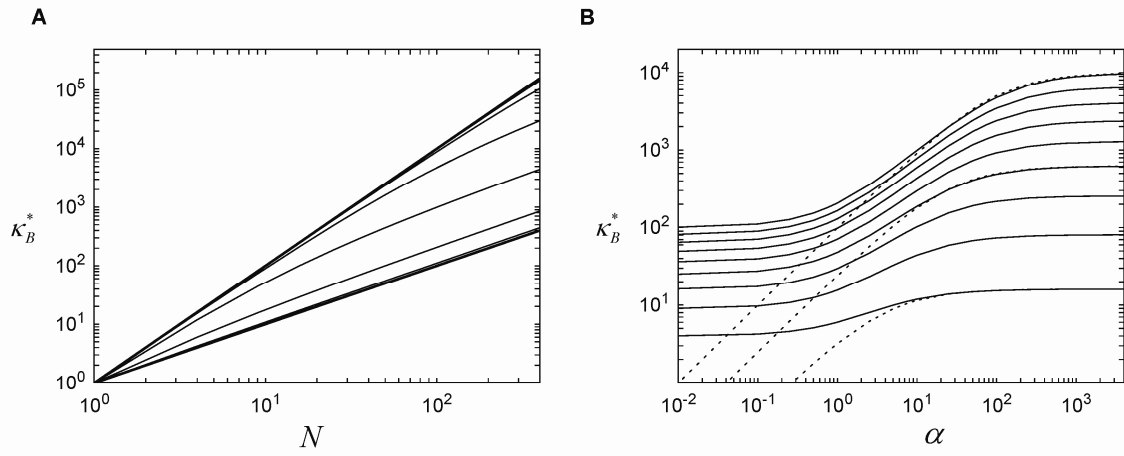


Figure 2



inset to 3B

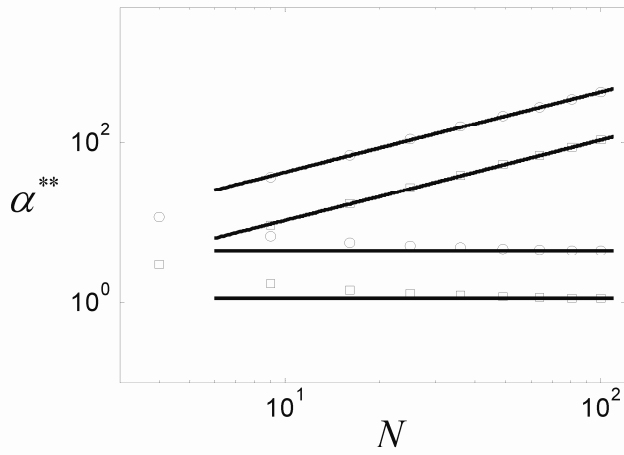


Figure 3

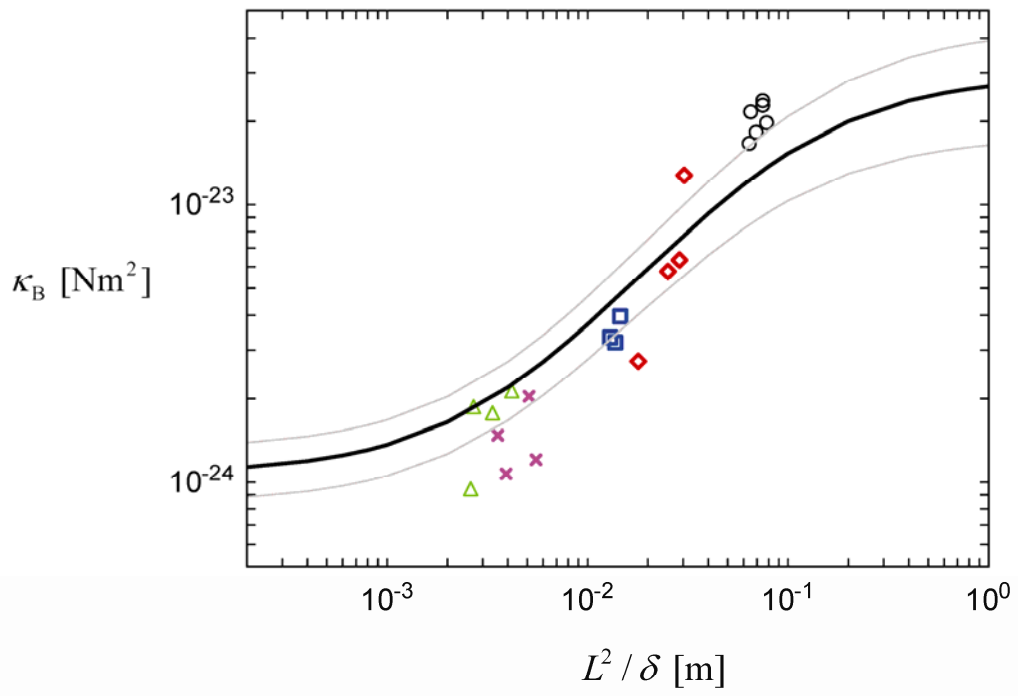


Figure 4

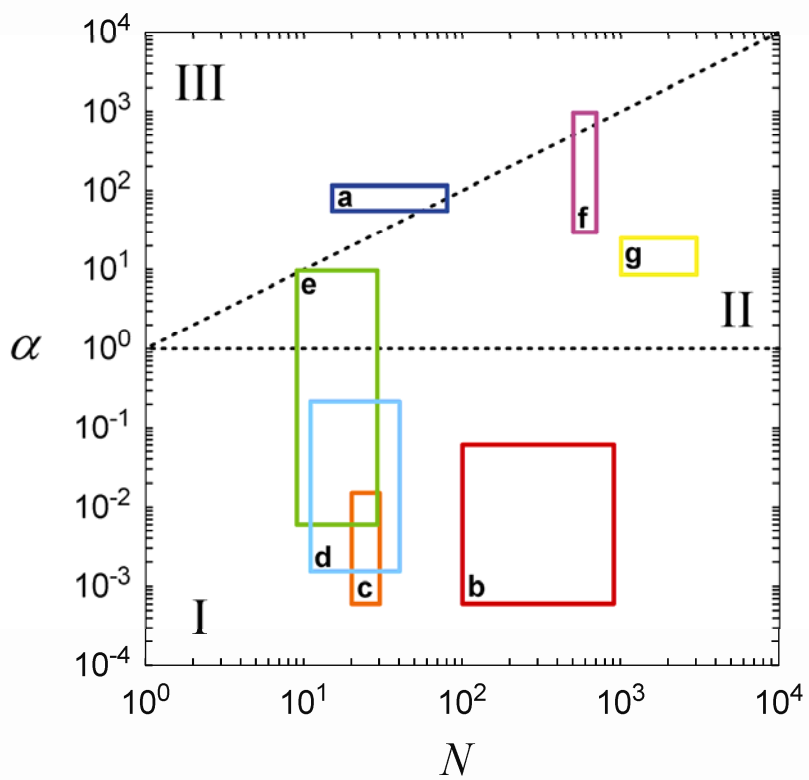


Figure 5

Supplementary Material: Effect of fiber fracture on bundle bending stiffness

Each original mother-fiber in the Finite Element model is divided into m daughter-fibers of equal length, $L_f < L$, where subdivisions on nearest-neighbor mother-fibers are randomly aligned with respect to one another. For any bundle size (M, L) we find two distinct regimes delineated by the critical ratio, $\phi^* \approx M$, where $\phi := L/L_f$ is the fracture number density per fiber. For $\phi \ll \phi^*$, the bending response of the bundle is unaffected by fiber fracture (Fig. S1). For $\phi \gg \phi^*$, however, the bundle response is strongly affected by fiber fracture and characterized by a renormalized coupling parameter $\alpha' := \alpha(\phi^*/\phi)^2$. In this regime, the bundle behaves like m smaller sub-bundles of length L_f . Fitting Eq. (2) to the numerical data by treating c as an adjustable parameter allows for the determination of ϕ^* (Fig. S2).

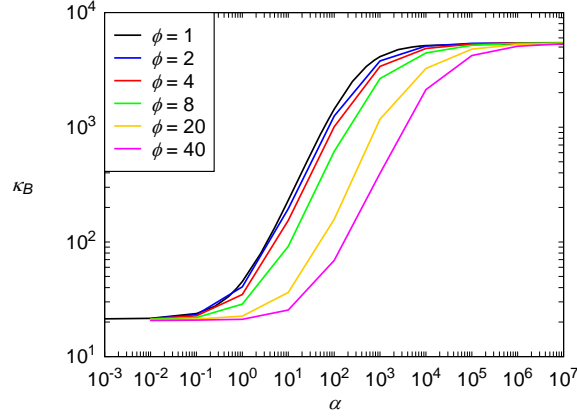


Fig. S1. Dependence of bundle bending stiffness on the fracture density, $\phi := L/L_f$, and the fiber coupling parameter, α , for $M = 8$.

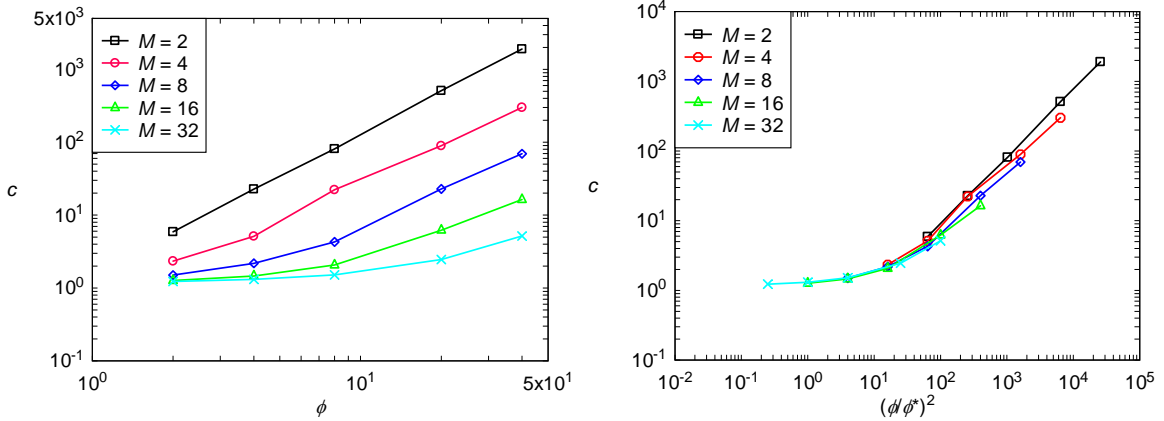


Fig. S2. Dependence of parameter c in Eq. (2) on fracture density for various bundle sizes, M . **A)** Before renormalization. **B)** After renormalization by $\phi^* = M/8$. The lack of perfect collapse in (B) and the presence of the small kinks in (A) for $M = 8$ and $M = 16$ are due to the fact that Eq. (2) is only applicable theoretically to the low-fracture-density regime, $\phi \ll \phi^*$. Above ϕ^* the

bundle consists of many sub-bundles that effectively have different boundary conditions than the original, mother-bundle.

7.2 Athermal Response

The following publications deal with the properties of stiff polymer networks at zero temperature. In “Floppy Modes and Nonaffine Deformations in Random Fiber Networks” and “Non-affine rubber elasticity for stiff polymer networks” the concept of the floppy modes is presented and discussed in detail. It is shown that the anomalous scaling properties of the elastic modulus in the random fibrous architecture, as determined by Wilhelm and Frey [82], can be reproduced with a self-consistent effective medium theory. Furthermore, a scaling analysis is presented that isolates the governing length-scale of the network.

It is argued that the floppy-mode framework is general enough to be applicable to a variety of network structures, both in two and three dimensions. In “Mechanics of Bundled Semiflexible Polymer Networks” the theory is combined with the WLB model and shown to correctly capture the macroscopic rheological properties of an experimental in-vitro system.

The article “Force distributions and force chains in random stiff fiber networks” discusses the properties of elastic forces. It contrasts with the previous publications that primarily deal with the properties of the elastic energy/modulus. Analogies are drawn with “propagation” of forces in granular media.

Floppy Modes and Nonaffine Deformations in Random Fiber Networks

Claus Heussinger and Erwin Frey

*Arnold Sommerfeld Center for Theoretical Physics and Center for NanoScience, Department of Physics,
Ludwig-Maximilians-Universität München, Theresienstrasse 37, D-80333 München, Germany*

(Received 26 March 2006; published 8 September 2006)

We study the elasticity of random fiber networks. Starting from a microscopic picture of the *nonaffine* deformation fields, we calculate the macroscopic elastic moduli both in a scaling theory and a self-consistent effective medium theory. By relating nonaffinity to the low-energy excitations of the network (“floppy modes”), we achieve a detailed characterization of the nonaffine deformations present in fibrous networks.

DOI: [10.1103/PhysRevLett.97.105501](https://doi.org/10.1103/PhysRevLett.97.105501)

PACS numbers: 62.25.+g, 81.05.Lg, 87.16.Ka

Materials as different as granular matter, colloidal suspensions, or lithospheric block systems share the common property that they may exist in a highly fragile state [1,2]. While, in principle, able to withstand static shear stresses, small changes in the loading conditions may lead to large scale structural rearrangements or even to the complete fluidization of the material [2–4]. To understand the extraordinary mechanical properties of these systems, new concepts have to be developed that go beyond the application of classical elasticity theory and that sufficiently reflect the presence of the microstructure [5]. One example is the “stress-only” approach to the elasticity of granular materials [6], where the elimination of the kinematic degrees of freedom accounts for the infinite stiffness of the grains. This seems to capture the inhomogeneous distribution of stresses in the sample and their concentration along the so-called force chains [7]. In jammed systems of soft spheres, on the other hand, fragility has recently been shown to directly affect the deformation response of the system. While it may induce anomalous deformation fields that strongly deviate from the expectations of homogeneous elasticity (“nonaffine” deformations) [8], it may also lead to a proliferation of low-frequency vibrational states far beyond the usual Debye behavior of ordinary solids [9]. It has been argued that these low-energy vibrations derive from a set of zero-frequency modes (floppy modes) that are present just below the jamming threshold [10] and relate to the ability of the structure to internally rearrange without any change in its potential energy. This concept of floppy modes has also been used in connection with elastic percolation networks where the fragile state is reached by diluting a certain fraction of nearest-neighbor contacts. In these systems, constraint-counting arguments may be used to determine the percolation transition at which the system loses its rigidity [11].

Here our focus is on a particular class of heterogeneous networks composed of cross-linked fibers. These systems have recently been suggested as model systems for studying the mechanical properties of paper sheets [12] or biological networks of semiflexible polymers [13,14].

While these networks are known to have a rigidity percolation transition at low densities [15,16], we show here that even networks in the high-density regime in many ways resemble the behavior of fragile matter, despite the fact that they are far away from the percolation threshold. We identify the relevant floppy modes and highlight their importance for understanding the macroscopic elasticity of the network. In particular, we will be able to explain the occurrence of an anomalous intermediate scaling regime observed in recent simulations [15,17,18]. In this regime, the shear modulus was found to depend on density (measured relative to the percolation threshold) as $G \sim \delta\rho^\mu$ with a fractional exponent as large as $\mu \approx 6.67$ [15]. Also, highly nonaffine deformations [17,19] as well as inhomogeneous distribution of stresses in the network have been found. Heuristic nonaffinity measures have been devised [17,19]; however, little is known about the actual nature of the deformations present. While the expression “nonaffine” is exclusively used to signal the absence of conventional homogeneous elasticity, scarce positive characterization of nonaffine deformations has been achieved up to now [20]. This Letter tries to fill this gap by characterizing in detail the nonaffine deformation field present in fibrous networks. By relating nonaffinity to the floppy modes of the structure, we can, starting from a microscopic picture, calculate the macroscopic elastic moduli in both a scaling theory and a self-consistent effective medium theory. In analogy with the affine theory of rubber elasticity for flexible polymer gels, our approach might very well serve as a second paradigm to understand the elasticity of microstructured materials. Because of the proximity to the fragile state, it might also be of relevance to force transmission in granular media and to the phenomenon of jamming.

The two-dimensional fiber network we consider is defined by randomly placing N elastic fibers of length l_f on a plane of area $A = L^2$ such that both the position and orientation are uniformly distributed. We consider the fiber-fiber intersections to be perfectly rigid but freely rotatable cross-links that do not allow for relative sliding

of the filaments. The randomness entails a distribution of angles $\theta \in [0, \pi]$ between two intersecting filaments

$$P(\theta) = \frac{\sin(\theta)}{2}, \quad (1)$$

while distances between neighboring intersections, the segment lengths l_s , follow an exponential distribution [21]

$$P(l_s) = \langle l_s \rangle^{-1} e^{-l_s/\langle l_s \rangle}. \quad (2)$$

The mean segment length $\langle l_s \rangle$ is inversely related to the line density $\rho = Nl_f/A$ as $\langle l_s \rangle = \pi/2\rho$. The segments are modeled as classical beams with cross-section radius r and bending rigidity κ . Loaded along their axis (“stretching”), such slender rods have a rather high stiffness $k_{\parallel}(l_s) = 4\kappa/l_s r^2$, while they are much softer with respect to transverse deformations $k_{\perp}(l_s) = 3\kappa/l_s^3$ (“bending”). Numerical simulations for the effective shear modulus G of this network have identified a crossover scaling scenario characterized by a length scale $\xi = l_f(\delta\rho l_f)^{-\nu}$ and $\nu \approx 2.84$ [15] that mediates the transition between two drastically different elastic regimes. For fiber radius $r \gg \xi$, the system is in an affine regime where the elastic response is dominated mainly by stretching deformations homogeneously distributed throughout the sample. The modulus in this regime is simply proportional to the typical stretching stiffness $G_{\text{aff}} \propto k_{\parallel}(\langle l_s \rangle)$ and independent of the fiber length l_f . This is in marked contrast to the second regime at $r \ll \xi$. There, only nonaffine bending deformations are excited, and the modulus shows a strong dependence on fiber length $G_{\text{na}} \propto k_{\perp}(\langle l_s \rangle)(l_f/\langle l_s \rangle)^{\mu-3}$. Using renormalization-group language, the parameters r and l_f may be viewed as scaling fields (measured in units of the “lattice constant” $\langle l_s \rangle$). The stretching dominated regime may then be characterized by an (affine) fixed point at $l_f \rightarrow \infty$ and finite radius $r \neq 0$. On the other hand, the (nonaffine) fixed point of the bending dominated regime is obtained by first letting $r \rightarrow 0$ and then performing $l_f \rightarrow \infty$. This suggests that the elastic properties in the latter regime may be analyzed at vanishing radius $r = 0$, that is, by putting the system on the stable manifold of the fixed point.

In the following, we will exploit this limit to calculate the modulus G_{na} in the nonaffine regime. Central to the analysis is the recognition that in this limit the ratio of bending to stretching stiffness $k_{\perp}/k_{\parallel} \propto r^2$ tends to zero and bending deformations become increasingly soft. We thus obtain the much simpler problem of a central-force network. However, as only two fibers may intersect at a cross-link, the coordination is $z < 4$ [22] and rigid regions may not percolate through the system [23,24]. This implies that, on a macroscopic level, the elastic moduli will be zero, while microscopically displacements can be chosen such that segment lengths need not be changed. These are the floppy modes of the structure that entail the fragility of the network in the bending dominated regime. It has been argued that a critical coordination of $z_c = 4$ is necessary to

give the network rigidity [24]. This value defines the “isostatic” point, which in our network corresponds to taking the limit $l_f \rightarrow \infty$. Thus, we arrive at the conclusion that isostaticity and the onset of rigidity seem to be intimately connected to the fixed point governing the nonaffine regime. While it is usually not possible to deduce the specific form of the floppy modes, the fibrous architecture allows for their straightforward construction (see Fig. 1). In a first step, we perform an arbitrary axial displacement δz of a given (primary) fiber as a whole. This, of course, will also affect the crossing (secondary) fibers such that the lengths of interconnecting segments change. In a second step, therefore, one has to account for the length constraints on these segments by introducing cross-link deflections $\bar{y}_i = -\delta z \cot\theta_i$ transverse to the contour of the primary fiber. As a result, all segment lengths remain unchanged to first order in δz [25]. The construction is, therefore, suitable to describe the linear response properties of the network, while at the same time it offers an explanation for the stiffening behavior found in fully nonlinear simulations [19,26]. Any finite strain necessarily leads to the energetically more expensive stretching of bonds and, therefore, to an increase of the modulus.

The identified modes take the form of localized excitations that affect only single filaments and their immediate surroundings. By superposition, we may therefore construct a displacement field that allows the calculation of macroscopic quantities such as the elastic moduli. To achieve this, we need to know the typical magnitude of displacements δz of a given fiber relative to its surroundings, the crossing secondary fibers. Since δz is defined on the scale of the complete fiber, we do not expect any dependence on average segment length $\langle l_s \rangle$, such that $\delta z \propto l_f$ remains as the only conceivable possibility. Alternatively, one may obtain the same result by assuming that the individual fiber *centers* follow the macroscopic strain

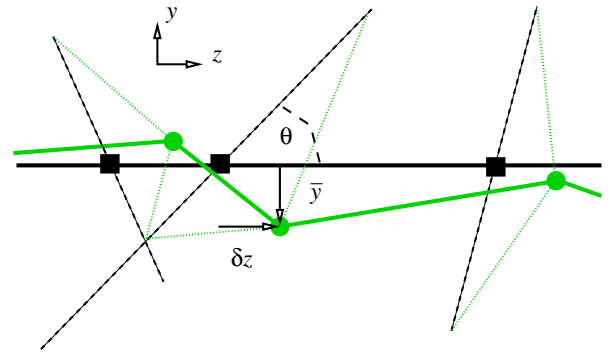


FIG. 1 (color online). Construction of a floppy mode by axial displacement δz of the primary fiber (drawn horizontally) and subsequent transverse deflection $\bar{y} = -\delta z \cot\theta$ of the cross-links to restore the segment lengths on the secondary fibers (dashed lines, possible to first order in δz). Initial cross-link positions are marked as black squares, final configurations as green circles.

field in an affine way. Then relative displacements of centers of neighboring fibers would be proportional to their typical distance. This is of the order filament length l_f and again $\delta z \propto l_f$. Note, however, that the assumption of affine displacement of the fiber centers cannot be literally true for fibers intersecting at very small angles $\theta \rightarrow 0$. To avoid a diverging transverse deflection $\bar{y}_i = -\delta z \cot \theta \rightarrow \infty$, the two fibers will most likely not experience any relative motion at all and $\delta z \rightarrow 0$. Truly affine displacements can, therefore, be established only on scales larger than the filament length. It should also be clear that the assumption of affine displacements of the fiber centers is different from the usual approach of assigning affine deformations on the scale of the single segment. The latter would lead to deformations $\delta_{\text{aff}} \propto l_s$, proportional to the length l_s of the segment. Instead, axial displacements of the fiber as a whole are, by construction of the floppy mode, directly translated into *nonaffine* deformations $\delta_{\text{na}} \propto l_f$, which do not depend on the length of the segment.

Restoring the radius r to its finite value, the floppy modes acquire energy and lead to bending of the fibers. A segment of length l_s will then typically store the energy $w_b(l_s) \simeq \kappa \delta_{\text{na}}^2 / l_s^3 \simeq \kappa l_f^2 / l_s^3$. By averaging over the segment length distribution Eq. (2), one may calculate the average bending energy $\langle W_b \rangle$, stored in a fiber consisting of $n \simeq \rho l_f$ segments,

$$\langle W_b \rangle \simeq \rho l_f \int_{l_{\min}}^{\infty} dl_s P(l_s) \frac{\kappa \delta_{\text{na}}^2}{l_s^3}. \quad (3)$$

We assume the integral to be regularized by a lower cutoff length l_{\min} that we now determine in a self-consistent manner. Physically, l_{\min} corresponds to the shortest segments along the fiber that contribute to the elastic energy. Even though we know [see Eq. (2)] that arbitrarily short segments do exist, their high bending stiffness $k_{\perp}(l_s) \propto l_s^{-3}$ makes their deformation increasingly expensive. Segments with length $l_s < l_{\min}$ will, therefore, be able to relax from their floppy mode deformation δ_{na} , thereby reducing their bending energy from $w_b(l_{\min})$ to nearly zero. However, due to the length constraints, this relaxation necessarily leads to the movement of an entire secondary fiber and to the excitation of a floppy mode there. By balancing $w_b(l_{\min}) = \langle W_b \rangle$, this gives $l_{\min} \simeq 1/\rho^2 l_f$ and for the average bending energy of a single fiber $\langle W_b \rangle \simeq \kappa / l_f (\rho l_f)^6$. This implies for the modulus $G_{\text{na}} \simeq \rho / l_f \langle W_b \rangle \propto \rho^7$, which compares well with the simulation result of $\mu = 6.67$. What is more, by equating the energy $\langle W_b \rangle$ with $\langle W_s \rangle \simeq \kappa l_f r^{-2}$ valid in the affine stretching regime, one can also infer the crossover exponent $\nu = 3$.

In summary, we have succeeded in explaining the elasticity of the bending dominated regime starting from the microscopic picture of the floppy modes that characterize directly the deformation field deep inside the nonaffine regime. Alternatively, one might try to understand the

emergent nonaffinity in a perturbative approach that considers deviations from an affine reference state. Such a line of reasoning has recently been suggested in Ref. [18], where nonaffine boundary layers, growing from the filament ends, are assumed to perturb the perfect affine order. However, comparing with their simulation data, the authors could not confirm the scaling picture unambiguously and acknowledged the need for further numerical as well as improved theoretical work [18]. Thus, nonaffine elasticity in fibrous networks appears to be intrinsically a nonperturbative strong-coupling phenomenon for which the floppy mode picture provides the correct low-energy excitations. As we will explicitly show next, one particular strength of our approach is that the scaling picture can readily be extended to a full theory that self-consistently calculates the modulus in a nonaffine effective medium theory.

To set up the theory, we consider a single filament together with its cross-links that provide the coupling to the medium. The energy of this assembly consists of two parts. First, the bending energy of the primary fiber

$$W_b[y(z)] = \frac{\kappa}{2} \int \left(\frac{\partial^2 y}{\partial z^2} \right)^2 dz, \quad (4)$$

due to a transverse deflection $y(z)$. A second stretching energy contribution arises whenever a cross-link deflection $y_i = y(z_i)$ differs from its prescribed value $\bar{y}_i = -\delta z \cot \theta_i$ and may be written in the form of an harmonic confining potential $W_s(y_i) = \frac{1}{2} k_i (y_i - \bar{y}_i)^2$ that acts individually on each of the $n \simeq \rho l_f$ cross-links. It allows the filament to reduce its own energy at the cost of deforming the elastic matrix into which it is imbedded. Performing a configura-

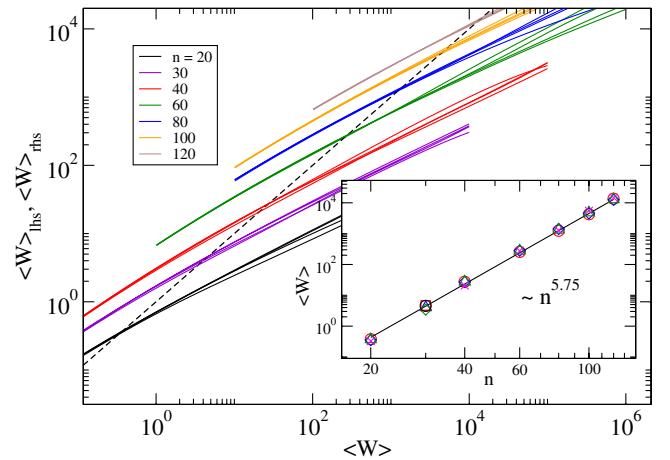


FIG. 2 (color online). Graphical solution of Eqs. (5) and (6) for various numbers n of cross-links obtained by calculating the intersection between the left side of the equation $\langle W \rangle_{\text{lhs}}$ (bisecting line, dashed curve) with the right side $\langle W \rangle_{\text{rhs}}$ (solid curves). The different curves for a given n correspond to ensembles of varying size. They seem to diverge in the limit $\langle W \rangle_{\text{rhs}} \gg \langle W \rangle_{\text{lhs}}$. In fact, there (and only there) the averaging procedure is ill-defined [26]. Inset: Resulting dependence of $\langle W \rangle$ on n .

tional average $\langle \cdot \rangle$ over cross-link positions z_i and orientations θ_i , we obtain the average elastic energy stored in a single fiber as

$$\langle W \rangle = \left\langle \min_{y(z)} \left(W_b[y(z)] + \sum_{i=1}^n \frac{k_i}{2} (y_i - \bar{y}_i)^2 \right) \right\rangle. \quad (5)$$

To solve the model, we further need to specify the stiffness $k_i = k(\theta_i)$ of the medium that relates to the relaxation mode of a cross-link on the primary filament from its floppy mode deflection. As we have argued above, any relaxation of this kind must act as axial displacement on a secondary fiber, thus exciting a new floppy mode there. The energy scale associated with this is $\langle W \rangle$ such that we can write

$$k(\theta_i) = 2\langle W \rangle \frac{\sin^2(\theta_i)}{\delta z^2}, \quad (6)$$

where the angular dependence derives from the projection onto the axis of the secondary filament. Equations (5) and (6) represent a closed set of equations to calculate the configurationally averaged deformation energy $\langle W \rangle$ as a function of the number of cross-links n . In implementing this scheme, we have generated ensembles of filaments with a distribution of cross-linking angles as given by Eq. (1) and segment lengths according to Eq. (2). Note that there is no free parameter in this calculation. The equations are solved graphically in Fig. 2 by plotting both sides of Eq. (5) as a function of $\langle W \rangle$. The point of intersection, which solves the equation, is shown in the inset as a function of the number of cross-links n . For the same parameter window as used in the network simulations [15], it yields the scaling behavior of $\langle W \rangle \propto n^{5.75}$. This implies for the modulus the exponent of $\mu = 6.75$, which improves upon the simple scaling picture presented above and provides a very accurate calculation of the scaling exponent μ .

In conclusion, we have succeeded in deriving the macroscopic elasticity of random fibrous networks starting from a microscopic description of the displacement field in a manner that does not rely on the notion of affine deformations. We have given a floppy mode construction that may be applied to any two- or three-dimensional network with fibrous architecture, for example, paper or biological networks of semiflexible filaments. It may also be shown to be relevant to systems where the constraint of straight fibers is relaxed [26]. The unusually strong density dependence of the modulus found here is a consequence of the exponential segment length distribution Eq. (2) and the presence of the length scale l_{\min} . While identification of the floppy modes has been recognized to be highly important for a description of force transmission in granular media or the jamming transition in colloidal systems, one can rarely give the exact form of these zero-energy excitations. On the contrary, we have achieved an explicit construction of

the floppy modes that can be put in the form of localized elementary excitations affecting only single filaments and their immediate surroundings.

It is a pleasure to acknowledge fruitful discussions with David Nelson and Mikko Alava.

-
- [1] *Soft and Fragile Matter*, edited by M. E. Cates and M. R. Evans (Institute of Physics, London, 2000).
 - [2] A. Soloviev and A. Ismail-Zadeh, in *Nonlinear Dynamics of the Lithosphere and Earthquake Prediction*, edited by V. I. Keilis-Borok and A. Soloviev (Springer, Berlin, 2003).
 - [3] M. E. Cates, J. P. Wittmer, J.-P. Bouchaud, and P. Claudin, *Phys. Rev. Lett.* **81**, 1841 (1998).
 - [4] E. I. Corwin, H. M. Jaeger, and S. Nagel, *Nature (London)* **435**, 1075 (2005).
 - [5] S. Alexander, *Phys. Rep.* **296**, 65 (1998).
 - [6] J. P. Wittmer, P. Claudin, M. E. Cates, and J.-P. Bouchaud, *Nature (London)* **382**, 336 (1996).
 - [7] J.-P. Bouchaud, P. Claudin, D. Levine, and M. Otto, *Eur. Phys. J. E* **4**, 451 (2001).
 - [8] A. Tanguy, J. P. Wittmer, F. Leonforte, and J.-L. Barrat, *Phys. Rev. B* **66**, 174205 (2002).
 - [9] L. E. Silbert, A. J. Liu, and S. R. Nagel, *Phys. Rev. Lett.* **95**, 098301 (2005).
 - [10] M. Wyart, S. R. Nagel, and T. A. Witten, *Europhys. Lett.* **72**, 486 (2005); *Ann. Phys. (Paris)* **30**, 1 (2005).
 - [11] D. J. Jacobs and M. F. Thorpe, *Phys. Rev. Lett.* **75**, 4051 (1995).
 - [12] M. Alava and K. Niskanen, *Rep. Prog. Phys.* **69**, 669 (2006).
 - [13] A. Bausch and K. Kroy, *Nature Phys.* **2**, 231 (2006).
 - [14] C. Heussinger and E. Frey, *Phys. Rev. Lett.* **96**, 017802 (2006); *cond-mat/0512557*.
 - [15] J. Wilhelm and E. Frey, *Phys. Rev. Lett.* **91**, 108103 (2003).
 - [16] M. Latva-Kokko and J. Timonen, *Phys. Rev. E* **64**, 066117 (2001).
 - [17] D. A. Head, A. J. Levine, and F. C. MacKintosh, *Phys. Rev. Lett.* **91**, 108102 (2003).
 - [18] D. A. Head, A. J. Levine, and F. C. MacKintosh, *Phys. Rev. E* **68**, 061907 (2003).
 - [19] P. R. Onck, T. Koeman, T. van Dillen, and E. van der Giessen, *Phys. Rev. Lett.* **95**, 178102 (2005).
 - [20] B. A. DiDonna and T. C. Lubensky, *Phys. Rev. E* **72**, 066619 (2005).
 - [21] O. Kallmes and H. Corte, *Tappi* **43**, 737 (1960).
 - [22] Because of the finite fiber length, there are also two- and threefold coordinated cross-links.
 - [23] M. Kellomäki, J. Åström, and J. Timonen, *Phys. Rev. Lett.* **77**, 2730 (1996).
 - [24] J. C. Maxwell, *Philos. Mag.* **27**, 294 (1864).
 - [25] A similar construction holds in 3D, where, in addition, each cross-link acquires a floppy “out-of-plane” degree of freedom.
 - [26] C. Heussinger and E. Frey (to be published).

Non-affine rubber elasticity for stiff polymer networks

Claus Heussinger, Boris Schaefer, and Erwin Frey

Arnold-Sommerfeld Center for Theoretical Physics and Center for NanoScience,
Department of Physics, Ludwig-Maximilians-Universität München,
Theresienstrasse 37, D-80333 München, Germany

(Dated: November 26, 2007)

We present a theory for the elasticity of cross-linked stiff polymer networks. Stiff polymers, unlike their flexible counterparts, are highly anisotropic elastic objects. Similar to mechanical beams stiff polymers easily deform in bending, while they are much stiffer with respect to tensile forces (“stretching”). Previous approaches have based network elasticity on the central-force stretching mode, in a manner similar to classical rubber elasticity for flexible polymers. In contrast, our theory properly accounts for the soft bending response inherent to any stiff polymer network. A self-consistent effective medium approach is used to calculate the macroscopic elastic moduli starting from a microscopic characterization of the deformation field in terms of “floppy modes” – low-energy bending excitations that retain a high degree of non-affinity. The length-scale characterizing the emergent non-affinity is given by the “fiber length” l_f , defined as the scale over which the polymers remain straight. The calculated scaling properties for the shear modulus are in excellent agreement with the results of recent simulations obtained in two-dimensional model networks. Furthermore, our theory can be applied to rationalize bulk rheological data in reconstituted actin networks.

PACS numbers: 62.25.+g, 87.16.Ka, 81.05.Lg

I. INTRODUCTION

The elasticity of flexible polymer gels is successfully described by the theory of rubber elasticity [1]. It ascribes the resistance to deformation to a reduction of conformational entropy induced by a changing end-to-end distance of individual polymer strands. In the classic approach, developed by Kuhn and others [2], the magnitude of the deformation of a single constituent polymer is usually assumed to derive from the macroscopically induced strain in an affine way. With this assumption the network problem is reduced to calculating the response of a single chain. In this sense affine deformations represent a mean-field assumption that neglects spatial correlations and therefore the coupling between the network structure (“architecture”) and the mechanical properties of its constituents.

In recent years a different class of cross-linked networks made of semiflexible or stiff polymers have gained widespread interest. Their importance for biological systems as the cytoskeleton or extra-cellular matrix makes understanding their properties highly rewarding [3]. Out of the variety of biological stiff polymers, F-actin has emerged as a model system, which allows precise *in vitro* rheological measurements, for example in determining the (complex) frequency-dependent shear modulus $G(\omega)$ and in particular its elastic component, the plateau modulus G_0 at intermediate frequencies. In these experiments various types of cross-linking proteins are being used [4, 5, 6, 7] and the influence of the degree of cross-linking on the elastic modulus is investigated.

Stiff polymers, unlike their flexible counterparts, are highly anisotropic in their elastic response and may be characterized in terms of two qualitatively different deformation modes (see Fig. 1) [8, 9]. The linear response to

longitudinal forces acting parallel to the contour (stretching/compression), is due to the presence of thermally excited undulations similar to the (isotropic) stiffness of flexible polymers. The resulting effective spring constant of a stiff polymer of contour length l_s , $k_{\parallel} \sim l_p/l_s^4$, depends on the temperature-dependent persistence length $l_p \sim T^{-1}$, which indicates the entropic origin. On the other hand, the resistance of the polymer to *transverse* forces (bending) is predominantly an energetic effect, leading to an increase in energy rather than to a decrease in entropy. Subsequently, the corresponding spring constant $k_{\perp} \sim l_s^{-3}$ is independent of temperature.

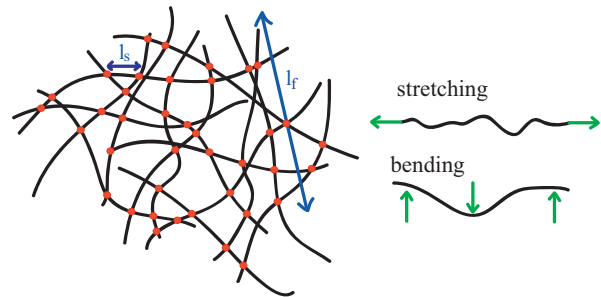


FIG. 1: Sketch of a stiff polymer network with filaments which are straight on a scale l_f and where the distances between crosslinks (“polymer segments”) on a given filament is denoted by l_s . The response of the constituent stiff polymers to external forces is anisotropic with spring constants k_{\parallel} and k_{\perp} , characterizing their resistance to stretching and bending deformations, respectively.

The presence of two elementary deformation modes complicates, but also enriches, the theoretical analysis of stiff polymer networks since it is not obvious which of the modes, or combination thereof, will dominate the macro-

scopic elastic response [10, 11]. Leaving aside these difficulties, recent approaches [9, 12, 13] have still adopted straightforward extensions of rubber elasticity to stiff polymer networks by assuming affine deformations to be present down to the scale of the individual polymer segment – the part of a polymer filament that connects two neighbouring cross-links (see Fig.1). In these models no bending deformations are present, leaving the stretching mode as the only possible source of elasticity.

In many systems of interest, however, the large value of the persistence length $l_p/l \gg 1$ calls this affine approach into question. This separation of length scales implies that the bending mode is in fact soft as compared to the stretching mode, since $k_{\parallel}/k_{\perp} \sim l_p/l \gg 1$. One would therefore expect the elastic energy to be dominated by low-energy bending deformations instead of highly expensive stretching modes [14]. Interestingly, recent simulations on random fibrous networks have shown that this is not always the case [10, 11, 15, 16, 17]. There, it was found that in networks with infinitely long filaments (for fixed density) the soft bending mode is suppressed and the elastic modulus is entirely given in terms of the stiffer stretching mode, similar to springs connected in parallel. In contrast, the same simulations performed in the more realistic situation of finite filament length have indeed identified an elastic regime that is dominated by soft bending deformations. The filament length thus strongly influences the elastic properties and is crucial for understanding the observed behaviour. The affine theory, by working on the smaller scale of the polymer segments, is incapable of accounting for these effects.

In the present article we expand on our recent publication [18] to develop an elastic theory that works on the scale of the whole polymer filament. The theory naturally explains the presence of a bending dominated regime as well as its suppression with increasing filament length. It is expected to be applicable to a broad class of filamentous networks with a soft bending mode.

Similar to the classic theory of rubber elasticity it assumes that the cross-links adjust to the macroscopically applied strain without showing thermal fluctuations. In contrast to rubber elasticity, however, the cross-link movements are chosen such that the polymer end-to-end distances are kept unchanged. This automatically avoids energetically highly expensive stretching deformations and results in elastic moduli that derive from the soft bending mode only.

In the following, we assume that stiff polymers, characterized by $k_{\parallel}/k_{\perp} \gg 1$, effectively behave as if they were strictly inextensible bars, i.e. having an infinite stretching stiffness $k_{\parallel} \rightarrow \infty$. Subsequently, we will construct sets of “admissible” cross-link displacements that respect this inextensibility and thus retain a highly non-affine character. These displacement modes are referred to as “floppy modes” [19], highlighting the fact that in an equivalent network of central force springs they would carry no energy. Here, the finite bending stiffness of the polymers associates an elastic energy to each mode,

which we use to calculate the macroscopic elastic constants of the network.

Section II will be concerned with the analysis of networks in the limit of diverging stretching stiffness $k_{\parallel} \rightarrow \infty$, which allows us to treat stiff polymers as inextensible bars. We will introduce the concept of the floppy modes and give an explicit construction valid for a broad class of network architectures.

In Section III we discuss the energy involved with exciting floppy modes in networks of stiff polymers, characterized by a finite, but soft, bending stiffness. Specifically, we will develop a theory that allows to calculate the network elastic constants in a self-consistent manner.

Section IV is devoted to the specific architecture of random fibrous networks in a planar geometry (two dimensional), where we check our ideas against simulations.

II. FLOPPY MODES

Here, we are concerned with some general properties of networks of inextensible bars, so called frameworks. While the bars are assumed to be perfectly rigid, they are allowed to freely rotate at the cross-links (“vertices”). In effect, both the stretching and the bending mode are eliminated, which leaves us with a purely geometric problem. By applying methods from rigidity theory [19] we will find that polymer networks when viewed as frameworks are not rigid and possess zero-energy deformation modes (“floppy modes”), for which we will give an explicit geometric construction. These modes, which may be viewed as the analog of the zero-energy shear modes of regular square lattices, characterize the deformation field of the network under external strain. By accounting for the finite bending stiffness of the polymers, they are used to calculate the elastic energy stored in polymer networks and thus the elastic moduli.

A. Maxwell counting

It has first been realized by Maxwell [20] that a framework, consisting of v vertices and b bars, can undergo a transition from a floppy to a rigid state by increasing the coordination number z . Assuming that each bar represents an independent constraint for the total of dv degrees of freedom in d spatial dimensions, Maxwell derived the condition $b - dv = 0$ determining the rigidity transition. As the number of vertices can be rewritten in terms of the coordination number as $v = 2b/z$, this immediately yields a critical coordination of $z_c = 2d$. According to this simple *Maxwell counting rule*, frameworks are rigid, whenever their vertices have more than z_c neighbors, while they will be floppy and allow for internal rearrangements otherwise.

With regard to stiff polymer networks this transition may be used to set up a classification where the elastic energy is dominated by either bending or stretching

modes. While for $z < z_c$ bending modes can stabilize the otherwise floppy (zero-energy) central-force network, they only provide minor contributions to the energy once $z > z_c$. The honeycomb lattice in 2d, for example, has a coordination of $z = 3$ and is therefore bending dominated, while the triangular lattice with $z = 6$ is clearly rigid and therefore stretching dominated. Imposing a deformation necessarily leads to the stretching of bonds. A particular case is the square lattice in two dimensions, which has precisely the critical coordination $z = z_c = 4$. Although being floppy with respect to shear deformations, the network may be stabilised by introducing suitable boundary constraints or by adding additional bars along the diagonals of some of the squares. It turns out that in the limit of infinite system size a non-extensive number of diagonal bars (which scales as the square root of the system size) is needed to stabilise the network [21].

Maxwell-counting is only approximate, since one can always add redundant bars that do not constrain any degrees of freedom. This effect is taken into account by the modified Maxwell relation $b - dv = s - m$ [22]. In this picture redundant bars create overconstrained regions where a total of s states of self-equilibrated internal stresses may exist. In general, a state of self-stress is defined as a set of bar tensions that is in static equilibrium with zero external force applied. At the same time underconstrained regions arise that allow for m zero energy deformation modes, i.e. internal rearrangements that can be accommodated without changing the lengths of any of the bars to first order in the magnitude of the imposed strain. These are usually referred to as mechanisms or floppy modes.

In principle, the floppy modes of a pin-jointed structure may be found by studying the kinematic matrix \mathbf{C} which relates vertex displacements \mathbf{d} to segment extensions $\mathbf{e} = \mathbf{C}\mathbf{d}$ [23]. The kinematic matrix thus constitutes a *linear* relation between displacements and extensions, which is only true for infinitesimally small displacements. The entries to the matrix can then easily be identified by considering the extension of a single bar oriented (in two dimensions) at an angle ϕ to the horizontal. For given displacements $\mathbf{d}_i = (u_i, v_i)$ at the two vertices $i = 1, 2$ the extension is found as

$$e = (u_2 - u_1) \cos \phi + (v_2 - v_1) \sin \phi. \quad (1)$$

The floppy modes then correspond to those vertex displacements that do not lead to any extensions in the bars. This amounts to calculating the null-space of the matrix, i.e. $\mathbf{C}\mathbf{d}_0 = \mathbf{0}$.

An elementary but illustrative example of a bar/joint network (adopted from Ref. [24]) is the “chair” shown in Fig. 2a. Having $b = 4$ bars and $v = 2$ vertices, Maxwell’s counting rule would imply that the structure is marginally rigid. Actually, there is also one floppy mode $m = 1$ as well as one state of self-stress $s = 1$. The former corresponds to the (infinitesimal) movement of the horizontal bar forming the seat, while the latter corresponds to a tension in the two vertical bars making the back.

For regular systems it is sometimes possible to guess

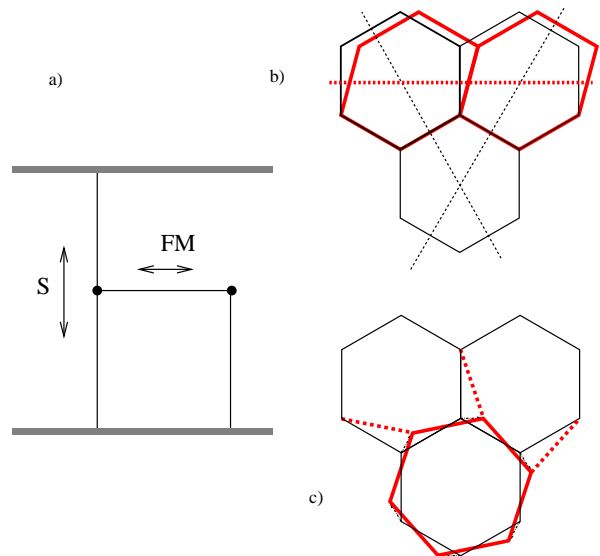


FIG. 2: Illustration of the floppy modes. The “chair” in a) has one floppy mode (FM) corresponding to the axial movement of the horizontal bar, as well as one state of self-stress (S) located in the two vertical bars. The floppy modes of the honeycomb lattice may be constructed, b) from the global shear deformations along any of the three dashed lines (as well as their parallels), or, c) from localized librations.

the modes. Consider, for the purpose of illustration, a honeycomb lattice in two dimensions, where a coordination of $z = 3$ implies $b - 2v = -v/2$. There is, accordingly, half a floppy mode per vertex. These modes are most easily identified with shear deformations along lines of symmetry (Fig. 2b). Probing the shear response of the honeycomb along a given direction will cause each of the N layers of cells to be displaced by a small amount δ , which eventually has to add up to the externally imposed deformation $\Delta = N\delta$. Thus, there is “sharing” of the deformations between the individual cells and each layer contributes a small amount to fulfilling the constraints imposed by the macroscopical strain field. In other words, the deformation field in the honeycomb lattice is affine down to the scale of the individual cell, which experiences deformations $\delta = \Delta/N \propto l_{\text{cell}}$ proportional to its own size.

Another possibility to construct the floppy modes of the honeycomb network is given by the librations of individual hexagons [25] (see Fig. 2c). These librations are, in contrast to the shear displacements, localized modes that are confined to a single cell and its immediate surroundings. Since there is one libration per cell and each of the six corresponding vertices belongs to three cells, this also makes one mode for every two vertices.

B. Floppy modes of stiff polymer networks

Proteins used to cross-link stiff polymers into networks often have only two heads [26] such that there can only be two-, three- and four-fold connected vertices. The average coordination number in stiff polymer networks is therefore $z < 4$, which would place it below the rigidity transition and render the network bending dominated.

In contrast to the very regular structures discussed above, stiff polymer networks are usually highly random. Nevertheless, as we will see below, the floppy modes can be constructed quite easily on scales l_f over which the undeformed polymers can be assumed to be represented by straight fibers. For isolated polymers the length-scale l_f can be identified with the persistence length l_p , while in networks the origin may be different and for example a consequence of the network generating process itself. It is the presence of the length-scale l_f which renders the structure of stiff polymer networks qualitatively different from flexible polymer gels. The resulting fibrous appearance may be inspected in the figures of Refs. [27, 28, 29]. We have recently argued that the “fiber length” l_f plays the role of the size of an effective unit cell [11]. This has to be contrasted to flexible polymer gels, where the unit size is set by the mesh-size. In the following we use the word “fiber” in connection with the length l_f over which the polymer remains straight. In later sections we will introduce a simple model system where fiber and polymer length are equal.

Consider (see Fig. 3a,b) a single (primary) fiber α of length l_f , which may be part of a longer polymer. It is imbedded into a network of other (secondary, tertiary, ...) fibers. Secondary fibers α_i are assumed to intersect the primary fiber α at the crosslinks $i = 1 \dots n_{cl}$, while tertiary fibers only intersect secondary fibers, e.t.c. The floppy-mode construction proceeds in two stages during which only the crosslinks on the primary fiber are being moved. The rest of the network, in particular the neighbouring secondary filaments will remain static such that the floppy mode stays highly localized similar to the librations of the hexagons discussed above. In the first step, we perform a small axial displacement δz_α of the primary fiber α as a whole. The axial movement of the cross-links pertaining to this fiber induces a change in length of all neighbouring segments on the crossing secondary fibers. In the second step, therefore, one has to account for the length constraints on these segments by introducing cross-link deflections $\bar{\mathbf{y}}_{\alpha,i}$ transverse to the primary fiber. It turns out that to *first order* in δz_α all segment lengths can be kept at their repose length by choosing

$$\bar{\mathbf{y}}_{\alpha,i} = -\delta z_\alpha \cot \theta_{\alpha,i} \hat{\mathbf{e}}_{\alpha,i} + \bar{\mathbf{y}}_{\alpha,i}^\perp, \quad (2)$$

where $\theta_{\alpha,i}$ is the angle between the two crossing fibers α and α_i at crosslink i . We denote by $\hat{\mathbf{e}}_{\alpha,i}$ a unit vector transverse to the primary fiber lying in the plane spanned by the two fibers, and by $\bar{\mathbf{y}}_{\alpha,i}^\perp$ an arbitrary vector perpendicular to this plane.

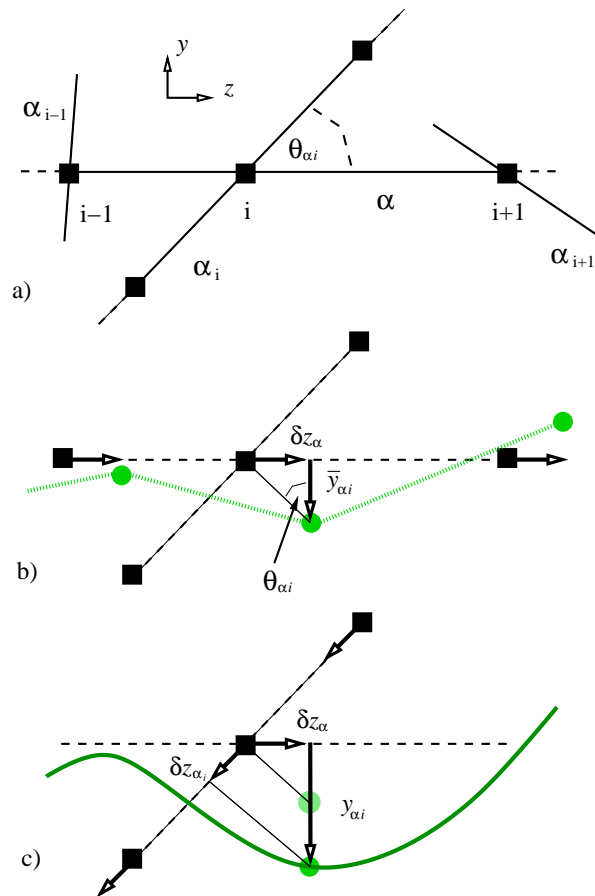


FIG. 3: Construction of a floppy mode starting from the initial geometry as drawn in a). In b), the horizontal fiber is moved, while the surrounding fibers remain in their original positions. This leads to the new cross-link positions (green circles) with transverse deflection $\bar{y}_{\alpha,i} = -\cot \theta_{\alpha,i} \delta z_\alpha$ (Eq. (2)). The component $\bar{\mathbf{y}}_{\alpha,i}^\perp$ (not drawn) is oriented perpendicular to the plane of the two fibers. In c), also the secondary fiber is moved, such that the cross-link is now deflected according to $y_{\alpha,i} = \bar{y}_{\alpha,i} + \delta z_{\alpha,i} / \sin \theta_{\alpha,i}$ (Eq. (3)). The solid green line represents the actual contour of the deformed fiber obtained by minimizing the bending energy along the entire fiber (see Eq. (5)).

We would like to emphasize that the construction only works for infinitesimal δz_α , while finite displacements necessarily lead to changes in bond lengths and therefore to stretching of bonds. As will be explained in more detail in Section IV A this has dramatic consequences on the nonlinear elasticity of the network, leading to strong strain stiffening behaviour.

The construction can be performed for any of the $\alpha = 1, \dots, N_f$ fibers, such that precisely N_f floppy modes are identified this way [42]. For the mode localized around fiber α one may define a vector $\mathcal{Y}_\alpha = (0, \dots, \bar{\mathbf{y}}_{\alpha,1}, \dots, \bar{\mathbf{y}}_{\alpha,n_{cl}}, 0, \dots)$, where the deflections of all crosslinks in the network are combined. It has nonzero components only at crosslinks belonging to fiber α . With

respect to the standard vector scalar product one can then show that the set of floppy modes $\{\mathcal{Y}_\alpha\}$ is linearly independent, however, not orthogonal. Since a given crosslink i always belongs to two filaments at the same time, there is obviously a coupling between the two corresponding modes.

In analogy to the shear modes of the honeycomb lattice one may also construct extended floppy modes for the fibrous network by superposition of the different \mathcal{Y}_α . This amounts to relaxing the constraint that a single fiber moves in a static environment where neighbouring fibers remain fixed to their initial positions. Instead, a different δz_α is assigned to each of the $\alpha = 1, \dots, N_f$ fibers. In this case, we find (see Fig. 3c) that the crosslink deflection $\bar{y}_{\alpha,i}$ of Eq. (2) has to be modified by a term $\delta z_{\alpha_i} / \sin \theta_{\alpha,i}$ due to the additional movement δz_{α_i} of the neighbouring filament α_i at crosslink i . This amounts to the overall deflection

$$\mathbf{y}_{\alpha,i} = \bar{\mathbf{y}}_{\alpha,i} + \frac{\delta z_{\alpha_i}}{\sin \theta_{\alpha,i}} \hat{\mathbf{e}}_{\alpha,i}. \quad (3)$$

For the particular architecture of a random fiber network in two dimensions (2d), to be introduced below (see Section IV), we have also obtained an orthonormal set of floppy modes. The appropriate values of $\mathbf{y}_{\alpha,i}$ and δz_α are found by performing a singular value decomposition of the compatibility matrix \mathbf{C} . One of the modes is visualized in Fig. 4, where the black lines indicate the floppy-mode displacements of the crosslinks. One remarkable property is the heterogeneous distribution of amplitudes x , which leads to polynomial tails in the probability distribution, $P(x) \sim x^{-3}$ (see Fig. 5). The exponent is a direct consequence of the random orientation of the filaments which induces a probability distribution of angles θ between two intersecting filaments, $P(\theta) \sim \sin \theta$ [43]. By a transformation of variables to the floppy mode deflection $\bar{y} \sim \cot \theta$ (and thus to x) one finds a distribution $P(\bar{y}) \sim \sin^3 \theta(\bar{y}) \rightarrow \bar{y}^{-3}$, where the latter limit corresponds to large $\bar{y} \gg 1$.

III. ENERGY OF FLOPPY MODES

Having constructed the floppy modes of the fibrous polymer network we now proceed to determine the energy associated with their excitation.

A. Effective medium theory

We calculate the response of the network to the axial movement δz_α of only one fiber α . This proceeds by first calculating the energy stored in the primary fiber, given that the surrounding fibers are not allowed to move. Subsequently, we will relax this constraint and also account for the energy induced in the secondary (tertiary, ...) fibers. We will find that infinitely many levels of neigh-

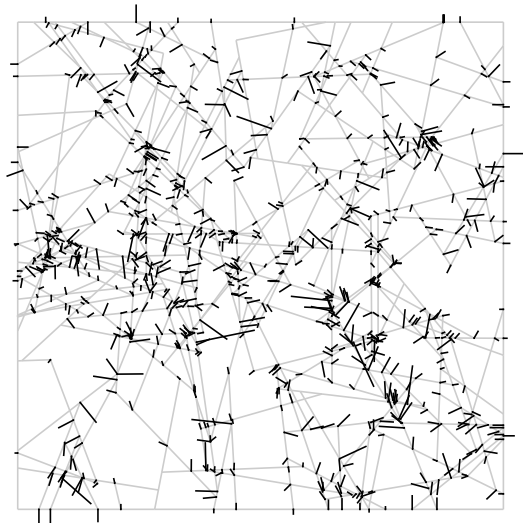


FIG. 4: Floppy mode of a random fiber network with 225 fibers (see Sect. IV). A fiber has the length of one third of the system size. Grey lines represent the network, black lines the floppy mode displacements. Note, that the overall amplitude of the mode is arbitrary.

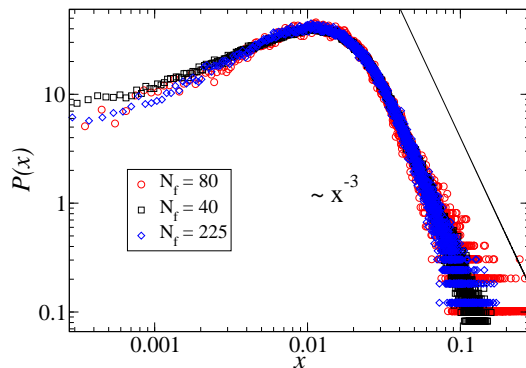


FIG. 5: Normalized probability distributions of absolute values of floppy mode displacements, as shown in Fig. 4. The distributions for different fiber numbers N_f can be rescaled on a single master curve by changing the overall amplitude of the modes.

boring fibers can be included by a formal resummation of the energy terms in a Cayley-tree approximation.

Quite generally, the bending energy of a polymer fiber with weakly undulating contour can be written as

$$W_b[\mathbf{y}_\alpha] = \frac{\kappa}{2} \int_0^{l_f} \left(\frac{d^2 \mathbf{y}_\alpha}{ds^2} \right)^2 ds, \quad (4)$$

where $\mathbf{y}_\alpha = \mathbf{y}(s_\alpha)$ denotes the transverse deflection at point s_α along the backbone of the polymer α . The bending rigidity κ is related to the persistence length by $\kappa = l_p k_B T$. The actual value of the energy contained in a localized floppy mode of amplitude δz_α can then be found by minimizing W_b for the given set of crosslink positions

$\mathbf{y}(s_{\alpha,i}) \stackrel{\perp}{=} \bar{\mathbf{y}}_{\alpha,i}$ (taken from Eq. (2)), and gives

$$W_0(\delta z_\alpha) = \min_{\mathbf{y}(s_\alpha), \mathbf{y}(s_{\alpha,i})=\bar{\mathbf{y}}_{\alpha,i}} W_b[\mathbf{y}_\alpha]. \quad (5)$$

Technically, this is achieved by performing a cubic spline interpolation through the set of points $\{(s_{\alpha,i}, \bar{\mathbf{y}}_{\alpha,i})\}_{i=1, \dots, n_{cl}}$. This can be shown to be equivalent to the minimization of the bending energy in Eq. (4) [30]. As $d^3 \mathbf{y}_{\alpha,i}/ds^3$ is proportional to the transverse force in the fiber, the discontinuities of the cubic spline in its third derivative reflect the external transverse force that is needed to keep the fiber in its deformed shape.

Now, we assume that neighbouring secondary fibers are free to react to the movement of the primary fiber. This allows the fiber deflection $\mathbf{y}_{\alpha,i}$ to be different from $\bar{\mathbf{y}}_{\alpha,i}$ and may lead to a reduction of the bending energy on the primary fiber, however, at the cost of deforming the surrounding, i.e. by spreading the mode to the neighbouring filaments. The amplitudes of the so generated secondary floppy modes may be found from solving Eq. (3) for δz_{α_i} . We thus find

$$\delta z_{\alpha_i} = \sin \theta_{\alpha,i} (\mathbf{y}_{\alpha,i} - \bar{\mathbf{y}}_{\alpha,i}) \cdot \hat{\mathbf{e}}_{\alpha,i}. \quad (6)$$

which highlights the fact that a secondary mode of amplitude δz_{α_i} occurs when the actual transverse deflection $\mathbf{y}_{\alpha,i}$ is different from the floppy-mode prescription $\bar{\mathbf{y}}_{\alpha,i}$. Furthermore, due to the scalar product with $\hat{\mathbf{e}}_{\alpha,i}$, the displacement \mathbf{y}_i^\perp perpendicular to the plane defined by the two intersecting polymers does not contribute, $\mathbf{y}_{\alpha,i}^\perp \cdot \hat{\mathbf{e}}_{\alpha,i} = 0$.

With Eq. (6) we find that Eq. (5) has to be modified by the bending energy contribution W_0 from the neighbouring filaments giving

$$W_1(\delta z_\alpha) = \min_{\mathbf{y}(s_\alpha)} \left(W_b[\mathbf{y}_\alpha] + \sum_{i=1}^{n_{cl}} W_0(\delta z_{\alpha_i}) \right). \quad (7)$$

Unlike in Eq. (5), where the crosslink variables on the primary fiber were constrained to be $\mathbf{y}(s_{\alpha,i}) = \bar{\mathbf{y}}_{\alpha,i}$, here they remain unconstrained and move such that the total energy, deriving from both primary and secondary fibers, is minimized. Note, however, that the deflections on the secondary fibers are still constrained and given by Eq. (2), $\mathbf{y}(s_{\alpha,i,j}) = \bar{\mathbf{y}}_{\alpha,i,j}$. This may be corrected for by taking into account further levels of filaments (tertiary, ...), thus defining a sequence of energies ($W_0, W_1, W_2, \dots, W_\infty$) the fixed point of which is found by substituting on both sides of Eq. (7) one and the same asymptotic function W_∞ .

Since the resulting expression still depends on the quenched random network structure in a complicated way, we have recently proposed an effective medium approximation that uses the averaged $\langle [W_\infty] \rangle \equiv W$ instead [18]. For reasons that will immediately become apparent we have defined two averaging procedures. The angular brackets $\langle \cdot \rangle$ denote averaging over the random

variables on the primary fiber, the crosslink positions $s_{\alpha,i}$ and angles $\theta_{\alpha,i}$. The probability distributions of these variables provide the most important characterization of the architecture of the network. The brackets $[\cdot]$ denote averaging with respect to the remaining randomness in the subsequent hierarchies of fibers. Mathematically, the effective medium approximation is implemented by interchanging this latter average with the minimization operation. Physically, this amounts to assuming that one and the same medium (W) is felt by all the crosslinks on the primary fiber. One thus arrives at the final equation

$$W(\delta z_\alpha) = \left\langle \min_{\mathbf{y}(s_\alpha)} \left(W_b[\mathbf{y}_\alpha] + \sum_{i=1}^{n_{cl}} W(\delta z_{\alpha_i}) \right) \right\rangle, \quad (8)$$

where δz_{α_i} is given by Eq. (6). In principle, Eq. (8) has to be solved self-consistently for the function $W(x)$. Since we are concerned with small displacements only, the energy may be expanded to harmonic order as $W(x) = kx^2/2$, which gives

$$W(\delta z_{\alpha_i}) = \frac{1}{2} k \sin^2 \theta_{\alpha,i} (y_{\alpha,i} - \bar{y}_{\alpha,i})^2, \quad (9)$$

where we defined $y_{\alpha,i} = \mathbf{y}_{\alpha,i} \cdot \hat{\mathbf{e}}_{\alpha,i}$ and similar for $\bar{y}_{\alpha,i}$. With this parametrization Eq.(8) has to be solved for the single unknown parameter k .

Eq. (8) can be interpreted as follows. The total energy stored in the network upon axially moving a single fiber the amount δz_α has two contributions. The first term, corresponding to the bending energy of the primary fiber, W_b , dominates if the crosslinks follow the local floppy-mode associated with δz_α , such that $\delta z_{\alpha_i} \approx 0$ ($y_{\alpha,i} \approx \bar{y}_{\alpha,i}$). On the other hand, the energy is mainly stored in the surrounding medium if the crosslinks deviate strongly from the floppy-mode, $y_{\alpha,i} \approx 0$, in which case the bending energy vanishes, $W_b \approx 0$. Since medium deformations can only occur in the form of floppy-modes, the stiffness k of the medium is the same as the stiffness of the fiber. This allows to solve the equation self-consistently, which can easily be done numerically as will be explained in the appendix. There, we will also solve Eq. (8) for some exemplary network structures.

It is worth mentioning that Eqs. (8) and (9) may be interpreted as the zero temperature limit (or the saddle-point approximation) to a fluctuating stiff polymer in a random array of harmonic pinning sites with stiffnesses given by $k \sin^2 \theta_{\alpha,i}$ (see Fig. 6). Compared to the ‘‘bare floppion’’ defined by the Eqs.(2)-(5), the excitation given by Eq. (8) is ‘‘dressed’’ and incorporates the interactions with the medium on a Cayley-tree level.

B. Elastic Modulus

In principle, the elastic modulus can be found by minimizing the energy, consisting of contributions of the type of Eq. (5) from each of the N_f fibers, with respect to the variables δz_α [44]. Compared to the full problem of

having to minimize the energy with respect to *all* degrees of freedom, that is all $N_{\text{cl}} \sim N_f n_{\text{cl}}$ crosslink coordinates, this is only a minimization with respect to $N_f \ll N_{\text{cl}}$ variables. Still, this poses a challenging quenched disorder problem which can only be tackled numerically.

Here we reduce the calculation to an effective single-fiber problem, by making a simplifying assumption about the magnitude of the individual δz_α . We assume, that the fiber centers-of-mass $\mathbf{r}_{\text{cm}}^\alpha = (X_\alpha, Y_\alpha, Z_\alpha)$ follow the macroscopic strain field in an affine way, just as the centers of the hexagons did in the honeycomb lattice. This is equivalent to assuming that the displacement field is affine on the scale of the fiber length l_f . Note, however, that this does by no means imply that the elastic elements themselves undergo affine deformations, as will become clear below [45]. For a given macroscopic shear $\gamma \equiv \gamma_{xy}$ we find $\delta \mathbf{r}_{\text{cm}}^\alpha = \gamma Y_\alpha \hat{\mathbf{e}}_x$ and thus

$$\delta z_\alpha = \gamma Y_\alpha \cos \phi_\alpha, \quad (10)$$

which is just the projection of the affine displacement on the fiber axis, oriented at an angle $\phi_\alpha \in [-\pi/2, \pi/2]$ with respect to the x -axis. Using Eqs. (10) and (2) one can write Eq. (3) as

$$\mathbf{y}_{\alpha,i} = -\delta z_\alpha^{\text{rel}} \cot \theta_{\alpha,i} \hat{\mathbf{e}}_{\alpha,i} + \bar{\mathbf{y}}_{\alpha,i}^\perp, \quad (11)$$

where we have defined

$$\delta z_\alpha^{\text{rel}} = \gamma \left(Y_\alpha \cos \phi_\alpha - Y_{\alpha_i} \frac{\cos(\theta_{\alpha,i} + \phi_\alpha)}{\cos \theta_{\alpha,i}} \right). \quad (12)$$

Upon comparison of Eq. (11) with Eq. (2) one may interpret $\delta z_\alpha^{\text{rel}}$ as specifying the movement of the primary fiber *relative* to its surrounding. Note, however, that this relative displacement $\delta z_\alpha^{\text{rel}}$ depends on the orientations ϕ_α and $\phi_\alpha + \theta_{\alpha,i}$ of the primary and the secondary fibers, as well as on the arc-length along the primary fiber (via Y_{α_i}). In contrast to Eq. (2), which follows from moving the primary fiber in a fixed environment, Eqs. (11) and (12) are derived from a joint movement of all fibers. For the following we are only interested in the typical magnitude of $\delta z_\alpha^{\text{rel}}$, which may be obtained by averaging over the angles ϕ_α and estimating the typical distance between the center of masses of the intersecting fibers as $Y_\alpha - Y_{\alpha_i} \sim l_f$. We thus find that $\delta z_\alpha^{\text{rel}} \propto \gamma l_f$.

By assuming affine displacements of the fiber centers, we have thus succeeded in reducing the many-body problem of the movement δz_α of N_f interacting fibers to the case of a single fiber moving the amount $\delta z_\alpha^{\text{rel}} \sim \gamma l_f$ relative to its surrounding. The modulus can thus be calculated from the knowledge of the energy $W(\delta z_\alpha^{\text{rel}})$ calculated in the previous section. From the definition of the modulus we find that $G\gamma^2/2 = N_f W/V$, where V is the volume of the system.

It should be made clear that the assumption of affine displacements of the fiber centers is different from the usual approach of assigning affine deformations on the scale of the single polymer segment [9, 12, 13]. The latter would lead to deformations $\delta_{\text{aff}} \propto \gamma l_s$, proportional to the

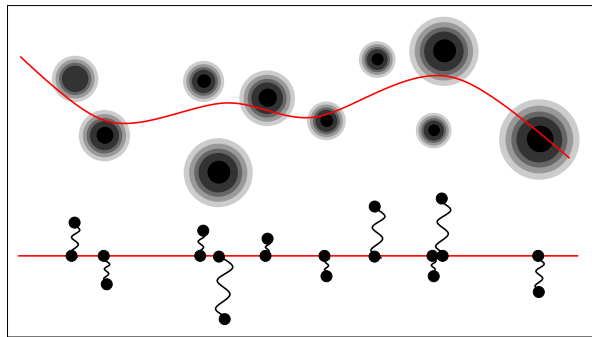


FIG. 6: The energy in Eq. (8) is that of a stiff polymer attached to springs of variable stiffness. It may therefore be interpreted as a polymer in a random potential. The potential is attractive and localized at pinning sites given by Eq. (2).

length l_s of the segment. Instead, axial displacements of the fiber as a whole are, by construction of the floppy mode, directly translated into *non-affine* deformations $\delta_{\text{na}} \propto \gamma l_f$, which do not depend on the length of the segment but rather on the scale of the fiber length l_f . We would like to emphasize the subtle difference between “affine displacements” of single points (the fiber centers-of-mass), and “affine deformations” of fiber segments of length l_s .

IV. RANDOM NETWORK IN 2D

Having presented the general concepts of the floppy modes and their energy we now proceed to introduce a simple model system where the ideas may be tested. The random two-dimensional network, the “Mikado model” [15], has the advantage that it only needs one structural parameter, the density of fibers ρ .

The network is defined by randomly placing N elastic fibers of length l_f on a plane of area $A = L^2$ such that both position and orientation are uniformly distributed [31, 32, 33]. The fiber-fiber intersections are assumed to be perfectly rigid, but freely rotatable crosslinks that do not allow for relative sliding of the filaments. The randomness entails a distribution of angles $\theta \in [0, \pi]$ between two intersecting filaments

$$P(\theta) = \frac{\sin \theta}{2}, \quad (13)$$

while distances between neighbouring intersections, the segment lengths l_s , follow an exponential distribution [34]

$$P(l_s) = \langle l_s \rangle^{-1} e^{-l_s/\langle l_s \rangle}. \quad (14)$$

The mean segment length $\langle l_s \rangle$ is inversely related to the line density $\rho = N l_f / A$ as $\langle l_s \rangle = \pi / 2 \rho$. The segments are modeled as classical beams with cross-section radius r and bending rigidity κ . Loaded along their axis

(“stretching”) such slender rods have a rather high stiffness $k_{\parallel}(l_s) = 4\kappa/l_s r^2$, while they are much softer with respect to transverse deformations $k_{\perp}(l_s) = 3\kappa/l_s^3$ (“bending”).

Numerical simulations [15, 16, 17] for the effective shear modulus G of this network have identified a crossover scaling scenario characterized by a length scale

$$\xi = l_f(\delta\rho l_f)^{-\nu} \quad (15)$$

with $\nu \approx 2.84$ [16] [46] that mediates the transition between two drastically different elastic regimes. For a fiber radius $r \gg \xi$ the system is in an affine regime where the elastic response is mainly dominated by stretching deformations homogeneously distributed throughout the sample. The modulus in this regime is simply proportional to the typical stretching stiffness, $G_{\text{aff}} \propto k_{\parallel}(\langle l_s \rangle)$ and independent of the fiber length l_f . This is in marked contrast to the second regime at $r \ll \xi$. There, only non-affine bending deformations are excited and the modulus shows a strong dependence on fiber length,

$$G_{\text{na}} \propto k_{\perp}(\langle l_s \rangle) \left(\frac{l_f}{\langle l_s \rangle} \right)^{\mu-3}, \quad (16)$$

and thus on density, $G_{\text{na}} \propto \delta\rho^{\mu}$ where $\mu = 2\nu + 1 \approx 6.67$.

As this latter non-affine regime is characterized by a ratio $k_{\parallel}(\langle l_s \rangle)/k_{\perp}(\langle l_s \rangle) \sim (\langle l_s \rangle/r)^2 \gg 1$, and therefore a bending mode that is soft as compared to the stretching mode, we may apply the floppy-mode picture developed in previous sections to calculate the exponent μ . To this end, we numerically solve Eq. (8) for varying numbers $n_{\text{cl}} \sim \rho l_f$ of crosslinks per fiber. The average $\langle \cdot \rangle$ is thereby defined in terms of the probability distributions of Eqs. (13) and (14). As a result, we find the fiber energy to scale as $W \sim n_{\text{cl}}^x \kappa/l_f^3$ and $x \approx 5.75$ (see Fig. 7). The shear modulus is inferred from W as $G = 2\rho W/l_f \gamma^2 \sim \rho^{6.75}$, which reproduces the exponent μ as measured in the simulation to a remarkable accuracy.

Based on the formalism of the preceding sections we have also developed [18] a scaling argument that allows approximate solution of Eq. (8) in terms of a single length-scale l_{min} , which on a microscopic scale governs the coupling of the fiber to the matrix. Since the stiffness $k_{\perp} \sim \kappa/l_s^3$ of the individual polymer segment is strongly increasing with decreasing its length l_s , we assume that segments with $l_s < l_{\text{min}}$ rather deform the surrounding medium than being deformed itself, while longer segments $l_s > l_{\text{min}}$ are not stiff enough to deform the medium. The scale l_{min} therefore plays the role of a minimal length below which segments are stiff enough to remain undeformed.

In terms of the crosslink deflections y_i , this implies that long (and soft) segments have $y_i \approx \bar{y}_i$, while short (and stiff) segments have crosslinks that are in their original position $y_i \approx 0$. Since the energy of a segment of length l_s can be written as $w(l_s) \sim k_{\perp} y_i^2 \sim \kappa y_i^2/l_s^3$, we find that the elastic energy is reduced by the amount

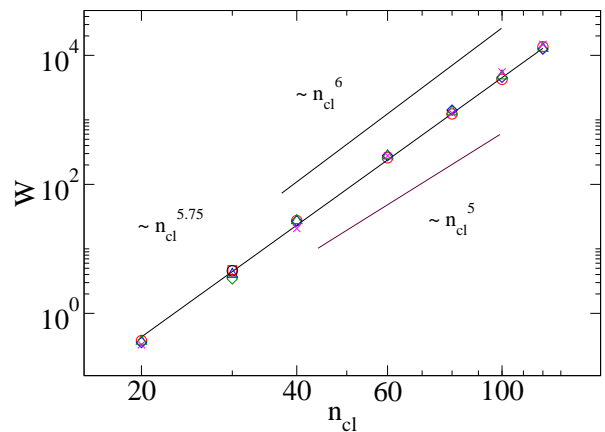


FIG. 7: Solution of Eqs. (8) and (9) for various numbers n_{cl} of crosslinks per filament. The randomness is defined by Eqs. (13) and (14). The different symbols at given n_{cl} relate to ensembles of varying size $N = 100 \dots 1000$. The lines $W \sim n_{\text{cl}}^5$ and $W \sim n_{\text{cl}}^6$ serve to illustrate the quality of the fit.

$w(l_{\text{min}}) \sim \kappa \bar{y}_i^2/l_{\text{min}}^3$ as compared to the situation where also the short segments are deformed. In turn, the energy in the neighbouring fiber is increased, where a floppy mode of amplitude $\delta z \sim \bar{y}_i$ is excited. The length-scale l_{min} can therefore be determined by equating the energy reduction in the small segments, $w(l_{\text{min}})$, with the energy increase due to the additional floppy mode in the neighbouring fiber. This latter contribution can be calculated as an average over all segments of length $l_s > l_{\text{min}}$ thus giving

$$W \simeq n_{\text{cl}} \int_{l_{\text{min}}}^{\infty} dl_s P(l_s) w(l_s) \stackrel{!}{=} w(l_{\text{min}}). \quad (17)$$

As a result, we find $l_{\text{min}} \simeq 1/\rho^2 l_f$ and thus for the average fiber energy $W \simeq \kappa(\rho l_f)^6/l_f$. This corresponds to an exponent $\mu = 7$, which confirms the previous analysis.

From Eq. (14) one may also induce a probabilistic interpretation of the length-scale l_{min} . Segments with lengths $l_s < l_{\text{min}}$ will occur on average only once along a given fiber. This may be seen from solving the equation

$$\int_0^{l_{\text{min}}} dl_s P(l_s) \sim \frac{1}{n_{\text{cl}}}, \quad (18)$$

stating that small segments will occur once in every $n_{\text{cl}} \sim \rho l_f$ crosslinks. There will therefore be typically one segment per fiber in the undeformed configuration $y_i \approx 0$, while all others follow the floppy mode.

These scaling arguments also provide additional insights into a more microscopic understanding of the crossover from affine to non-affine elasticity in random rod networks [16]. Upon rewriting the crossover scale ξ as $\xi \sim l_f(l_{\text{min}}/l_f)^{3/2}$ the scaling variable $x = r/\xi$ of Eq. (2) in [16] takes the alternative form $x^{-2} \sim k_{\parallel}(l_f)/k_{\perp}(l_{\text{min}})$ such that the crossover scaling law of the modulus reads

$$G(r, \rho) = \rho^{\mu} g(k_{\parallel}(l_f)/k_{\perp}(l_{\text{min}})). \quad (19)$$

The scaling argument now identifies a competition between the relative stiffness of the stretching and bending modes on the scale of the *whole polymer fiber* as the driving force of the affine to non-affine crossover. For large scaling arguments, $k_{\parallel}(l_f) \gg k_{\perp}(l_{\min})$, bending is the weaker mode and yields a non-affine response in the form of floppy modes. Stretching deformations become dominant as soon as $k_{\parallel}(l_f)$ becomes smaller than $k_{\perp}(l_{\min})$; this happens if the rigidity scale $l_{\min} \leq (r^2 l_f)^{1/3}$.

The only requirement for the presence of a bending dominated regime (beyond the scale separation $k_{\parallel}/k_{\perp} \gg 1$) is a low coordination number, which for the random fiber network can be calculated as $z = 4(1 - (\rho l_f)^{-1})$. This places the network below the rigidity transition for any finite l_f , while increasing the filament length $l_f \rightarrow \infty$ the critical coordination of $z_c = 4$ is asymptotically reached. As an implication the bending mode must eventually be suppressed.

The above analysis clearly shows that the proposed floppy mode concept can be utilized to understand the bending dominated elasticity in the random fibrous network. It allows to extract the length-scale l_{\min} that is ultimately responsible for the strong density-dependence of the elastic modulus as found in the simulations. Most importantly, the length-scale l_{\min} is a special feature of the random architecture studied here. Other network structures will not necessarily feature the same length-scale even though the basic formalism of the floppy bending modes can still be applied. The exponents characterizing the elastic response will thus depend on network architecture, a fact which is also exemplified in the Appendix.

In Ref. [27] we have furthermore applied the theory to explain the mechanics of reconstituted actin networks, where filaments are crosslinked and bundled by fascin. By taking into account the fact that bundles have to be characterized by a length-dependent bending rigidity $\kappa(L)$ [35, 36, 37] it was possible to explain the observed dependence of the elastic modulus on actin and fascin concentration.

A. Nonlinear elasticity arising from geometric effects

Here, we report on additional simulations probing the nonlinear modulus of the structure. Note, that in these simulations the material properties of the fibers remain linear, such that the nonlinearities result from geometrical effects only. As one can infer from Fig. 8 the network is strongly stiffening already at very small values of strain. Similar results have recently been reported in [38], where the stiffening behaviour was attributed to a crossover from bending to stretching dominated elasticity. The floppy mode picture allows to give this crossover a microscopic explanation. As argued in Section II B, the floppy modes of the fibrous network are only adequate for infinitesimally small displacements δz . The construction embodied in Eq. (2) keeps segment lengths invariant to

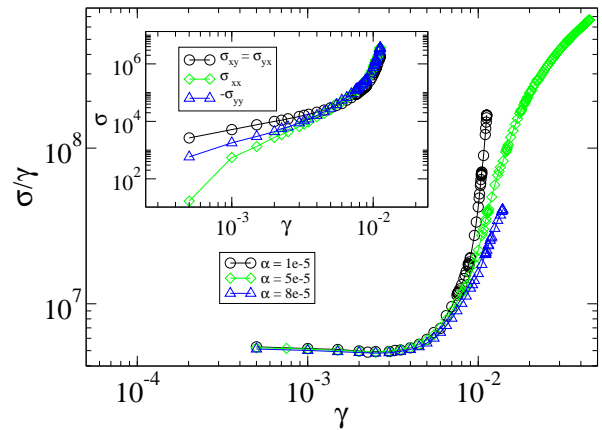


FIG. 8: Nonlinear “modulus” σ/γ in the bending dominated regime ($\rho l_f = 30$) for various values of the aspect ratio $\alpha = r/l_f$. Inset: The stress increases linearly up to a strain of about 1%. Normal stresses quickly rise in magnitude and eventually are of the same order and proportional to the shear stress.

first order in δz only, such that any finite deformation will necessarily lead to stretching of the bonds.

Note, that this stiffening mechanism is not mediated by non-linear material properties of the fibers but rather is of geometric origin and is due to the specific structural arrangement in the fibrous architecture. It is therefore of different nature than the stiffening mechanism inherent to single semiflexible polymers, where an applied tension can stretch the polymer only as far as there is stored length available [39].

In the nonlinear regime we have also measured the normal stresses σ_{xx} and σ_{yy} that act perpendicular to the principal strain direction. We found (see inset to Fig. 8) that these stresses can become of the order of the shear stresses σ_{xy} and have a negative sign indicating that the network “pulls in” during the course of the deformation. A similar effect has recently been observed in rheological measurements on F-actin networks [40] and rationalized in terms of the highly nonlinear entropic stretching response of single polymers. Note, that in our simulations the same effect occurs within a purely mechanical picture, where no material non-linearities are present. It is explained with the fact, that the additional amount of contour length necessary to undergo a finite floppy mode can only come from pulling in the fiber ends. This is equivalent to a network contraction which leads to the observed large normal stresses.

B. Nonstraight fibers

In real networks fibers will never be perfectly straight. We have argued above that in this case the scale of the fiber-length l_f must be viewed as the length-scale over which the polymer remains straight. With this in mind

our theory also holds for networks where fibers are non-straight, as long as the undulation wavelength $\lambda \sim l_f$ is larger than the distance between crosslinks $\langle l_s \rangle$.

In this section we investigate the effects of introducing undulations with wavelengths comparable to the crosslink distance, $\lambda \sim \langle l_s \rangle$. To this end we have manually generated zig-zag fibers by randomly displacing the crosslinks by some maximal amount $\Delta \cdot l_f$. A similar analysis has been performed in Ref. [38], where a substantial decrease in the degree of non-affinity of the deformation field has been found. Similarly, we find that the system develops a new crossover to a regime of affine bending deformations (see Fig. 9), where the modulus scales as $G \propto \delta\rho^3$, a behaviour well known from bending dominated cellular foams [11, 14, 41].

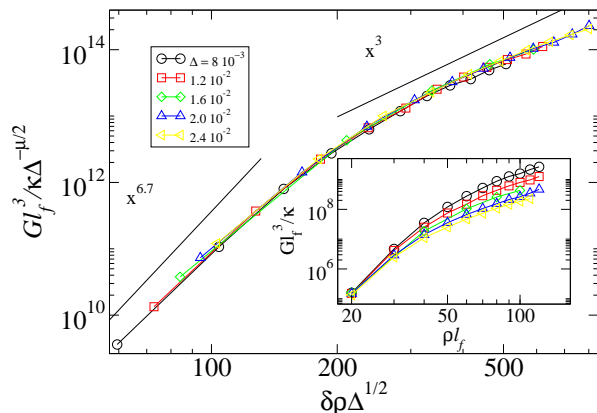


FIG. 9: Shear modulus G (inset) and scaling function g of Eq. (20) for various values of Δ . Collapse is achieved by plotting $G\Delta^{\mu/2}$ as a function $x = \delta\rho\Delta^{1/2}$ and known exponent $\mu = 6.7$ [16]. The asymptotic regimes show the scaling properties of straight fibers, $g(x) \sim x^{6.7}$, and foams, $g(x) \sim x^3$, respectively.

In this new regime the bending deformations come from pulling out the zig-zags similar to the pulling of thermally activated polymer undulations. We find that the curves may be scaled by using the same length-scale $l_{\min} \sim \delta\rho^{-2}$ that served as a lower cut-off in segment lengths. The modulus thus takes the following scaling form

$$G(\Delta, \delta\rho) = \Delta^{-\mu/2} g(\Delta/l_{\min}), \quad (20)$$

where the scaling function has the limiting form $g(x \ll 1) \sim x^{\mu/2}$ to eliminate the Δ -dependency. For large values of the scaling variable $x \gg 1$ we have to recover the scaling properties characteristic for foams, giving $g(x \gg 1) \sim x^{3/2}$. This analysis highlights once more the fundamental role played by the length-scale l_{\min} in establishing the elastic response of the network. Here, it acts as a crossover scale, that mediates the transition to a foam-like bending regime at strong disorder $\Delta \gg l_{\min}$.

Note, that by introducing kinks in the contour of the fibers, the floppy modes start to spread beyond the single

fiber to which they were confined originally. A kink is most conveniently characterized by the angle ψ through which the direction of the fiber changes at the location of the kink. By displacing a crosslink by the amount Δ one thus finds for the angle $\sin\psi = \Delta/l_s$, where l_s is the length of the segment that ends at the crosslink. Exciting the fiber with a floppy mode of amplitude δz , a finite kink-angle ψ leads to the fraction $\delta z' \sim \delta z \sin\psi \sim \delta z \Delta/l_s$ being coupled into the neighbouring fiber. At the crossover, defined by $x = \Delta/l_{\min} \sim 1$, we therefore find that for a segment of length $l_s = l_{\min}$, $\delta z'(l_{\min}) \approx \delta z$. In this situation the floppy mode is transmitted to the neighbouring fiber without attenuation of its amplitude. Since segments of length l_{\min} statistically occur once per filament, the crossover point also marks the onset of a complete delocalization of the floppy modes.

V. CONCLUSION

We started our discussion with the assumption that the elasticity of stiff polymer networks is governed by the action of the bending mode. This assumption is based on the recognition that in systems where the persistence length is large, bending as compared to stretching is by far the softer mode. The respective spring constants are scale-separated and obey the relation $k_{\parallel}/k_{\perp} \sim l_p/l \gg 1$.

One immediate implication of this scenario is that polymer end-to-end distances have to stay constant, which necessitates deformations that are highly non-affine. We have characterized this non-affine deformation field by constructing the floppy modes of the structure [18]. These are defined as the set of crosslink displacements that do not lead to any stretching of bonds. With this microscopic deformation field it is possible to calculate the macroscopic elastic moduli on the level of a self-consistent effective medium theory that incorporates fiber-medium interactions within a Cayley-tree approximation.

As a result the anomalous scaling properties of the linear shear modulus as determined by computer simulations of two-dimensional random networks [16, 17] are explained. The exponents are found to be a consequence of the special architecture of the network that features two different length-scales. On the mesoscopic scale the fiber length l_f induces a non-affine deformation field, with segment deformations δ_{na} following the macroscopic strain γ as $\delta_{\text{na}} \sim \gamma l_f$, instead of as $\delta_{\text{aff}} \sim \gamma l_s$, which would result from an affine deformation field. Microscopically, a second length l_{\min} plays the role of a minimal length below which segments are stiff enough to remain undeformed.

We would like to emphasize that the construction of the floppy modes only relies on the presence of the mesoscopic length l_f , which is applicable to a broad class of networks. In the particular case of a random rod network we have found that the anomalous scaling properties of the shear modulus, previously found in simulations, crucially depend on the presence of a second length-scale

l_{\min} , which is a special property of this random architecture. The exponents found for random rod networks are therefore not immediately applicable to other systems. Having established the general theoretical framework, it is nevertheless straightforward to calculate the exponents for other types of networks in two and three dimensions. Indeed, we have applied the theory to reconstituted actin networks crosslinked and bundled with fascin, and found that the calculated exponents are in good agreement with the experimental results [27].

Finally, we also conducted simulations probing the non-linear elasticity of the random fibrous network as well as modified the network structure by introducing kinks in the contour of the polymers. The results confirm the governing role of the identified length-scales and firmly establish that the non-affine floppy mode picture captures the essential physics of stiff polymer networks similar in spirit to affine rubber elasticity for flexible polymer gels. In view of this conceptual analogy, the next step could be to assess the importance of crosslink fluctuations, which have been neglected here (as in classical rubber elasticity). By greatly reducing the number of fluctuating degrees of freedom to one per fiber (namely δz), the theory developed here may very well provide a new starting point for the analysis of the statistical mechanics of stiff polymer networks.

Acknowledgments

We gratefully acknowledge fruitful discussions with Mark Bathe and Camilla Mohrdieck. Financial support from the German Science Foundation (SFB 486) and the German Excellence Initiative via the program "Nanosystems Initiative Munich (NIM)" is gratefully acknowledged.

APPENDIX A: SOLUTION OF EQ. (8) FOR VARIOUS NETWORK STRUCTURES

In this appendix we provide some technical details on how to solve Eq. (8) for various network architectures in two spatial dimensions. We will measure lengths in units of the fiber length l_f and energies in units of κ/l_f , where κ is the bending stiffness of the fiber. Assuming harmonic energies $W(x) = kx^2/2$ we rewrite Eq. (8) symbolically as

$$k = \langle f(k, n_{cl}; \{z_i, \theta_i\}) \rangle, \quad (\text{A1})$$

where the function f is defined by

$$f = \min_{y(z)} \left(\frac{2W_b}{\delta z^2} + k \sum_{i=1}^{n_{cl}} \sin^2(\theta_i) \left(\frac{y(z_i)}{\delta z} + \cot \theta_i \right)^2 \right), \quad (\text{A2})$$

and we used Eq. (2) to substitute $\bar{y}_i = -\cot \theta_i \delta z$.

The network structure enters Eqs.(A1) and (A2) via the variables $\{z_i, \theta_i\}$, which relate to the locations z_i

of the cross-links on the backbone of the primary fiber as well as the angles θ_i between primary and secondary fibers. The ensemble average $\langle \cdot \rangle$ can then be defined by the probability distributions $P(\{\theta_i\})$ and $P(\{l_i\})$, where segment lengths are given by $l_i = z_{i+1} - z_i$.

To illustrate the importance of structural features on the elastic properties of the network we solve Eq. (A2) for two types of distributions, relating to random and regular structures, respectively. The random network is characterized by probability distributions as given in Eqs. (13) and (14). The regular network has only one segment length $l_0 = l_f/(n_{cl} - 1)$ and an angular distribution similar to Eq. (13) but restricted to the interval $[\theta_{\min}, \pi - \theta_{\min}]$.

For a given realization of the randomness the function f is calculated by performing the minimization with respect to the contour $y(z)$. This is achieved in two steps, where first the bending energy $W_b[y]$ is minimized for a *given* set of values $\{y(z_i)\}$. As explained in the main text, this is equivalent to a cubic spline interpolation. The second step consists of a minimization with respect to the remaining variables $\{y(z_i)\}$.

Finally solving Eq. (A1) the fiber stiffness $k^*(n_{cl})$ is determined as a function of the number n_{cl} of crosslinks per fiber. A graphical solution for $n_{cl} = 40$ for various network structures is presented in Fig. 10. The function $\langle f(k) \rangle$ is plotted as function of k . The sought after value k^* is found at the point of intersection with the bisecting curve.

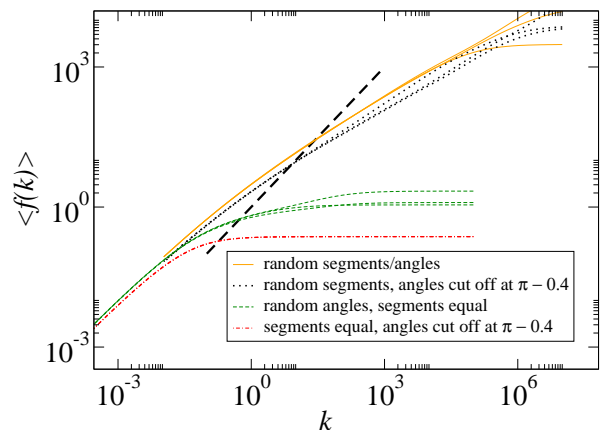


FIG. 10: Graphical solution of Eq. (A2) for a fiber with $n_{cl} = 40$ crosslinks imbedded in networks of varying architectures. $\langle f(k) \rangle$ is plotted as a function of k for ensembles of varying sizes. The solution to Eq. (A2) is found by intersecting the curves with the bisecting line (dashed).

The different curves for a given network structure correspond to ensembles of varying size. They seem to diverge in the limit $k \rightarrow \infty$. In fact, in this limit only the bending energy W_b contributes to Eq. (A2) and $y_i \approx \bar{y}_i$. This may make the averaging procedure ill defined, for example in the case of Eq. (14) where the segment lengths l_s can become arbitrarily small. The resulting segmental

bending energy $w_b \sim l_s^{-3}$ shows a divergence and does not have a well defined average value.

As one can see from Fig. 10 the resulting fiber stiffness k^* very sensitively depends on the randomness in the segment lengths, while crosslink angles only play a minor role. This is made particularly clear by comparing the random-segment and the regular-segment network in

terms of the exponent x , which is defined by $k^* \sim n_{cl}^x$. As stated in the main text the random network has $x \approx 6$, while for the regular network we find $x \approx 4$. We have shown above that the former result derives from the presence of the length-scale l_{min} . In contrast, the latter is simply obtained by calculating the bending energy of n_{cl} segments each of length l_0 , $W_b \sim n_{cl}\kappa/l_0^3 \sim n_{cl}^4$.

-
- [1] M. Rubinstein and R. H. Colby, *Polymer Physics* (Oxford University Press, 2003).
- [2] W. Kuhn, *Kolloid Zeits.* **76**, 258 (1936), F. T. Wall, *J. Chem. Phys.* **10**, 132 (1941), P. J. Flory and J. Rehner Jr., *J. Chem. Phys.* **11**, 512 (1943).
- [3] A. Bausch and K. Kroy, *Nature Physics* **2**, 231 (2006).
- [4] B. Wagner, R. Tharmann, I. Haase, M. Fischer, and A. R. Bausch, *PNAS* **103**, 13974 (2006).
- [5] R. Tharmann, M. M. A. E. Claessens, and A. R. Bausch, *Phys. Rev. Lett.* **98**, 088103 (2007).
- [6] M. L. Gardel, J. H. Shin, F. C. MacKintosh, L. Mahadevan, P. A. Matsudaira, and D. A. Weitz, *Science* **304**, 1301 (2004).
- [7] Y. Tseng, B. W. Schafer, S. C. Almo, and D. Wirtz, *J. Biol. Chem.* **277**, 25609 (2002).
- [8] K. Kroy and E. Frey, *Phys. Rev. Lett.* **77**, 306 (1996).
- [9] F. C. MacKintosh, J. Käs, and P. A. Janmey, *Phys. Rev. Lett.* **75**, 4425 (1995).
- [10] C. Heussinger and E. Frey, *Phys. Rev. Lett.* **96**, 017802 (2006).
- [11] C. Heussinger and E. Frey, *Phys. Rev. E* **75**, 011917 (2007).
- [12] J. H. Shin, M. L. Gardel, L. Mahadevan, P. Matsudaira, and D. A. Weitz, *PNAS* **101**, 9636 (2004).
- [13] C. Storm, J. J. Pastore, F. C. MacKintosh, T. C. Lubensky, and P. A. Janmey, *Nature* **435**, 191 (2005).
- [14] L. J. Gibson and M. F. Ashby, *Cellular Solids: Structure and Properties* (Cambridge University Press, Cambridge, 1999).
- [15] E. Frey, K. Kroy, J. Wilhelm, and E. Sackmann, in *Dynamical Networks in Physics and Biology*, edited by G. Forgacs and D. Beysens (Springer, Berlin, 1998), Chap. 9.
- [16] J. Wilhelm and E. Frey, *Phys. Rev. Lett.* **91**, 108103 (2003).
- [17] D. A. Head, A. J. Levine, and F. C. MacKintosh, *Phys. Rev. Lett.* **91**, 108102 (2003); *Phys. Rev. E* **68**, 61907 (2003).
- [18] C. Heussinger and E. Frey, *Phys. Rev. Lett.* **97**, 105501 (2006).
- [19] *Rigidity Theory and Applications*, edited by M. F. Thorpe and P. M. Duxbury (Kluwer Academic/Plenum Publishers, 1999).
- [20] J. C. Maxwell, *Philos. Mag.* **27**, 27 (1864).
- [21] V. S. Deshpande, M. F. Ashby, and N. A. Fleck, *Acta mater.* **49**, 1035 (2001).
- [22] C. R. Calladine, *Int. J. Solids Struct.* **14**, 161 (1978).
- [23] S. Pellegrino and C. R. Calladine, *Int. J. Solids Struct.* **22**, 409 (1986).
- [24] S. Pellegrino, *Int. J. Solids Struct.* **30**, 3025 (1993).
- [25] S. Alexander, *Phys. Rep.* **296**, 65 (1998).
- [26] S. J. Winder and K. R. Ayscough, *Journal of Cell Science* **118**, 651 (2005).
- [27] O. Lieleg et. al., *Phys. Rev. Lett.* **99**, 088102 (2007).
- [28] R. Götter, K. Kroy, E. Frey, M. Barmann, and E. Sackmann, *Macromolecules* **29**, 30 (1996).
- [29] J.-P. Collet, H. Shuman, R. E. Ledger, S. Lee, and J. W. Weisel, *PNAS* **102**, 9133 (2005).
- [30] J. Stoer and R. Bulirsch, *Introduction to Numerical Analysis* (Springer, 2002).
- [31] J. A. Åström, J. P. Mäkinen, M. J. Alava, and J. Timonen, *Phys. Rev. E* **61**, 5550 (2000).
- [32] J. A. Åström, S. Saarinen, K. Niskanen, and J. Kurkijärvi, *J. Appl. Phys.* **75**, 2383 (1994).
- [33] M. Latva-Kokko and J. Timonen, *Phys. Rev. E* **64**, 066117 (2001).
- [34] O. Kallmes and H. Corte, *Tappi* **43**, 737 (1960).
- [35] M. Bathe, C. Heussinger, M. Claessens, A. Bausch, and E. Frey, q-bio.BM/0607040, 2006.
- [36] C. Heussinger, M. Bathe, and E. Frey, *Phys. Rev. Lett.* **99**, 048101 (2007).
- [37] M. M. A. E. Claessens, M. Bathe, E. Frey and A. R. Bausch, *Nat. Mater.* **5**, 748 (2006)
- [38] P. R. Onck, T. Koeman, T. van Dillen, and E. van der Giessen, *Phys Rev Lett* **95**, 178102 (2005).
- [39] J. F. Marko and E. D. Siggia, *Macromolecules* **28**, 8759 (1995).
- [40] P. A. Janmey, M. E. McCormick, S. Rammensee, J. L. Leight, P. C. Georges, and F. C. MacKintosh, *Nature Mat.* **6**, 48 (2007).
- [41] A. M. Kraynik and W. E. Warren, in *Low density cellular plastics*, edited by H. Hilyard and C. Cunningham (Kluwer Academic Publisher, Amsterdam, 1994), Chap. 7.
- [42] This exhausts all possible floppy modes in two spatial dimensions, while in three dimensions additional modes are found that relate to the deflection \mathbf{y}^\perp of individual cross-links.
- [43] The probability of intersection of two fibers with relative angle θ is proportional to the excluded volume $A = \sin \theta l_f^2/2$.
- [44] By minimizing the energy, instead of calculating the partition function associated with the variables δz_α , one neglects fluctuations of the crosslinks.
- [45] Similarly, the elements of the honeycomb unit cell do not undergo affine deformations [14], even though the unit cell as a whole does.
- [46] The density $\delta\rho$ is measured relative to the rigidity percolation transition occurring at $\rho_{clf} = 6.7$

Mechanics of Bundled Semiflexible Polymer Networks

O. Lieleg,¹ M. M. A. E. Claessens,¹ C. Heussinger,² E. Frey,² and A. R. Bausch¹

¹*Lehrstuhl für Biophysik E22, Technische Universität München, James-Frank-Strasse 1, 85748 Garching, Germany*

²*Arnold Sommerfeld Center (ASC) for Theoretical Physics and Center for NanoScience (CeNS), Ludwig-Maximilians-Universität München, Theresienstrasse 37, D-80333 München, Germany*

(Received 27 November 2006; published 22 August 2007)

While actin bundles are used by living cells for structural fortification, the microscopic origin of the elasticity of bundled networks is not understood. Here, we show that above a critical concentration of the actin binding protein fascin, a solution of actin filaments organizes into a pure network of bundles. While the elasticity of weakly cross-linked networks is dominated by the affine deformation of tubes, the network of bundles can be fully understood in terms of nonaffine bending undulations.

DOI: [10.1103/PhysRevLett.99.088102](https://doi.org/10.1103/PhysRevLett.99.088102)

PACS numbers: 87.15.La

The mechanical properties and dynamic organization of the cytoskeleton determine the morphology and mechanical response of eukaryotic cells. To ensure adaptability of both organization and mechanics, cells exploit the dynamic interplay between semiflexible polymers such as microtubules and actin filaments using a multitude of associated binding proteins. In particular, the local elastic properties are regulated by the activation of auxiliary proteins which, e.g., cross-link and/or bundle the filamentous networks into complex scaffolds. Given the importance of the actin cytoskeleton for force generation and transduction there is much interest in understanding the mechanical properties of different network structures and the physical origin of the transitions between them. This is best studied in *in vitro* model systems [1]. In the absence of cross-links actin solutions are successfully described by the spatial confinement of thermal bending undulations upon affine tube deformation [2]. Cross-linked semiflexible polymer networks, on the other hand, are in general dominated by an interplay between polymer stretching and bending modes, the precise form of which, as well as the degree of non-affinity, strongly depends on the network microstructure [3]. So far the mechanical response of highly cross-linked actin networks, also in the presence of bundles and composite phases, has mainly been described assuming purely affine entropic stretching deformations [4–7]. However, an applied tension can stretch a thermally undulating polymer only as far as there is excess contour length available. As the maximal amount of stored length is inversely proportional to the persistence length, entropic stretching is suppressed in networks of stiff polymer bundles, where the persistence length grows with bundle size [8,9]. Moreover, the highly nonlinear nature of the force-extension relation of semiflexible polymers implies that linear elasticity is applicable as long as only a fraction of the total excess length is pulled out. As an alternative the recently introduced concept of the “floppy modes” may be better suited to describe the polymer elasticity in situations where entropic effects are suppressed [10]. These floppy modes constitute bending excitations which, unlike the affine

stretching deformations, retain a highly nonaffine character.

In this Letter we show that above a critical concentration of the actin binding protein (ABP) fascin a solution of actin filaments organizes into a homogeneous network whose building blocks are bundles only. At low cross-linker concentration, the network response is dominated by the affine deformation of reptation tubes and the ensuing changes in confinement free energy [11]. The observed mechanical and structural transition between both phases can be described by a simple relation between the ABP concentration and the entanglement length. It is proposed to rationalize the scaling of the elastic modulus in the bundled regime in terms of the floppy mode picture. A model based on affine stretching deformations only fits the data if additional assumptions about the bundle structure are made.

G-actin is obtained from rabbit skeletal muscle and stored in lyophilized form at $-21\text{ }^{\circ}\text{C}$ [12]. For measurements the lyophilized actin is dissolved in deionized water and dialyzed against G-buffer (2 mM Tris, 0.2 mM adenosine triphosphate (ATP), 0.2 mM CaCl_2 , 0.2 mM dithiothreitol (DTT), and 0.005% NaN_3 , pH 8) at $4\text{ }^{\circ}\text{C}$. The G-actin solutions are kept at $4\text{ }^{\circ}\text{C}$ and used within 7 days of preparation. The average length of the actin filaments is controlled to $21\text{ }\mu\text{m}$ using gelsolin which is prepared from bovine plasma serum following [13]. Recombinant human fascin (55 kD) was prepared by a modification of the method of [14] as described by [15]. In the experiments the molar ratio R between fascin and actin, $R = c_f/c_a$, is varied over almost three decades.

To resolve the structure and mechanical properties of actin-fascin networks actin is polymerized in F-buffer (2 mM Tris, 2 mM MgCl_2 , 0.2 mM CaCl_2 , 0.2 mM DTT, 100 mM KCl, and 0.5 mM ATP, pH 7.5). For fluorescence microscopy filaments are stabilized with tetramethyl rhodamine iso-thiocyanate (TRITC)-phalloidin; either labeled reporter filaments (1 per 400) or continuous labeling is used at distinct amounts of fascin. To avoid photobleaching 0.6 μM glucose oxidase, 0.03 μM catalase, and 0.01 M glucose are added. The samples for trans-

mission electron microscopy (Philips EM 400T) are adsorbed to glow-discharged carbon-coated formvar films on copper grids. The samples are washed in a drop of distilled water and negatively stained with 0.8% uranyl acetate; excess liquid is drained with filter paper. The viscoelastic response of actin-fascin networks is determined by measuring the frequency-dependent viscoelastic moduli $G'(\omega)$ and $G''(\omega)$ with a stress-controlled rheometer (Physica MCR 301, Anton Paar, Graz, Austria) within a frequency range of three decades. Approximately 520 μl sample volume are loaded within 1 min into the rheometer using a 50 mm plate-plate geometry with 160 μm plate separation. To ensure linear response small torques are applied. Actin polymerization is carried out *in situ*, measurements are taken 60 min after the polymerization was initiated.

Fluorescence images show that in the presence of high concentrations of fascin, actin filaments organize into a network of bundles [Fig. 1(a)] while below a critical value $R^* \approx 0.01$ no bundles can be observed. Both fluorescence and transmission electron microscopy do not show any signs of composite phases or microdomains as observed in the presence of other ABPs [6,16,17]. Moreover, the existence of a purely bundled phase is demonstrated by a cosedimentation assay (see supplementary material [18]). The bundles formed are very long ($> 100 \mu\text{m}$) and straight, which is consistent with the measured bending rigidity κ [8]. TEM micrographs reveal that above R^* the actin-fascin bundle thickness D and therefore the number of actin filaments per bundle N increases weakly with R

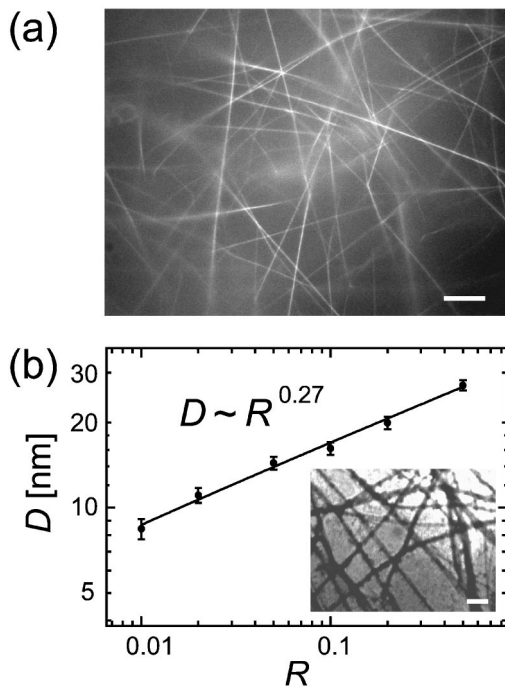


FIG. 1. (a) Fluorescence micrograph of an actin-fascin network (0.1 mg/ml actin): for high fascin concentrations a purely bundled network is formed (scale bar is 10 μm). (b) From TEM pictures (inset, scale bar is 0.2 μm) a scaling relation for the average bundle diameter D is obtained.

[Fig. 1(b)]. The bundle thicknesses are extracted from the TEM micrographs by fitting a Gaussian to the intensity profiles, obtaining a scaling of $D \sim N^{1/2} \sim R^x$ with $x = 0.27$. Concomitant with the structural changes the viscoelastic properties of the network alter: with increasing R both the storage modulus $G'(\omega)$ and the loss modulus $G''(\omega)$ increase over the whole frequency range probed. The storage modulus $G'(\omega)$ exhibits a plateau at low frequencies, while the loss modulus $G''(\omega)$ reveals a well-defined minimum which shifts to higher frequencies with increasing R . The plateau modulus $G'(10 \text{ mHz})$ plotted against R shows two distinct regimes in the elastic response. At low R , G_0 is only slightly dependent on R , $G_0 \sim R^{0.1 \pm 0.1}$, while above a critical value R^* , G_0 increases with $G_0 \sim R^{1.5 \pm 0.2}$ (Fig. 2). This exponent fits the data for both actin concentrations probed ($c_a = 0.2 \text{ mg/ml}$ and $c_a = 0.4 \text{ mg/ml}$). The transition point R^* agrees well with the structural transition at R^* observed in microscopy. Below $R^* = R^*$ the plateau modulus scales with the actin concentration as $G_0 \sim c_a^{1.3}$ suggesting that entanglements dominate the elastic response [2]. Above R^* a different scaling regime occurs with $G_0 \sim c_a^{2.4}$.

With the observed scaling behavior $G_0(R, c_a)$ the plateau modulus is parametrized in both regimes, before and after the structural transition. At the crossover concentration $R = R^*$ these two parametrizations have to be equal. This uniquely determines the scaling of R^* with the actin concentration, $R^* \sim c_a^{-0.79}$, which results in the constraint $c_f c_a^{-0.21} \sim 1$. This can be approximated to $c_f l_e^{1/2} \sim 1$ using the entanglement length $l_e \sim c_a^{-2/5}$. This surprisingly simple criterion for the bundling transition defies an obvious explanation and a detailed theoretical model is still lacking. It would need to account for the subtle interplay between confinement free energy of polymers in both the

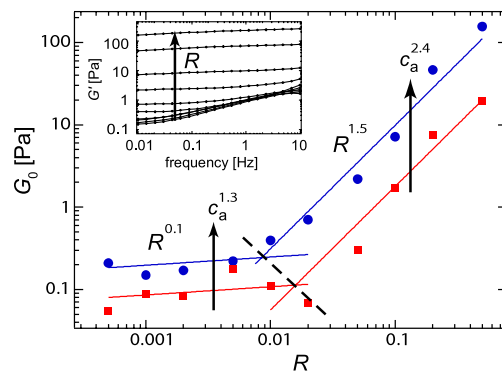


FIG. 2 (color online). Plateau modulus G_0 as a function of the molar ratio R of fascin with respect to actin for two different concentrations of actin: 0.4 mg/ml (circles) and 0.2 mg/ml (squares). The dependence of G_0 on c_a is obtained by scaling the fits for the 0.2 mg/ml actin data upon the 0.4 mg/ml data points. The dashed line shows the boundary separating the two scaling regimes. The original frequency spectra for 0.4 mg/ml actin at different cross-linker concentrations ($R = 0, 0.001, 0.002, 0.005, 0.01, 0.02, 0.05, 0.1, 0.2, 0.5$) are depicted in the inset.

bundle and the network as well as the binding enthalpy of the cross-linking proteins.

The mechanical properties inside the bundled regime may, on the other hand, be understood in terms of the nonaffine floppy mode model [10], where network elasticity is attributed to bending modes of wavelength comparable to the distance between cross-links l_c and with stiffness $k_{\perp} \sim \kappa/l_c^3$. In this picture typical deformations of the network do not follow the macroscopic strain affinely but scale as $\delta_{na} \sim \gamma L_B$, where L_B is a constant length over which an individual bundle within the network can be assumed to be straight. From our fluorescence and TEM pictures, we would expect this length to be comparable to the bundle length. As a consequence the linear elastic modulus reads

$$G_0 \sim \nu k_{\perp} \delta_{na}^2 \quad (1)$$

with the polymer density $\nu \sim 1/\xi^2 l_c$. This model can be tested by relating the structural parameters of the network, mesh size ξ and l_c , and the bending elasticity κ of the bundle segment to the concentration of actin and fascin monomers (c_a, c_f).

The structural information obtained by TEM and fluorescence microscopy justifies the assumption that the bundles form an isotropic network similar to an entangled structure of single filaments. With increasing R , filaments and smaller bundles reorganize to form larger bundles that are spaced farther apart. The mesh size ξ of this self-similar structure therefore depends on R as $\xi \sim \xi_0 N^{1/2}$, where $\xi_0 \sim c_a^{-1/2}$ is the mesh size of the filamentous network. Cross-linking will typically occur on the scale of the entanglement length l_e , which plays the role of a distance between bundle-bundle intersections (entanglement points). Since on average only a fraction of those will be occupied we can assume that distances between cross-links along the same bundle are given by $l_c \sim R^{-y} l_e$ [6,7]. Doubling the cross-linker concentration R should halve the distance between them, suggesting an exponent $y \approx 1$.

For a description of the elastic properties of the bundles it is necessary to realize that fascin only leads to loosely coupled bundles, where bending is dominated by the shear stiffness of the cross-linking proteins [8,9]. The key quantity in this context is the bundle coupling parameter $\alpha(l_c) = (l_c/b)^2$, where the length scale $b \sim \delta^{1/2}$ encodes the properties of the ABPs inside the bundle, in particular δ will depend on the concentrations c_f and c_a ; however, the precise relationship is not known. From fluorescence images the mesh size of the bundled network at $R = 0.5$ can be approximated which allows one to calculate l_e and thus l_c . From this one can estimate the coupling parameter to be $\alpha > 1$ for the whole bundle regime, implying that the effective bundle bending stiffness κ acquires a wavelength dependence [9], leading to $\kappa(\lambda) \sim N \kappa_f \alpha(\lambda)$, where λ is the wavelength of the deformation mode. This stands in marked contrast to what is known for single filaments or scruin-bound bundles where a fully coupled bending re-

gime, $\kappa \sim N^2 \kappa_f$, has been assumed [19]. The wavelength dependence of the bundle stiffness has far reaching consequences for the static as well as dynamic properties of semiflexible polymer bundles [20]. In particular, it implies that the entanglement length l_e has to be reevaluated. As it derives from the suppression of long wavelength fluctuations by confining a polymer into a tube [21], it is highly sensitive to a wavelength dependent $\kappa(\lambda)$. This results in $l_e^3 \sim (N l_p) \xi^4 / b^2$, which is different from the usual expression $l_e^5 \sim l_p \xi^4$ valid for single filaments, where in both cases $l_p = 17 \mu\text{m}$ [22] denotes the persistence length of a single actin filament. Combining the above results and setting the deformation mode length λ equal to l_c , one finally arrives at the following prediction

$$G_0 \sim R^z c_a^w \delta^{-1/3}, \quad (2)$$

where the exponents are given by $z = 2y - 4x$ and $w = 7/3$. Thus the scaling exponent of the plateau modulus can be related to parameters describing the microstructure such as the scaling of the mesh size as well as the dependence of the bundle thickness and elasticity on R . From our measurements of $x = 0.27$ and $z = 1.5$, and by assuming δ to be a constant, a value of $y = 1.29$ is obtained, which is in reasonable agreement with the expected $y \approx 1$. This result is largely insensitive to the assumption of constant δ , since by assuming δ to change according to simple Langmuir kinetics an exponent $y \approx 1.21$ is obtained.

To further characterize the elastic properties in the bundled regime, the nonlinear elasticity of the network is investigated. For samples with $R > R^*$ a constant shear rate is applied and the resulting stress is reported. From the smoothed $\sigma(\gamma)$ relation the numerical derivative yielding the differential modulus $K = \partial\sigma/\partial\gamma$ is calculated (Fig. 3). For small strains of $\gamma = 1\%$ – 10% linear behavior is observed, where the differential modulus follows $K \sim R^{1.5}$ in agreement with our oscillatory measurements. A nonlinear response is observed above γ_c , which is determined as the strain at which K deviates by 5% from its value in the

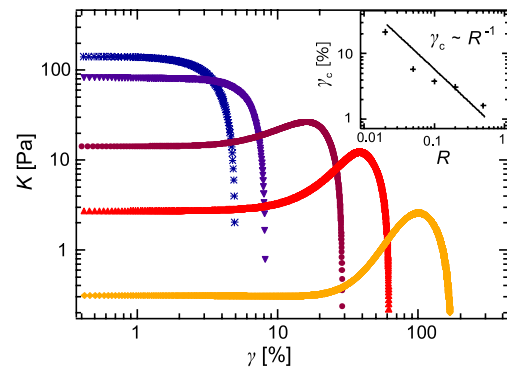


FIG. 3 (color online). Differential modulus $K = d\sigma/d\gamma$ plotted versus deformation γ for fascin networks in the bundle phase ($c_a = 0.4 \text{ mg/ml}$ and increasing R : diamonds $R = 0.02$; upright triangles: $R = 0.05$; circles: $R = 0.1$; downright triangles: $R = 0.2$; stars: $R = 0.5$). The inset shows the critical strain γ_c in dependence on R .

linear regime. Up to $R = 0.1$ a strain hardening occurs while for very high values of R the linear regime is directly followed by strain weakening. The disappearance of the strain hardening at high concentrations of fascin might be the result of the rupturing of fascin-actin bonds—very similar to what was reported for rigor heavy meromyosin (HMM) networks [7]. The floppy mode description also has implications on the onset of the nonlinear behavior. As has been argued in [10] large strains necessarily lead to stretching even if the deformations were only of bending character. The bundle stretching Δ is related to the transverse displacement δ_{na} by simple geometric considerations as $l_c^2 + \delta_{\text{na}}^2 = (l_c + \Delta)^2$. The floppy mode description thus applies as long as this stretching is small compared to the available thermal excess length $\Delta\Lambda \sim l_c b/Nl_p$ [20]. This defines a critical strain $\gamma_c \sim l_c(b/N)^{1/2} \sim R^{-y+x}b^{-1/6} \sim R^{-1.0}\delta^{-1/12}$ for the onset of nonlinear effects. The scaling with R is in excellent agreement with our measurements (see inset of Fig. 3). The weak dependence on the cross-linker spacing $\gamma_c \sim \delta^{-1/12}$ also implies that this result is insensitive towards any putative dependence on the fascin concentration via $\delta = \delta(c_f)$.

On the other hand, if one were to apply an affine stretching model, a different picture emerges, where $\delta(c_f)$ has to be tuned to obtain a reasonable data fit. In such a model one would assume the modulus to be given by $G_{\text{aff}} \sim \nu k_{\parallel} \delta_{\text{aff}}$, where $k_{\parallel} \sim \alpha^{3/2}(N\kappa_f)^2/l_c^4$ is the stretching stiffness of the bundle [20]. The deformations are assumed to be affine, implying $\delta_{\text{aff}} \sim \gamma l_c$. The modulus thus reads as $G_{\text{aff}} \sim R^{2x}c_a \delta^{-3/2}$ [18] while the critical strain $\gamma_c \sim \delta^{1/2}R^{-2x}$ is obtained by equating $\Delta\Lambda$ with the affine deformation $\delta_{\text{aff}} \sim \gamma l_c$. This model can only fit the data by assuming $\delta \sim c_f^{-\beta}$ with an exponent in the range of $\beta = 0.6$ – 0.9 , such that for $\beta = 0.6$ the R dependence of the modulus and for $\beta = 0.9$ the c_a dependence of the modulus is reproduced. To finally decide whether or not the application of an affine stretching model is equally successful as the floppy mode approach, $\delta(c_f)$ would have to be determined by scattering experiments.

In summary, on the basis of a combined microscopy and rheology study we have shown that the actin binding protein fascin mediates a transition from an entangled polymer solution to a homogeneously cross-linked bundle phase. These phases differ both in structure and mechanical properties. The location of the transition is given by a simple relation between the ABP concentration and the entanglement length. Moreover, this transition point seems to be more general since it also occurs at similar ABP concentrations in other systems such as isotropically cross-linked networks or even composite networks [4,7,17]. The transition is a consequence of the interplay between the chemical kinetics of the binding proteins, the bending rigidity of the polymers, and the entropic forces between those components. How the concerted action of those driving forces leads to such a structural transition is an

interesting theoretical problem. The elasticity in the bundled phase is well explained in terms of a recently developed floppy mode picture [10]. We have argued that in the absence of a significant amount of stored length in the bundles, nonaffine bending is the dominant low energy excitation. It explains both the linear elasticity and the onset of nonlinear behavior. This model has to be seen as an alternative to affine models where the elastic response is due to pulling out stored length fluctuations. While the elasticity of isotropic networks may be predominantly determined by such an entropic stretching of single filaments between the cross-linking points, we suppose that the elastic response of composite phases may instead be dominated by nonaffine deformations of bundles as described by floppy modes. The detailed understanding of the presented purely bundled network, composed of shear dominated bundles, provides a benchmark for addressing the further challenge to describe the mechanics of networks, which are dominated by structural heterogeneities.

We thank M. Rusp for the actin preparation. This work was supported by Deutsche Forschungsgemeinschaft through the DFG-Cluster of Excellence Nanosystems Initiative Munich (NIM) and No. SFB 413. Oliver Lieleg was supported by CompInt in the framework of the ENB Bayern.

-
- [1] A. R. Bausch and K. Kroy, *Nature Phys.* **2**, 231 (2006).
 - [2] B. Hinner *et al.*, *Phys. Rev. Lett.* **81**, 2614 (1998).
 - [3] C. Heussinger and E. Frey, *Phys. Rev. Lett.* **96**, 017802 (2006).
 - [4] M. L. Gardel *et al.*, *Science* **304**, 1301 (2004).
 - [5] F. C. MacKintosh *et al.*, *Phys. Rev. Lett.* **75**, 4425 (1995).
 - [6] J. H. Shin *et al.*, *Proc. Natl. Acad. Sci. U.S.A.* **101**, 9636 (2004).
 - [7] R. Tharmann *et al.*, *Phys. Rev. Lett.* **98**, 088103 (2007).
 - [8] M. M. A. E. Claessens *et al.*, *Nat. Mater.* **5**, 748 (2006).
 - [9] M. Bathe *et al.*, arXiv:q-bio/0607040.
 - [10] C. Heussinger and E. Frey, *Phys. Rev. Lett.* **97**, 105501 (2006).
 - [11] E. Frey, in *Advances in Solid State Physics*, edited by B. Kramer (Springer, Berlin, 2001), Vol. 41.
 - [12] J. A. Spudich and S. Watt, *J. Biol. Chem.* **246**, 4866 (1971).
 - [13] H. Kurokawa *et al.*, *Biochem. Biophys. Res. Commun.* **168**, 451 (1990).
 - [14] S. Ono *et al.*, *J. Biol. Chem.* **272**, 2527 (1997).
 - [15] D. Vignjevic *et al.*, *J. Cell Biol.* **160**, 951 (2003).
 - [16] M. Tempel *et al.*, *Phys. Rev. E* **54**, 1802 (1996).
 - [17] B. Wagner *et al.*, *Proc. Natl. Acad. Sci. U.S.A.* **103**, 13974 (2006).
 - [18] See EPAPS Document No. E-PRLTAO-99-069734 for supplementary information. For more information on EPAPS, see <http://www.aip.org/pubservs/epaps.html>.
 - [19] J. H. Shin *et al.*, *J. Mol. Biol.* **337**, 255 (2004).
 - [20] C. Heussinger *et al.*, *Phys. Rev. Lett.* **99**, 048101 (2007).
 - [21] T. Odijk, *Macromolecules* **16**, 1340 (1983).
 - [22] L. LeGoff *et al.*, *Phys. Rev. Lett.* **89**, 258101 (2002).

Force distributions and force chains in random stiff fiber networks

C. Heussinger^a and E. Frey

Arnold Sommerfeld Center for Theoretical Physics and Center for NanoScience (CeNS), Department of Physics, Ludwig-Maximilians-Universität München, Theresienstrasse 37, D-80333 München, Germany

Received 10 May 2007

Published online: 3 September 2007 – © EDP Sciences / Società Italiana di Fisica / Springer-Verlag 2007

Abstract. We study the elasticity of random stiff fiber networks. The elastic response of the fibers is characterized by a central force stretching stiffness as well as a bending stiffness that acts transverse to the fiber contour. Previous studies have shown that this model displays an anomalous elastic regime where the stretching mode is fully frozen out and the elastic energy is completely dominated by the bending mode. We demonstrate by simulations and scaling arguments that, in contrast to the bending dominated *elastic energy*, the equally important *elastic forces* are to a large extent stretching dominated. By characterizing these forces on microscopic, mesoscopic and macroscopic scales we find two mechanisms of how forces are transmitted in the network. While forces smaller than a threshold F_c are effectively balanced by a homogeneous background medium, forces larger than F_c are found to be heterogeneously distributed throughout the sample, giving rise to highly localized force chains known from granular media.

PACS. 62.25.+g Mechanical properties of nanoscale materials – 87.16.Ka Filaments, microtubules, their networks, and supramolecular assemblies

1 Introduction

It has been well known for more than a century that networks of central force springs lose their rigidity when the number of connected neighbours is lower than a certain threshold value [1]. To guarantee the rigidity of these otherwise “floppy” networks, additional contributions to the elastic energy, beyond central-force stretching, have to be introduced [2]. Here our focus is on a particular class of heterogeneous networks composed of crosslinked fibers, whose length l_f is much larger than the typical distance l_s between two fiber-fiber intersections (see Fig. 1). These systems have recently been suggested as model systems for studying the mechanical properties of paper sheets [3] or biological networks of semiflexible polymers [4–6]. As only two fibers may intersect at a given cross-link, the average number of neighbouring cross-links is $z < 4$. This places them below the rigidity transition both in two and in three spatial dimensions. Several strategies have been used to elastically stabilize a central-force fiber network [7]. Here, we use an additional energy cost for fiber “bending”. The bending mode penalizes deformations transverse to the contour of the fiber while to linear order the distance between cross-links, *i.e.* the length of the fiber, remains unchanged.

The two-dimensional fiber network we consider is defined by randomly placing N initially straight elastic fibers

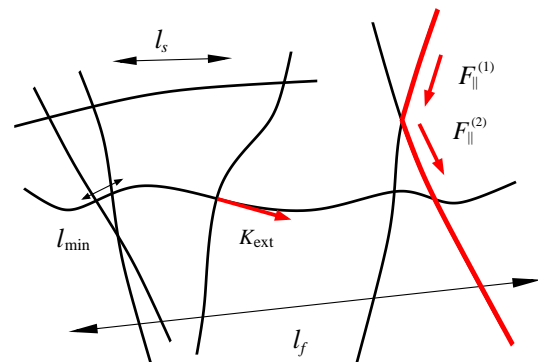


Fig. 1. (Colour on-line) Illustration of the local network structure and the relevant length scales in the random fiber network (drawn in the deformed configuration): the fiber length l_f , the typical segment length l_s and the shortest deformed segment of length l_{\min} . K_{ext} signifies the bending force that the crossing fiber exerts in the axial direction of the horizontal fiber. $F_{\parallel}^{(1)}$ and $F_{\parallel}^{(2)}$ correspond to axial forces that are directly transmitted from one fiber to a neighbouring fiber at the crosslink. This mechanism forms the basis for the establishment of force chains; see main text.

of length l_f on a plane of area $A = L^2$ such that both position and orientation are uniformly distributed. The fiber density is thus defined as $\rho = Nl_f/A$. We consider the fiber-fiber intersections to be perfectly rigid, but freely

^a e-mail: claus.heussinger@physik.lmu.de

rotatable cross-links that do not allow for relative sliding of the fibers. The elastic building blocks of the network are the fiber segments, which connect two neighbouring cross-links. A segment of length l_s is modeled as a classical beam with cross-section radius r and bending rigidity κ [8]. Loaded along its axis (central force “stretching”) such a slender rod has a rather high stiffness, characterized by the spring constant $k_{\parallel}(l_s) \sim \kappa/l_s r^2$, while it is much softer with respect to transverse deformations $k_{\perp}(l_s) \sim \kappa/l_s^3$ (“bending”).

While this random fiber network is known to have a rigidity percolation transition at a density ρ_c [9–11], we have recently shown [12,13] how the network’s inherent fragility, induced by its low connectivity z , determines the properties even in the high-density regime far away from the percolation threshold, $\rho \gg \rho_c$. In particular, it was possible to explain the anomalous scaling properties of the shear modulus as found in simulations [10,14]. The unusually strong density dependence of the elastic shear modulus $G \sim (\rho - \rho_c)^{6.67}$ [10] is found to be a consequence of the architecture of the network that features various different length scales [12,13] (see Fig. 1). On the mesoscopic scale the fiber length l_f induces a highly non-affine deformation field, where segment deformations δ_{na} follow the macroscopic strain γ as $\delta_{\text{na}} \sim \gamma l_f$. This is in stark contrast to an affine deformation field where deformations scale with the size of the object under consideration. For a segment of length l_s the affine deformation therefore is $\delta_{\text{aff}} \propto \gamma l_s$. Microscopically, a second length l_{min} governs the coupling of a fiber segment to its neighbours on the crossing fiber [12,13]. Due to the fact that the bending stiffness $k_{\perp} \sim l_s^{-3}$ of a segment is strongly increasing with shortening its length, it is found that segments with $l_s < l_{\text{min}}$ rather deform their neighbours than being deformed, while longer segments $l_s > l_{\text{min}}$ are not stiff enough to induce deformations in the surrounding. Thus l_{min} plays the role of a *rigidity scale*, below which segments are stiff enough to remain undeformed. As a consequence the elastic properties of the fiber as a whole are not governed by the *average* segment \bar{l}_s , but rather by the *smallest loaded* segment l_{min} .

In the observed scaling regime the elastic modulus does originate exclusively in the bending of the individual fibers, and thus reflects the stabilising effect of this soft deformation mode. In contrast, stretching deformations in this non-affine bending-dominated regime can be assumed to be frozen out completely. In our previous articles [12,13] we have dealt with the properties of the bending mode, k_{\perp} , and its implications on the *elastic energy*. Here we focus on the stretching mode, k_{\parallel} , and its role in the occurrence of *elastic forces*. As the non-affine bending regime is relevant for slender fibers with a small cross-section radius, $r \rightarrow 0$, it is characterized by a scale separation, $k_{\parallel}/k_{\perp} \sim r^{-2} \rightarrow \infty$, which assures that no stretching deformations, δ_{\parallel} , occur. Thus, the fibers effectively behave as if they were inextensible bars. Closer inspection of the limiting process reveals, however, that the stretching deformations tend to zero as $\delta_{\parallel} \sim 1/k_{\parallel}^1$. This makes the

contribution to the total energy $W_s \sim k_{\parallel} \delta_{\parallel}^2 \sim k_{\parallel}^{-1}$ negligible, as required, but also implies that finite stretching forces F_{\parallel} will occur:

$$F_{\parallel} \sim k_{\parallel} \delta_{\parallel} \rightarrow \text{const}. \quad (1)$$

Indeed, these forces, acting axially along the backbone of the fibers, are absolutely necessary to satisfy force-balance at the intersection of two fibers. With two fibers intersecting at a finite angle it is intuitively clear that a change in transverse force in one fiber has to be balanced by an axial force in the second.

For thicker fibers with a larger cross-section radius r , a second elastic regime occurs, where the bending instead of the stretching mode is frozen out. This regime formally corresponds to the limit $k_{\parallel}/k_{\perp} \sim r^{-2} \rightarrow 0$. It is characterized by stretching deformations of mainly affine character [14]. The elastic shear modulus (as well as the Young’s modulus) have been shown to depend linearly on density [10,15,16], $G \sim \rho$, which is in striking contrast to the strong susceptibility to density variations found in the non-affine bending regime.

In the following we will present results of simulations that characterize in detail the occurring axial forces in both elastic regimes, the non-affine bending as well as the affine stretching regime. In the simulations we subject the network to a macroscopic deformation and determine the new equilibrium configuration by minimizing the elastic energy. The minimization procedure is performed with the commercially available finite element solver MSC.MARC. Further details of the simulation procedure can be found in our previous publications [6]. Starting with the average force profile along the fibers we then proceed by giving the full probability distribution of forces. We show that its tails are heterogeneously distributed throughout the system, similar to force chains in granular media. We find that most of the features can be understood with the help of the two basic length scales, the filament length l_f and the rigidity scale l_{min} .

2 Effective medium theory

In this section we will characterize the configurationally averaged force profile along a fiber. In the spirit of an effective medium theory, one can think of the fiber as being imbedded in an elastic matrix that, on a coarse-grained scale, acts continuously along the backbone. The associated force \mathcal{K}_{ext} , which is imposed on the fiber, leads to a change in axial force according to [8]

$$\frac{\partial F_{\parallel}}{\partial s} = -\mathcal{K}_{\text{ext}}, \quad (2)$$

where s is the arclength along the fiber backbone.

a system of two springs connected in series. Minimizing the energy for fixed overall deformation δ , one finds $\delta_{\parallel} = k_{\perp} \delta / (k_{\parallel} + k_{\perp})$, which shows the required scaling $\delta_{\parallel} \sim k_{\parallel}^{-1}$ in the limit $k_{\parallel} \rightarrow \infty$.

¹ This may be seen by considering the following simplified energy function, $W = k_{\perp}(\delta - \delta_{\parallel})^2 + k_{\parallel} \delta_{\parallel}^2$, which represents

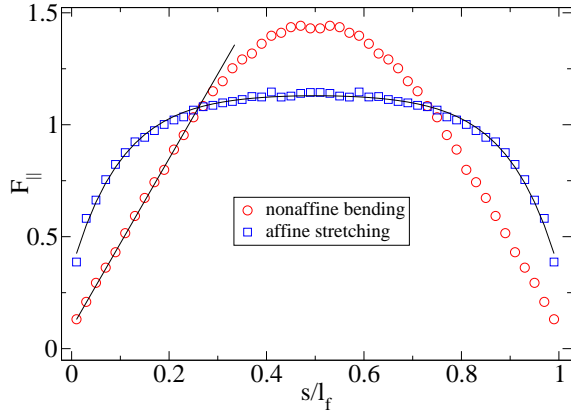


Fig. 2. (Colour on-line) Variation of average axial force F_{\parallel} along the backbone $s = [0, l_f]$ of the fibers (symmetrized around $s = l_f/2$). The symbols are the results of our simulations. Towards the fiber ends the force relaxes exponentially in the affine stretching regime (full curve is a fit to the Cox model), and linearly in the non-affine bending regime.

A while back, Cox [17] provided a second, constitutive equation that allows to solve for the force profile $F_{\parallel}(s)$. He assumed the medium to be characterized by an affine deformation field $\delta_{\text{aff}}(s) \sim \gamma s$. The external force \mathcal{K}_{ext} is assumed to be non-vanishing only when the actual fiber deformation δ_{\parallel} is different from this affine deformation field,

$$\mathcal{K}_{\text{ext}}(s) = k (\delta_{\parallel} - \delta_{\text{aff}}(s)). \quad (3)$$

Equations (2) and (3) can easily be solved and result in a force profile that shows a plateau in the center of the fiber as well as boundary layers where the force decreases exponentially, $F_{\parallel}(s) = a - b \cosh[c(s - l_f/2)]$, with a , b , and c appropriately chosen constants.

Åström *et al.* [16] have applied this model to the affine stretching regime and found the boundary layers to grow as the fiber cross-section radius is decreased. Figure 2 shows results of our simulations for the force profile both in the affine stretching regime (squares, blue on-line) and the non-affine bending regime (circles, red on-line). Apparently the Cox-model accounts very well for the force profile in the stretching regime, while it fails completely in the bending regime, where the simulation data clearly show that the force increases linearly from the boundary towards the center of the fiber.

Cox ideas can be generalized to the non-affine bending regime, where the elastic medium entirely consists of bending modes. In this regime the axial forces in the fiber arise due to the pulling and pushing of its crossing neighbours that try to transfer their high bending load in a kind of lever-arm effect (see Fig. 1). As explained above, the deformation field is non-affine and, instead of δ_{aff} , one has to use $\delta_{\text{na}} \sim \gamma l_f$ [13], which is proportional to the fiber length l_f . Since we are interested in the limit where stretching deformations vanish, $\delta_{\parallel} \rightarrow 0$, the resulting external force is arclength independent, $\mathcal{K}_{\text{ext}} = -k\delta_{\text{na}} \sim -l_f$ and constant along the backbone. The axial force profile $F_{\parallel}(s)$ is thus

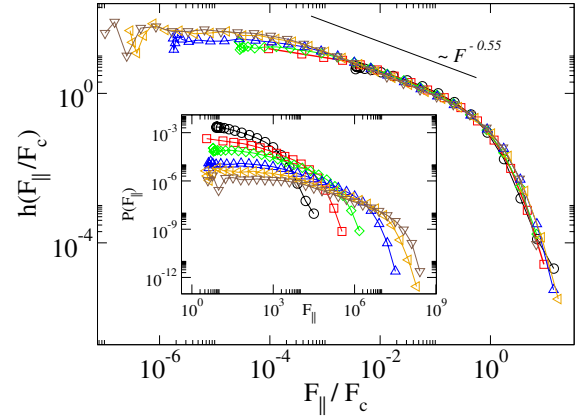


Fig. 3. (Colour on-line) Probability distribution $P(F_{\parallel})$ (inset) and scaling function h in the non-affine bending regime with aspect ratio $r/l_f = 5 \cdot 10^{-6}$ for various densities $\rho l_f = 20 \dots 100$. The force scale used to obtain the data collapse is $F_c = \kappa \rho_c^2 (\delta \rho / \rho_c)^5$.

expected to be linearly increasing from the boundaries towards the center, in agreement with the simulations.

Recently, Head *et al.* [14] have suggested growing boundary layers to play a key role for the cross-over from the affine stretching to the non-affine bending regime. Here, we have shown that these growing boundary layers are rather a consequence of a transition from an exponential to a linear force profile in the boundary layers. This follows naturally from the fact that non-affine deformations, δ_{na} , scale with the fiber length l_f and not with the segment length l_s . As we have analyzed in detail in reference [13], this scaling property, which originates in the network architecture, can be understood within a “floppy mode” concept. Therefore, the growing boundary layers should be viewed as a consequence rather than the driving force of the affine to non-affine transition.

3 Force distribution

We now turn to a discussion of the full probability distribution of axial forces, instead of just the average value as we have done in the previous section. In Figure 3 we display the distribution function $P(F_{\parallel})$ for various densities ρ deep in the non-affine regime. Remarkably, the curves for different densities collapse on a single master curve by using the scaling ansatz

$$P(F_{\parallel}) = F_c^{-1} h(F_{\parallel}/F_c), \quad (4)$$

with the force scale $F_c = \kappa \rho_c^2 (\delta \rho / \rho_c)^5$, where $\delta \rho = \rho - \rho_c$.

Its appearance in equation (4) indicates that F_c is the average axial force. We now show that it is furthermore equivalent to the average bending force $F_c = \langle k_{\perp}(l_s) \cdot \delta_{\text{na}} \rangle$ that is needed to impose the non-affine bending deformation δ_{na} on a segment of bending stiffness k_{\perp} .

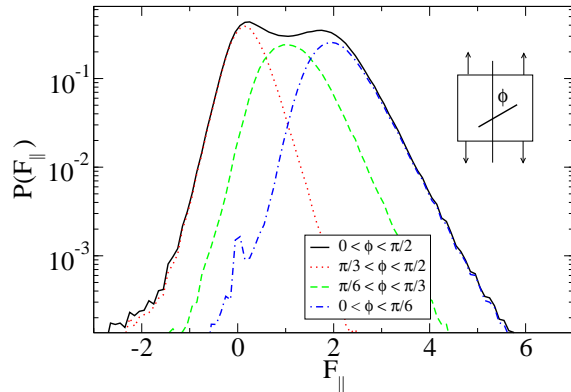


Fig. 4. (Colour on-line) Probability distribution $P(F_{\parallel})$ of axial forces in the affine-stretching-dominated regime for $\rho l_f = 60$ and aspect ratio $r/l_f = 0.05$. The system is subject to uniaxial stretching, as indicated in the inset. Note the linear scale on the x -axis. The peak of the distribution is strongly correlated with the orientation, ϕ , of the fiber relative to the principal stretching direction.

The average $\langle \cdot \rangle$ is performed over the segment-length distribution $P(l_s)$ ², restricted to those segments that are longer than the rigidity scale l_{\min} . Recall, that l_{\min} plays the role of the shortest deformed segment such that shorter segments do not contribute to the averaging. The equivalence of both expressions for the force scale becomes evident by writing the average explicitly,

$$F_c = \int_{l_{\min}}^{\infty} dl_s P(l_s) k_{\perp}(l_s) \delta_{\text{na}}, \quad (5)$$

and inserting $k_{\perp} \sim l_s^{-3}$. The integral is dominated by its lower limit, which leads to $F_c \sim \kappa(\rho l_f)^5/l_f^2$ as required.

Hence, the force scale F_c has been identified as the average force that induces the non-affine bending of a fiber. At the same time it occurs in the probability distribution of stretching forces as depicted in Figure 3. This two-fold role reflects the interplay of bending and stretching in the effective medium theory, where stretching forces in one fiber have to be balanced by bending forces in its neighbours. We can thus conclude that the effective medium picture is the appropriate description for forces up to the threshold F_c , *i.e.* for the “typical” properties of the system.

Interestingly, for forces smaller than F_c the probability distribution displays an intermediate power law tail $h(x) \sim x^{-\beta}$, with an exponent $\beta \approx 0.55$, which as yet defies a simple explanation. For forces larger than F_c , one may even speculate about the existence of a second power law regime with a much higher exponent $\beta' \approx 5$. While in this regime the distribution does not seem to decrease exponentially, the available range of forces is too small to reach any final conclusions as to the functional form.

The axial forces in the affine stretching regime follow a completely different probability distribution, as can be

² In the random network structure considered here, this distribution is exponential, $P(l_s) = \rho \exp(-l_s \rho)$.

seen from Figure 4. The solid black line relates to the probability distribution of all segments, irrespective of their orientation ϕ , with respect to the imposed strain field (in this case: uniaxial extension along the y -direction). The broken lines only include segments with orientations ϕ in a particular interval, as denoted in the figure legend. The tails of the distribution are exponential (as has previously been observed in Ref. [16]), while the peak force strongly depends on the orientation ϕ of the segments. The position of the peak follows naturally from the assumption that segments undergo affine deformations with $\delta_{\text{aff}} = \gamma l_s \cos^2 \phi$. Since the resulting affine forces $F_{\text{aff}}(\phi) = k_{\parallel}(l_s) \delta_{\text{aff}} \sim \kappa \gamma \cos^2 \phi$ do not depend on the length of the segments, one expects only a single, orientation-dependent force, that is a delta-function distribution $P(F, \phi) \sim \delta(F - F_{\text{aff}}(\phi))$. The broadening of the distribution relative to the singular delta-function can be rationalized with the fact that the affine strain field can only fulfill force equilibrium if the fibers are infinitely long. For finite fibers the force has to drop to zero at the ends (as discussed above), leading to additional (non-affine) deformations and therefore to a broadening of the peak.

4 Force chains

In the preceding two sections we have characterized the occurring axial forces on the scale l_f of a single fiber as well as on the smaller scale of an individual fiber segment l_s . We now proceed to discuss the properties of the forces on a larger, mesoscopic scale. To this end, we probe the Green’s function of the system and impose a localized perturbation in the center of the network. Fixing the boundaries, we displace a single crosslink and monitor the resulting

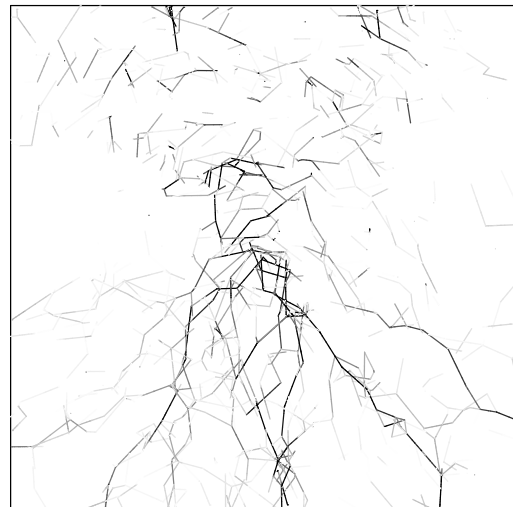


Fig. 5. Picture of a network in the non-affine-bending-dominated regime. The grey scale is chosen according to the axial force in the segment. Force chains are clearly visible, and follow a zig-zag course from the center towards the lower boundary.



Fig. 6. Picture of a network in the affine-stretching-dominated regime. The grey scale is chosen according to the axial force in the segment. No force chains are present.

response of the network. Similar studies have been conducted in reference [18], where ensemble averaging is used to discuss the applicability of homogeneous elasticity theory. Here, we focus on the individual network realization to better characterize the spatial organization of the forces.

In Figures 5 and 6 we show pictures of a network, where the grey scales of the segments are chosen according to the magnitude of the forces they carry. The higher the force the darker the segment. While the quenched random structure is the same in both plots, the fiber aspect ratio $\alpha = r/l_f$ is chosen such that the network lies deep in the non-affine bending ($\alpha = 10^{-5}$) or the affine stretching regime ($\alpha = 10^{-1}$), respectively. As is clearly visible in Figure 5 the non-affine response is characterized by well-defined paths of high forces that extend from the center, where the force is applied, to the boundaries. These forces are transmitted from fiber to fiber along a zig-zag course. Upon comparison with the distribution function for axial forces (like those shown in Fig. 3), we find that the force chains are constituted by forces with magnitude larger than F_c (*i.e.* above the intermediate power law regime). In contrast, in the affine regime a rather homogeneous distribution of forces is observed (Fig. 6).

The observation that the highest occurring forces are connected in chains, suggests a mechanism that allows direct transmission of an axial load from one fiber to the next. This has to be contrasted with the results of Section 2, where we have developed an effective medium picture that constitutes an indirect load transfer, in which axial forces in one fiber are balanced by transverse (bending) forces in the neighbouring fiber. The difference between both mechanisms becomes evident by considering the load transfer at a fiber-fiber intersection that coincides with the end-point of one of the two fibers; see Figure 7 for an illustration. An axial load $F_{\parallel}^{(1)}$ that is coupled into fiber (1) at

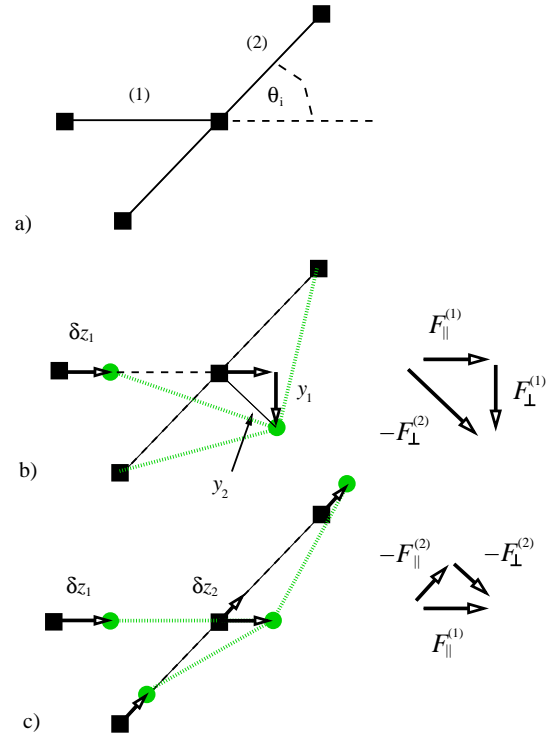


Fig. 7. (Colour on-line) Illustration of the two mechanisms of load transfer for a fiber segment (1) ending at a crossing fiber (2). The displacement δz_1 of the horizontal fiber leads to deformations in both fibers. The indirect load transfer, b), couples axial forces into bending deformations, while the direct transfer, c), transmits the axial force directly into axial forces in the neighbouring fiber.

its left end has to be taken up by the crossing fiber (2) at the distal end of fiber (1). Assume that this applied force in the horizontal fiber, $F_{\parallel}^{(1)}$, is accompanied with an axial displacement δz_1 , which translates the fiber along its axis.

In the indirect load transfer the axial force $F_{\parallel}^{(1)}$ is balanced by bending forces $F_{\perp}^{(1,2)}$ oriented perpendicular to the contour of both fibers. The force balance reads

$$F_{\parallel}^{(1)} + F_{\perp}^{(1)} = -F_{\perp}^{(2)}. \quad (6)$$

The angle between both fibers being θ , the associated bending displacements are (Fig. 7b)

$$y_1 = -\delta z \cot \theta, \quad y_2 = \delta z / \sin \theta. \quad (7)$$

This mechanism forms the basis of the effective medium theory applied in Section 2 to explain the average force profile along the fibers. It has also been shown to allow a direct calculation of the macroscopic elastic moduli of the network [12, 13].

We now proceed to discuss the second mechanism. It can immediately be seen from the θ -dependence that the bending displacements $y_{1/2}$ of equation (7) can become increasingly large, if the fibers intersect at small enough angles, $\theta \rightarrow 0$. Then, the network responds in a different way.

As can be inferred from Figure 7c the large bending contributions may be avoided by additionally moving the secondary fiber along its own axial direction, $\delta z_2 = \delta z_1 \cos \theta$. This leaves the primary fiber straight while the bending displacement in the secondary fiber becomes $y_2 = \delta z_1 \sin \theta$. The force balance must therefore be written as

$$F_{\parallel}^{(1)} = -(F_{\parallel}^{(2)} + F_{\perp}^{(2)}). \quad (8)$$

The smaller the angle θ the larger is the contribution of $F_{\parallel}^{(2)}$, which is just the forward “scattering” of forces, seen in Figure 5.

The existence of force chains is intimately connected to the presence of long fibers, $\rho l_f \gg 1$. Since the coordination can be written as $z = z_c(1 - O(\rho l_f)^{-1})$ [13], the system will become completely rigid by increasing the fiber length, $l_f \rightarrow \infty$. There, the force scale F_c diverges and axial forces imposed on a fiber will propagate along the fiber completely uncorrelated with forces on its neighbours. As the number of intersections $n_{cl} \sim \rho l_f$ per fiber is proportional to the fiber length, the probability distribution for the angle between two intersecting fibers is sampled to an increasing degree. In particular, the smallest angle that will occur in a finite sample of n_{cl} intersections is calculated from

$$\int_0^{\theta_{\min}} d\theta P(\theta) = 1/n_{cl}, \quad (9)$$

as $\theta_{\min} \sim l_f^{-1/2}$, where we have used $P(\theta) \sim \theta$ for small values of θ . With increasing fiber length ever smaller angles occur. As explained above, the presence of small angles necessarily lead to forward scattering of axial forces, and thus to the emergence of force chains. The presence of force chains is therefore a consequence of the special geometry of the network that allows the fibers to intersect at arbitrarily small angles. To support this view, we have conducted additional simulations in which the localized perturbation is applied in varying directions. As a result, the structure of the force chains remain unchanged while their amplitudes are modulated.

5 Conclusion and outlook

In conclusion, we have characterized in detail the properties of forces occurring in two-dimensional random fiber networks. We have shown that the previously identified *rigidity scale* l_{\min} , in addition to the *structural scale* of the fiber length l_f , governs the occurrence of stretching forces in an elastic regime, where the energy derives from the bending mode only ($k_{\parallel}/k_{\perp} \rightarrow \infty$). The probability distribution of forces shows scaling behaviour with the force scale $F_c = \kappa \rho_c^2 (\delta \rho / \rho_c)^5$ that can be identified with the average force needed to deform a fiber segment by the non-affine deformation $\delta_{na} \sim \gamma l_f$.

Two types of force transmission have been identified. Forces up to the scale F_c are transmitted from one fiber to the next by an *indirect mechanism*, where stretching

forces are balanced by bending forces and vice versa. This is best illustrated by the action of a lever-arm that tries to transmit its bending load to the neighbouring fiber, which subsequently starts to stretch (see \mathcal{K}_{ext} in Fig. 1). This mechanism of force transmission can be used to understand the average force profile along a fiber, and also forms the basis for the calculation of the scaling properties of the elastic modulus [12,13]. In a second *direct mechanism* axial forces are also transmitted directly to their neighbours, giving rise to highly localized force chains that are heterogeneously distributed throughout the sample. This mechanism is only active for forces larger than F_c . In contrast to the indirect mechanism, which probes the center of the force distribution and therefore typical properties of the network, the direct mechanism reflects the properties of the extremal values of the distribution.

The observation of force chains suggests an analogy with granular media [19]. The scale separation $k_{\parallel} \gg k_{\perp}$ implies that the fibers behave as if they were inextensible. The network of inextensible segments may therefore loosely be viewed as the contact network of a system of rigid grains. Due to the low coordination number, the fiber network has to be stabilised by the action of the bending mode directed perpendicularly to the fiber axis. This bears some similarity to a friction force in granular systems, which is directed tangentially to the grain surfaces. Indeed, it has been argued that stable granular systems with a coordination as low as found here may only be achieved if frictional forces are taken into account [20]. The occurrence of force chains in our “frictional” system is, however, due to the vicinity of the isostatic point with regard to the *frictionless* system ($z_c = 4$). Since the coordination may be written as $z = 4(1 - O(\rho l_f)^{-1})$ the isostatic point is reached by increasing the fiber length $l_f \rightarrow \infty$.

We gratefully acknowledge fruitful discussions with Klaus Kroy. Financial support of the German Science Foundation (SFB486) and of the German Excellence Initiative via the program “Nanosystems Initiative Munich (NIM)” is gratefully acknowledged.

References

1. J.C. Maxwell, *Philos. Mag.* **27**, 27 (1864).
2. M. Sahimi, *Heterogeneous Materials* (Springer, New York, 2003).
3. M. Alava, K. Niskanen, *Rep. Prog. Phys.* **69**, 669 (2006).
4. E. Frey, K. Kroy, J. Wilhelm, E. Sackmann, in *Dynamical Networks in Physics and Biology*, edited by G. Forgacs, D. Beysens (Springer, Berlin, 1998) Chapt. 9.
5. A. Bausch, K. Kroy, *Nat. Phys.* **2**, 231 (2006).
6. C. Heussinger, E. Frey, *Phys. Rev. Lett.* **96**, 017802 (2006); *Phys. Rev. E* **75**, 011917 (2007).
7. M. Latva-Kokko, J. Mäkinen, J. Timonen, *Phys. Rev. E.* **63**, 046113 (2001).
8. L.D. Landau, E.M. Lifshitz, *Theory of Elasticity*, Vol. **7**, 3rd ed. (Butterworth-Heinemann, Oxford, 1995).
9. M. Latva-Kokko, J. Timonen, *Phys. Rev. E* **64**, 066117 (2001).

10. J. Wilhelm, E. Frey, Phys. Rev. Lett. **91**, 108103 (2003).
11. D.A. Head, A.J. Levine, F.C. MacKintosh, Phys. Rev. E **68**, 25101 (2003).
12. C. Heussinger, E. Frey, Phys. Rev. Lett. **97**, 105501 (2006).
13. C. Heussinger, B. Schaefer, E. Frey, cond-mat/0703095.
14. D.A. Head, A.J. Levine, F.C. MacKintosh, Phys. Rev. Lett. **91**, 108102 (2003); Phys. Rev. E **68**, 61907 (2003).
15. J.A. Åström, J.P. Mäkinen, M.J. Alava, J. Timonen, Phys. Rev. E **61**, 5550 (2000).
16. J.A. Åström, S. Saarinen, K. Niskanen, J. Kurkijärvi, J. Appl. Phys. **75**, 2383 (1994).
17. H.L. Cox, Br. J. Appl. Phys. **3**, 72 (1952).
18. D.A. Head, A.J. Levine, F.C. MacKintosh, Phys. Rev. E **72**, 061914 (2005).
19. H.M. Jaeger, S.R. Nagel, Rev. Mod. Phys. **68**, 1259 (1996).
20. T. Unger, J. Kertész, D.E. Wolf, Phys. Rev. Lett. **94**, 178001 (2005).

7.3 Thermal Response

The two articles “Stiff Polymers, Foams, Fiber Networks” and “The Role of Architecture in the Elastic Response of Semiflexible Polymer and Fiber Networks” deal with the elastic properties of stiff polymer networks at finite temperature.

We study a variety of network structures and discuss the influence of structural randomness on the scaling properties of the elastic moduli. The fiber length l_f is found to play a decisive role in mediating the elastic response.

Stiff Polymers, Foams, and Fiber Networks

Claus Heussinger and Erwin Frey

Arnold Sommerfeld Center for Theoretical Physics and CeNS, Department of Physics, Ludwig-Maximilians-Universität München, Theresienstrasse 37, D-80333 München, Germany

Hahn-Meitner-Institut, Glienicker Strasse 100, D-14109 Berlin, Germany

(Received 15 March 2005; published 9 January 2006)

We study the elasticity of fibrous materials composed of generalized stiff polymers. It is shown that, in contrast to cellular foamlike structures, affine strain fields are generically unstable. Instead, a subtle interplay between the architecture of the network and the elastic properties of its building blocks leads to intriguing mechanical properties with intermediate asymptotic scaling regimes. We present exhaustive numerical studies based on a finite element method complemented by scaling arguments.

DOI: [10.1103/PhysRevLett.96.017802](https://doi.org/10.1103/PhysRevLett.96.017802)

PACS numbers: 61.41.+e

Cellular and fibrous materials (see Fig. 1) are ubiquitous in nature and in many areas of technology. Examples range from solid or liquid foams over wood and bone to the protein fiber network of cells [1–3]. On a mesoscopic level, these materials are comprised of struts and membranes with anisotropic elastic properties. The systems differ widely in architecture. One finds patterns which are as regular as a honeycomb, as sophisticated as the particular design of a dragonfly’s wing, or simply random [4]. The manifold combinations of architecture and elastic properties of the building blocks allow for a rich spectrum of macroscopic elastic responses. For regular cellular structures, macroscopic elasticity can already be understood by considering the response of a single cell [2,5]. In these systems, local stresses acting on an individual cell are the same as those applied on the macroscopic scale. In other words, the local deformation δ of a cell with linear dimension l_s follows the macroscopic strain γ in an *affine way* such that it scales as $\delta \propto \gamma l_s$. Since in affine models there can be no cooperativity between the elastic responses of individual cells, the effect of the assembled structure can be predicted simply by counting the number of cells. Fibrous networks, on the other hand, are dramatically different already in their morphology as can be inferred from Fig. 1. The presence of fibers introduces the additional mesoscopic scale of the fiber length l and, by hierarchically cutting cells into smaller and smaller compartments, generates a broad distribution of pore sizes that, in contrast to foams, has a nonvanishing weight even for the smallest cells [6]. This difference in architecture crucially affects the mechanical properties. Recently, a nonaffine regime has been identified [7] and characterized [8–10] in two-dimensional networks of classical beams (“Mikado model”) commonly used to model the mechanical properties of paper sheets [11–14]. The nonaffinity of the deformation field necessarily implies that in these networks cooperativity effects play an important role.

In this Letter, we will contrast the two systems of foams and fiber networks and relate their different linear elastic properties to their specific structural features. By system-

atically tuning the force response properties of the individual elements, we will be able to show that the hierarchical architecture of the fiber network leads to a new length scale, below which correlations drive the system away from the state of affine deformations. We will, moreover, describe the mechanism that generates this length and calculate the resulting power law behavior of the elastic modulus by a scaling argument.

The fiber network is defined as follows. N anisotropic elastic elements, geometrically represented by straight lines of length l , are placed on a plane of area $A = L^2$ such that both the position and the orientation of the elements are uniformly randomly distributed. The length of the segments, i.e., the distance l_s between any two neighboring intersections, follows an exponential distribution [6]

$$P(l_s) = \langle l_s \rangle^{-1} e^{-l_s/\langle l_s \rangle}, \quad (1)$$

with a mean value that is given in terms of the density $\rho = Nl/A$ as $\langle l_s \rangle = \pi/2\rho$. At any intersection, a permanent cross-link with zero extensibility is generated. This constrains the relative translational motion of the two filaments, while leaving the rotational degrees of freedom independent. Not allowing for kinking, filaments are assumed to remain straight at the cross-links. The simplicity of this network structure (one parameter ρ) makes it an

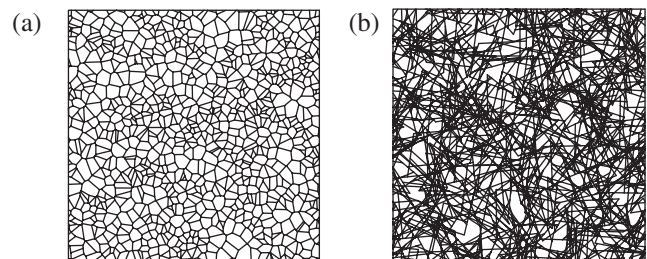


FIG. 1. Illustration of the different architecture of (a) cellular and (b) fibrous materials. The foam in (a) is constructed by a Voronoi tessellation from the centers of the fibers in (b).

ideal candidate to obtain physical insight into the relation of architecture and elastic properties of the constituents, which we specify next. Previous studies [8,9] have considered classical beams of radius r and bending stiffness κ . Loaded along their axis (“stretching”), such slender rods have a rather high stiffness $k_s = 4\kappa/l_s r^2$, while they are much softer with respect to transverse deformations $k_\perp(l_s) = 3\kappa/l_s^3$ (“bending”). Here we consider elastic elements where, in addition to the mechanical stiffness of beams, a more general stretching coefficient

$$k_{\parallel}(l_s) = 6\kappa \frac{l_p^\alpha}{l_s^{3+\alpha}} \quad (2)$$

is introduced. This may result from thermal fluctuations of the filament immersed in a heat bath of solvent molecules. The prefactor is chosen such that k_{\parallel} for $\alpha = 1$ reduces to the longitudinal entropic elasticity of a stiff polymer described by the wormlike chain model grafted at one end [15]. In this case, the material length l_p is called the persistence length of the polymer and quantifies the ratio of bending to thermal energy $l_p = \kappa/k_B T$. The phenomenological exponent α allows us to extend our discussion to the broad class of systems for which k_{\parallel} is a monomial (with units energy per area) involving one additional material length l_p . Having two longitudinal deformation modes, the effective stretching stiffness is equivalent to a serial connection of the “springs” k_s and k_{\parallel} . Setting $l_p = cr$, we can write $k_s \propto k_{\parallel}(\alpha = -2)$. The constant c is a material property of the specific polymer and has been chosen as $c = 1.5 \times 10^4$, which roughly corresponds to the biopolymer F-actin. The precise value, however, is irrelevant with regard to the thermal response k_{\parallel} and specifies only the location of the crossover to k_s . The description of a thermally fluctuating network in terms of force constants k_{\parallel} , k_s , and k_\perp is in the spirit of a Born-Oppenheimer approximation that neglects the fluctuations of the “slow variables,” the cross-link positions, while assuming the “fast” polymer degrees of freedom to be equilibrated. By minimization of the internal energy with respect to the slow parameters, we calculate the shear modulus G for a given macroscopic shear strain of $\gamma = 0.01$. This procedure is performed with the commercially available finite element solver MSC.MARC using periodic boundary conditions on all four sides of the simulation box.

As indicated in the introduction, the complement to the fiber network is a regular foamlike material that one can describe by a mean-field approach [2,5]. Assuming correlations between neighboring segments to be absent, the response is fully described by the properties of an average segment of length $\langle l_s \rangle \propto \rho^{-1}$. Marking the force constants of this segment by an overbar, we can express them in the form (neglecting numerical prefactors) $\bar{k}_\perp \approx \kappa \rho^3$, $\bar{k}_{\parallel} \approx \bar{k}_\perp (\rho l_p)^\alpha$, and $\bar{k}_s \approx \bar{k}_\perp (\rho r)^{-2}$, respectively. The deformation modes will act as springs connected in series [5] such that the modulus takes the form

$$G_{\text{foam}}^{-1} = a\bar{k}_{\parallel}^{-1} + b\bar{k}_\perp^{-1} + c\bar{k}_s^{-1}. \quad (3)$$

The foam will thus show a crossover from thermal stretching to bending at $l_p \approx \langle l_s \rangle$ and to mechanical stretching at $r \approx \langle l_s \rangle$. This behavior, and for illustration also that of a completely random foam, are indicated by the dashed lines in Figs. 2 and 3, where they can be compared with the actual results of our numerical analysis on the fiber system. In Fig. 2, the normalized shear modulus $G l^3 / \kappa$ is shown as a function of dimensionless persistence length l_p / l for a set of dimensionless densities ρl for the special case of $\alpha = 1$. At large l_p / l (right part of the plot), we recover purely mechanical behavior characterized by $G \propto \bar{k}_s$ consistent with the mean-field picture of Eq. (3) [8,9,11]. Our main interest, however, lies in the regime of small l_p / l (left part of the plot), where the persistence length is small enough for thermal fluctuations to become relevant. To analyze the modulus in the thermal regime ($k_s \rightarrow \infty$), it will be helpful to use dimensional analysis and write the modulus in terms of the two remaining response coefficients \bar{k}_\perp and \bar{k}_{\parallel} of an average segment

$$G(\kappa, l, l_p, \rho) = \bar{k}_\perp g(\rho l, \bar{k}_{\parallel} / \bar{k}_\perp). \quad (4)$$

The first argument of the scaling function g , the density $x = \rho l$, is of geometrical origin and counts the number of cross-links per filament. The second argument, $y = \bar{k}_{\parallel} / \bar{k}_\perp \approx \rho l_p$, relates to the energy balance between stretching and bending of an average segment and marks a crossover at $y \approx 1$ or $l_p \approx \langle l_s \rangle$. From Fig. 2 and the inset in Fig. 3, one infers that for *low densities* $g = y f(x)$, implying for the modulus $G = \bar{k}_{\parallel} f(\rho l)$. This linear dependence on the “preaveraged” stretching compliance \bar{k}_{\parallel} hints at a foamlike stretching dominated regime [10] where correlations are absent. As one can also infer from these figures, the domain of validity of this linear regime is

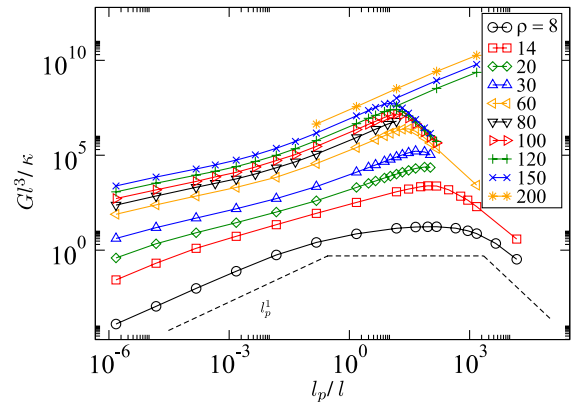


FIG. 2 (color online). Shear modulus $G l^3 / \kappa$ as function of persistence length l_p / l for various densities ρl and $\alpha = 1$. The second branch in the upper right corner ($\rho l \geq 120$) is obtained by suppressing the mechanical response (“ $k_s \rightarrow \infty$ ”). The dashed line indicates the three regimes as obtained by Eq. (3).

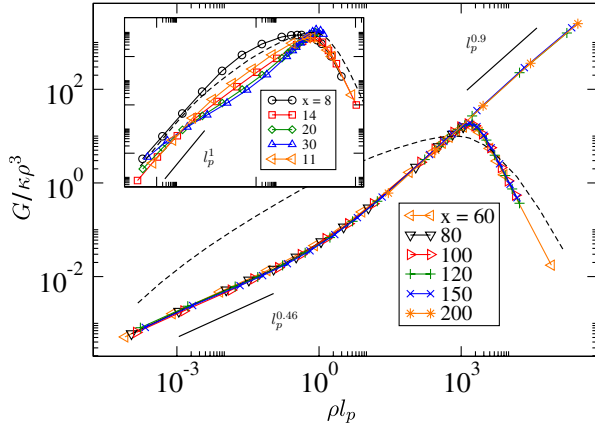


FIG. 3 (color online). Scaling function g as a function of ρl_p for various values of $x = \rho l$. For comparison, we present also the scaling function of a *random* foam (dashed line).

extremely narrow and confined to low densities $x \leq 20$ and persistence lengths $y \ll 1$. For *medium and high densities*, Fig. 3 shows two nontrivial scaling regimes where $g(x \gg 1, y) = y^z$ becomes independent of x (and, therefore, of the filament length l) and exhibits power law behavior with exponents $z = 0.46$ and $z = 0.9$ for small and large values of y , respectively. In both cases, the modulus can be written as a generalized geometric average

$$G \propto \bar{k}_\perp^{1-z} \bar{k}_\parallel^z, \quad (5)$$

which has to be contrasted with Eq. (3), where bending and stretching modes are assumed to superimpose linearly. Here correlation effects between the segments induce the nontrivial form of the modulus and distinguish the fiber network from the ordinary foamlike behavior obtained by single segment considerations. Whereas foams may be considered as a limit where the number of cross-links per fiber is small (filament length identical to the cell size), the scaling limit of fiber networks corresponds to infinite fiber length.

To understand the origin of the correlations, one has to take into account the full distribution of segment lengths, Eq. (1). This will have a pronounced effect on an affine deformation field $\delta_{\text{aff}} \propto \gamma l_s$, as can be seen by considering the axial force f_\parallel along an affinely stretched segment of length l_s , $f_\parallel = k_\parallel \delta_{\text{aff}} \approx \kappa l_p^\alpha \gamma / l_s^{2+\alpha}$. In any but the purely mechanical situation, where $\alpha = -2$ (and, thus, $f_s \approx \kappa \gamma / r^2$), f_\parallel strongly depends on the segment length. This implies that, in general, two neighboring segments on the same filament produce a net force at their common node that has to be taken up by the crossing filament which then, preferentially, will start to bend. From the exponential distribution of segment lengths in Eq. (1), one can easily show that the size of these residual forces δf can be arbitrarily large. The corresponding probability distribution $Q(\delta f)$ shows polynomial (fat) tails

$$Q(\delta f) \propto \delta f^{-(3+\alpha)/(2+\alpha)} P(0), \quad \delta f \rightarrow \infty, \quad (6)$$

and has a diverging mean value. This is due to the finite probability $P(0) = P(l_s = 0) \neq 0$ of finding segments with zero length. As a consequence, there are always residual forces high enough to cause significant bending of the crossing filament. Hence, we conclude that an affine deformation field is unstable and that the system can easily lower its energy by redistributing the stresses to relieve shorter segments and remove the tails of the residual force distribution $Q(\delta f)$.

This mechanism can be used to derive an expression for the modulus in the parameter region $y \ll 1$, where the value of the exponent $z = 0.46$ indicates that bending and stretching deformations contribute equally to the elastic energy. We assume that segments up to a critical length l_c —to be determined self-consistently—will fully relax from their affine reference state to give all their energy to the neighboring segment on the crossing filament. The energy of segments with $l_s > l_c$ will then have two contributions: first, a stretching part from the imposed affine strain field (for simplicity, we will set $\alpha = 1$ in what follows.)

$$w_s(l_s) \approx k_\parallel \delta_{\text{aff}}^2 \approx \kappa \gamma^2 \frac{l_p}{l_s}, \quad (7)$$

second, a bending part

$$w_b(l_s) \approx k_\perp \delta_{\text{aff}}^2 \approx \kappa \gamma^2 \frac{l_s^2}{l_p^3}, \quad (8)$$

that arises only if the segment under consideration is neighbor to an element on the crossing filament with $l'_s < l_c$ (the prime refers to the neighboring small segment). Adding both contributions and averaging over all segments $l_s > l_c$ and $l'_s < l_c$, we arrive at the expression $w \approx \kappa \gamma^2 \rho (\rho l_p / x_c + x_c)$, where $x_c := \rho l_c \ll 1$ in the parameter range of interest. Minimizing with respect to x_c gives the required expressions $x_c^{\text{min}} \approx (l_p \rho)^{1/2}$ and $G \approx \rho^2 w_{\text{min}} / \gamma^2 \approx \kappa \rho^{7/2} l_p^{1/2}$, corresponding to a value $z = 1/2$ for the exponent that compares well with the measured value $z = 0.46$. Repeating the calculation for general values of α gives $z(\alpha) = \alpha / (1 + \alpha)$. We have verified this result by simulations with an accuracy of about 10% [16]. The nontrivial behavior of G observed in Figs. 2 and 3 can thus be explained by a length scale $l_c = \langle l_s \rangle (l_p / \langle l_s \rangle)^{1/2}$, below which the affinity of the deformation field breaks down. The mechanism is illustrated in Fig. 4, where a histogram for the fraction of energy stored in segments of various lengths is shown. Increasing the persistence length, the short segments one after the other lose their energies in favor of additional excitations in longer segments.

When, eventually, $l_c \approx l_p \approx \langle l_s \rangle$ ($y \approx 1$), the affine strain field does not serve as a reference configuration any more, since it is strongly perturbed by a majority of

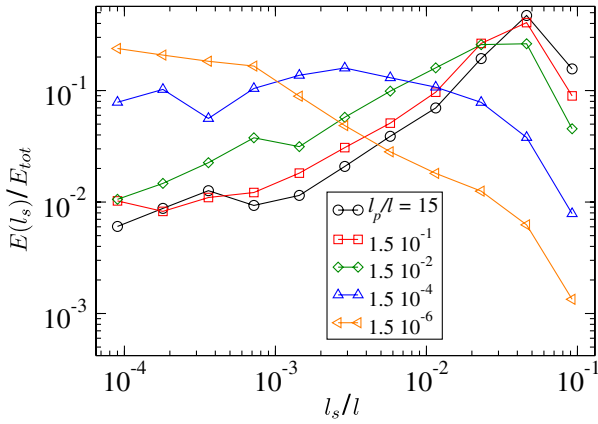


FIG. 4 (color online). Fraction of energy stored in the various segment lengths; the curves correspond to different persistence lengths at a density of $\rho l = 80$, equivalent to $\langle l_s \rangle / l \approx 2 \times 10^{-2}$.

segments with $l_s < l_c$. Moreover, the unloading of the smaller segments now produces significant stretching deformations of their neighbors on the *same* filament such that the available energy for bending of the *crossing* filament is reduced. At this stage, one enters the second intermediate asymptotic regime where, as in the affine regime at low densities, stretching modes dominate the modulus. As can be seen in Fig. 4, only the longest segments carry substantial amounts of energy such that the displacement field must be highly nonaffine. For $l_p/l \geq 1.5 \times 10^{-2}$, about 90% of the energy is stored in the longest 30% of the segments. In this parameter range, bending is on average the softer mode $y = \bar{k}_{\parallel} / \bar{k}_{\perp} \gg 1$ and, therefore, contributes only very little to the total energy. Raising the density to still higher values, it is conceivable from our data that the exponent $z = 0.9$ approaches $z = 1$, which would mean that the energy in the bending modes is completely negligible and $G \sim \bar{k}_{\parallel}$ as in the affine regime. A transition into a regime dominated by the low-energy bending modes would not be favorable, however. As is known from the mechanical fiber model [8], such a regime must not be characterized by the preaveraged force constant $\bar{k}_{\perp} = k_{\perp}(\langle l_s \rangle)$ but by an effective stiffness $\langle k_{\perp} \rangle \approx \kappa / \xi^3$ with a new length scale $\xi = l(\rho l)^{-\mu/3}$ and $\mu \approx 6.7$ that is highly dependent on fiber length l .

In summary, we found that, for a broad range of parameters, the macroscopic shear modulus of fibrous networks is asymptotically independent of the fiber length. Affine stretching is energetically unstable towards a redistribution of energies in favor of longer segments. This gives rise to a correlation-induced elasticity that cannot be explained within a “single cell” model. This physical picture is of general validity and will apply whenever the distribution of segment lengths is sufficiently broad. Cellular systems, being the appropriate structures for rather flexible poly-

mers, will therefore show nonaffine behavior only if they are highly irregular [16–18]. In the complementary case of the fiber network with its hierarchical, scale-invariant architecture, the nonaffinity even leads to asymptotic scaling regimes. These networks are particularly well suited to describe the macroscopic linear response of stiff polymer networks. Therefore, our results may be directly relevant for two-dimensional networks of the filamentous biopolymer F-actin, assembled on top of microfabricated pillars [19]. In addition, it might shed new light on very recent rheological measurements on cross-linked actin networks [20,21], which emphasize the single-polymer origin of the measured elastic moduli. Our simulations, on the contrary, highlight the potentially nontrivial effects of interpolymer correlations on the macroscopic elasticity.

- [1] D. Weaire and S. Hutzler, *The Physics of Foams* (Oxford University Press, Oxford, 2001).
- [2] L. J. Gibson and M. F. Ashby, *Cellular Solids: Structure and Properties* (Cambridge University Press, Cambridge, England, 1999).
- [3] B. Alberts *et al.*, *Molecular Biology of the Cell* (Garland Publishing, New York, 1994).
- [4] D. W. Thompson, *On Growth and Form* (Cambridge University Press, Cambridge, England, 1961).
- [5] A. M. Kraynik and W. E. Warren, in *Low Density Cellular Plastics*, edited by H. Hilyard and C. Cunningham (Kluwer Academic, Amsterdam, 1994), Chap. 7.
- [6] O. Kallmes and H. Corte, *Tappi* **43**, 737 (1960).
- [7] E. Frey, K. Kroy, J. Wilhelm, and E. Sackmann, in *Dynamical Networks in Physics and Biology*, edited by G. Forgacs and D. Beysens (Springer, Berlin, 1998).
- [8] J. Wilhelm and E. Frey, *Phys. Rev. Lett.* **91**, 108103 (2003).
- [9] D. A. Head, A. J. Levine, and F. C. MacKintosh, *Phys. Rev. Lett.* **91**, 108102 (2003).
- [10] D. A. Head, A. J. Levine, and F. C. MacKintosh, *Phys. Rev. E* **68**, 061907 (2003).
- [11] J. A. Åström, J. P. Mäkinen, M. J. Alava, and J. Timonen, *Phys. Rev. E* **61**, 5550 (2000).
- [12] J. A. Åström, S. Saarinen, K. Niskanen, and J. Kurkijärvi, *J. Appl. Phys.* **75**, 2383 (1994).
- [13] M. Latva-Kokko and J. Timonen, *Phys. Rev. E* **64**, 066117 (2001).
- [14] S. Heyden, Ph.D. thesis, Lund University, 1996.
- [15] K. Kroy and E. Frey, *Phys. Rev. Lett.* **77**, 306 (1996).
- [16] C. Heussinger and E. Frey, cond-mat/0512557.
- [17] A. Fazekas, R. Dendievel, L. Salvo, and Y. Bréchet, *Int. J. Mech. Sci.* **44**, 2047 (2002).
- [18] M. J. Silva, W. C. Hayes, and L. J. Gibson, *Int. J. Mech. Sci.* **37**, 1161 (1995).
- [19] W. H. Roos *et al.*, *Chem. Phys. Chem.* **4**, 872 (2003).
- [20] M. L. Gardel *et al.*, *Science* **304**, 1301 (2004).
- [21] J. H. Shin *et al.*, *Proc. Natl. Acad. Sci. U.S.A.* **101**, 9636 (2004).

The Role of Architecture in the Elastic Response of Semi-flexible Polymer and Fiber Networks

Claus Heussinger and Erwin Frey

*Arnold Sommerfeld Center for Theoretical Physics and CeNS,
Department of Physics, Ludwig-Maximilians-Universität München,
Theresienstrasse 37, D-80333 München, Germany and
Hahn-Meitner-Institut, Glienicker Strasse 100, D-14109 Berlin, Germany*
(Dated: August 29, 2007)

We study the elasticity of cross-linked networks of thermally fluctuating stiff polymers. As compared to their purely mechanical counterparts, it is shown that these thermal networks have a qualitatively different elastic response. By accounting for the entropic origin of the single-polymer elasticity, the networks acquire a strong susceptibility to polydispersity and structural randomness that is completely absent in athermal models. In extensive numerical studies we systematically vary the architecture of the networks and identify a wealth of phenomena that clearly show the strong dependence of the emergent macroscopic moduli on the underlying mesoscopic network structure. In particular, we highlight the importance of the polymer length that to a large extent controls the elastic response of the network, surprisingly, even in parameter regions where it does not enter the macroscopic moduli explicitly. Understanding these subtle effects is only possible by going beyond the conventional approach that considers the response of *typical polymer segments* only. Instead, we propose to describe the elasticity in terms of a *typical polymer filament* and the spatial distribution of cross-links along its backbone. We provide theoretical scaling arguments to relate the observed macroscopic elasticity to the physical mechanisms on the microscopic and the mesoscopic scale.

PACS numbers: 87.16.Ka, 62.20.Dc, 82.35.Pq

I. INTRODUCTION

Classical elasticity is a continuum theory that deals with the large scale deformation properties of solid systems. It relates stresses and strains by introducing a host of phenomenological parameters, e.g. shear and bulk modulus for isotropic media, that characterize the elastic properties on wave lengths large compared with any other material length scale [1]. Biological systems like the cell or sub-cellular organelles are often characterized by a highly heterogeneous structure with a multitude of hierarchical levels of organization [2]. Due to these large scale inhomogeneities that may extend up to the scale of the system size, the applicability of elasticity theory on smaller length scales has to be critically examined. In particular, the actual deformations in the system are expected to relate to the externally applied stresses in a non-trivial way that crucially depends on the specific structural details.

To shed some light on the relevance of structure to the effective elasticity this article deals with the calculation of elastic constants in networks of semi-flexible polymers. In eukaryotic cells these networks assemble to form the cytoskeleton that plays a central role in many cellular functions such as locomotion, adhesion or cell division. From the point of view of structure already a one-component isotropic solution of semi-flexible polymers represents an interesting model-system being studied for many years [3, 4, 5]. One of the main quantities of interest is the plateau value of the shear modulus found at intermediate timescales where single polymer bending fluctuations are equilibrated, yet center of mass motion

is negligible. The generally accepted theory for the concentration dependence of the plateau modulus is based on the free energy change of confining a polymer to a tube [3, 6, 7, 8], the diameter of which is a consequence of the structural organization of the tubes in the form of a random assembly of cylinders [9]. Even though this is well known for more than a decade, computer simulations to study the geometrical as well as elastic properties in this fibrous architecture have only recently been realized [10, 11].

Upon the addition of cross-linking agents or other regulating proteins one can induce structural changes to modify the network architecture in many ways [12, 13, 14, 15, 16]. There have been attempts to describe the phase diagram of these systems [17, 18], the detailed mechanisms that lead to a particular structure, however, are far from being understood. In general, there will be a complex interplay of polymer kinetics, thermal fluctuations and chemical as well as mechanical properties of the polymers and the cross-linking agents yielding a particular architecture relevant for a given physical situation.

A complementary approach to describe cross-linked networks is to neglect these intricate “dynamic” aspects of the network, and to concentrate on a “static” architecture and its effect on the macroscopic elasticity [19, 20, 21, 22, 23, 24]. In the structural engineering community, for example, it is of tantamount importance to analyze the architecture of structures made of beams or trusses. A common way to take advantage of the reduced weight compared to the bulk material without suffering from a loss of stiffness is a triangulation of the basic cells. This eliminates the soft bending modes of the beams and makes it possible to construct huge cantilever

bridges like that over the Firth of Forth in Scotland or towers like Eiffel’s tower in Paris. Since the rigidity of these structures is not due to the individual beam but to a non-local back-coupling effect induced by the architecture of the network, the triangulation is therefore one example on how cooperativity among the building blocks may be possible.

To address this question of cooperativity in the context of the elasticity of cross-linked stiff polymer networks we will concentrate in the following on two generic structures, *cellular* and *fibrous* networks, that may serve as reference systems for the classification of real polymer networks. While cellular structures may be characterized by the amount of randomness in size and type of their unit cells (see Fig.1b-d), fibrous networks have a hierarchical structure, where smaller cells are generated within larger cells within even larger cells (Fig.1a). This is a consequence of the presence of the additional mesoscopic scale of the fiber length. As we will see, this length-scale is ultimately responsible for the intricate scaling properties of the elasticity of fibrous polymer networks. The goal of this article is to identify these mechanisms, that couple the particular network structure to the properties of the individual polymers and effectuate the macroscopic elasticity of the system.

In contrast to the purely mechanical systems relevant for engineering applications [19, 20, 21, 25], the systems we would like to study are immersed in a thermal environment. This implies that in addition to the usual enthalpic polymer elasticity also entropic effects have to be accounted for. We have published a brief account of this study recently [23]. It will turn out that by accounting for the entropic origin of the single-polymer elasticity, the networks acquire a strong susceptibility to polydispersity and structural randomness that is completely absent in athermal models.

The article is organized as follows. In Sect.II we motivate our modeling approach of thermally fluctuating networks of stiff polymers. This will lead us to the definition of effective elastic properties of the “polymer segments” that constitute the elementary building blocks of the network. In Sect.III and IV these polymer segments are assembled into cellular and fibrous networks, respectively. The macroscopic elastic constants of these structures are calculated and related to the particular architectural features. Finally, in Sect.V we present our main conclusions and hint at implications for experiments.

II. MODEL DEFINITION

To study the elastic properties of thermally fluctuating cross-linked stiff polymer networks we calculate numerically the low frequency shear modulus. Assuming a time-scale separation between the fast bending fluctuations of the single polymer and their very slow center of mass motion, we adopt a description of the system in the spirit of a Born-Oppenheimer approximation. This neglects en-

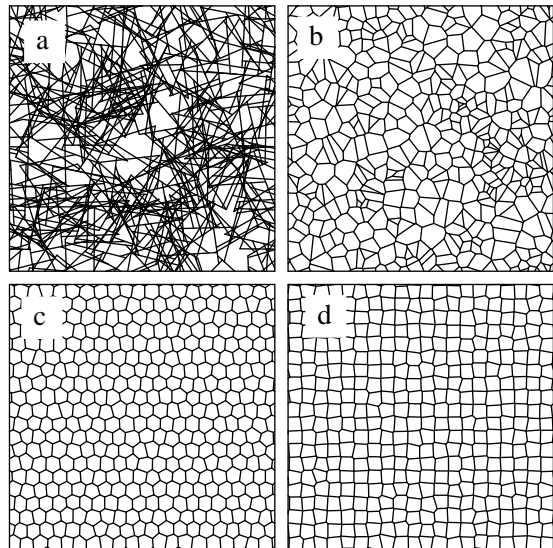


FIG. 1: Illustration of the different architectures of (a) fibrous and (b-d) cellular materials in two dimensions. While (a) and (b) are random structures generated by Poisson point processes, (c) and (d) are quite regular networks based on honeycomb and square lattices, respectively.

tropic contributions from the “slow variables”, the cross-link positions, while assuming the “fast” polymer degrees of freedom to be equilibrated at all times. Macroscopic quantities will then depend parametrically on the set of cross-link variables. A macroscopic shear strain γ constrains the cross-links at the boundaries, while those in the bulk are moving freely to minimize the elastic energy E . The shear modulus is defined as its second derivative with respect to the shear strain, $G = V^{-1} \partial^2 E_{\min} / \partial \gamma^2$, where V is the system volume.

By keeping the positions of the cross-links fixed, the energy can be written as a sum

$$E = \sum_{\alpha} \epsilon(\delta \mathbf{x}^{\alpha}), \quad (1)$$

over contributions from individual polymer segments α , each of which connects a given pair of cross-links (see Fig.2). The single segment energy e depends on the generalized “displacement-vector” $\delta \mathbf{x}^{\alpha}$, which incorporates the degrees of freedom, displacements \mathbf{u} and rotations $\boldsymbol{\theta}$, of the two cross-links pertaining to the segment.

In the numerical section we focus on two-dimensional systems such that a vector $\delta \mathbf{x}_{2d} = (\mathbf{u}_0, \theta_0, \mathbf{u}_l, \theta_l)$ has six components. Those are in-plane displacements $\mathbf{u}_{0,l}$ and z-axis rotations $\theta_{0,l}$, at both ends $0, l$ of the segment with length l (see Fig.2). Note, that the additional variable of cross-link rotation sets our system apart from bond-bending and related models [26] where only translational degrees of freedom are accounted for. As a consequence one also has to account for the presence of torques as the conjugate variable to rotations.

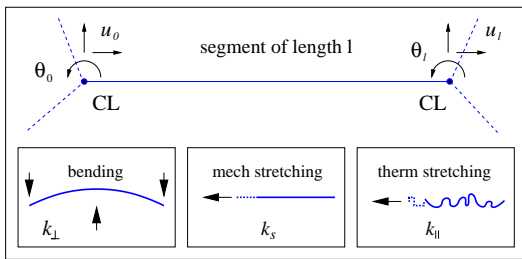


FIG. 2: Illustration of a polymer segment of length l and its connection to the network (dashed lines) at the cross-links (CL). The three degrees of freedom at each cross-link are denoted by \mathbf{u} and θ , respectively. Identification of the three possible modes of deformation and their stiffnesses k_{\perp} , k_s and k_{\parallel} as defined in the text.

To leading order, in linear elasticity, the single segment quantity e is a quadratic function of its coordinates

$$e(\mathbf{x}) = \frac{1}{2} \mathbf{x}^T \mathbf{K} \mathbf{x}, \quad (2)$$

which defines the “stiffness matrix” \mathbf{K} (spring constants) of the polymer strand.

In models of classical beams with cross-section radius r the matrix elements are well established and relate to the two deformation modes of stretching (s) and bending (\perp), respectively. While the former is characterized by the Young’s modulus E of the material, the latter depends on the bending stiffness $\kappa = E\pi r^4/4$, here taken for circular cross-sections. To calculate the bending response, standard Euler-Bernoulli beam theory [1] is used.

While we refer to Appendix A for a derivation of the complete matrix, it turns out that the response of a beam of length l is sufficiently characterized already by two elements of \mathbf{K} ,

$$k_s(l) = 4\kappa/lr^2, \quad k_{\perp}(l) = 3\kappa/l^3, \quad (3)$$

relating to either deformation mode. Due to their small aspect ratios $r/l \ll 1$ slender rods are highly anisotropic and much softer in bending than in stretching, $k_{\perp}/k_s \propto (r/l)^2$. In this approximation the two deformation modes are decoupled such that, for example, pre-stretching does not influence the bending response. Therefore, Euler-buckling cannot be accounted for.

Here, we consider thermally fluctuating stiff polymers immersed in a heat bath of solvent molecules. In these systems, the effects of temperature on the elastic properties of the polymer can be quantified by defining the persistence length l_p as the ratio of bending stiffness to thermal energy $l_p = \kappa/k_B T$. With this definition we have, in addition to the enthalpic stiffness of the classical beam, an entropic contribution

$$k_{\parallel}(l) = \zeta \kappa \frac{l_p}{l^4}, \quad (4)$$

to the polymer’s stretching compliance that can be calculated within the wormlike chain model [27, 28]. The

prefactor ζ depends on the specific boundary conditions chosen at the ends of the polymer segment. Its value can be absorbed in the persistence length, and therefore only quantitatively affects the results. To avoid a large numerical offset with respect to Eq.(3), we have chosen $\zeta = 6$, which corresponds to a boundary condition with one end clamped [27]. Having two longitudinal deformation modes k_s and k_{\parallel} the effective stretching stiffness is equivalent to a serial connection

$$k_{\text{eff}}^{-1} = k_s^{-1} + k_{\parallel}^{-1}. \quad (5)$$

Thus, the elastic properties of the polymer segments are given by the classical theory of beam bending supplemented by a generalized stretching stiffness, that also includes entropic effects. While the stiffness matrix has only been set up for the two-dimensional problem, the governing entries in three dimensions will still be the same Eqs.(3) and (4).

As one can infer from Eqs.(3) and (4), at a given temperature T there are two length scales characterizing the material properties of the polymers, the radius r and the persistence length l_p . Typical biological polymers are characterized by a ratio $R = l_p/r \gg 1$. F-actin, for example, a key component of the cytoskeleton has $R = O(10^4)$ ($r \approx 5\text{nm}$, $l_p \approx 17\mu\text{m}$), while microtubules, most important for cell-division and intra-cellular transport, have an even larger $R = O(10^6)$. For specificity, we require in the following a constant $R = 1.5 \cdot 10^4$, the precise value, however, is irrelevant if one is interested only in the thermal response where the radius does not enter and $k_s \rightarrow \infty$ [45]. Occasionally, we will perform this limit to highlight features that are independent of the mechanical stretching response. On the other hand, the location of the cross-over point, where the mechanical stretching becomes relevant, does indeed depend on the choice of R . By definition, it determines the relative magnitude of the two stretching compliances $k_s/k_{\parallel} \simeq R^2(l/l_p)^3$.

The dependence of the three force constants k_{\perp} , k_s and k_{\parallel} , Eqs.(3) and (4), on the ratio of persistence length to segment length l_p/l is illustrated in Fig.3. One can clearly distinguish three regimes, in each of which one of the spring constants is by far smaller than the remaining two. The dashed line corresponds to a hypothetical spring where the deformation modes are coupled in series $k^{-1} = k_{\perp}^{-1} + k_s^{-1} + k_{\parallel}^{-1}$. If the segment length l was representative for the network under consideration, that is the network was characterized by only small polydispersity, then we would expect the macroscopic modulus to be well approximated by the microscopic single segment behavior considered here. We will later refer to this behavior as the “affine model”. It will be shown to be valid only in regular cellular structures.

This completes the specification on the microscopic scale of the elastic properties of the single polymer segments. We now proceed to assemble the segments into networks of varying architecture to identify the physical principles which determine the elastic response on the macroscopic scale.

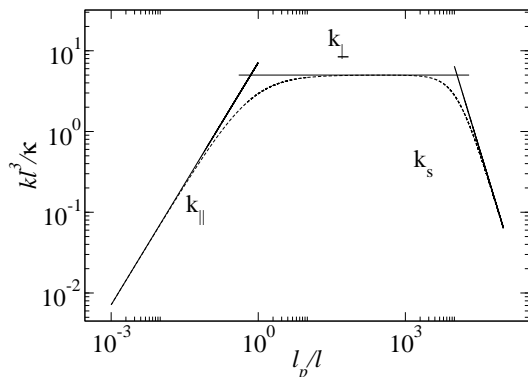


FIG. 3: Dependence of the three spring constants k_{\parallel} , k_{\perp} and k_s on persistence length l_p/l . The dashed line corresponds to a hypothetical spring with the three deformation modes connected in series.

To determine the elastic shear modulus, we apply a small shear strain of $\gamma = 0.01$ to stay in the regime of linear elasticity and use periodic boundary conditions on all four sides of the simulation box. The numerical procedure is performed with the commercially available finite element solver MSC.MARC. The results will be complemented by scaling arguments.

We will find that in *regular cellular architectures*, to be discussed next, macroscopic elasticity can trivially be explained by the microscopic constitutive laws given in terms of the stiffness matrix \mathbf{K} . In sufficiently *random cellular systems*, however, this picture is changed. The macroscopic response takes up nontrivial features that cannot be explained by single polymer elasticity. In *fibrous architectures*, subject of Sect.IV, we will find this anomalous elasticity again but in more striking form.

III. CELLULAR ARCHITECTURE

A cellular structure is most conveniently constructed from a Voronoi tessellation of a distribution of points which may either be chosen regularly or by some random process [29]. With each point we associate a Voronoi cell that is defined to enclose that region in space which is closer to the given point than to any of its neighbors. This procedure is equivalent to the Wigner-Seitz construction known from solid-state physics. In three dimensions the elastic elements are defined to be the lines of intersection of two neighboring cell walls, while in two dimensions (see Fig.1) they are represented by the cell walls themselves. We will call these elastic building blocks of the network *polymer segments* and associate to them the material properties, respectively the stiffness matrix \mathbf{K} , introduced in the preceding section. By its definition, a segment spans the distance between two vertices and is therefore “end-linked” to the rest of the network.

Depending on the spatial distribution of Voronoi

points there will also be a distribution $P(l_s)$ of segment lengths l_s . Only in regular structures, for example the (anisotropic) two-dimensional honeycomb structure, this distribution will degenerate into one (or several) delta-function peaks.

The first moment of this distribution, the average segment length \bar{l}_s , is naturally the most important quantity to describe the geometrical aspects of a cellular structure. In $d = 2, 3$ dimensions this “mesh-size” may be reparametrized in terms of the density ρ as

$$\bar{l}_s \propto \rho^{-1/(d-1)}, \quad (6)$$

where we defined ρ as the total polymer length per system size. While there are practical reasons to use ρ as a measure for the density in the simulations, in experimental work it is sometimes easier to control the monomer concentration c . This can be found as $rc \propto \rho$, where the cross-section radius r is assumed proportional to the monomer size.

A. Mechanical Behavior: Beams

In the engineering literature the cellular structures defined above are well known as foams and are ubiquitous in nature and many areas of technology. Examples range from liquid foams and froths well known from drinks or household detergents, to plastic and metallic foams used for insulation or shock absorption [29, 30]. It is well known that naturally occurring foams have to obey Plateau’s laws to reach an equilibrium state. We do not require these laws to hold in the following, since we are interested in the dependence of elastic properties on the architectural features in general, and not in the specific details of the dynamic properties of foams.

For purely mechanical cellular foams, where thermal fluctuations are neglected altogether, the only material length scale is the radius r of the cross-section. By identifying κ/\bar{l}_s as an energy scale, we can use dimensional analysis to write the shear modulus G as

$$G = \frac{\kappa}{\bar{l}_s^{d+1}} g(r/\bar{l}_s), \quad (7)$$

where the occurrence of the spatial dimension d highlights the fact that the modulus has units of an energy density. In writing this, we have not made explicit the dependence on the higher moments of the probability distribution P . As will become clear below, these can be used to characterize the randomness of the structure and will be considered separately. If one defines force-constants at the scale of the average mesh-size

$$\bar{k}_{\perp} \simeq \kappa/\bar{l}_s^3, \quad \bar{k}_s \simeq \kappa/\bar{l}_s r^2, \quad (8)$$

the scaling variable can alternatively be written as $r/\bar{l}_s \simeq \sqrt{\bar{k}_{\perp}/\bar{k}_s}$, and therefore characterizes the relative stiffness of the bending to the stretching mode.

B. Regular Structures and Affine Models

Restricting our attention for the moment to regular structures, macroscopic elasticity can already be understood by considering the response of a single cell [30, 31, 32]. In these systems it seems reasonable that local stresses acting on an individual cell are the same as those applied on the macroscopic scale. In other words, the local deformation δ of a cell with linear dimension \bar{l}_s follows the macroscopic strain γ in an *affine way* such that it scales as $\delta \propto \gamma \bar{l}_s$. With this assumption the scaling function can be calculated [31] and one generically finds for the modulus

$$G_{\text{aff}}^{-1} = \bar{l}_s^{d-2} (a \bar{k}_\perp^{-1} + b \bar{k}_s^{-1}), \quad (9)$$

where the details of the particular structure may enter the numbers a and b in an involved way. The important conclusion to be drawn is that the deformation modes act as if they were springs connected in series. For slender beams with $r \ll \bar{l}_s$ the bending mode is softer than the stretching mode and therefore dominates the modulus – mechanical foams are *bending dominated*.

While we argue here that the modulus in Eq.(9) represents the generic case, there may be special cases where the prefactors a or b are suppressed by the specific choice of the unit cell. The triangulated network is one example where $a = 0$ and the bending mode is suppressed. Below we will encounter another example when studying the square lattice. For these systems the special geometry of the unit cell, or more generally, the local architecture has to be taken into account. This is indeed the main focus of this article. On the other hand, by assuming affine displacements no cooperativity between the elastic responses of neighboring cells is possible. The macroscopic modulus G directly reflects the elastic properties of the single cell. The local geometry is being hidden in the prefactors a and b , while the effect of the assembled structure may simply be predicted by counting the numbers of cells.

C. Cell Polydispersity

We have tested the validity of the affine model in a simple two-dimensional cellular structure with varying degree of randomness. We have taken the seeds for a Voronoi construction of a regular, honeycomb lattice structure and randomly displaced them with a uniform probability distribution of width $\Delta \cdot \bar{l}_s$. The influence of randomness on the elastic properties of mechanical (non-fluctuating) foams has been studied extensively by various authors [33, 34, 35]. Here, we also include effects from thermal fluctuations such that the response of a polymer segment is characterized by three deformation modes with stiffnesses k_s, k_\parallel and k_\perp , respectively. The affine prediction for the modulus of this system ($d = 2$)

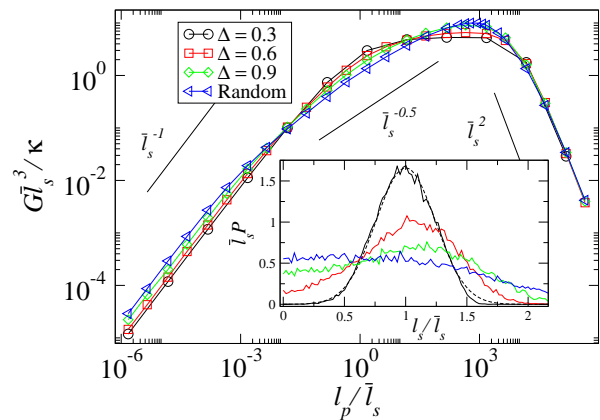


FIG. 4: Shear modulus $G \bar{l}_s^3 / \kappa$ as a function of l_p / \bar{l}_s for a 2d honeycomb foam structure with varying degree of randomness Δ . The blue curve (“Random”) corresponds to a “maximally” random foam generated from a Poisson point process. Inset: Distribution P of segment lengths for the same systems. At low levels of randomness ($\Delta = 0.3$) it can be approximated by a Gaussian probability distribution (dashed line), while it shows significant broadening upon increasing the randomness to $\Delta = 0.6, 0.9$. The peak disappears completely in the case of the maximally random Poisson foam.

can be inferred from Eq.(9). By defining

$$\bar{k}_\parallel \simeq \kappa l_p / \bar{l}_s^4, \quad (10)$$

and substituting $\bar{k}_s^{-1} \rightarrow \bar{k}_s^{-1} + \bar{k}_\parallel^{-1}$ one finds for the modulus

$$G_{\text{aff}}^{-1} = \bar{k}_\perp^{-1} h(l_p / \bar{l}_s) = \frac{\bar{l}_s^3}{\kappa} \left[a + b \left(\frac{R \bar{l}_s}{l_p} \right)^{-2} + c \frac{\bar{l}_s}{l_p} \right], \quad (11)$$

where we have inserted Eqs.(8) and (10) and used the relation $R = l_p / r$. This has to be compared with the actual results of our numerical analysis in Fig.4. The normalized shear modulus $G \bar{l}_s^3 / \kappa$ is shown as a function of persistence length l_p / \bar{l}_s expressed in units of the average segment length. The curves correspond to varying degrees of randomness Δ .

We find that regular networks (black curve, circles) characterized by a single mesh-size \bar{l}_s indeed display the functional form expressed through Eq.(11). For mesh-sizes much larger than the persistence length $\bar{l}_s \gg l_p$ the network deforms by pulling out thermal undulations and $G \propto \bar{k}_\perp \propto \bar{l}_s^{-4}$ (left part of Fig.4). Decreasing the mesh-size beyond $\bar{l}_s \approx r$ stretching of the polymer backbone dominates the modulus $G \propto \bar{k}_s \propto \bar{l}_s^{-1}$ (right part of Fig.4). The physically relevant situation for studying stiff polymers, however, corresponds to the intermediate regime, where the persistence length is much larger than the mesh-size, which is still much larger than the polymer radius $l_p \gg \bar{l}_s \gg r$. Typical actin networks with $l_p = 17 \mu\text{m}$ and $r = 5 \text{nm}$ may have mesh-sizes in the sub-micron range $\bar{l}_s \approx 100 \text{nm}$. In this regime, most

of the energy is stored in the bending modes leading to $G \propto \bar{k}_\perp \propto \bar{l}_s^{-3}$ corresponding to the plateau region visible in Fig.4.

Using the values $a = 0.2$, $b = 0.35$ and $c = 0.14$ we managed to fit the scaling function of Eq.(11) to the numerical data (in fact, this is the dashed line in Fig.3). Increasing the level of randomness the presence of the additional variable Δ spoils the scaling property and a fit is no longer possible. The power law regimes gradually shrink and the cross-over regions increase in size. While the mechanical stretching regime is hardly affected by the randomness at all, this effect is most pronounced in the cross-over from the bending to the thermal stretching dominated regime. The physically most relevant intermediate plateau regime disappears completely and shows strong amplitude modulations.

We have also generated foams by Voronoi tessellation of a fully random distribution of points, corresponding to a Poisson process (blue curve, left triangles). For these “maximally random foams” one could rather use an expression $G \propto \bar{l}_s^{-7/2}$ to characterize the modulus at these intermediate parameter values. At this point this is only an empirical observation. Later, in the context of the fibrous architecture, we will see how this exponent can be derived from a scaling argument that properly takes into account the randomness in the system.

One may infer from the inset of Fig.4 that deviations from the scaling form presented in Eq.(11) are indeed intimately connected to a broadening of the segment length distribution $P(l_s)$. In the regular structure the distribution can very well be described by a Gaussian centered around the average mesh-size \bar{l}_s (dashed line in Fig.4). Random foams, on the contrary, display significantly broader distributions and even have non-negligible weight on very small segments.

We will see below that the different effect of randomness in the thermal and the mechanical stretching regimes can be traced back to the unusually strong length dependence of the entropic stretching stiffness $k_\parallel \propto l_s^{-4}$ as compared to $k_s \propto l_s^{-1}$. We will find that this leads to the breakdown of the affine model whenever there is a sufficiently broad distribution of segment lengths. Thermal networks are thus inherently more sensitive to elements of randomness than purely mechanical systems.

It is instructive to consider yet another lattice structure as a basis for our foam model (see Fig. 1). By placing the Voronoi points on a slightly randomized square lattice one can generate a foam with a bimodal segment length distribution having a second peak at some small length l_1 (see inset Fig.6). To understand this, one has to realize that a generic foam structure generated by Voronoi tessellation has only three-fold connected vertices, while they are four-fold connected in the square network. A small amount of randomness therefore induces a bifurcation of a four-fold vertex into a short segment with three-fold connected vertices at its ends (see Fig.5). Unlike the honeycomb foam, the resulting structure is elastically anisotropic and has 3 distinct moduli [36]. In addition to

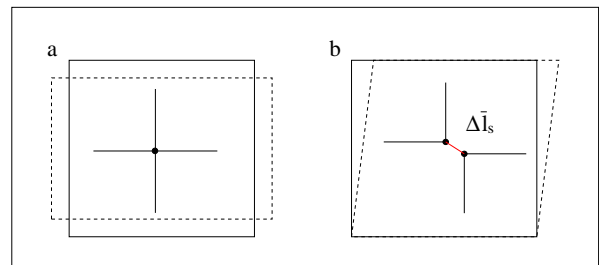


FIG. 5: (a) Pure shear deformation of the square lattice and (b) simple shear. Illustration of the bifurcation leading from a four-fold connected vertex to a three-fold connected one by introducing small amounts of randomness $\Delta\bar{l}_s$.

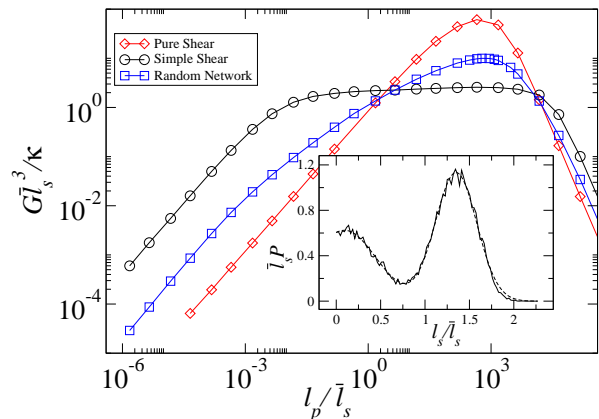


FIG. 6: The two different shear moduli for the slightly randomized square lattice ($\Delta = 0.3$) as shown in Fig.1. Also shown is the modulus of the highly random Poisson foam. Inset: Distribution of segment lengths for the same network. The dashed line is a fit to a sum of two Gaussians centered around $l_1/\bar{l}_s = 0.092$ and $l_2/\bar{l}_s = 1.35$.

the bulk modulus there are two shear moduli corresponding to simple and pure shear deformations. These two modes are schematized in Fig.5, while the corresponding moduli (together with the isotropic shear modulus of the Poisson foam) are shown in Fig.6. Pure shear leads to deformations along the main axis of symmetry of the unit squares and thus to stretching of the elements. The bending regime is therefore strongly suppressed. On the other hand, simple shear deforms the squares along their diagonals and thus favors the bending mode. Only when the stretching energy stored in the small segments $w_\parallel = k_\parallel(l_1)\delta_{\text{aff}}(l_1)^2 \propto l_p/l_1^2$ equals the bending energy in the average segment $w_\perp = k_\perp(\bar{l}_s)\delta_{\text{aff}}(\bar{l}_s)^2 \propto \bar{l}_s^{-1}$ does the system cross-over to a stretching dominated network. Noting (from the inset of Fig.6) that $l_1 \approx \bar{l}_s/10$ we find that this happens when $l_p \approx 10^{-2}\bar{l}_s$ in accord with Fig.6. It is interesting to see that the network loses its anisotropy at the two points $\bar{l}_s = l_p$ and $\bar{l}_s = r$, where the modulus takes the same value as that of the Poisson foam. This follows from the fact that the stiffness of the

average polymer segments is isotropic at these parameter values and either $k_{\parallel} \approx k_{\perp}$ or $k_s \approx k_{\perp}$. Comparing absolute values we find that the shear modulus in the thermal regime, strongly influenced by the presence of the small segments, can vary orders of magnitude while the mechanical stretching regime is hardly affected at all.

To conclude this section we emphasize once again that polydispersity in the segment lengths can have strong effects on the macroscopic elasticity of a cellular polymer network. It can lead to modifications of the scaling properties, as we have found in the most random foams, as well as to quantitative changes of the modulus by several orders of magnitude as in the anisotropic square structure. As a consequence, experiments which are limited to restricted parameter windows would most likely measure effective exponents that lie in between the extremal values given by pure stretching and bending. One, therefore, has to be cautious interpreting experimental data within the context of the foam-model, without the knowledge of the polydispersity of the structure.

IV. FIBROUS ARCHITECTURE

Looking at pictures of cross-linked actin networks reconstituted in vitro [12, 15] one might wonder whether a description in terms of a cellular architecture is actually relevant for these systems at all. Besides having a strong polydispersity in cell sizes, real polymer networks seem to have a hierarchical architecture that allows for smaller cells to be generated within larger cells within even larger cells. On the contrary, foams only have one of these hierarchies (see Fig.1). What is more, cellular structures do not account for the effects of the polymer length l_f , which constitutes an additional mesoscopic scale in the problem.

In the following we want to quantify the effects of the polydispersity in connection with the length scale l_f by studying the elastic properties of a generic two-dimensional fibrous structure which is defined as follows. N anisotropic elastic elements, geometrically represented by straight lines of length l_f , are placed on a plane of area $A = L^2$ such that both position and orientation of the elements are uniformly random distributed. This randomness entails a distribution of angles $\theta \in [0, \pi]$ between two intersecting filaments

$$P(\theta) = \frac{\sin(\theta)}{2}, \quad (12)$$

which has a maximum for filaments at right angles. At any intersection a permanent cross-link with zero extensibility is generated. This constrains the relative translational motion of the two filaments. For the rotational degree of freedom one may introduce an energy contribution $W_{\text{rot}} = m(\phi - \phi_0)^2$ for the change of relative cross-link angles ϕ from their initial values ϕ_0 . We restrict ourselves to the study of the two limiting cases, where the potential is either soft ($m \rightarrow 0$) and therefore allows

for free relative rotations of the filaments (free hinges), or infinitely stiff ($m \rightarrow \infty$) and inhibits any change of the angles at the cross-links (fixed angles).

The remaining elastic building blocks of the network, the *polymer segments*, span the distance between two neighboring cross-links on the same polymer. Their length can be shown to follow an exponential distribution [37]

$$P(l_s) = \bar{l}_s^{-1} e^{-l_s/\bar{l}_s}. \quad (13)$$

The mean value \bar{l}_s is given in terms of the density $\rho = Nl/A$ as

$$\bar{l}_s = \pi/2\rho, \quad (14)$$

which is a realization of Eq.(6). On average there are, thus, $x = l_f/\bar{l}_s \approx l_f\rho$ segments per polymer. The simplicity of this network, which has only one structural parameter ρ , makes it an ideal candidate to obtain physical insight into the relation between architecture and elastic properties of the constituents. This model has frequently been used to study the elastic and brittle properties of athermal paper sheets [25, 38, 39, 40]. In the context of biological networks of stiff polymers it has been introduced in [24] and recently studied by various authors [19, 20, 21]. In all this work, however, the elastic properties of the polymers are modeled by the classical theory of Euler-Bernoulli beams. Here, we concentrate on the effects of thermal fluctuations, a brief account of which we have published recently [23].

A. Simulation Results

In Figs. 7 and 8 the results of our simulations are shown for fibrous networks with a varying number x of cross-links per polymer. The axes are the same as in previous plots. The normalized shear modulus $G\bar{l}_s^3/\kappa$ is shown as a function of persistence length $y = l_p/\bar{l}_s$ expressed in units of the average segment length. Short fibers with few cross-links, corresponding to low densities are depicted in Fig. 7, long fibers or high densities in Fig. 8. In both figures we find a regime at large values of the persistence length l_p/\bar{l}_s (right part of the plot) where the dimensionless shear modulus decreases as $G \propto l_p^{-2} \propto r^{-2}$. This corresponds to a purely mechanical stretching regime where $G \propto \bar{k}_s$ consistent with the mean-field picture of Eq.(11) [19, 20, 24, 25].

Our main interest, however, lies in the regime of $l_p/\bar{l}_s \leq 10^3$, where the persistence length is small enough for thermal fluctuations to become relevant. In this regime one may safely neglect the mechanical stretching stiffness and set $k_s \rightarrow \infty$. Then, dimensional analysis for the shear modulus requires

$$G = \frac{\kappa}{\bar{l}_s^3} g(x, y), \quad (15)$$

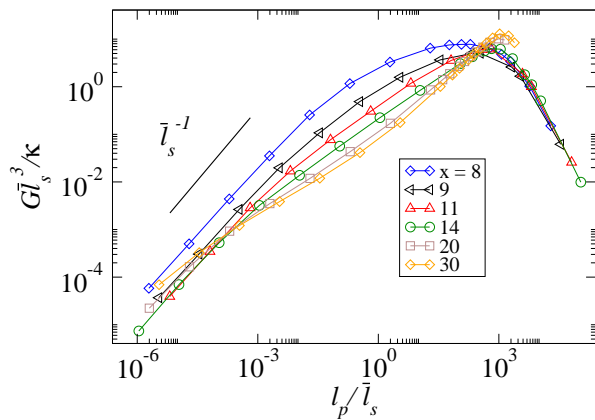


FIG. 7: Scaling function g as a function of $y = l_p/\bar{l}_s$ for various $x = l_f/\bar{l}_s \leq 30$ (from networks with freely hinged cross-links); For rather small values of $x = 8, 9$ the curves resemble the results from the cellular networks. At intermediate values $10^{-3} \leq y \leq 10^2$ the modulus shows strong modulation and develops a dip with increasing x .

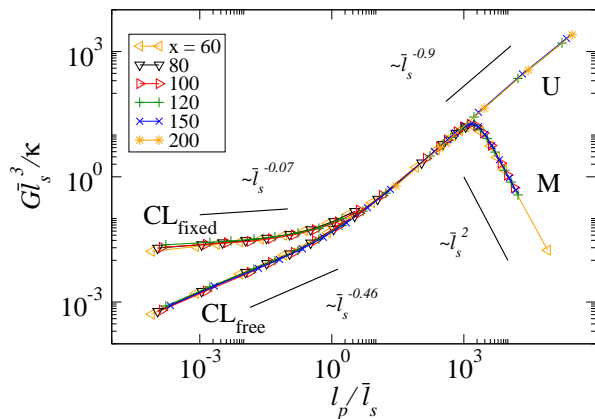


FIG. 8: Scaling function g as a function of $y = l_p/\bar{l}_s$ for various $x = l_f/\bar{l}_s \geq 60$; In contrast to Fig.7 no dependence on x is observed any more and new scaling regimes emerge. The two branches in the cross-link dominated regime ($y \ll 1$) correspond to freely hinged (CL_{free}) or fixed (CL_{fixed}) cross-link angles, respectively. For $y \gg 1$ one encounters a universal thermal regime (U) independent of the cross-link properties as well as a mechanical regime (M).

where we have introduced the scaling variables

$$x = l_f/\bar{l}_s \simeq l_f\rho, \quad y = l_p/\bar{l}_s \simeq l_p\rho. \quad (16)$$

Comparing to Eq.(7) there is an additional argument in the scaling function g , the polymer length $x = l_f/\bar{l}_s$. This purely geometrical variable counts the number of cross-links (or equivalently: segments) per filament. The second argument may be written in the alternative form $y \simeq \bar{k}_{\parallel}/\bar{k}_{\perp}$. It characterizes the relative stiffness of stretching and bending mode for a typical segment.

From Fig. 7 one infers that for *low densities* $g = yf(x)$,

implying for the modulus $G = \bar{k}_{\parallel}f(\rho l_f)$. This linear dependence on the “pre-averaged” stretching compliance \bar{k}_{\parallel} hints at an entropic stretching dominated regime similar to that found in the cellular structures discussed above. This regime has been suggested in [21], where a scaling argument is developed relying on the affine assumption borrowed from the mechanical stretching regime. Our analysis shows that the domain of validity of this linear regime is extremely narrow and confined to short filaments $x \leq 20$ and persistence lengths $y \ll 1$. What is more, due to the non-trivial density-dependence expressed through the function $f(x)$, the modulus does not even display a power-law behavior in the density. Instead, we find that the modulus shows complex dependence on its variables and develops a dip in the intermediate parameter region where $10^{-3} \leq y \leq 10^2$. This is also the relevant parameter range for networks of F-actin, where the ratio of persistence length to mesh-size $l_p/\bar{l}_s \approx 10 - 100$.

For *medium and high densities* Fig. 8 shows non-trivial scaling regimes where the scaling function g becomes independent of x and therefore of the filament length l_f . This highly non-trivial observation has important implications and allows the system to exhibit power law behavior $g \propto y^z$. We find non-trivial fractional exponents $z = 0.46(0.07)$ and $z = 0.9$ for small and large values of y , respectively. In the figure one can distinguish four branches that belong to different realizations of the network. While branch M (mechanical regime, $G \propto \bar{k}_s$) has been discussed already, the remaining three are obtained by setting $k_s \rightarrow \infty$. The two branches found at small values $y \ll 1$ relate to networks where the cross-link angles are either free to vary (CL_{free} , $z = 0.46$) or are perfectly fixed to their initial values (CL_{fixed} , $z = 0.07$), respectively. We term this regime “cross-link dominated” since tuning the cross-link properties may have strong effects on the elastic modulus by driving the system from one branch towards the other. Both branches merge at $y \approx 1$ where we enter a universal regime (branch U, $z = 0.9$) which is completely independent of the elasticity of the cross-links and which therefore is termed “filament dominated”.

In all cases, the modulus can be written as a generalized geometric average

$$G \propto \bar{k}_{\perp}^{1-z} \bar{k}_{\parallel}^z, \quad (17)$$

which has to be contrasted with Eq.(11), where bending and stretching modes are assumed to superimpose linearly (see Table I for a direct comparison of the various regimes). There, the system is described either by $z = 0$, if bending dominates, or by $z = 1$ if stretching is the main deformation mode. Values different from the two limiting cases $z = 0, 1$ cannot be described by the mean-field approach, hence the assumption of affine deformations applied on the level of the polymer segments (or the cell size) necessarily has to fail. This will become especially clear in the following section, where we review the application of affine theories to fibrous architectures. We will

		z	z_{Theory}	z_{Foam}
CL _{fixed}	$r \ll l_p \ll \bar{l}_s$	0.07	0	1
CL _{free}	$r \ll l_p \ll \bar{l}_s$	0.46	1/2	–
U	$r \ll \bar{l}_s \ll l_p$	0.9	1	0
M	$\bar{l}_s \ll r \ll l_p$	(1)	(1)	(1)

TABLE I: Compilation of the different elastic regimes of the fibrous network. The modulus is given by $G \sim \bar{k}_\perp^{1-z} \bar{k}_\parallel^z$ with the appropriate values for the exponent z . For comparison also the predictions from the theoretical analysis (see below) as well as the exponents for the foam structure are given. The latter only for fixed cross-link angles (CL_{fixed}), which is necessary to make the structure stable. The mechanical regime M corresponds to the exponent $z = 1$, however with \bar{k}_\parallel substituted by \bar{k}_s .

illustrate its failure and highlight the physical principles involved. To go beyond we will introduce a model that accounts for the spatial distribution of cross-links along the backbone of a *typical polymer filament* instead of just considering a single *typical polymer segment*. This new approach will allow us to understand all the features of the macroscopic elasticity encountered in Fig.8.

B. Affine Models in Fibrous Architectures

In some of the earlier approaches to describe the elastic moduli of stiff polymer networks the assumption of affine deformations has been applied on the level of the average segment which can be characterized by “pre-averaged” response coefficients $\langle k(l_s) \rangle \rightarrow \bar{k} = k(\bar{l}_s)$ introduced in Eqs.(8) and (10). The characteristic fibrous structure of stiff polymer networks is not accounted for and effectively substituted by a highly regular cellular structure. The modulus in the thermal regime is then obtained simply by replacing in Eq.(9) the mechanical stretching response \bar{k}_s with its thermal counterpart \bar{k}_\parallel . Several variants of this model have been considered in the literature [27, 28, 41] that only differ in the specific (ad hoc) choice of the prefactors a, b . The stretching dominated model [28] (setting $a = 0$ in Eq.(9)) with a modulus depending on density as

$$G_\parallel \sim \rho^{(2+d)/(d-1)}, \quad (18)$$

and its extensions to nonlinear elasticity [42], have widely been used to fit experimental data for the plateau modulus in cross-linked F-actin networks [12, 15, 43]. Despite this apparent success, it is not clear a priori why in the parameter regime of interest the mesh-work should deform by the stretching of bonds when actually bending is by far the softer mode ($\bar{k}_\parallel/\bar{k}_\perp \simeq l_p/\bar{l}_s \gg 1$). In general, such a regime can only occur if the specific architecture suppresses the soft bending modes as in the triangulated structure with its highly coordinated vertices. A second approach seems to repair this deficiency by setting in

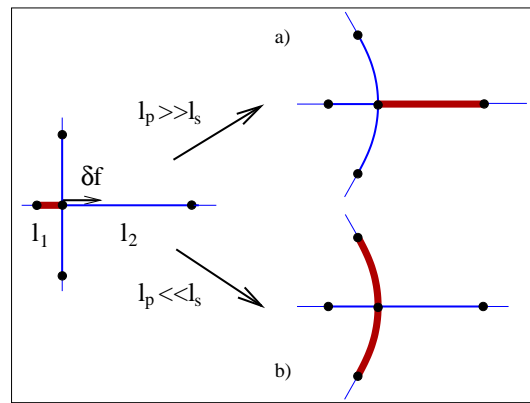


FIG. 9: Illustration of the effects of non-zero residual forces. The relaxation of the small segment l_1 from its overly stressed state goes to the cost of additional deformations in its neighbors. Depending on the value of the persistence length the energy will mainly be stored in a) the stretching mode ($l_p \gg l_s$) or b) the bending mode ($l_p \ll l_s$).

Eq.(9) $b = 0$. The modulus in this theory

$$G_\perp \sim \rho^{(1+d)/(d-1)}, \quad (19)$$

only differs by a factor of $\rho^{1/(d-1)}$ from the stretching dominated modulus of Eq.(18). However, neither theory provides justification for neglecting the effects of the polydispersity in the fibrous system. In fact, if one extends the approach to include the distribution of segment lengths, such theories necessarily have to fail, as we will explain in the next section.

C. Effects of the Segment Length Distribution

To understand the origin of this failure consider an affine deformation field $\delta_{\text{aff}} \propto \gamma l_s$ being applied to a random network of stiff polymers with a distribution $P(l_s)$ of segment lengths l_s . The axial forces f_\parallel generated by such a deformation field can simply be calculated by multiplying the deformation with the stretching stiffness of the segment

$$f_\parallel = k_\parallel \delta_{\text{aff}} \simeq \kappa l_p \gamma / l_s^3. \quad (20)$$

Note that in contrast to the purely mechanical situation, where the axial force $f_s = k_s \delta_{\text{aff}} \simeq \kappa \gamma / r^2$ is independent of length, f_\parallel strongly increases with shortening the segment length. This implies that, in general, two neighboring segments on the same filament produce a net force δf at their common node that has to be taken up by the crossing filament. There, it leads to additional deformations that eventually destroy the affine order. This mechanism is illustrated in Fig.9 where the relaxation of the small segment l_1 leads to bending of its neighbor on the crossing filament (b). Also the segment l_2 on the

same filament is affected by the relaxation and experiences an additional stretching contribution (a). Whether the available energy is stored in the stretching or the bending mode depends crucially on the value of the persistence length, as is indicated in the figure.

One may calculate the probability distribution Q for residual forces by summing over all segment lengths that are consistent with a given force δf ,

$$Q(\delta f) = \langle \delta(|f_{\parallel}(l_1) - f_{\parallel}(l_2)| - \delta f) \rangle. \quad (21)$$

The averaging procedure defined by the angular brackets

$$\langle A \rangle = \int dl_1 \int dl_2 P(l_1, l_2) A(l_1, l_2), \quad (22)$$

involves the two-point probability $P(l_1, l_2)$ of finding neighboring segments with lengths l_1 and l_2 , respectively. In the special case of the random network considered here, there are no correlations between neighboring segment lengths such that the distribution factorizes. The formula can thus be evaluated by substituting $f_{\parallel} \propto l_s^{-3}$ taken from Eq.(20). This inverse relationship between forces and segment lengths translates the weight of the probability distribution $P_0 = P(l_s \rightarrow 0) \neq 0$ at small segment lengths into polynomial (fat) tails of the corresponding distribution of residual forces

$$Q(\delta f \rightarrow \infty) \propto \delta f^{-4/3} P_0, \quad (23)$$

which has a diverging mean value. The exponent can readily be derived from evaluating the integral measure $df_{\parallel} \propto l^{-4} dl \propto f_{\parallel}^{4/3} dl$. As a consequence there are always residual forces high enough to cause additional deformation of the crossing filament. Hence we conclude that an affine deformation field is unstable and that the system can easily lower its energy by redistributing the stresses to relieve shorter segments and remove the tails of the residual force distribution $Q(\delta f)$.

Even though we have evaluated Eq.(21) for the special case of an exponential segment length distribution Eq.(13), it is important to note, that the observed sensitivity is not a special feature of the fibrous architecture, but applies to any polymer network with a broad distribution of segment lengths independent of the dimensionality of the network. Due to the strong length dependence of $k_{\parallel}(l_s)$ the thermal response is highly sensitive to even small polydispersity as we have already seen in the random cellular network of Sect.III C. On the contrary, these effects are completely absent in purely mechanical models and also in models of flexible polymers, where the distribution $Q(\delta f)$ degenerates into a delta-function peak at the value $\delta f = 0$, and explains the robustness of these regimes to randomness.

If we want to include the effects of randomness into a microscopic theory we cannot naively apply the conventional picture of affine deformations on the scale of the single segment. This can safely be done only in highly ordered structures like regular cellular materials. Instead,

we have to adopt a description of the deformations (at least) on the larger scale of the complete polymer. In the following we therefore consider a *typical polymer filament*, which is composed of a sequence of segments drawn from the distribution $P(l_s)$. To describe the elastic properties correctly, we will also have to consider the connections of the polymer to the surrounding network matrix, in addition to the elastic properties of the segments themselves. We may now employ this picture to explain the intricate scaling properties of the polymer network in all the parameter regimes displayed in Fig.8.

D. Cross-link dominated Regime

1. Freely hinged cross-links

We start with the description of the system in the parameter region $y \ll 1$ ($l_p \ll \bar{l}_s$), where the properties of the cross-links strongly influence the system's response. The idea is to impose a virtual affine deformation on every segment and calculate, as a perturbative correction, the contribution to the elastic energy resulting from the relaxation out of this reference state. This procedure will lead to good predictions only when the corrections are small and the affine deformations are only weakly perturbed. As we will see below, this is the case in the parameter region $y \ll 1$. However, it will also become clear, that a small perturbation for the deformations is sufficient to generate completely different scaling properties for the macroscopic modulus. For the moment we restrict our attention to free relative cross-link rotations (branch CL_{fixed}), since then the affine reference state is particularly simple and contains stretching contributions only.

As explained above any deviation from the affine reference state, induced by relaxation of non-zero residual forces, will lead to additional deformations in the crossing filaments. Since it is more likely that two filaments cross each other at an angle close to 90° , the induced non-affine deformations will mainly be oriented transverse to the contour of the crossing filament and are therefore of bending character. The value of the exponent $z = 0.46$ supports this assumption and indicates that bending and stretching deformations in this regime contribute equally to the elastic energy even though the bending mode is very stiff ($\bar{k}_{\parallel}/\bar{k}_{\perp} \sim y \ll 1$). Therefore any relaxation of residual stretching forces, will be punished by high amounts of bending energy (see Fig. 9b). Only the smallest segments on the polymer, corresponding to the outermost tails of the residual force distribution, will have sufficient energy to perturb the deformation field and relax to a state of lower strain.

In the following, we will assume that segments up to a critical length l_c – to be determined self-consistently – fully relax from their affine reference state to give all their energy to the neighboring segment on the crossing filament. The total energy of the polymer can then be

calculated from segments with $l_s > l_c$ only. There are two contributions. First, a stretching energy

$$w_s(l_s) \simeq k_{\parallel} \delta_{\text{aff}}^2 \simeq \kappa \gamma^2 \frac{l_p}{l_s^2}, \quad (24)$$

from the imposed affine strain field $\delta_{\text{aff}} \propto \gamma l_s$. Second, a bending energy that is due to the relaxation of a neighboring segment on the crossing filament out of its affine reference state. This process requires that the segment of length \hat{l}_s moves the distance $\hat{\delta}_{\text{aff}} = \gamma \hat{l}_s$, which corresponds to its own affine deformation. The resulting bending energy

$$w_b(l_s) \simeq k_{\perp} \hat{\delta}_{\text{aff}}^2 \simeq \kappa \gamma^2 \frac{\hat{l}_s^2}{l_s^3}, \quad (25)$$

now depends on the length l_s of the segment under consideration as well as on the length \hat{l}_s of the neighboring (now relaxed) segment. As we have assumed above, the second contribution w_b only arises if the length \hat{l}_s is shorter than the critical length l_c . The total deformation energy along the polymer is then obtained by adding both contributions and integrating over all segments $l_s > l_c$ along the filament as well as averaging over neighbors with $\hat{l}_s < l_c$,

$$W_{\text{pol}} \simeq (l_f \rho) \kappa \gamma^2 \int_{l_c}^{\infty} dl_s P(l_s) \left(\frac{l_p}{l_s^2} + l_s^{-3} \int_0^{l_c} d\hat{l}_s P(\hat{l}_s) \hat{l}_s^2 \right), \quad (26)$$

where the prefactor $l_f \rho$ just counts the number of segments per polymer. For simplicity, we have not considered any dependence of the deformations on the orientation relative to the macroscopic strain field. In essence, this would only introduce some additional numerical prefactors that are irrelevant for the scaling picture developed here. The integrations are reparametrized by introducing the non-dimensional variable $\lambda = \rho l_s$ such that we arrive at the expression for the average polymer energy

$$W_{\text{pol}} \simeq \kappa \gamma^2 l_f \rho^2 (\rho l_p / \lambda_c + \lambda_c), \quad (27)$$

where numerical constants have been dropped and $\lambda_c := \rho l_c \ll 1$ in the parameter range of interest. Minimizing with respect to λ_c determines a new non-affinity length

$$l_c^{\text{min}} = \lambda_c^{\text{min}} \bar{l}_s \simeq \sqrt{l_p \bar{l}_s}, \quad (28)$$

that sets the maximal scale up to which the destruction of affine deformations lead to a lowering of the elastic energy. Inserting this length into Eq.(27) and multiplying by the number-density of filaments ρ/l_f one arrives at an expression for the modulus $G \simeq W_{\text{pol}}^{\text{min}} \cdot \rho/l_f \gamma^2 \simeq \kappa \rho^{7/2} l_p^{1/2}$. Rewriting the result as

$$G \simeq \sqrt{\bar{k}_{\perp} \bar{k}_{\parallel}} \propto \bar{l}_s^{-7/2}, \quad (29)$$

we immediately see that our theory reproduces the empirical result of Eq.(17) with an exponent $z = 1/2$, which compares well with the measured value of $z = 0.46$.

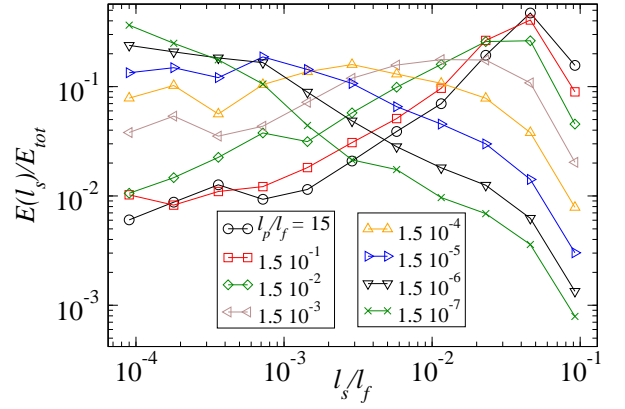


FIG. 10: Fraction of energy stored in the various segment lengths; the curves correspond to different persistence lengths at a density of $l_f/\bar{l}_s = 80$, equivalent to $\bar{l}_s/l \approx 2 \cdot 10^{-2}$.

The non-trivial behavior of G observed in Fig. 8 can thus be explained by a non-affinity length scale $l_c^{\text{min}} \simeq \sqrt{\bar{l}_s l_p}$ below which the affinity of the deformation field breaks down. Recapitulating the results from the cellular networks in Fig.4, we observe that the same intermediate scaling behavior of $G \propto \bar{l}_s^{-7/2}$ is found in both architectures. We have thus established the microscopic origin of the scaling law. It derives from a continuous unloading of smaller segments driven by an interplay between segment length distribution and elastic properties of the single polymer. This mechanism is illustrated in Fig. 10, where a histogram for the fraction of energy stored in segments of various lengths is shown. For very small persistence length, a significant fraction of the energy is stored in the shortest segments. Affine deformations can be seen as a good approximation. Increasing the persistence length, the short segments one after the other loose their energies in favor of additional excitations in longer segments. This is fully consistent with the assumption of a growing non-affinity scale l_c^{min} below which no energy is stored.

It is important to realize that our derivation of the exponent does not make use of the precise form of the segment length distribution $P(l_s)$. In fact, there is no need to perform the integrations explicitly and only the limiting behavior of $P(l_s \rightarrow 0)$ enters. Thus, the conclusions are valid for a general class of functions that may even be slowly vanishing at zero segment length.

We have also conducted simulations that assume a more general form for the stretching stiffness

$$k_{\parallel}(\alpha) = 6\kappa \frac{l_p^\alpha}{l_s^{3+\alpha}}, \quad (30)$$

which reduces to the original definition for $\alpha = 1$. Since the relative stiffness of the deformation modes is now $k_{\parallel}/k_{\perp} \propto (l_p/l_s)^\alpha$ we can think of the phenomenological exponent α to tune the anisotropy of the individual segment. It allows us to extend our discussion to the broad

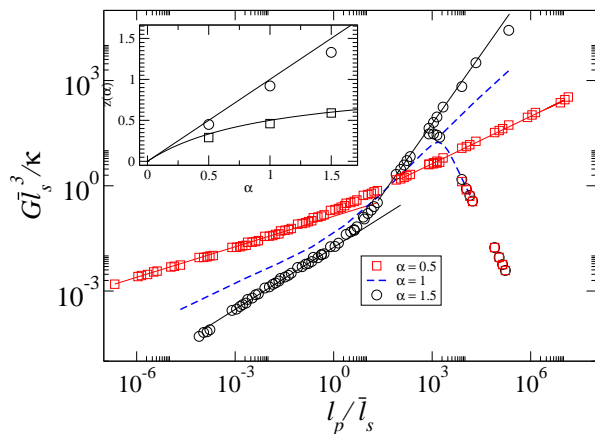


FIG. 11: Scaling function g as a function of $y = l_p/\bar{l}_s$; the symbols correspond to values of $\alpha = 0.5, 1.5$. In addition the scaling function for $\alpha = 1$ taken from Fig.8 is shown (dashed line). Inset: Exponents z determined from the slopes of the branches CL_{free} (squares) and U (circles), respectively. The solid lines correspond to the curves $z = \alpha$ and $z = \alpha/(1 + \alpha)$ as derived in the main text.

class of systems for which k_{\parallel} is a monomial (with units energy per area) involving one additional material length l_p . Repeating the scaling theory for general values of α gives $z(\alpha) = \alpha/(1 + \alpha)$ which is verified by the results of the simulations presented in Fig.11. It provides further evidence for the validity of our scaling picture.

2. Fixed Cross-link Angles

If we want to apply the same reasoning to the network with the fixed cross-link angles, we face the problem that even a perfectly affine displacement of all the cross-links induces some amount of bending of the segments, in addition to the usual contribution from the stretching deformations. While an affine strain γ would change all angles by an amount $\Delta\phi \propto \gamma$, due to the infinite rotational stiffness in the cross-links this cannot actually occur. The segments therefore have to experience an extra bending contribution induced by cross-link rotations ($-\Delta\phi$) that restore the angles to their original values. In the parameter regime $y \ll 1$, where bending is the stiffer mode, we therefore expect strong contributions to the energy from the bending mode already in the affine reference state. Allowing for the relaxation of the smallest segments from their stretched state to even stronger reduce the amount of stretching we might find an exponent as low as $z = 0.07$, signalling nearly exclusive contributions from the bending mode, not too surprising. In fact, we will argue below that neglecting the stretching energies, i.e. assuming an exponent of $z = 0$, represents a reasonable approximation to the elasticity in this regime.

E. Universal Regime

By increasing y from its small value we soften the bending mode and therefore reduce the influence of the fixed cross-link angles on the elastic energy. At the same time the non-affinity scale $l_c^{\text{min}} \propto y^{1/2}$ increases, indicating ever stronger deviations from the affine reference state. When, eventually, $l_c^{\text{min}} \approx l_p \approx \bar{l}_s$ ($\lambda_c^{\text{min}} \approx y \approx 1$) the affine strain field does not serve as a reference configuration any more, since it is strongly perturbed by a majority of segments with $l_s < l_c^{\text{min}}$. At this stage, the two branches, present in the cross-link dominated regime, merge and one enters a universal filament-dominated regime. There, the specific properties of the cross-links do not influence the macroscopic elasticity notably.

While the scaling argument presented for the hinged network ceases to be applicable, the remaining residual forces δf continue to lead to a redistribution of stresses from shorter to longer segments, albeit at higher scales. As we have shown in [23], eventually about 90% of the energy is stored in the longest 30% of the segments only. The new feature as compared to the regime CL_{free} is that unloading of a segment from its stretched configuration will also lead to stretching of its immediate neighbor on the *same* filament (see Fig.9a). This way, the available energy for bending of the *crossing* filament, which was the primary contribution in Eq. (26), is reduced. In the limit $y \gg 1$ we can neglect these contributions and calculate the energy from the polymers' stretching stiffness only. The physical picture is that of a serial connection of infinitely many segments along the backbone of a "typical" polymer. The stiffness of this polymer, and therefore the modulus, may be obtained from the stretching spring constants of the individual segments $k_{\parallel}(l_s)$ as

$$G^{-1} = \int dl_s P(l_s) k_{\parallel}(l_s)^{-1} \propto \bar{k}_{\parallel}^{-1}, \quad (31)$$

corresponding to the exponent $z = 1$. For the more general response coefficient of Eq.(30) this argument predicts $z = \alpha$, a result which is closely confirmed by the results of the simulation as can be seen from the inset of Fig.11. Note, that the shear modulus in this asymptotic region takes the same form as postulated by the affine theory in Eq.(11). However, using Eq.(31) one can resolve the effects according to segment length to find that the contribution to the total energy from segments with length l_s grows as $W(l_s) \propto l_s^4$. This strong increase is in accord with the assumption of a large non-affinity scale, below which no energy is stored, and in striking contrast to the affine theory that would yield $W_{\text{aff}}(l_s) \propto k_{\parallel}(l_s) \delta_{\text{aff}}^2 \propto l_s^{-2}$.

V. CONCLUSION

We have studied the macroscopic elastic properties of networks of semi-flexible polymers. We provide exhaustive numerical studies supplemented by scaling arguments that elucidate the subtle interplay between the

architecture of the network and the elastic properties of its building blocks.

The main conclusion to be drawn is that, irrespective of the specific architecture chosen, thermally fluctuating stiff polymer networks are inherently more sensitive to polydispersity and randomness than their purely mechanical counterparts. This is due to their strongly length-dependent entropic stretching response $k_{\parallel}(l) \propto \kappa^2/l^4$ which has to be contrasted with the mechanical stretching stiffness $k_s(l) \propto \kappa/l$.

Although simulations have only been conducted in two-dimensional networks, the identified mechanism by which the structural randomness influences the elastic properties is expected to be of universal character and hold independent of dimensionality. As we have shown, the actual consequences of this susceptibility (e.g. scaling behaviour of elastic moduli) may vary from system to system and certainly also with the dimension. A precise knowledge of the network architecture is therefore indispensable for the interpretation of experimental data. For this it will be most important to develop new techniques that allow the characterization of the microstructure and monitor its changes upon deformation. As exemplified by the discussion in the universal regime Sec. IV E, where the (non-affine) elastic modulus turns out to be similar to that in an affine theory, we have shown that macroscopic measurements alone do not suffice to extract the network mechanics also on the microscopic scale.

We have described how the polymer length l_f can be used to drive the system from a simple cellular structure with filaments as short as the mesh-size $l_f \approx \bar{l}_s$, to a fully scale-invariant fibrous structure characterized by infinitely long filaments $l_f \rightarrow \infty$. Especially the latter limit allows for intricate scaling behavior that impressively demonstrates the qualitative difference between thermally fluctuating and purely mechanical elastic networks.

The elasticity of a simple cellular structure may be described by a serial connection of their elementary deformation modes bending and stretching, respectively. This leads to the modulus of Eq.(9)

$$G^{-1} = a\bar{k}_{\perp}^{-1} + b\bar{k}_{\parallel}^{-1}. \quad (32)$$

In this picture, deformations can be drawn from either mode and it will be the softer one that dominates the modulus. In fibrous networks with fixed cross-link angles we have shown that the modes rather act as if they were springs connected in parallel. The modulus can then be approximated by

$$G = a\bar{k}_{\perp} + b\bar{k}_{\parallel}, \quad (33)$$

where the prefactors a, b depend weakly on the scaling variable $y \sim \bar{k}_{\parallel}/\bar{k}_{\perp} \sim l_p/\bar{l}_s$. The network elasticity is therefore always dominated by the stiffer mode, qualitatively similar to a triangulated network, where the specific geometry of the unit cell always imposes stretching deformations on the system, no matter how soft the

bending mode actually is. The fibrous architecture apparently also suppresses the transition into regimes where the softer mode is dominant. This conclusion is consistent with recent simulations on the purely mechanical fiber model [19, 20], where a transition into a regime dominated by soft bending modes ($y \gg 1$) could only be observed at finite values for the filament length l_f . Increasing the length to asymptotic values $l_f \rightarrow \infty$, as we have done here, such a ‘‘bending-soft’’ regime is strongly suppressed and eventually cannot occur any more. Instead, the elasticity is governed by the much stiffer (mechanical) stretching mode. A detailed theoretical explanation of how this suppression is generated in mechanical fiber networks will appear elsewhere [44], however, it is clear that the mechanism that leads to bending in cellular structures cannot work in fibrous networks. The fact, that any segment is part of the larger structure of the polymer fiber leads to strong geometric correlations and imposes very strict conditions on possible segmental deformations.

Allowing the filaments to freely rotate at the cross-links, a situation which may be relevant for F-actin networks cross-linked for example with α -actinin, we also find an asymptotic scaling regime where stretching and bending modes contribute equally to the elastic energy, Eq.(17),

$$G \propto \bar{k}_{\perp}^{1-z} \bar{k}_{\parallel}^z. \quad (34)$$

By quantifying the degree of co-operation between neighboring elements in the network we were able to identify a non-affinity length-scale l_c below which the state of affine deformations is rendered unstable. A scaling argument is supplied that allows the calculation of the effective macroscopic exponents starting from this microscopic picture.

It seems that the effects described above can only be accounted for by going beyond the conventional approach that considers *typical polymer segments* only. Instead, we propose to describe the elasticity in terms of a *typical polymer filament* and the spatial distribution of cross-links along its backbone. By controlling the architecture of the network, the scale of the polymer length l_f therefore seems to implicitly influence the elastic properties of the system even in parameter regions where it does not enter the macroscopic elastic moduli explicitly.

Acknowledgments

We gratefully acknowledge fruitful discussions with Mark Bathe, Oskar Hallatscheck and Klaus Kroy.

APPENDIX A: STIFFNESS MATRIX

This appendix derives an expression for the stiffness matrix of a polymer segment imbedded in a two-dimensional network.

The differential equation governing the bending of a beam of length l is given by $\kappa X^{(4)} = 0$, where the transverse deflection X is induced by the forces F_0, F_l as well as the torques M_0, M_l acting on both ends. The solution can then be written as

$$X(s) = X_0 + X'_0 s + \frac{s^2}{2\kappa}(M_0 - sF_0/3), \quad (\text{A1})$$

while equilibrium conditions require that

$$F_l = -F_0, \quad M_l = -(M_0 - F_0 l). \quad (\text{A2})$$

Stretching the beam to the position Z is governed by the equation

$$Z(s) = Z_0 + s - \frac{s}{EA}T_0, \quad (\text{A3})$$

with the condition

$$T_l = -T_0, \quad (\text{A4})$$

balancing the axial forces T .

The two variables (X, Z) are the coordinates (in the frame of the fiber) of the vector \mathbf{u} introduced in the main text. The rotation is given by $\theta = X'$. The four Eqs. (A1), (A2), (A3) and (A4) can now be inverted to yield the forces in terms of the displacements at the beam ends (cross-links)

$$\begin{pmatrix} F_0 \\ T_0 \\ M_0 l \\ F_l \\ T_l \\ M_l l \end{pmatrix} = \frac{\kappa}{l^3} \begin{pmatrix} -12 & 0 & -6 & 12 & 0 & -6 \\ 0 & \Lambda & 0 & 0 & -\Lambda & 0 \\ -6 & 0 & -4 & 6 & 0 & -2 \\ 12 & 0 & 6 & -12 & 0 & 6 \\ 0 & -\Lambda & 0 & 0 & \Lambda & 0 \\ -6 & 0 & -2 & 6 & 0 & -4 \end{pmatrix} \begin{pmatrix} X_0 \\ Z_0 \\ X'_0 l \\ X_l \\ Z_l \\ X'_l l \end{pmatrix}, \quad (\text{A5})$$

where we have defined $\Lambda = l^2 A/I = 4(l/r)^2$. The second equality only holds for circular beam cross-sections, where the moment of area $I = \pi r^4/4$. The corresponding matrix is called the stiffness matrix.

If, in addition to Eq.(A3), we assume that the stretching response is governed by that of a thermally fluctuating stiff polymer we have to take into account k_{\parallel} of Eq.(4). This is achieved by letting both stretching modes

act in series and substitute $k_s^{-1} \rightarrow k_s^{-1} + k_{\parallel}^{-1}$. Equivalently, one can assign an effective polymer radius

$$r_{pol}^2 = r^2 + \frac{4l^3}{\zeta l_p}, \quad (\text{A6})$$

which now depends on the segment length l as well as on the persistence length l_p of the polymer.

-
- [1] L. D. Landau and E. M. Lifshitz, *Theory of Elasticity*, 3rd ed. (Butterworth-Heinemann, Oxford, 1995), Vol. 7.
- [2] B. Alberts *et al.*, *Molecular biology of the cell* (Garland Publishing, New York, 1994).
- [3] B. Hinner *et al.*, Phys. Rev. Lett. **81**, 2614 (1998).
- [4] J. Xu, A. Palmer, and D. Wirtz, *Macromolecules* **31**, 6486 (1998).
- [5] M. M. A. E. Claessens, R. Tharmann, K. Kroy, and A. R. Bausch, *Nature Physics* **2**, 186 (2006).
- [6] T. Odjik, *Macromolecules* **16**, 1340 (1983).
- [7] W. Helfrich and W. Harbich, *Chem. Scr.* **25**, 32 (1985).
- [8] H. Isambert and A. C. Maggs, *Macromolecules* **29**, 1036 (1996).
- [9] A. P. Philipse, *Langmuir* **12**, 1127 (1996).
- [10] D. Rodney, M. Fivel, and R. Dendievel, Phys. Rev. Lett. **95**, 108004 (2005).
- [11] S. R. Williams and A. P. Philipse, Phys. Rev. E **67**, 51301 (2003).
- [12] J. H. Shin *et al.*, PNAS **101**, 9636 (2004).
- [13] M. Tempel, G. Isenberg, and E. Sackmann, Phys. Rev. E **54**, 1802 (1996).
- [14] O. Pelletier *et al.*, Phys Rev Lett **91**, 148102 (2003).
- [15] R. Tharmann, M. M. A. E. Claessens, and A. R. Bausch, *Biophys. J.* **90**, 2622 (2006).
- [16] L. Limozin and E. Sackmann, Phys Rev Lett **89**, 168103 (2002).
- [17] I. Borukhov, R. F. Bruinsma, W. M. Gelbart, and A. J. Liu, PNAS **102**, 3673 (2005).
- [18] A. G. Zilman and S. A. Safran, *Europhys. Lett.* **63**, 139 (2003).
- [19] J. Wilhelm and E. Frey, Phys. Rev. Lett. **91**, 108103 (2003).
- [20] D. A. Head, A. J. Levine, and F. C. MacKintosh, Phys. Rev. Lett. **91**, 108102 (2003).
- [21] D. A. Head, A. J. Levine, and F. C. MacKintosh, Phys. Rev. E **68**, 61907 (2003).

- [22] P. R. Onck, T. Koeman, T. van Dillen, and E. van der Giessen, *Phys Rev Lett* **95**, 178102 (2005).
- [23] C. Heussinger and E. Frey, *Phys. Rev. Lett.* **96**, 017802 (2006).
- [24] E. Frey, K. Kroy, J. Wilhelm, and E. Sackmann, in *Dynamical Networks in Physics and Biology*, edited by G. Forgacs and D. Beysens (Springer, Berlin, 1998), Chap. 9.
- [25] J. A. Åström, J. P. Mäkinen, M. J. Alava, and J. Timonen, *Phys. Rev. E* **61**, 5550 (2000).
- [26] M. Sahimi, *Heterogeneous Materials* (Springer, New York, 2003).
- [27] K. Kroy and E. Frey, *Phys. Rev. Lett.* **77**, 306 (1996).
- [28] F. C. MacKintosh, J. Käs, and P. A. Janmey, *Phys. Rev. Lett.* **75**, 4425 (1995).
- [29] D. Weaire and S. Hutzler, *The physics of foams* (Oxford University Press, Oxford, 2001).
- [30] L. J. Gibson and M. F. Ashby, *Cellular Solids: Structure and Properties* (Cambridge University Press, Cambridge, 1999).
- [31] A. M. Kraynik and W. E. Warren, in *Low density cellular plastics*, edited by H. Hilyard and C. Cunningham (Kluwer Academic Publisher, Amsterdam, 1994), Chap. 7.
- [32] H. X. Zhu, J. F. Knott, and N. J. Mills, *J. Mech. Phys. Solids* **45**, 319 (1997).
- [33] M. J. Silva, W. C. Hayes, and L. J. Gibson, *Int. J. Mech. Sc.* **37**, 1161 (1995).
- [34] H. X. Zhu, J. R. Hobdell, and A. H. Windle, *Acta mater.* **48**, 4893 (2000).
- [35] A. Fazekas, R. Dendievel, L. Salvo, and Y. Bréchet, *Int. J. Mech. Sc.* **44**, 2047 (2002).
- [36] D. Boal, *Mechanics of the Cell* (Cambridge University Press, Cambridge, 2002).
- [37] O. Kallmes and H. Corte, *Tappi* **43**, 737 (1960).
- [38] J. A. Åström, S. Saarinen, K. Niskanen, and J. Kurkijärvi, *J. Appl. Phys.* **75**, 2383 (1994).
- [39] M. Latva-Kokko and J. Timonen, *Phys. Rev. E* **64**, 066117 (2001).
- [40] S. Heyden, Ph.D. thesis, Lund University, 1996.
- [41] R. L. Satcher and C. F. Dewey, *Biophys. J.* **71**, 109 (1996).
- [42] C. Storm *et al.*, *Nature* **435**, 191 (2005).
- [43] M. L. Gardel *et al.*, *Science* **304**, 1301 (2004).
- [44] C. Heussinger and E. Frey, cond-mat/0603697.
- [45] This limit corresponds to taking $r \rightarrow 0$ and the Young's modulus $E \rightarrow \infty$ in such a way that the bending stiffness $\kappa \sim Er^4$ stays constant. As a consequence the stretching stiffness diverges, $k_s \sim Er^2 \rightarrow \infty$, and the beam becomes inextensible.

Appendix A

Fascin Networks

Above a critical concentration of the actin-binding protein fascin, a solution of actin filaments organizes into a pure network of bundles. As we show here the mechanical properties inside this bundled regime may be understood in terms of the floppy-mode theory presented in Section 4.2.

To derive a scaling theory for the plateau modulus, we assume the network structure to be characterized by the length-scale l_c , which denotes the typical distance between neighboring cross-links along a bundle.

Within the floppy-mode theory the linear elastic modulus reads

$$G \sim \nu \cdot k_{\perp}^B \cdot \delta_{\text{na}}^2, \quad (\text{A.1})$$

with the polymer density $\nu \sim 1/a^2 l_c$, the bending stiffness $k_{\perp}^B \sim N\kappa/l_c \lambda^2$, which is taken from the worm-like bundle model, Eq.(3.4), and the non-affine deformation $\delta_{\text{na}} \sim \gamma_0 l_f$.

The most important distinction between the non-affine theory, Eq. (A.1), and the result of the affine theory, Eq. (2.8), is the scaling of the polymer deformation, $\delta_{\text{na}} \sim \gamma_0 l_f$, as compared $\delta_{\text{aff}} \sim \gamma_0 a$ in the affine case ¹.

To test this model we need to know how bundle size N , mesh-size a , and cross-link distance l_c depend on the experimental control parameters, which are the actin concentration c_a and the fascin-to-actin ratio $R = c_f/c_a$.

TEM micrographs reveal that the actin/fascin bundle thickness and therefore the number of actin filaments per bundle, N , increases weakly with R as $N \sim R^{2x}$ and $x \approx 0.27$. With increasing R , filaments and smaller bundles reorganize to form larger bundles that are spaced further apart. The mesh size a of this coarsening, self-similar structure therefore depends on R as $a \sim a_0 N^{1/2}$, where $a_0 \sim c_a^{-1/2}$ is the mesh size of the filamentous network. Cross-linking will typically occur on the scale of the deflection length l_d , which plays the role of a distance between bundle-bundle intersections. Since on average only a fraction of those will be occupied we can assume that distances between cross-links along

¹Sometimes one also finds the choice $\delta \sim \gamma_0 l_c$. All these choices are “ad hoc” and not motivated by any physical principles. In contrast, the non-affine scaling $\delta_{\text{na}} \sim \gamma_0 l_f$ derives directly from the assumptions of the floppy-mode theory.

the same bundle are given by $l_c = R^{-y}l_d$ [74, 69] with an as yet undetermined exponent y . The deflection length must be calculated with the wormlike bundle model and is found as $l_d^3 \sim Na^4l_p/\lambda^2$.

Combining the above results one finally arrives at the following prediction

$$G \sim R^z c_a^w \lambda^{-2/3}, \quad (\text{A.2})$$

where the exponents are given by $z = 2y - 4x$ and $w = 7/3$.

The length-scale λ depends on the mechanical and geometrical properties of the cross-linking fascin molecules, in particular on the average distance between neighbouring cross-links and thus possibly on the fascin-to-actin ratio R . As the dependence on λ is only weak, we can assume it to be constant in what follows ².

The scaling with actin concentration compares well with the measured value of $w \approx 2.4$. From the measurements of $x \approx 0.27$ and $z \approx 1.5$ a value of $y \approx 1.29$ is obtained, which can be tested by measuring the non-linear elasticity of the network. By applying a constant shear rate the critical strain γ_c , marking the onset of non-linear behaviour, is determined as $\gamma_c \sim R^{-1}$. We will now argue, that this critical strain is equivalent to the point where the floppy mode description breaks down.

As has been argued in Section 4.2 large strains necessarily lead to stretching even if the deformations were only of bending character. The bundle stretching Δ is related to the transverse bending displacement δ_{na} by simple geometric considerations as $l_c^2 + \delta_{\text{na}}^2 = (l_c + \Delta)^2$, which for small deflections gives $\Delta \sim \delta_{\text{na}}^2/l_c \sim \gamma_0^2/l_c$. The floppy mode description only applies as long as this stretching is small compared to the available thermal stored length $\Delta\Lambda$, which must again be calculated with the wormlike bundle model. The straightforward calculation gives $\Delta\Lambda \sim l_c\lambda/Nl_p$. By equating $\Delta = \Delta\Lambda$ a critical strain is defined as $\gamma_c \sim l_c(\lambda/N)^{1/2} \sim R^{-y+x}\lambda^{-1/6}$ for the onset of non-linear effects. Using the values of the exponent as determined above one finds $\gamma_c \sim R^{-1.0}$ in agreement with the experimentally determined exponent.

We thus conclude that the floppy mode theory, when combined with the wormlike bundle model, is capable of explaining the observed rheological properties of an isotropic network of actin bundles crosslinked with fascin.

²Alternatively, one could assume the cross-link distance to change according to a Langmuir-kinetic. As expected this does not change the exponents markedly.

Bibliography

- [1] M. Alava and K. Niskanen: *The physics of paper. Rep. Prog. Phys.* **69** (2006), 669.
- [2] B. Alberts, D. Bray, J. Lewis, M. Raff, K. Roberts and J.D. Watson: *Molecular biology of the cell*. Garland Publishing, New York, 1994.
- [3] S. Alexander: *Amorphous solids: their structure, lattice dynamics and elasticity. Phys. Rep.* **296** (1998), 65.
- [4] J.A. Åström, J.P. Mäkinen, M.J. Alava and J. Timonen: *Elasticity of poissonian fiber networks. Phys. Rev. E* **61** (2000), 5550.
- [5] P. Benetatos and A. Zippelius. *Anisotropic random networks of semiflexible polymers*. arXiv:0706.0508v1, 2007.
- [6] M. Born and K. Huang: *Dynamical theory of crystal lattices*. Oxford University Press, London, 1966.
- [7] I. Borukhov, R.F. Bruinsma, W.M. Gelbart and A.J. Liu: *Structural polymorphism of the cytoskeleton: a model of linker-assisted filament aggregation. Proc. Natl. Acad. Sci. USA* **102** (2005), 3673.
- [8] C.R. Calladine: *Buckminster Fuller's "tensegrity" structures and Clerk Maxwell's rules for the construction of stiff frames. Int. J. Solids Struct.* **14** (1978), 161.
- [9] C.R. Calladine and S. Pellegrino: *First-order infinitesimal mechanisms. Int. J. Solids Struct.* **27** (1991), 505.
- [10] M.V. Chubynsky and M.F. Thorpe: *Self-organization and rigidity in network glasses. Curr. Op. Sol. Stat. & Mat. Sci.* **5** (2001), 525.
- [11] J.P. Collet, H. Shuman, R.E. Ledger, S. Lee and J.W. Weisel: *The elasticity of an individual fibrin fiber in a clot. Proc. Natl. Acad. Sci. USA* **102** (2005), 9133.
- [12] H.L. Cox: *The elasticity and strength of paper and other fibrous materials. Br. J. Appl. Ph.* **3** (1952), 72.
- [13] B.A. DiDonna and T.C. Lubensky: *Nonaffine correlations in random elastic media. Phys. Rev. E* **72** (2005), 66619.

- [14] A.R.T. van Eerd, W.G. Ellenbroek, M. van Hecke, J.H. Snoeijer and T.J.H. Vlugt: *Tail of the contact force distribution in static granular materials*. *Phys. Rev. E* **75** (2007), 060302.
- [15] W.G. Ellenbroek, E. Somfai, M. van Hecke and W. van Saarloos: *Critical scaling in linear response of frictionless granular packings near jamming*. *Phys. Rev. Lett.* **97** (2006), 258001.
- [16] R. Everaers, R. Bundschuh and K. Kremer: *Fluctuations and stiffness of double stranded polymers: railway track model*. *Europhys. Lett.* **29** (1995), 263.
- [17] A. Fazekas, R. Dendievel, L. Salvo and Y. Bréchet: *Effect of microstructural topology upon the stiffness and strength of 2D cellular structures*. *Int. J. Mech. Sci.* **44** (2002), 2047.
- [18] H. Felgner, R. Frank and M. Schliwa: *Flexural rigidity of microtubules measured with the use of optical tweezers*. *J. Cell Sci.* **109** (1996), 509.
- [19] P.J. Flory and J. Rehner Jr.: *Statistical mechanics of cross-linked polymer networks I Rubberlike elasticity*. *J. Chem. Phys.* **11** (1943), 512.
- [20] E. Frey, K. Kroy, J. Wilhelm and E. Sackmann. *Dynamical networks in physics and biology*. Springer, Berlin, 1998. Chapt. 9.
- [21] M.L. Gardel, J.H. Shin, F.C. MacKintosh, L. Mahadevan, P.A. Matsudaira and D.A. Weitz: *Elastic behavior of cross-linked and bundled actin networks*. *Science* **304** (2004), 1301.
- [22] M.L. Gardel, J.H. Shin, F.C. MacKintosh, L. Mahadevan, P.A. Matsudaira and D.A. Weitz: *Scaling of F-actin network rheology to probe single filament elasticity and dynamics*. *Phys. Rev. Lett.* **93** (2004), 188102.
- [23] L.J. Gibson and M.F. Ashby: *Cellular solids: structure and properties*. Cambridge University Press, Cambridge, 1999.
- [24] F. Gittes, B. Mickey, J. Nettleton and J. Howard: *Flexural rigidity of microtubules and actin-filaments measured from thermal fluctuations in shape*. *J. Cell Biol.* **120** (1993), 923.
- [25] I. Goldhirsch and C. Goldenberg: *On the microscopic foundations of elasticity*. *Eur. Phys. J. E* **9** (2002), 245.
- [26] R. Götter, K. Kroy, E. Frey, M. Bärmann and E. Sackmann: *Dynamic light scattering from semidilute actin solutions: a study of hydrodynamic screening, filament bending stiffness, and the effect of tropomyosin/troponin-binding*. *Macromolecules* **29** (1996), 30.

- [27] D.A. Head, A.J. Levine and F.C. MacKintosh: *Deformation of cross-linked semiflexible polymer networks*. *Phys. Rev. Lett.* **91** (2003), 108102.
- [28] D.A. Head, A.J. Levine and F.C. MacKintosh: *Distinct regimes of elastic response and deformation modes of cross-linked cytoskeletal and semiflexible polymer networks*. *Phys. Rev. E* **68** (2003), 061907.
- [29] D.A. Head, A.J. Levine and F.C. MacKintosh: *Non-universality of elastic exponents in random bond-bending networks*. *Phys. Rev. E* **68** (2003), 25101.
- [30] D.A. Head, A.J. Levine and F.C. MacKintosh: *Mechanical response of semiflexible networks to localized perturbations*. *Phys. Rev. E* **72** (2005), 061914.
- [31] W. Helfrich and W. Harbich: *Adhesion and cohesion of tubular vesicles*. *Chem. Scr.* **25** (1985), 32.
- [32] B. Hinner, M. Tempel, E. Sackmann, K. Kroy and E. Frey: *Entanglement, elasticity and viscous relaxation of actin solution*. *Phys. Rev. Lett.* **81** (1998), 2614.
- [33] E.K. Hobbie and D.J. Fry: *Nonequilibrium phase diagram of sticky nanotube suspensions*. *Phys. Rev. Lett.* **97** (2006), 036101.
- [34] E.K. Hobbie and D.J. Fry: *Rheology of concentrated carbon nanotube suspensions*. *J. Chem. Phys.* **126** (2007), 124907.
- [35] L.A. Hough, M.F. Islam, P.A. Janmey and A.G. Yodh: *Viscoelasticity of single wall carbon nanotube suspensions*. *Phys. Rev. Lett.* **93** (2004), 168102.
- [36] H. Isambert and A.C. Maggs: *Dynamics and rheology of actin solutions*. *Macromolecules* **29** (1996), 1036.
- [37] H. Isambert, P. Venier, A.C. Maggs, A. Fattoum, R. Kassab, D. Pantaloni and M.F. Carlier: *Flexibility of actin-filaments derived from thermal fluctuations - effect of bound nucleotide, phalloidin, and muscle regulatory proteins*. *J. Biol. Chem.* **270** (1995), 11437.
- [38] H.M. Jaeger, S.R. Nagel and R.P. Behringer: *Granular solids, liquids, and gases*. *Rev. Mod. Phys.* **68** (1996), 1259.
- [39] P.A. Janmey, S. Hvidt, J. Käs, D. Lerche, A. Maggs, E. Sackmann, M. Schliwa and T.P. Stossel: *The mechanical-properties of actin gels - elastic-modulus and filament motions*. *J. Biol. Chem.* **269** (1994), 32503.
- [40] J. Kierfeld, O. Niamploy, V. Sa-yakanit and R. Lipowsky: *Stretching of semiflexible polymers with elastic bonds*. *Eur. Phys. J. E* **14** (2004), 17.
- [41] A.M. Kraynik and W.E. Warren. *Low density cellular plastics*. Kluwer Academic Publisher, Amsterdam, 1994. Chapt. 7.

- [42] L. Kreplak, H. Bar, J.F. Leterrier, H. Herrmann and U. Aebi: *Exploring the mechanical behavior of single intermediate filaments*. *J. Mol. Biol.* **354** (2005), 569.
- [43] K. Kroy and E. Frey: *Force-extension relation and plateau modulus for wormlike chains*. *Phys. Rev. Lett.* **77** (1996), 306.
- [44] W. Kuhn: *Relationship between molecular size, static molecular shape and elastic characteristics of high polymer materials*. *Kolloid Zeits.* **76** (1936), 258.
- [45] L.D. Landau and E.M. Lifshitz: *Theory of elasticity*, Vol. 7. 3. Edition. Butterworth-Heinemann, Oxford, 1995.
- [46] L. Limozin and E. Sackmann: *Polymorphism of cross-linked actin networks in giant vesicles*. *Phys. Rev. Lett.* **89** (2002), 168103.
- [47] C.H. Liu, S.R. Nagel, D.A. Schecter, S.N. Coppersmith, S. Majumdar, O. Narayan and T.A. Witten: *Force fluctuations in bead packs*. *Science* **269** (1995), 513.
- [48] J. Liu, G.H. Koenderink, K.E. Kasza, F.C. MacKintosh and D.A. Weitz: *Visualizing the strain field in semiflexible polymer networks: strain fluctuations and nonlinear rheology of F-actin gels*. *Phys. Rev. Lett.* **98** (2007), 198304.
- [49] F.C. MacKintosh, J. Käs and P.A. Janmey: *Elasticity of semiflexible biopolymer networks*. *Phys. Rev. Lett.* **75** (1995), 4425.
- [50] C.E. Maloney and A. Lemaître: *Amorphous systems in athermal, quasistatic shear*. *Phys. Rev. E* **74** (2006), 016118.
- [51] E. Mandelkow and E.M. Mandelkow: *Microtubules and microtubule-associated proteins*. *Curr. Op. Cell Biol.* **7** (1995), 72.
- [52] J.C. Maxwell: *On the calculation of the equilibrium and stiffness of frames*. *Philos. Mag.* **27** (1864), 27.
- [53] T. Odjik: *On the statistics and dynamics of confined or entangled stiff polymers*. *Macromolecules* **16** (1983), 1340.
- [54] C. O'Hern, L.E. Silbert, A.J. Liu and S.R. Nagel: *Jamming at zero temperature and zero applied stress: The epitome of disorder*. *Phys. Rev. E* **68** (2003), 11306.
- [55] P.R. Onck, T. Koeman, T. van Dillen and E. van der Giessen: *Alternative explanation of stiffening in cross-linked semiflexible networks*. *Phys. Rev. Lett.* **95** (2005), 178102.
- [56] S. Ostojic, E. Somfai and B. Nienhuis: *Scale invariance and universality of force networks in static granular matter*. *Nature* **439** (2006), 828.
- [57] A. Palmer, J. Xu, S.C. Kuo and D. Wirtz: *Diffusing wave spectroscopy of actin filament networks*. *Biophys. J.* **76** (1999), 1063.

- [58] F. Pampaloni, G. Lattanzi, A. Jonás, T. Surrey, E. Frey and E.L. Florin: *Thermal fluctuations of grafted microtubules provide evidence of a length-dependent persistence length. Proc. Natl. Acad. Sci. USA* **103** (2006), 10248.
- [59] O. Pelletier, E. Pokidysheva, L.S. Hirst, N. Bouxsein, Y. Li and C.R. Safinya: *Structure of actin cross-linked with α -actinin: a network of bundles. Phys. Rev. Lett.* **91** (2003), 148102.
- [60] A.J. Rader, B.M. Hespeneide, L.A. Kuhn and M.F. Thorpe: *Protein unfolding: rigidity lost. Proc. Natl. Acad. Sci. USA* **99** (2002), 3540.
- [61] S. Ramanathan and D.C. Morse: *Brownian dynamics algorithm for entangled wormlike threads. J. Chem. Phys.* **126** (2007), 94906.
- [62] D. Rodney, M. Fivel and R. Dendievel: *Discrete modeling of the mechanics of entangled materials. Phys. Rev. Lett.* **95** (2005), 108004.
- [63] M. Rubinstein and R.H. Colby: *Polymer physics*. Oxford University Press, Oxford, 2003.
- [64] N. Saitô, K. Takahashi and Y. Yunoki: *The statistical mechanical theory of stiff chains. J. Phys. Soc. J. 2* **22** (1967), 219.
- [65] R.L. Satcher and C.F. Dewey: *Theoretical estimates of mechanical properties of the endothelial cell cytoskeleton. Biophys. J.* **71** (1996), 109.
- [66] B. Schaefer: Diplomarbeit, 2007.
- [67] F.G. Schmidt, B. Hinner, E. Sackmann and J.X. Tang: *Viscoelastic properties of semiflexible filamentous bacteriophage fd. Phys. Rev. E* **62** (2000), 5509.
- [68] A.N. Semenov: *Dynamics of concentrated solutions of rigid-chain polymers part 1 – brownian motion of persistent macromolecules in isotropic solution. J. Chem. Soc. Faraday Trans.* **86** (1986), 317.
- [69] J.H. Shin, M.L. Gardel, L. Mahadevan, P. Matsudaira and D.A. Weitz: *Relating microstructure to rheology of a bundled and cross-linked F-actin network in vitro. Proc. Natl. Acad. Sci. USA* **101** (2004), 9636.
- [70] L.E. Silbert, A.J. Liu and S.R. Nagel: *Vibrations and diverging length scales near the unjamming transition. Phys. Rev. Lett.* **95** (2005), 98301.
- [71] M.J. Silva, W.C. Hayes and L.J. Gibson: *The effects of nonperiodic microstructure on the elastic properties of 2-dimensional cellular solids. Int. J. Mech. Sci.* **37** (1995), 1161.
- [72] C. Storm, J.J. Pastore, F.C. MacKintosh, T.C. Lubensky and P.A. Janmey: *Nonlinear elasticity in biological gels. Nature* **435** (2005), 191.

- [73] A. Tanguy, J.P. Wittmer, F. Leonforte and J.L. Barrat: *Continuum limit of amorphous elastic bodies: A finite size study of low-frequency harmonic vibrations*. *Phys. Rev. B* **66** (2002), 174205.
- [74] R. Tharmann, M. Claessens and A.R. Bausch: *Micro- and macrorheological properties of actin networks effectively crosslinked by depletion forces*. *Biophys. J.* **90** (2006), 2622.
- [75] R. Tharmann, M. Claessens and A.R. Bausch: *Viscoelasticity of isotropically cross-linked actin networks*. *Phys. Rev. Lett.* **98** (2007), 88103.
- [76] Y. Tseng, B.W. Schafer, S.C. Almo and D. Wirtz: *Functional synergy of actin filament cross-linking proteins*. *J. Biol. Chem.* **277** (2002), 25609.
- [77] B. Wagner, R. Tharmann, I. Haase, M. Fischer and A.R. Bausch: *Cytoskeletal polymer networks: The molecular structure of cross-linkers determines macroscopic properties*. *Proc. Natl. Acad. Sci. USA* **103** (2006), 13974.
- [78] F.T. Wall: *Statistical thermodynamics of rubber*. *J. Chem. Phys.* **10** (1942), 132.
- [79] D. Weaire and S. Hutzler: *The physics of foams*. Oxford University Press, Oxford, 2001.
- [80] J.W. Weisel: *The mechanical properties of fibrin for basic scientists and clinicians*. *Biophys. Chem.* **112** (2004), 267.
- [81] J. Wilhelm and E. Frey: *Radial distribution function of semiflexible polymers*. *Phys. Rev. Lett.* **77** (1996), 2581.
- [82] J. Wilhelm and E. Frey: *Elasticity of stiff polymer networks*. *Phys. Rev. Lett.* **91** (2003), 108103.
- [83] S.R. Williams and A.P. Philipse: *Random packings of spheres and spherocylinders simulated by mechanical contraction*. *Phys. Rev. E* **67** (2003), 51301.
- [84] S.J. Winder and K.R. Ayscough: *Actin-binding proteins*. *J. Cell Sci.* **118** (2005), 651.
- [85] G.C.L. Wong, A. Lin, J.X. Tang, Y. Li, P.A. Janmey and C.R. Safinya: *Lamellar phase of stacked two-dimensional rafts of actin filaments*. *Phys. Rev. Lett.* **91** (2003), 18103.
- [86] M. Wyart: *On the rigidity of amorphous solids*. *Ann. Phys. Fr.* **30** (2005), 1.
- [87] M. Wyart, S.R. Nagel and T.A. Witten: *Geometric origin of excess low-frequency vibrational modes in weakly connected amorphous solids*. *Europhys. Lett.* **72** (2005), 486.

-
- [88] M. Wyart, L.E. Silbert, S.R. Nagel and T.A. Witten: *Effects of compression on the vibrational modes of marginally jammed solids. Phys. Rev. E* **72** (2005), 51306.
- [89] J. Xu, A. Palmer and D. Wirtz: *Rheology and microrheology of semiflexible polymer solutions: actin filament networks. Macromolecules* **31** (1998), 6486.
- [90] H.X. Zhu, J.R. Hobdell and A.H. Windle: *Effects of cell irregularity on the elastic properties of 2D Voronoi honeycombs. J. Mech. Phys. Sol.* **49** (2001), 857.
- [91] A.G. Zilman and S.A. Safran: *Role of cross-links in bundle formation, phase separation and gelation of long filaments. Europhys. Lett.* **63** (2003), 139.

Danksagung

Abschließend möchte ich mich für die Unterstützung bedanken, die ich in den Jahren der Doktorarbeit erhalten habe.

Der meiste Dank gebührt sicherlich Prof. Dr. Erwin Frey, dessen Kreativität und Motivation wesentlich dazu beigetragen haben, diese Doktorarbeit zum Erfolg zu führen. Seine Fähigkeit, komplexe Sachverhalte präzise auf den Punkt zu bringen, hat mir oft geholfen. Auch wenn er als Lehrstuhlleiter vielfältige Verpflichtungen hatte, waren die Treffen mit ihm nie gehetzt, immer fruchtbar und intensiv. Nicht unerwähnt lassen möchte ich, dass er es mir ermöglicht hat, zu verschiedenen Konferenzen im In- und Ausland zu fahren. Insbesondere wenn man sieht, wie knapp Reisemittel an manchen Lehrstühlen sind, so muss das hier besonders gewürdigt werden. Schließlich schulde ich Erwin Frey Dank für die Unterstützung während und auch nach meiner Elternzeit, die es mir erlaubte, im fernen Lüneburg zu arbeiten.

Eine besondere Bereicherung waren die wissenschaftlichen Diskussionen, die ich mit vielen führen konnte; vor allem mit Dr. Mark Bathe und Prof. Dr. Klaus Kroy (der mir in Berlin buchstäblich im Nacken saß). Eine besondere Ehre war es mir, während meiner Münchener Zeit, in Klaus' Wohnung leben zu dürfen. Vielleicht habe ich sogar etwas vom "wissenschaftlichen Geist" profitiert, der in der Wohnung immer zu spüren war.

Eine große Hilfe zur Bewältigung alltäglicher, jedoch für mich unlösbarer Probleme, leistete Frederik Wagner mit seinem unermüdlichen (sowie unerschütterlichen) Einsatz als Systembetreuer.

Eine große Unterstützung waren alle, die mich im letzten Jahr bei meinen zahlreichen Besuchen in München aufgenommen haben. Mein Dank geht an Mark und Tina (deren Apartment ich manchmal etwas unaufgeräumt verlassen habe), Sebastian und Andrea (deren köstliche Abendessen ich mit meinen Soja-Desserts "bereichert" habe), Hauke (dessen Telefonrechnung ich überstrapaziert habe), Ralf (dessen Monaco-Franze Kollektion ich durcheinander gebracht habe), sowie an Paolo, dessen Pariser Wohnung ich nutzen durfte.

Die Berliner Zeiten sind zwar schon lange her, an unsere nachmittägliche Scopa-Runde denke ich aber immer noch gerne zurück.

Zum Schluß- und am allerwichtigsten – möchte ich mich bei meiner Antje und bei meinen Eltern bedanken, ohne deren langjährige Unterstützung nichts von all dem möglich gewesen wäre. Meinem Sohn Cederic bin ich für seine Lebensfreude dankbar, die mir auch über anstrengende Arbeitstage hinweggeholfen hat.